AN ELECTRONICALLY-CONTROLLED EXCITATION SYSTEM FOR A SMALL ALTERNATOR

AN ELECTRONICALLY-CONTROLLED EXCITATION SYSTEM FOR A SMALL ALTERNATOR

A Thesis

Presented to

the Faculty of Graduate Studies

The University of Manitoba

In Partial Fullfillment

of the Requirements for the Degree

Master of Science in Electrical Engineering

---

by

Wilhelm Joseph Tishinski

March 1959

THE UNIVERSITY OF MANITOBA LIBRARY

ABSTRACT

The design of an electronic voltage regulator for a small alternator is presented. Stability of the regulating system is predicted with servomechanism theory. Having constructed a regulator in accordance with the design data, oscillograms were taken of its performance and are included in the thesis, confirming results from the stability criteria.

The system is found to be unstable and a corrective network is introduced to provide stability at no-load conditions.

Theory is presented evaluating the transient response of the alternator terminal voltage upon application and removal of load with the regulating system in action. Test results are included to substantiate the validity of the theoretical calculations.

TABLE OF CONTENTS

CHAPTER		PAGE
I	BASIC THEORY	
	1.1 Servomechanism Fundamentals	1
II	DESIGN OF THE FORWARD CONTROL ELEMENTS	
	2.1 Exciter Field Supply	4
	2.2 Thyratron Triggering Pulse	8
	2.3 The Cathode-Coupled Clipper.	12
	2.4 Power Amplification of the "Spiked"-Wave	18
	2.5 Coupling the "Spike"-Generating Circuit to the Thyratron Grid	22
	2.6 The Amplification of the Forward Control and Controlled Elements.	25
	2.7 The Transfer Function of the Forward Elements.	33
III	DESIGN OF THE FEEDBACK ELEMENT	
	3.1 Filtering Qualities of the Detector Circuit.	40
	3.2 Transfer Function of the Feedback Circuit.	54
IV	DESIGN OF THE REFERENCE SUPPLY	
	4.1 Required Voltage Output.	71
V	BLOCK DIAGRAM OF CLOSED-LOOP UNCOMPENSATED REGULATING SYSTEM	
	5.1 Connection of Control Elements to Form a Closed Loop .	75
	5.2 Loading on the Detector Circuit.	78
VI	STABILITY OF THE UNCOMPENSATED REGULATING SYSTEM	
	6.1 The Nyquist Diagram.	83
	6.2 The Bode Diagram	88
VII	STABILIZING NETWORKS FOR THE REGULATING SYSTEM	
	7.1 The Lag and Lead Networks.	91
	7.2 Feedback Stabilization	96
	7.3 Effect of Saturation on Stability.	121

CHAPTER PAGE

VIII STEADY-STATE AND TRANSIENT PERFORMANCE OF ALTERNATOR WITH REGULATING SYSTEM

8.1 Alternator Regulation 126
8.2 Transient Response with Suddenly-Applied Loads. . . 132
8.3 Maximum Voltage Rise Upon Removal of Load 159

IX PRACTICAL DIFFICULTIES WITH CIRCUIT OPERATION

9.1 Ripple in the Actuating Error Signal. 177

X CONCLUSIONS. 185

APPENDICES

A WAVE SHAPE RECORDING TECHNIQUE

A.1 The Phantastron Circuit. 187
A.2 Application of the Phantastron for Control of the Oscilloscope Beam. 195

B MACHINE CONSTANTS

B.1 Three-Phase Short-Circuit Current Analysis. 200
B.2 Self-Inductance of Exciter and Alternator Fields . . . 215
B.3 Equivalent Time Constant T_e of a Loaded Exciter. . . . 220
B.4 The Slip Test. 224
B.5 Exciter Armature Inductance. 225
B.6 Exciter and Alternator Resistances 226

C CURRENT WAVEFORMS IN THE EXCITER FIELD. 227
D INDUCTANCE OF THE SATURABLE REACTOR CONTROL WINDINGS. 232
E CONSTANTS OF 25VA TRANSFORMER, #50711, USED IN FEEDBACK CIRCUIT 251
F OPERATING PROCEDURE 252

BIBLIOGRAPHY. 253

LIST OF FIGURES

FIGURE		PAGE
1.1	Block Diagram of Simplified Feedback Control System	2
2.1	Components Providing Alternator Field Supply	5
2.2	Characteristics of an EL CIB/A Grid-Controlled Rectifier Tube	7
2.3	Circuit for Producing Thyratron Triggering Pulse	10
2.4	Cathode-Coupled Clipper Output and Grid Signal Input	17
2.5	Clipper Output and Differentiated Signal.	17
2.6	Power Amplifier Output and Grid Signal Input	17
2.7	Clamped and Unclamped Triggering Waves for Thyratron	17
2.8	Differentiating Circuit For an R-C Coupled Amplifier	19
2.9	Coupling "Spiked"-Wave to the Thyratron.	23
2.10	Error-Voltage Control of Saturable Reactor D-C Current	29
2.11	Maximum Phase Shift Possible	32
2.12	Minimum Phase Shift Possible	32
2.13	Voltage Across Thyratron for Small Field Current	32
2.14	Voltage Across Thyratron for Large Field Current	32
2.15	Transient Response of Saturable Reactor with Control Winding in Load Circuit of 6AC7 Pentode.	38
3.1	Rectifier and Filter in Feedback Circuit	41
3.2	Schematic and Equivalent Circuit of Detector	44
3.3	Rectifier Current for 120-Volt Input	47
3.4	Capacitor Discharge Through Back-Resistance of Rectifiers.	47
3.5	Ripple Voltage at Rectifier Output with No Filter Section and 120-Volt Input	47
3.6	Ripple Voltage at Rectifier Output with Filter Section Connected and 120-Volt Input	47
3.7	Individual Rectifier Arrangement in the Detector Circuit	49
3.8	Ripple Voltage at Filter Output With 120-Volt Input.	60
3.9	Response of Detector to a Unit-Step Input.	60
3.10	Decay of Detector Voltage with a Step Input.	60

FIGURE PAGE

4.1 Reference Supply Circuit. 72
5.1 Schematic of Uncompensated Voltage-Regulating System. . . 76
5.2 Detector Circuit with Loading 79
5.3 Block Diagram of Uncompensated Voltage-Regulating System. 81
6.1 Performance of Unstable Voltage-Regulating System 87
7.1 Equalizer Networks. 92
7.2 Minor-Loop Feedback Circuit 98
7.3 Schematic of Compensated Voltage-Regulating System. . . . 100
7.4 Block Diagram of Compensated Voltage-Regulating System. . 104
7.5 Treatment of Non-Linear Elements. 122
8.1 Vector Diagram for Full Load at 80% PF, Lagging 127
8.2 Vector Diagram for Full Load at Unity Power Factor. . . . 128
8.3 Transient Response of Alternator Upon Sudden Application of Full Load at 80% PF, Lagging, and with 71% Feedback. 144
8.4 Transient Response of Alternator Upon Sudden Application of Full Load at 80% PF, Lagging, and with 71% Feedback. 145
8.5 Transient Response of Alternator Upon Sudden Application of Full Load at 80% PF, Lagging, and with 100% Feedback 146
8.6 Transient Response of Alternator Upon Sudden Application of Full Load at 100% PF.. 150
8.7 Transient Response of Alternator Upon Sudden Application of Full Load at 94% PF, Leading 154
8.8 Transient Response of Alternator Upon Application of a Single-Phase Load at 100% PF. 156
8.9 Transient Response of Alternator Upon Starting a Wound Rotor Induction Motor 158
8.10 Transient Response of Alternator Upon Sudden Removal of Full Load at 80% PF, Lagging and with 100% Feedback . . 170
8.11 Transient Response of Alternator Upon Sudden Removal of Full Load at 80% PF, Lagging and with 71% Feedback. . . 171
8.12 Transient Response of Alternator Upon Sudden Removal of Full Load at 100% PF. 173

FIGURE PAGE

9.1 Portion of Regulating Circuit Contributing Ripple Components 178
9.2 Ripple Across Points a and b 179
9.3 Ripple Across f and ground 179
9.4 Ripple Across b and ground 179
9.5 Actuating Error Signal With No Filter Capacitor. 179
9.6 Ripple in Actuating Error Signal With 60% Feedback 183
9.7 Ripple in Actuating Error Signal With 100% Feedback. 183
9.8 Ripple in Actuating Error with 60% Feedback. 183
9.9 Ripple in Actuating Error with Full Load at 100% PF Applied to Alternator. 183
A.1 Cathode-Coupled Phantastron Controlling Oscilloscope Beam. .189
A.2 Theoretical Voltage Waveforms in Cathode-Coupled Phantastron. 192
A.3 Recorded Waveforms in Cathode-Coupled Phantastron. 193
A.4 Test Circuit for Determining Beam Triggering Characteristics of the Mark I Cossor 196
A.5 Potentiometer Arrangement for Bias Voltages. 196
B.1 Short-Circuit Currents of Alternator 207
B.2 Response of Exciter Field Current to a Unit-Step Input Voltage. 217
B.3 Response of Alternator Field Current to a Unit-Step Input Voltage. 217
B.4 Response of Loaded Exciter 222
B.5 Line Current and Voltage During Slip Test. 225
B.6 Thyratron and Exciter Field Current. 225
B.7 Back-Rectifier Current and Exciter Field Voltage 225
B.8 Theoretical Voltage and Current Wave Shapes Associated with Exciter Field 228
B.9 Flux Paths in Reactor When A-C Windings Energized. 240

FIGURE PAGE

B.10 Flux Paths in Reactor When Control Windings Energized. . . .240
B.11 Build-Up of A-C Current in Saturable Reactor with a Unit-Step Input in Control Voltage. 246
B.12 Build-Down of Saturable Reactor Load Current with Step Input in Control Voltage 246
B.13 Build-Up of Load Current with Unit-Step Input in Control Voltage. 246

LIST OF GRAPHS

GRAPH		PAGE
2.1	Phase-Shifting Properties of the Saturable Reactor with Load Resistance as a Parameter	11
2.2	Graphical Analysis of the Cathode-Coupled Clipper	14
2.3	Theoretical and Actual Clipper Output Wave Shapes	16
2.4	Graphical Analysis of Power Amplifier Producing Thyratron Triggering Wave	20
2.5	Effect of Saturable Reactor Control Current on the Exciter Field Current and Thyratron Firing Angle	26
2.6	Relation Between Saturable Reactor Control Current and Exciter Field Voltage	28
2.7	Dynamic Transfer Characteristics of 6AC7 Pentode with Control Winding of Saturable Reactor as Load	31
2.8	Load Line of Error-Amplifying 6AC7 Pentode	37
3.1	Volt-Ampere Characteristics of Selenium Rectifiers, Type, "Pyramid Ks 150"	46
3.2	Response of Detector Circuit to a Unit-Step Input	62
3.3	Voltage Decay at Detector Output With a Step Input	69
6.1	Polar Plot of Transfer Function for Uncompensated Voltage-Regulating System	85
6.2	Bode Diagram of Uncompensated Open-Loop Transfer Function	90
7.1	Effect of Lag Network on Unstable System	94
7.2	Bode Diagram of the Minor Open-Loop Transfer Function	105
7.3	Bode Diagram of Compensated System - Transfer Function A_{M2}	107
7.4	Calculated Effect of Feedback Signal on Degree of Stability	108
7.5	Bode Diagram of Compensated System - Transfer Function A_{M1}	112
7.6	Effect of Alternator Terminal Voltage and Feedback on System Stability	115
7.7	Polar Plot of Minor Loop	117
7.8	Polar Plots of Corrected and Uncorrected Transfer Functions for Voltage-Regulating System	120

GRAPH PAGE

8.1 Voltage Regulation of Alternator with and without Regulator. 133
8.2 Calculated and Recorded Alternator Terminal Voltage for Sudden Application of Full Load at 80% PF, Lagging 143
8.3 Calculated and Recorded Alternator Terminal Voltage for Suddenly Applied Load at 100% PF 149
8.4 Approximate Rate of Decay of Exciter Voltage Upon Load Removal. 164
8.5 Calculated and Recorded Alternator Terminal Voltage Upon Sudden Removal of Full Load at 80% PF, Lagging 169
8.6 Calculated and Recorded Alternator Terminal Voltage Upon Sudden Removal of Full Load at 100% PF. 175
B.1 Alternator Voltage Characteristics 201
B.2 Voltage Regulation and Field Compounding Characteristics of Alternator. 202
B.3 Exciter Saturation Curves - No-Load and Loaded Conditions. .203
B.4 Hysteresis Effect on Exciter Terminal Voltage for Various Ranges of Field Current - Exciter Loaded 204
B.5 Relation Between Exciter and Alternator Field Currents . . .205
B.6 Subtransient and Transient Short-Circuit Armature Currents .210
B.7 Excess D-C Component of Field Current. 211
B.8 D-C Components of the Armature Short-Circuit Currents. . . .213
B.9 No-Load Symmetrical Three-Phase Short-Circuit Armature Currents 214
B.10 Evaluating the Self-Inductance of the Exciter and Alternator Fields 219
B.11 Evaluation of T_e, the Loaded-Exciter Time Constant 223
C.1 Calculated and Experimental Current Wave Shapes and Magnitudes in Exciter Field. 231
D.1 Characteristic Curves of Saturable Reactor 235
D.2 Chart for Fitting a Power to a Saturation Curve. 236
D.3 Universal Curves for a Ninth Power Saturation Curve. 236
D.4 Control Winding Magnetization Curve and Relation Between Load Current and Control Current for Resistive Load. . . .244
D.5 Build-Up and Build-Down Currents in a Saturable Reactor with a Unit-Step Input Control Voltage. 249

LIST OF TABLES

TABLE		PAGE
3.1	Recorded Voltage Rise of Detector Circuit	59
3.2	Voltage Decay of Capacitor C_1 with a Step Input	66
3.3	Voltage Decay at Output with a Step Input	67
3.4	Voltage Decay at Output after Transition Takes Place	67
3.5	Recorded Voltage Decay with a Step Input	67
6.1	Tabulation of Points for Polar Plot of $A_1 (j\omega)$	84
6.2	Tabulation of Points for Polar Plot of $A_2 (j\omega)$	86
7.1	Relation Between R_b and Phase Shift of Transfer Function $A_{M2} (j\omega)$	110
7.2	Relation Between R_b and Phase Shift of Transfer Function $A_{M1} (j\omega)$	111
7.3	Minimum Amount of Anti-Hunt Signal That Will Maintain Stability at Various Alternator Terminal Voltages	113
7.4	Tabulation of Points for Polar Plot of $A_m (j\omega)$	116
7.5	Tabulation of Calculated Points for Polar Plot of A_{M2}	119
7.6	Tabulation of Calculated Points for Polar Plot of A_{M1}	119
8.1	Test Data for Full Load at 80% PF, Lagging	130
8.2	Test Data for Full Load at 100% PF	131
8.3	Test Data for Full Load at 94% PF, Leading	132
8.4	Computations of e_t for Full Load at 80% PF, Lagging	141
8.5	Computations of e_t for Full Load at 100% PF	148
8.6	Computations of e_t After Dropping Full Load at 80% PF, Lagging	167
8.7	Computations of e_t After Dropping Full Load at 100% PF	172
9.1	Harmonic Content of the Exciter at Various D-C Voltage Levels	180
A.1	Beam-Triggering Characteristics of the Mark I Cossor	197
A.2	Beam-Triggering Characteristics of the Mark II Cossor	197
B.1	Analysis of Short-Circuit Currents	206
B.2	Analysis of Unidirectional Component of Field Current	212
B.3	Evaluation of the Exciter Field Inductance from Oscillograph Tracings	216

TABLE PAGE

B.4 Evaluation of the Alternator Field Inductance from Oscillograph Tracings. 218

B.5 Evaluation of the Equivalent Time Constant T_e of the Exciter from Oscillograph Tracings 221

B.6 Data on Supplying A-C Power to the Exciter Armature. 224

B.7 Exciter and Alternator Resistances 226

D.1 Reactor Saturation Curve 233

D.2 Data for Plot of Load Line on Reactor Characteristic Curves.237

D.3 Evaluated Turns Ratio of the Saturable Reactor 239

D.4 Calculation of the Control Winding Flux Linkages 242

D.5 Tabulation of Points for Evaluating Time Constant of Reactor. 245

Please Note:

Many double-subscripted terms appear throughout this thesis. Due to the spacing of the typewriter, it was rather difficult to align both subscripts. For example, a term such as "v_{c_2}" does not mean that the subscript c is raised to the power two, but rather that c and 2 are individual subscripts. This applies to all subscripts comprised of a letter and a number.

W.J.T.

PREFACE

Voltage regulation of a-c generators is important not only for the maintenance of a constant voltage output, but also for system stability. Fast-acting regulators are a vital element in power plants in order to keep the generator from falling out of step when a disturbance occurs.

A 7.5 kva alternator, present in the electrical engineering department at the University of Manitoba, had poor regulation characteristics and it was felt that the design of a voltage regulator for this machine would be analogous in many respects to that for a large alternator found in a power plant. The shaft power was supplied by a 10 hp, d-c motor. When the alternator was loaded the speed of the M-G set decreased, because of the speed regulation of the motor. Therefore, the regulator to be devised had to be insensitive to speed variations.

Some of the design was carried out by trial and error, but all performance is proven by theory. This method of design was necessary because of unexpected complications due to ripple components in the exciter voltage, unequal line voltages at the alternator terminal when at no load, and to the non-linearities of some components.

A basic knowledge of servomechanisms is necessary in order to follow certain portions of this thesis. Several references in this field are listed in the bibliography section.

Nameplate data of the alternator was omitted from the graphs since only the one machine is treated throughout the entire thesis. Characteristic curves of the alternator and exciter were determined at rated speed unless otherwise specified. All timing waves are 60 cps, except where a note has been made to the contrary. All symbols used in the diagrams are as outlined in the manual - National Research Council of Canada, Proposed Standard for Electrical and Electronic Symbols, Jan., 1951.

Finally, the writer wishes to express his thanks to Professor R. A. Johnson for his assistance in problems of analysis, and to his advisor, Professor J. P. C. McMath, who was most helpful by his clairvoyant insight into the subtleties of circuit operation.

CHAPTER I

BASIC THEORY

1.1 Servomechanism Fundamentals

All servomechanism and regulator systems are basically identical in that they are automatically controlled. Any servomechanism system can be reduced to a simple feedback control system as shown in Fig. 1.1.

An actuating error E(s) is obtained from the difference of the reference input R(s) and some function of the controlled variable B(s) at the summing point. This actuating error supplies a signal to the control elements and controlled system. The amplified actuating error signal endeavors to reduce to zero the difference between R(s) and B(s). An external source of power is available at various points in such systems for amplification of some signals. This may produce self-excited oscillations or instability.

In a regulating system there are elements which have fixed characteristics such as the alternator and exciter fields and there are those elements whose characteristics can be controlled by the designer. Intuitively, one can see that if C(s) is experiencing a change, this change should be reported to the summing point as soon as possible so that corrective measures can take place and restore C(s) to its initial value. Thus, the feedback element H(s) should have a small delay, as should any other elements in the forward transfer function.

Suppose the controlled element is a generator which momentarily has a fluctuation in voltage. The time taken by the feedback element to transfer this change to the summing point is in question, but undoubtedly a delay is experienced. As soon as the summing point detects the variation in C(s) it will immediately take corrective measures to restore the output C(s) to its initial level. However, if there are further delays in the forward elements, the actuating error will not be able to immediately bring C(s) back to normal.

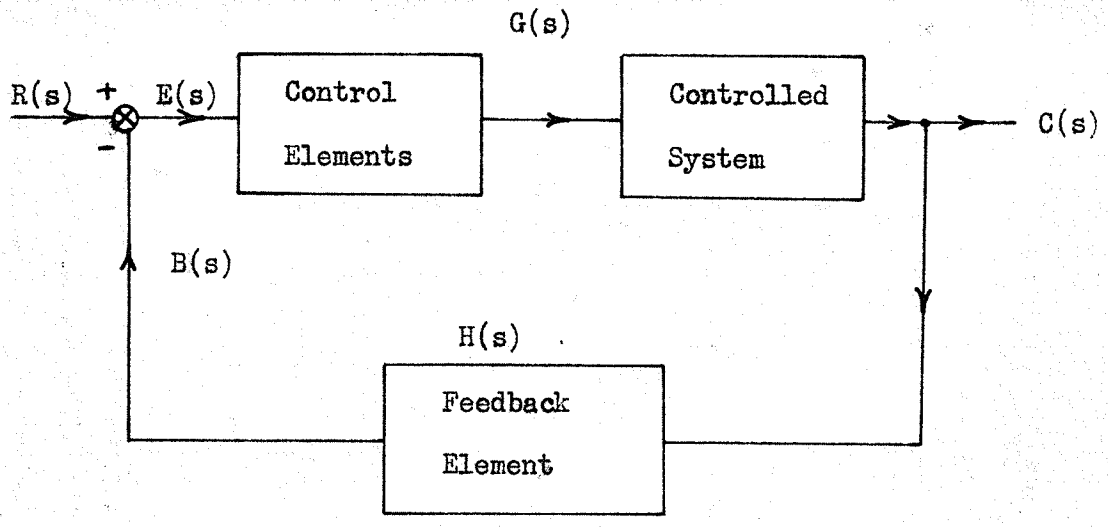

FIG. 1.1 BLOCK DIAGRAM OF SIMPLIFIED FEEDBACK CONTROL SYSTEM

E(s) will be of a greater magnitude than was necessary to restore C(s); thus, the voltage may be driven from a below-normal value to one above the desired value. This rise is, of course, detected by the feedback element and is transferred to the summing point where the error signal swings in a direction opposite to that of its original motion. The above action is called instability in the general servomechanism field, but in the case of electrical machines it is specifically known as "hunting."

There are three factors to contend with in designing a regulating system for an alternator:

1. Steady-state stability must be present.

2. Upon loading, the deviation of the terminal voltage from the open-circuit value must be as small as possible in the steady-state sense.

3. When load is suddenly applied, the terminal voltage should be brought back to normal in as short a time as possible, that is, the transient response must be relatively fast.

CHAPTER II

DESIGN OF THE FORWARD CONTROL ELEMENTS

2.1 Exciter Field Supply

As shown in Fig. 2.1 (a), the machine in question has an exciter which feeds the alternator field, thus the control of the alternator voltage can be accomplished by varying the field current of the exciter. Since the rating of the field current is 350 ma, this magnitude of current can readily be supplied by a grid-controlled, gas-filled rectifier. Numerous circuits are available for supplying current to a resistive and inductive load (exciter field) by a controlled rectifier. The one considered most economical and efficient for this purpose[1] was a half-wave controlled rectifier with a gas diode placed across the load, Fig. 2.1 (b). This arrangement is ~~most~~ efficient where large inductances are involved. The self-inductance, as found in Appendix B.2 is 19.0 henries, and the resistance is 198 ohms. Hence, the power factor angle of the field is

$$\theta = \tan^{-1} \omega \frac{L}{R}$$

$$= \tan^{-1} \frac{377 \times 19.0}{198}$$

$$= 88^{\circ}40'$$

which indicates a highly inductive load.

The thyratron selected was a type EL C1B/A, with characteristics ~~whose nameplate is~~ reproduced in Fig. 2.2. This selection was based on the tube current rating, peak inverse voltage rating, and on the reasonable cost. The back rectifier selected was a type EL 1C, whose capacity is identical to that of the thyratron. Theoretical voltage and current waveshapes are drawn in Fig. 2.1 (c).

If the tube fires at an angle β, only that portion of the sine wave voltage beyond β is impressed across the field. At the angle π, the thyratron ceases to conduct and ceases to permit any further flow

---

1. J.H. Bennett, Fast Response - High Current Thyratron Supplies for Inductive Loads, Electrical Engineering, Vol. 72, pp. 627, April, 1953.

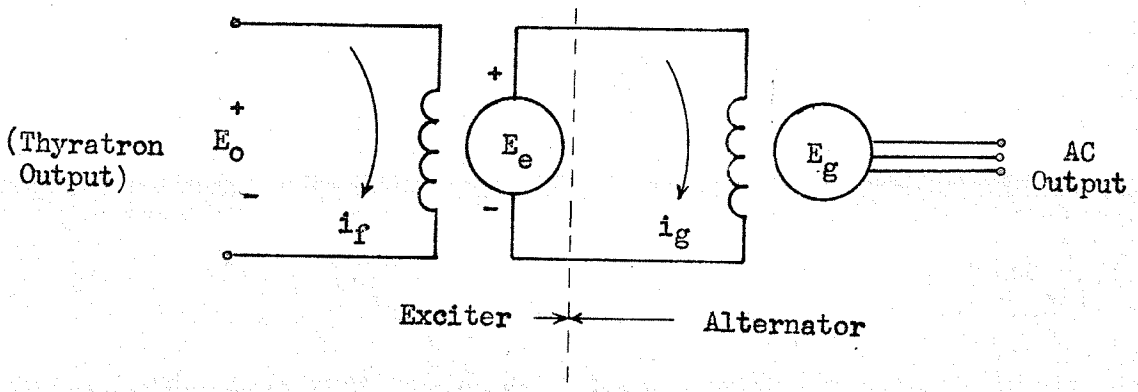

(a) ONE COMPONENT OF ALTERNATOR EXCITATION SYSTEM

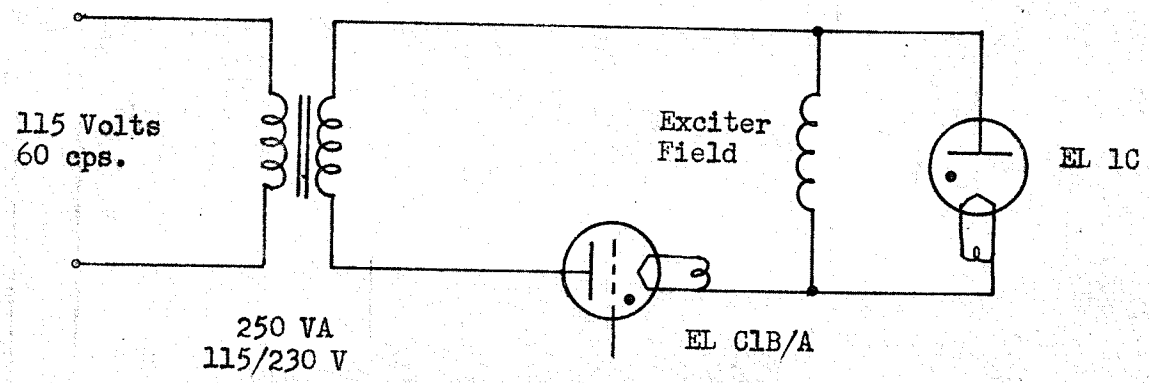

(b) CONTROL OF EXCITER FIELD CURRENT

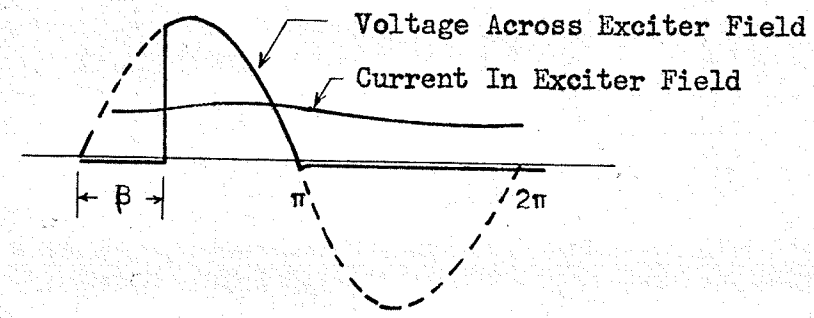

(c) THEORETICAL CURRENT AND VOLTAGE WAVE-SHAPES

FIG. 2.1 COMPONENTS PROVIDING ALTERNATOR FIELD SUPPLY

of current into the field. However, the theorem of constant flux linkages states that the current in an inductance cannot change instantaneously, that is, become zero when the impressed voltage becomes zero. Thus, the current in the field decays through the back rectifier, with the time constant of the field, until the thyratron fires again.

The average field current can be determined by the relation[1]:

$$I_{dc} = \frac{E_M}{2\pi R} (1 + \cos \beta) \qquad - - - - - - - - (2.1)$$

where E_M = peak value of the rectified voltage

R = exciter field resistance

= 198 ohms at 75°C

Field compounding curves, Appendix B.1, show that an exciter field current of 350 ma is necessary to maintain an alternator terminal voltage of 120 volts for full-load, 80% pf, lagging conditions. Also, an exciter field current of 100 ma is necessary to provide an alternator terminal voltage of 120 volts at no load. It would be undesirable to have the thyratron conduct for 180 degrees in providing 350 ma to the exciter field, since the field current would approach this value exponentially upon sudden loading, and the transient response of the over-all system would be relatively slow. However, if the field supply transformer voltage is so chosen that for 180-degree conduction of the thyratron, the average current would be, say 550 ma, ~~when it the thyratron suddenly started to fire from the 0 degree position to the 180 degree position~~, the transient rise in current would reach 350 ma in a much shorter time. This would improve the over-all transient response.

If 550 ma is selected as the maximum field current that would ever be required, then by using equation 2.1 to calculate E_M under 180-degree conducting conditions, the secondary voltage rating would be

$$0.550 = \frac{E_M}{2\pi 198} (1 + 1)$$

or E_M = 342 volts

and $E = 342/\sqrt{2}$

= 242 volts rms

---

1. W.L. Davis and H.R. Weed, Industrial Electronic Engineering, pp. 116, Prentice - Hall, 1954.

GRID CONTROL RECTIFIER TUBE

TANTALUM ANODE AND XENON GAS FILLING

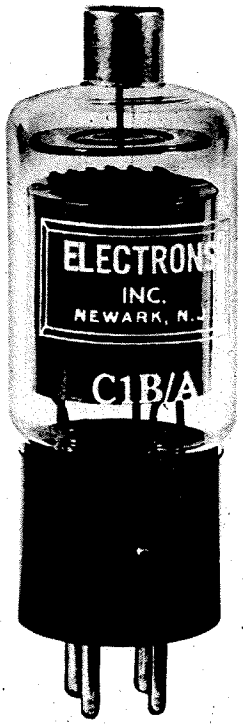

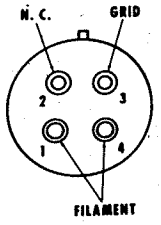

BOTTOM VIEW
OF BASE

Maximum Rated Anode Current	
D-c. Meter Value-Continuous	1.0 amp
D-c. Meter Value-Overload less than 3 sec.	1.5 amps
Oscillograph Peak-Continuously recurring	8.0 amps
Peak Forward Voltage (Max. Instantaneous)	750 volts
Peak Inverse Voltage (Max. Instantaneous)	1250 volts
Max. Commutation Factor (V/usec x A/usec) at a maximum initial inverse voltage of 500 volts	0.15
Filament	
Voltage	2.5 volts
Current	6.3 ± 0.8 amps
Heating Time (minimum)	25 secs
Average Arc Drop	
Average Tube	8 volts
Highest Tube at end of life	14 volts
Anode Starting Voltage (D.C.) @ +4V d-c. grid voltage	
Average Tube	30 volts
Highest Tube	75 volts
Grid Characteristics	
Critical Grid Voltage @ 750 p.f.v.	-4.0 ± 2.0 volts
Critical Grid Current	Less than 5 uamps
Grid-Anode Capacitance	approx. 2 uuf
Grid-Filament Capacitance	approx. 7.5 uuf
Maximum Negative Grid Voltage	100 volts
Deionization Time	Less than 1000 usecs
Max. Peak A-c Fault Current (Max. duration 0.1 sec.)	77 amps
Ambient Temperature Limits	-55° to +75° C
Mounting Position	Any
Overall Dimensions	1-9/16" x 4-3/4" Max.
Weight	~3 ozs.
Connections	
Filament and Grid	Medium 4-pin bayonet base A4-10
Anode	C1-5 cap at top (0.56" dia.)

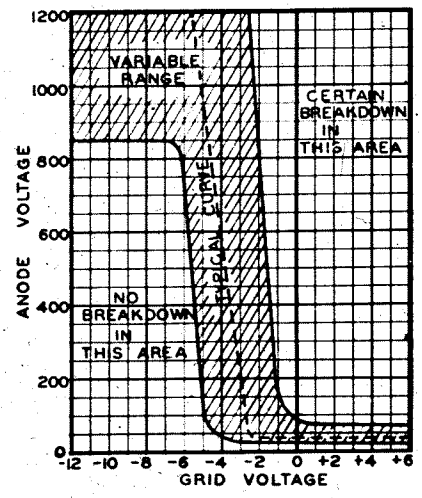

The filament must be lit before drawing d-c. load current.

The anode is designed to operate at red heat when under full load.

All of the above values are for returns to the filament transformer center tap.

The Engineering Manual contains additional information which should be considered in the circuit design.

ELECTRONS, INCORPORATED
127 Sussex Avenue
Newark 3, New Jersey

7/1/55

FIG. 2.2 CHARACTERISTICS OF AN EL C1B/A GRID-CONTROLLED RECTIFIER TUBE

This is practically twice the building supply voltage so the voltage ratio for the supply transformer can be specified as 2:1. For a half-wave rectifier with resistance loading, the utilization factor[2] is

$$VA = 4.95\ E_{dc}\ I_{dc}$$

To provide the alternator with 120 volts at full-load conditions of 80% pf, lagging, the power input to the field should be

$$P_{dc} = E_{dc}\ I_{dc}$$
$$= I_{dc}^{2}R$$
$$= 0.350^{2} \times 198$$
$$= 24.3 \text{ watts}$$

Therefore, the transformer rating should be

$4.95 \times 24.3 = 120$ VA

Conforming with the calculated voltage and power requirements, the following transformer was selected as being the supply for the exciter field:

Hammond Transformer
Type E6J5J
VA 250
Volts 230/115

The above transformer was more than double the required capacity, but since the larger transformer could be obtained with little additional cost, it was felt that this was worth the extra margin of safety provided.

2.2 Thyratron Triggering Pulse

Basically, a thyratron will fire whenever the negative grid bias is raised beyond a certain critical value. The firing characteristics of the EL C1B/A tube are shown in Fig. 2.2. Thus, for an anode supply of 340 volts, the grid should be raised to at least -1.0 volts to fire the tube and be below -5.4 volts to prevent firing.

Two methods are possible for controlling a thyratron:

(1) Varying the d-c grid bias until the critical grid-voltage curve is intersected permits control over only a 90-degree range of the sine wave.

---

2. Ibid., pp. 91.

(2) Maintaining a grid signal of constant amplitude, but varying the position of this signal along the time axis of the sine wave, permits control over 180 degrees.

The latter method appears to be more desirable, since, not only does it provide a wider range of control but the triggering pulse can be made into a "spiked"-wave, thus producing definite and precise firing.

The phase-shifting network can consist of an R-C combination or an R-L combination. Fig. 2.3(a) and (b) illustrate the schematic of the network selected[1] and the corresponding vector diagram. If the inductance is the variable component, then the grid signal voltage can be made to shift from a small angle to almost 180 degrees by making the inductance very small or very large respectively.

A saturable reactor was selected to function as the variable inductance component. This reactor consists of two windings - one, the a-c or load winding; the other, the d-c or control winding. With no current in the control winding the impedance of the reactor is relatively large and a large phase shift is obtained. As the d-c control current is increased the iron operates at a higher flux density. Lower permeability results and this produces a lower reactance. Most saturable reactors are so designed as to have a sharp bend at the "knee" in their control characteristics, that is, when the control current is increased beyond a critical value, the iron becomes completely saturated and further increases in the control current yield no change in the reactance. For the phase-shifting purposes the "knee" of the saturation curve must be avoided and the operation take place entirely along the proportional part of the curve. More data on the saturable reactor can be found in Appendix D.

Several tests were run on the phase-shifting network to determine the optimum value of the resistance R to be used in combination with the saturable reactor. The data obtained from the tests is plotted on Graph 1.

---

1. H.J. Bichsel, Circuits for Industrial Control, Westinghouse Industrial Electronics Reference Book, pp. 283, J. Wiley and Sons, 1948.

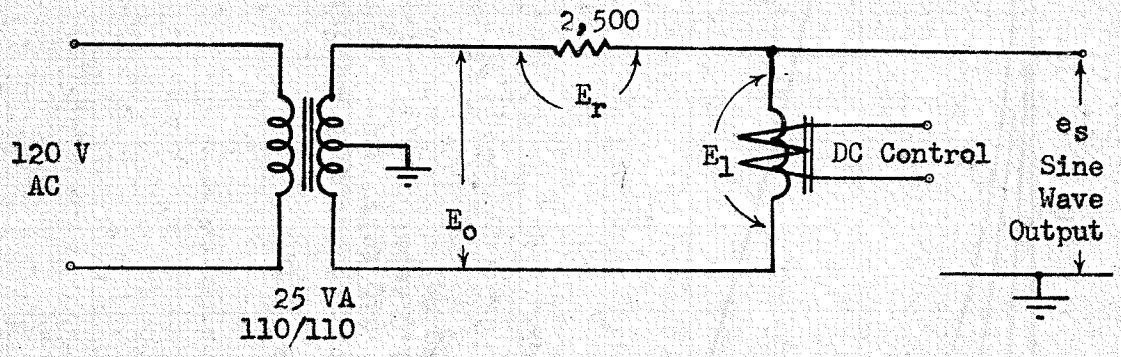

(a) PHASE-SHIFTING CIRCUIT

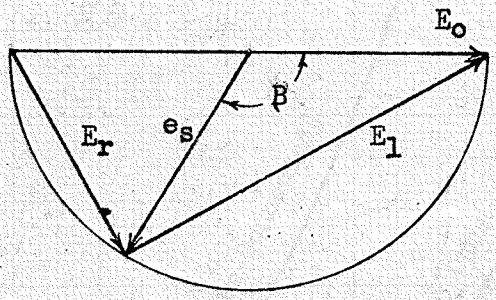

(b) VECTOR DIAGRAM OF THE PHASE-SHIFTING CIRCUIT

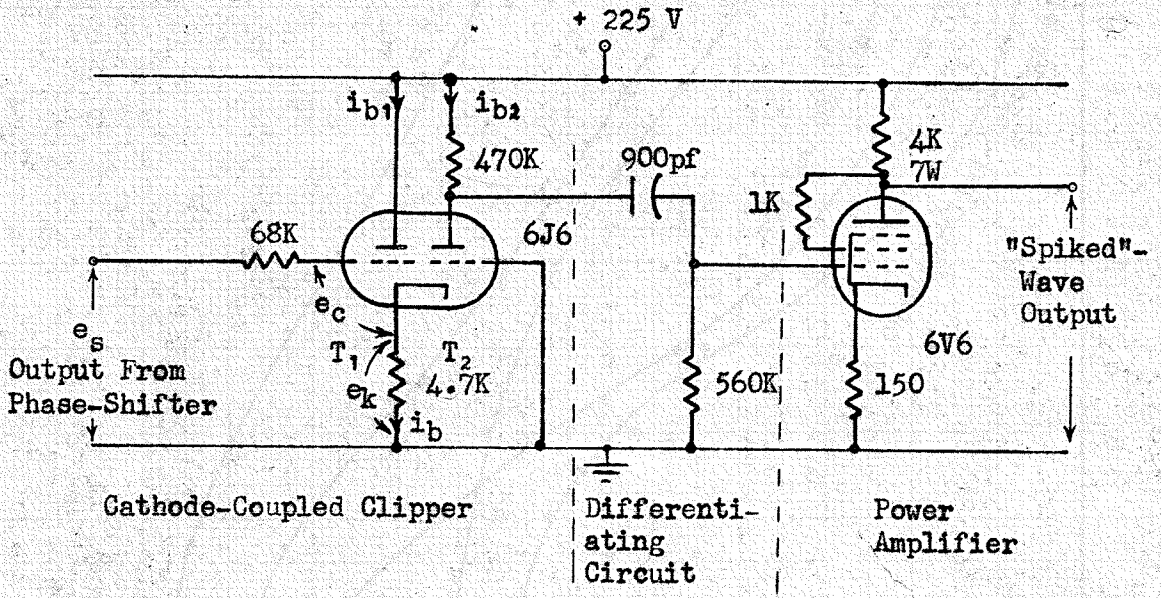

(c) Converting a Sine Wave into a "Spiked" - Wave

FIG. 2.3 CIRCUIT FOR PRODUCING THYRATRON TRIGGERING PULSE

THIS MARGIN RESERVED FOR BINDING.

IF SHEET IS READ THE OTHER WAY (VERTICALLY), THIS MUST BE LEFT-HAND SIDE.

GRAPH 2. 1 PHASE-SHIFTING PROPERTIES OF THE SATURABLE REACTOR WITH LOAD RESISTANCE AS A PARAMETER

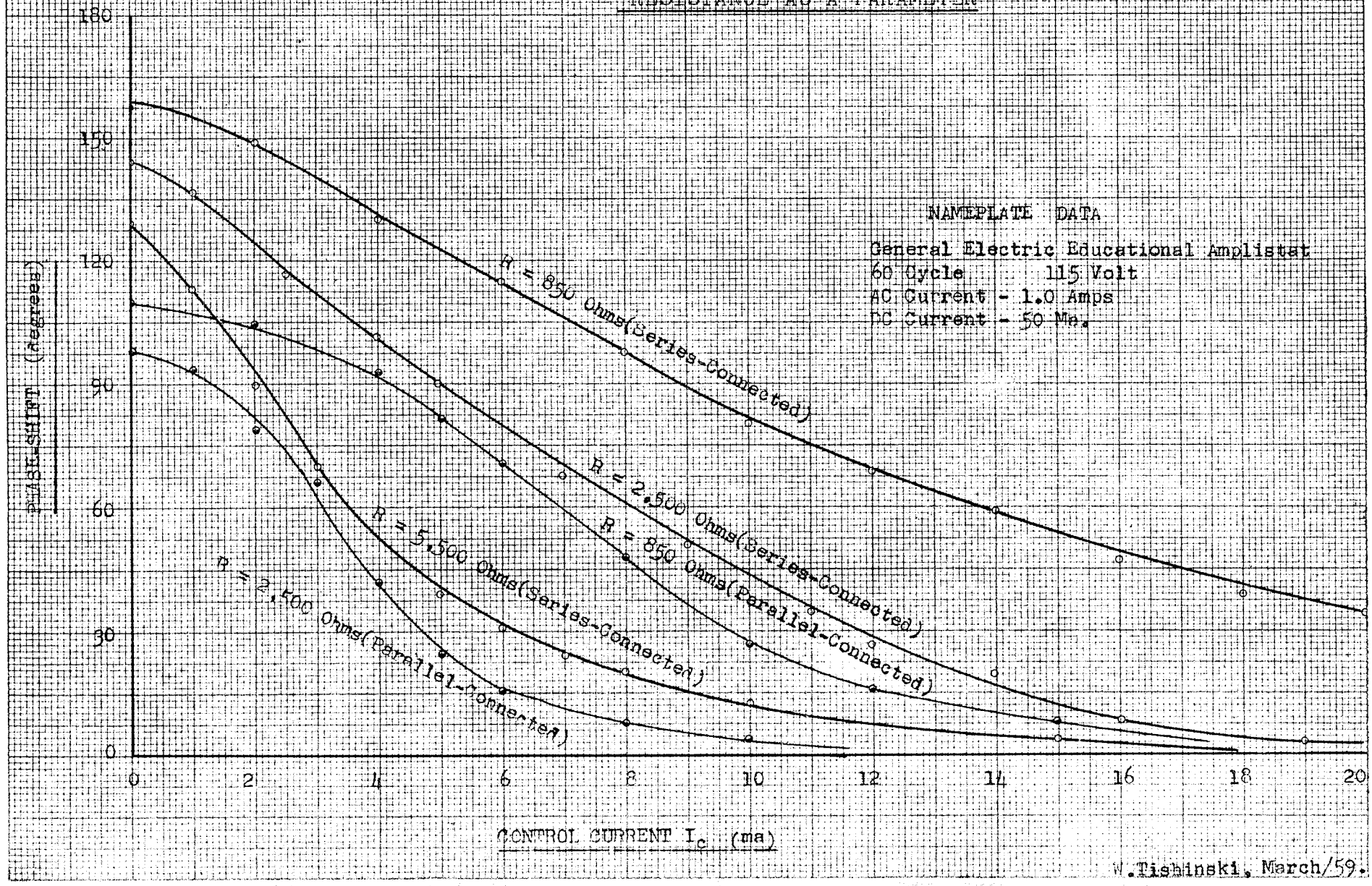

W.Tishinski, March/59.

MANUFACTURED BY RENOUF PUBLISHING CO., MONTREAL

FORM 1001

11

It is noted that as wide a range of phase-shifting is not obtained by connecting the reactor a-c windings in parallel as by connecting them in series. Furthermore, the transient response of a series-connected saturable reactor is more rapid than that for a parallel-connection.

Again, using equation 2.1, the firing angles β, to yield 100 ma and 350 ma are 130 degrees and 73 degrees respectively. It should be mentioned at this stage that the thyratron tube drop had been neglected in the above calculations. This is permissible since the design thus far is not concerned with precise values.

The 2,500-ohm resistor, with the saturable reactor series-connected, was selected as the optimum value since the corresponding curve indicates that the desired range of phase-shift can be obtained, as well as providing a shift which is quite sensitive to a change in the control current. The 5,300-ohm (series) curve indicates a greater amplification, that is, a larger phase-shift per unit of control current, but the 73-degree to 130-degree range is not available.

The output of the phase-shifting circuit could now be coupled to the grid of the thyratron with suitable grid bias and grid protecting resistors. However, as was mentioned previously, it was desired to have a "spiked"-wave fire the thyratron. Two more stages will be coupled to change the output sine wave into a "spiked"-wave.

(1) A clipper circuit will produce a square wave from the sine wave input.

(2) A power amplifier will amplify the differentiated square wave, (which is a "spiked"-wave) thus the "spiked"-wave will possess sufficient power to trigger the thyratron.

2.3 The Cathode-Coupled Clipper

The cathode-coupled clipper circuit[1] utilizes the simple differential amplifier circuit. Small signals at the grid give linear performance but large signals produce clipping. The schematic is shown in Fig. 2.3 (c), with the clipping action analysed on Graph 2.2

---

1. L.A. Goldmuntz, A Cathode-Coupled Clipper Circuit, Proc. I R E, Vol. 36, pp. 1172, September, 1948.

Due to the fact that the load of T_2 is relatively large (470K) compared with the load of T_1 (4.7K), it may be legitimate to assume that, away from cut-off conditions, the current in R_k is determined solely by the current through T_1. This assumption is not valid at cut-off conditions of T_1 because then the current through T_2 is of comparable magnitude with that of T_1.

The basic operation of this circuit is as follows:

As the grid of T_1 swings positive, more current passes through T_1 and a larger drop is experienced across R_k. Since the grid of T_2 is tied to ground, a larger drop across R_k produces cut-off conditions on T_2. Similarly, as the grid voltage of T_1 swings negatively, cut-off occurs on T_1, which decreases the biasing potential of T_2. Then T_2 conducts heavily, dropping the output voltage.

In the above outline, one important item was neglected; namely, that, as the voltage through R_k changes, not only will it affect the grid voltage of T_2, but it will also modify that of T_1. T_1 must be treated as a cathode-follower, therefore, a relation must be found between ib_1 and e_c, where e_c is the grid to cathode voltage of T_1. Having this information, another relation can be drawn between e_s and e_k. Once e_k is known, the output of T_2 can be readily determined.

For a graphical analysis, it is first necessary to plot the load lines of each half of the 6J6 vacuum tube on the average plate characteristics. The plate voltage is 225 volts. The load line of T_1 intersects the ordinate at

$$i_b = \frac{225}{4,700} = 48.0 \text{ ma}$$

and that of T_2 at

$$i_b = \frac{225}{470,000} = 0.48 \text{ ma}$$

It is immaterial whether R_k is included in the load of T_2 because it is relatively small compared to R_L. The grid bias line is also drawn:

$$e_k = -i_b R_k = -4,700\ i_b$$

THIS MARGIN RESERVED FOR BINDING.

IF SHEET IS READ THIS WAY (HORIZONTALLY), THIS MUST BE TOP.

IF SHEET IS READ THE OTHER WAY (VERTICALLY), THIS MUST BE LEFT-HAND SIDE.

GRAPH 2.2 GRAPHICAL ANALYSIS OF THE CATHODE-COUPLED CLIPPER

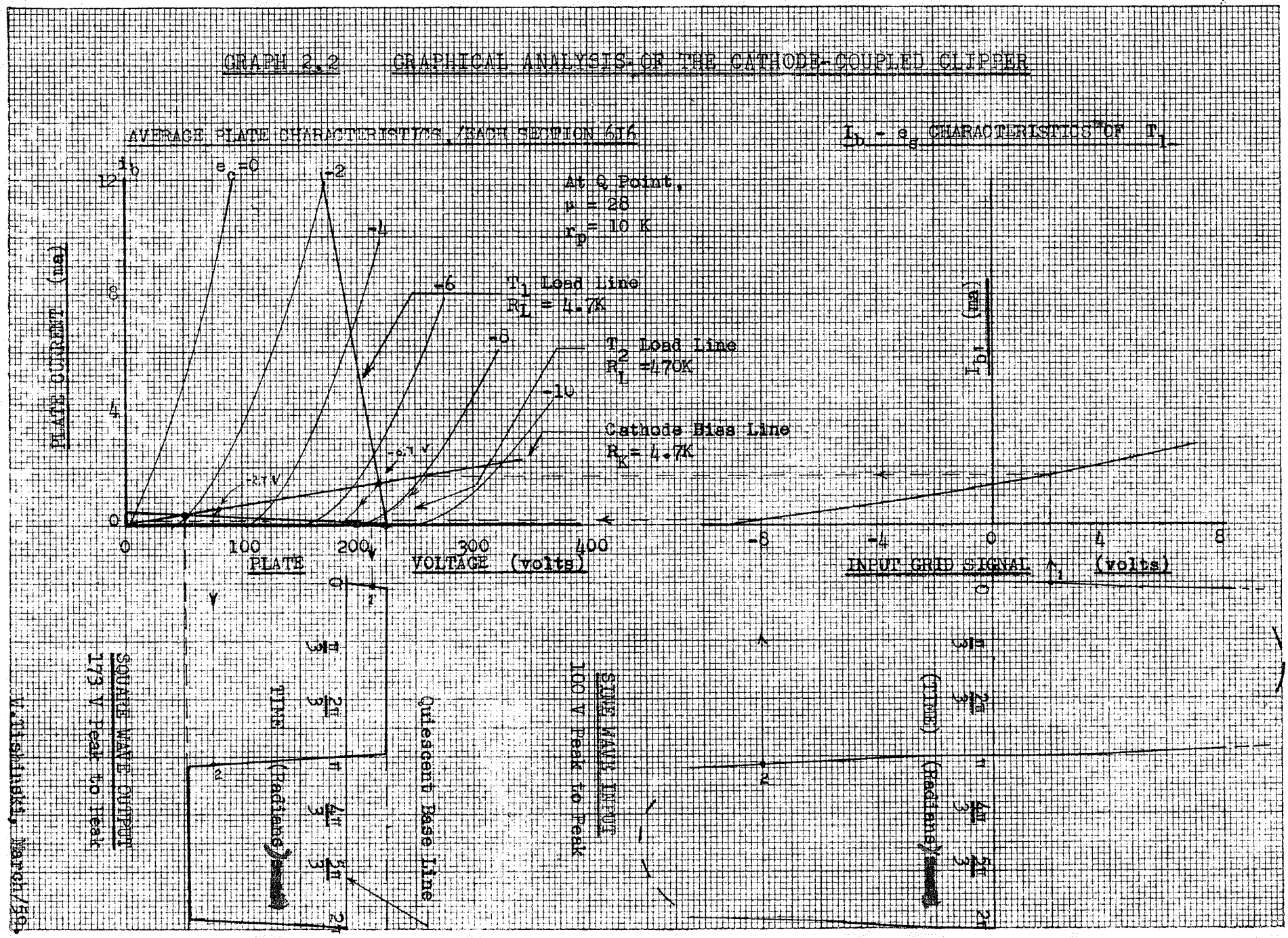

MANUFACTURED BY REHOUF PUBLISHING CO. MONTREAL

FORM 100

Now a signal applied to the grid of T_1 can be expressed as[1]:

$$e_s = e_c + e_k = e_c + i_{b1}R_k$$

Choosing appropriate values of i_{b1} along the T_1 load line, at specified values of e_c, e_k can be calculated. Then by simple addition e_s is obtained, giving the relation between e_s and i_{b1}. The following are actual points located on the graph:

e_c(volts)	i_{b1} (ma)	E_k (volts)	e_s (volts)
- 4.0	6.30	29.6	+ 25.6
- 6.0	2.30	10.8	+ 4.8
- 8.0	0.48	2.3	- 5.7
- 8.8	0	0	- 8.8

It must be pointed out now that the last two values of e_k are not exact, error becoming more pronounced as cut-off is approached. This is because i_{b1} was assumed to be the only current through R_k. However, this is not strictly true, since i_{b2} will continue to flow even though T_1 is cut off. e_s is not affected to any large extent and the error will be rectified as described in the following paragraph.

Below the i_b - e_s characteristics is shown a sine wave input, with a peak value of 50 volts, applied to the grid of T_1. Only the base portion need be shown since the upper part produces cut-off.

Point 1 on the signal input is at a 2-volt potential and approximately at a 2-degree displacement on the time base. At this potential, the i_b - e_s characteristics show that a cathode current of 1.7 ma flows. The cathode bias line shows that a bias of -8.2 volts exists on the grid of T_2. Locating this bias on the T_2 load line indicates a plate voltage of 212 volts. A corresponding point 1 is placed on the plate voltage curve at the same time displacement of 2 degrees. It should be noted now that i_{b2} was very small and i_b, for all practical purposes, was equal to i_{b1}.

---

1. T.S. Gray, Applied Electronics, pp. 430. J. Wiley and Sons, 1954.

IF SHEET IS READ THE OTHER WAY (VERTICALLY), THIS MUST BE LEFT-HAND SIDE.

GRAPH 2.3 THEORETICAL AND ACTUAL CLIPPER OUTPUT WAVESHAPES

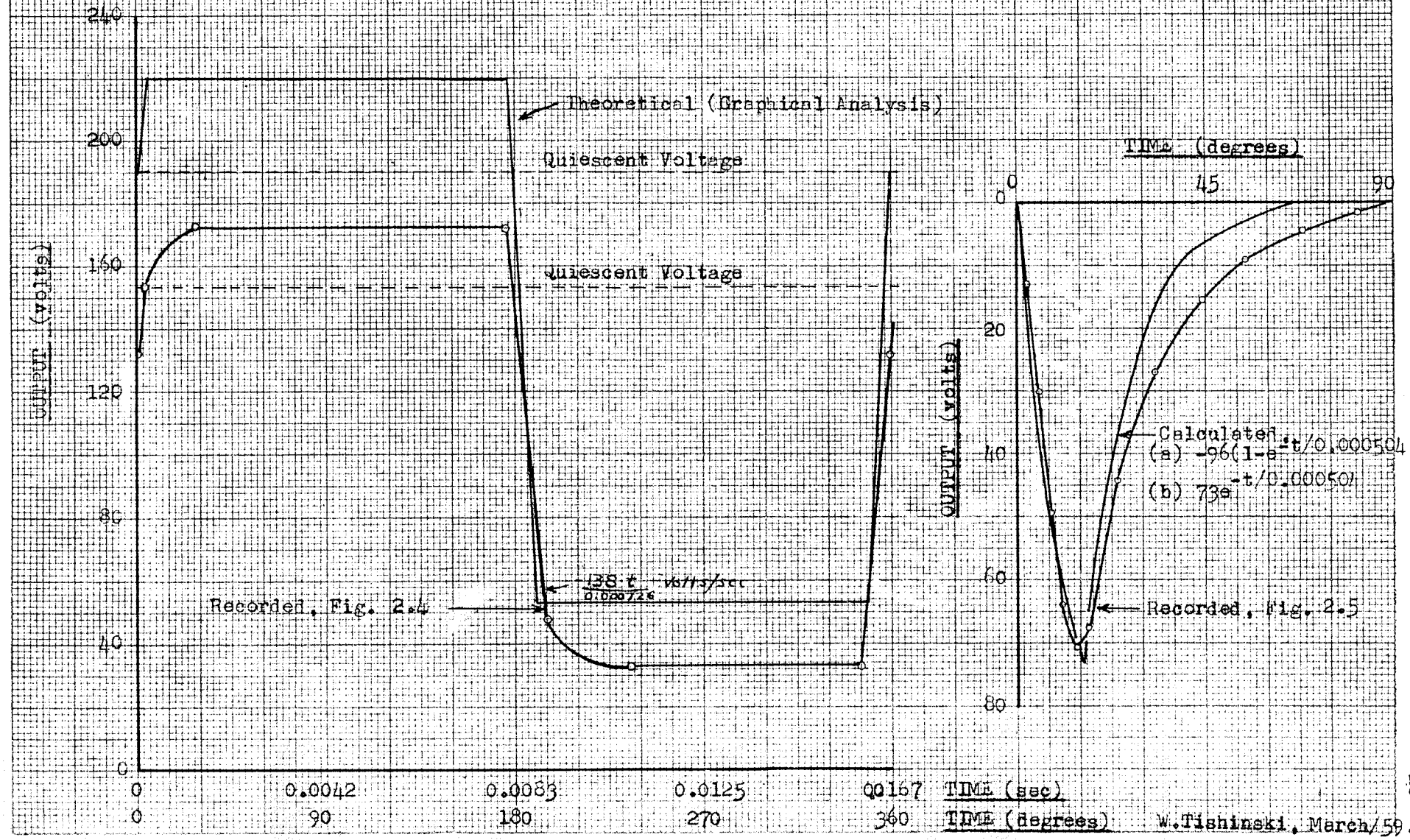

MANUFACTURED BY RENOUF PUBLISHING CO., MONTREAL FORM 100

W. Tishinski, March/59.

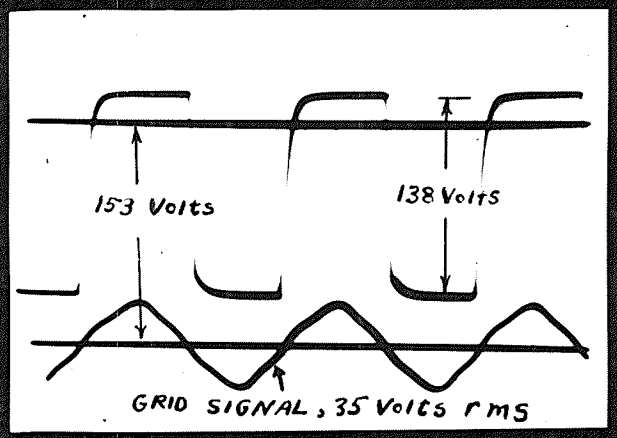

FIG. 2.4 CATHODE-COUPLED CLIPPER OUTPUT AND GRID SIGNAL INPUT

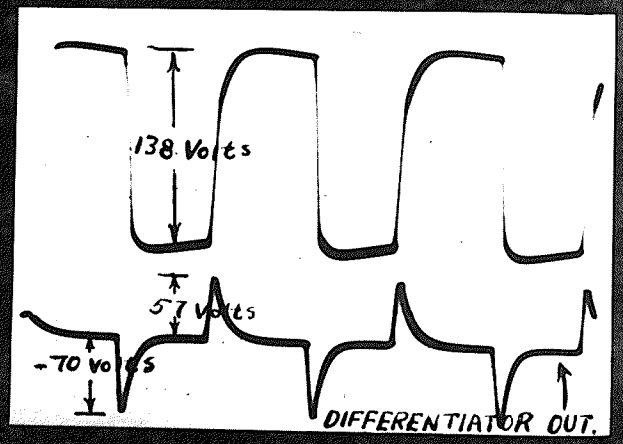

FIG. 2.5 CLIPPER OUTPUT AND DIFFERENTIATED SIGNAL

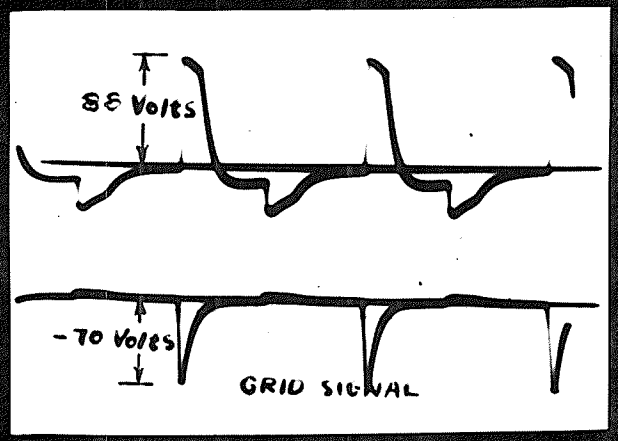

FIG. 2.6 POWER AMPLIFIER OUTPUT AND GRID SIGNAL INPUT

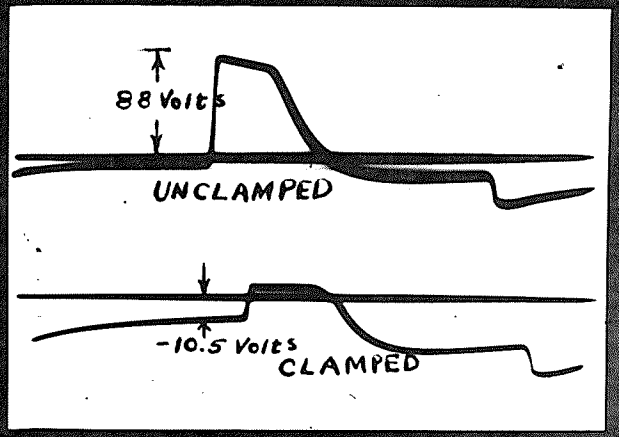

FIG. 2.7 CLAMPED AND UNCLAMPED TRIGGERING WAVES FOR THYRATRON

Plate voltage cannot rise above 225 volts, hence the output will stay at this value until the input signal starts on its downward trend.

Selecting a point 2, on the input signal, shows that a T_1 current of 0.20 ma flows at this instant. Projecting to the cathode bias line, e_k appears to be approximately -0.8 volts. However, at this bias i_{b2} is approximately 0.40 ma giving a total i_b of 0.60 ma. This makes $e_k = -2.7$ volts, and the plate voltage as determined from the T_2 load line, at this grid bias voltage, is 75 volts, which locates a corresponding point 2 on the output wave.

Under no condition can the plate voltage drop below 52 volts, since this is the intersection point of the T_2 load line and the cathode bias line.

Graph 2.3(a) shows the measured and theoretical wave shapes from the output of the cathode-coupled clipper. The theoretical peak to peak value of 173 volts compares with the actual 138 volts as recorded in Fig. 2.4. The discrepancy can be attributed to:

(1) Errors in measurement by the Cossor oscilloscope.

(2) The differences in the existing average plate characteristics and the theoretical as obtained from the tube manual.

The grid bias voltage of T_1 at quiescent conditions as noted on the graph, was -6.7 volts, while the measured quiescent bias voltage of the same tube was -9.5 volts.

As was mentioned previously, a signal with a leading vertical edge would be used to trigger the thyratron. This vertical edge is present in the square wave just obtained, but the wave possesses insufficient power capacity. The peak to peak value of the output current from the clipper is approximately 0.40 ma. Furthermore, the output impedance as determined analytically[1] is rather high:

$$Z_o = r_p + (u + 1)\, R_K // R_L$$

$$= \frac{[10K + (28 + 1)\, 4.7K] \times 470K}{10K + (28 + 1)\, 4.7K + 470K} = 112K$$

2.4 Power Amplification of the "Spiked"-Wave

The power output can be increased by adding a resistance-capacitance coupled power amplifier to the clipper circuit, Fig. 2.3(c). a Beam Power 6V6-GT tube was selected to perform the amplification.

---

1. J. Millman and H. Taub, Pulse and Digital Circuits, p. 8, McGraw-Hill, 1956.

Since a pentode has a relatively high plate resistance, the output impedance would be governed solely by the load resistance, if it was much smaller than r_p. However, when the screan grid is tied to the plate, the tube essentially becomes a triode with a low plate resistance, but it still maintains a high power output. The 1K resistor is inserted between the plate and screen in order to limit any large currents through the screen. Average plate characteristics were determined by test, and are drawn on Graph 24.

The R-C coupling between the clipper circuit and the power amplifier constitutes a differentiating circuit. It is necessary to determine what wave shape is fed to the grid of the power amplifier. Only the negative signal applied to the amplifier grid is of interest here, since it will produce a positive "spike" at the output. The negative signal will be produced by the dropping edge of the clipper output which has the equation:

$$\frac{-138.t}{0.000726} \quad \text{volts/sec}$$

The grid signal will be calculated and compared with the actual recorded wave.

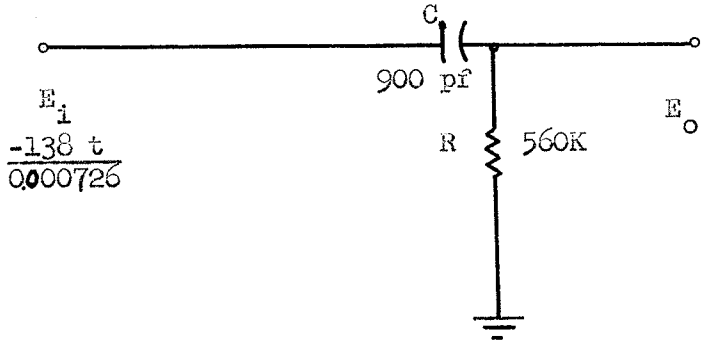

Fig. 2.8 Differentiating Circuit for an R-C-Coupled Amplifier

Applying Laplace transforms the transfer function is

$$\frac{E_o(s)}{E_i(s)} = \frac{s}{s + 1/RC}$$

Substituting for $E_i(s)$

$$E_o(s) = \frac{-138}{0.000726\ s(s + 1/RC)}$$

MANUFACTURED BY. REKOUF PUBLISHING CO., MONTREAL

FORM 100

IF SHEET IS READ THE OTHER WAY (VERTICALLY), THIS MUST BE LEFT-HAND SIDE.

GRAPH 2-4

GRAPHICAL ANALYSIS OF POWER AMPLIFIER PRODUCING THYRATRON TRIGGERING WAVE

AVERAGE PLATE CHARACTERISTICS FOR 6V6-GT *

TRIODE CONNECTION

$i_b - e_s$ CHARACTERISTICS

At Q Point, $\mu = 11$, $r_p = 3$ K

Load Line $R_L = 4.15$K

Cathode Bias Line $R = 150$ Ω

PLATE CURRENT (ma)

PLATE VOLTAGE (volts)

GRID INPUT (volts)

PEAKED-WAVE INPUT

TIME (degrees)

POWER-AMPLIFIED PEAKED-WAVE OUTPUT

W. Tichinicki, March/59.

Expanding by partial fractions

$$E_o(s) = \frac{-138}{0.000726}\left(\frac{RC}{s} - \frac{RC}{s + 1/RC}\right)$$

By taking the inverse Laplace transform

$$e_o(t) = \frac{-138}{0.000726} RC\,(1 - e^{-t/RC})$$

$$= -96\,(1 - e^{-t/0.000504})$$

This equation applies only for the period $0 \geqq t \geqq 0.000726$ sec.

At time $t = 0.000726$

$e_o(t) = -73.0$ volts, which compares favorably with the oscillogram tracing, Graph 3 (b).

During the horizontal portion of the clipper output, the capacitor discharges through the 560K resistor and the voltage decays according to the formula,

$$-E_o\, e^{-t/RC}$$

where $E_o = -73.0$ volts

Since the power amplifier tube is driven to cut-off conditions, a graphical analysis is the most direct method of solution. A cathode-follower action occurs with this amplifier, just as it did with the cathode-coupled clipper. As before, the input signal is composed of the grid signal and the drop across the biasing resistor,

$$e_s = e_c + e_k$$

where $e_k = i_b \times 150$

The $i_b - e_s$ characteristics must be determined as before,

e_c (volts)	i_b (ma)	e_k (volts)	e_s (volts)
- 3.00	25.0	3.75	+ 0.75
- 6.00	20.3	3.02	- 2.98
- 9.00	16.3	2.44	- 6.55
- 12.00	12.7	1.90	-10.10
- 15.00	8.6	1.30	-13.70
- 22.00	3.2	0.48	-21.52

The shape and magnitude of the output wave as determined graphically, is similar to the recorded wave, Fig. 2.6, as can be seen from Graph 2.3(b).

With the quiescent current being 23.5 ma in the power amplifier, a sufficient amount of power should be available to trigger the thyratron. The output impedance will also be relatively low. It is found to be[1]

$$Z_o = \frac{[3K + (11 + 1)\ 150] \times 4K}{3K + (11 + 1)\ 150 + 4K} = 2.2K$$

2.5 Coupling the "Spike"-Generating Circuit to the Thyratron Grid

The "spiked"-wave output from the power amplifier is superimposed on a positive d-c component which is blocked out by the 1.0μf capacitor. The triggering wave is then coupled to the thyratron grid through a grid protecting resistor R_3, Fig. 2.9. R_3 has two purposes:

(1) To limit the grid current before and after the tube conducts.

(2) To discharge from the grid capacitor any voltage accumulated on it because of surges in the anode circuit.

To perform the first function the resistor should be large, but to perform the latter it should be small. Therefore, the selection is a compromise.

The grid capacitor is used mainly to prevent the tube from "shocking-over" or conducting if voltage is suddenly applied to the anode circuit.[2] A 100 pf capacitor was found to function satisfactorily.

As mentioned previously, the grid must be held at a negative bias, preferably double the critical grid voltage. The triggering pulse is superimposed on this bias and must be of sufficient height to intersect the critical grid voltage locus. For the particular case considered it was found that an additional biasing element, such as a battery, was not necessary. This was due to the clamping action of the grid.

When the thyratron heaters are switched off, no conduction of current takes place from grid to cathode on a positive pulse. However, as the filaments heat up, conduction commences, thus clamping occurs.

---

1. Ibid., p. 8.
2. H.J. Bichsel, Circuits for Industrial Control, Westinghouse Industrial Electronics Reference Book, p. 280, J. Wiley and Sons, 1948.

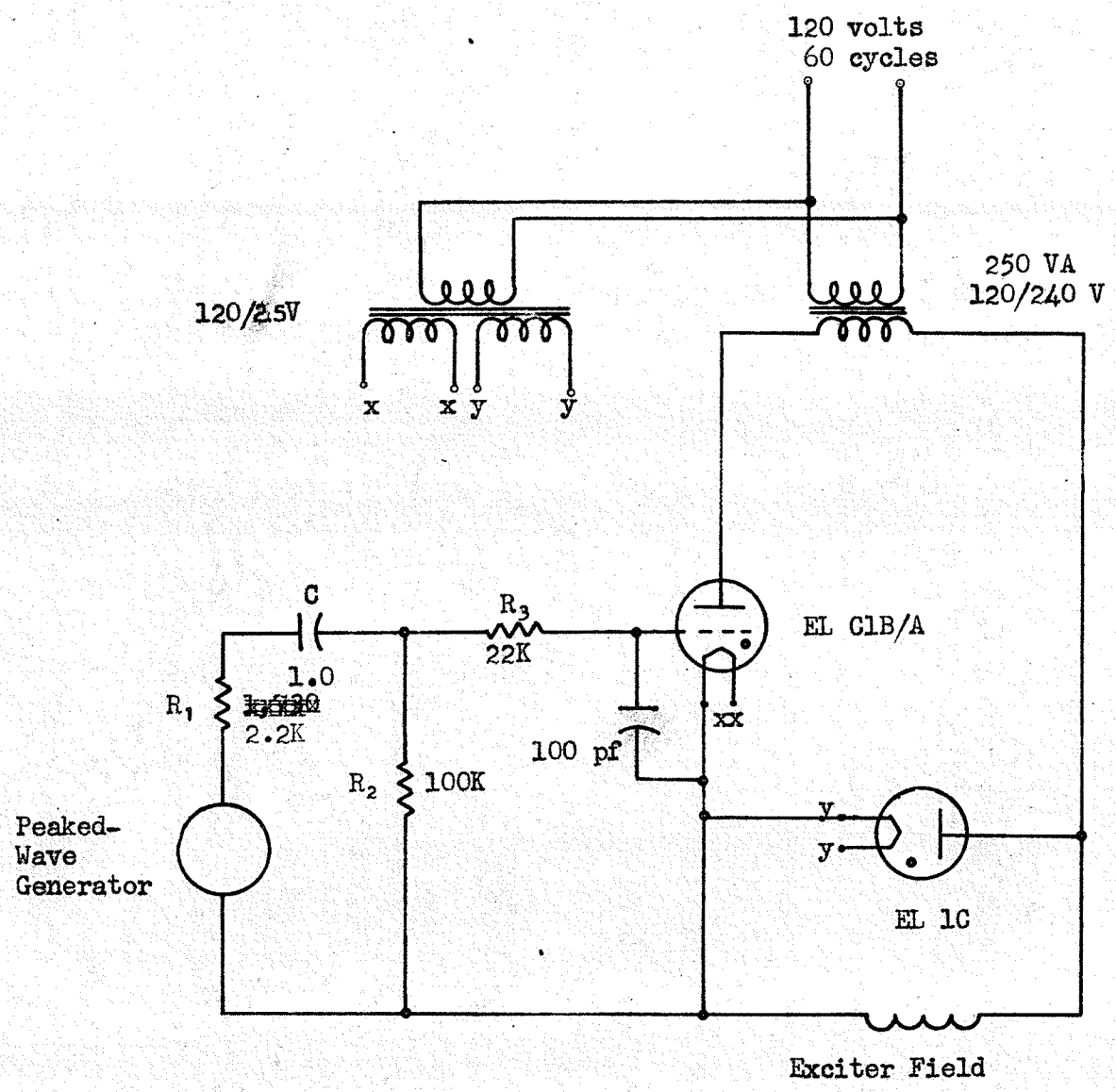

FIG. 2.9 COUPLING "SPIKED"-WAVE TO THE THYRATRON

A clamping process simply raises or lowers a varying wave above or below a reference line. Fig. 2.7 shows the grid wave prior to the clamping effect. It is noted that the wave has centered itself about a reference line over a period of one cycle, that is, the positive area equals the negative area. Conduction occurs only from grid to cathode, but not in the reverse direction. On the positive swing of the triggering wave the voltage distribution is determined solely by the resistance values, since a capacitor acts as a short circuit during sudden changes. During the horizontal portion of the triggering wave, the input voltage decays with a time constant,

$$T_1 = (R_3^1 + R_1)\, C = 0.0267 \text{ sec}$$

where R_3^1 = 22K + grid-cathode resistance (several thousand ohms)

R_1 = generator output impedance, 1730 ohms

C = 1.0 μf

R_2 is neglected since it is much larger than R_3^1.

At the edge of the horizontal portion the wave begins its downward trend. If the initial jump had been E volts and if the ~~down fall~~ drop had also been a vertical edge of E volts, then the resulting falling edge would have ended up below the reference line. This is due to the decay~~ing~~ process, which took place during the horizontal portion of the triggering wave. The above explanation has been based on a vertical falling edge, and although no such edge exists in the actual wave, the assumption facilitates the explanation.

When the input wave swings below the reference line, grid to cathode conduction ceases, and the wave decays with a time constant,

$$T_2 = (R_1 + R_2)\, C = 0.101 \text{ sec}$$

where R_2 = 100K

R_3 is no longer in the circuit, since this loop has been broken by the high grid-cathode impedance offered in the reverse direction. While the input wave is below the reference line the decaying process takes place with a time constant of 0.101 sec. Thus, on the positive swing, the voltage decays more rapidly, with T_1 = 0.0267 sec, than on the negative portion, with T_2 = 0.101 sec. The net effect is that the whole wave will shift downward with respect to the reference axis. Fig. 2.7 illustrates the actual clamped-wave experienced.

The positive portion of the triggering wave is no longer as high as it was on open-circuit, because of the drops across R_1 and R_3.

A high degree of clamping[1] is obtained if

$(R_1 + R_2)C$ is large

$(R_1 + R_3^1)$ is small

On examining the above conditions, it is seen that the clamping action is best when R_2 is high and R_1 and R_3^1 are small.

During the test work it was found that with R_3 = 1.5K, the negative bias on the clamped wave was -15.0 volts, while, with R_3 = 22K, the bias was reduced to -10.5 volts, thus verifying one of the above regulations.

The triggering wave, Fig. 2.6, is not a true "spiked"-wave, but it was so termed due to lack of a more appropriate word to describe the non-uniform shape. This is permissible, since the rising vertical edge, which is the part of interest, is common to both a "spiked"-wave, and to the actual wave obtained.

2.6 The Amplification of the Forward Control and Controlled Elements

The circuit thus far developed has provided a means of varying the field current in the exciter by varying the phase shift of the triggering pulse, which in turn was controlled by the d-c current in the saturable reactor and the average voltage of the thyratron as impressed on the exciter field.

A test was conducted to determine the above relation and simultaneously the relation between the control current and the firing angle. The obtained data were plotted on Graph 2.5. Two methods are now available for evaluating the average d-c voltage impressed on the exciter field:

(1) By the IR relation,

where I = exciter field current

R = exciter field resistance; 165 ohms at 23°C

(2) By the equation

$$E_{dc} = \frac{E_M}{2\pi}(1 + \cos\beta)$$

---

1. S. Seely, Electronic Engineering, pp. 207, McGraw-Hill, 1956.

THIS MARGIN RESERVED FOR BINDING.

IF SHEET IS READ THE OTHER WAY (VERTICALLY), THIS MUST BE LEFT-HAND SIDE.

GRAPH 2.5 EFFECT OF SATURABLE REACTOR CONTROL CURRENT ON THE EXCITER FIELD CURRENT AND THYRATRON FIRING ANGLE

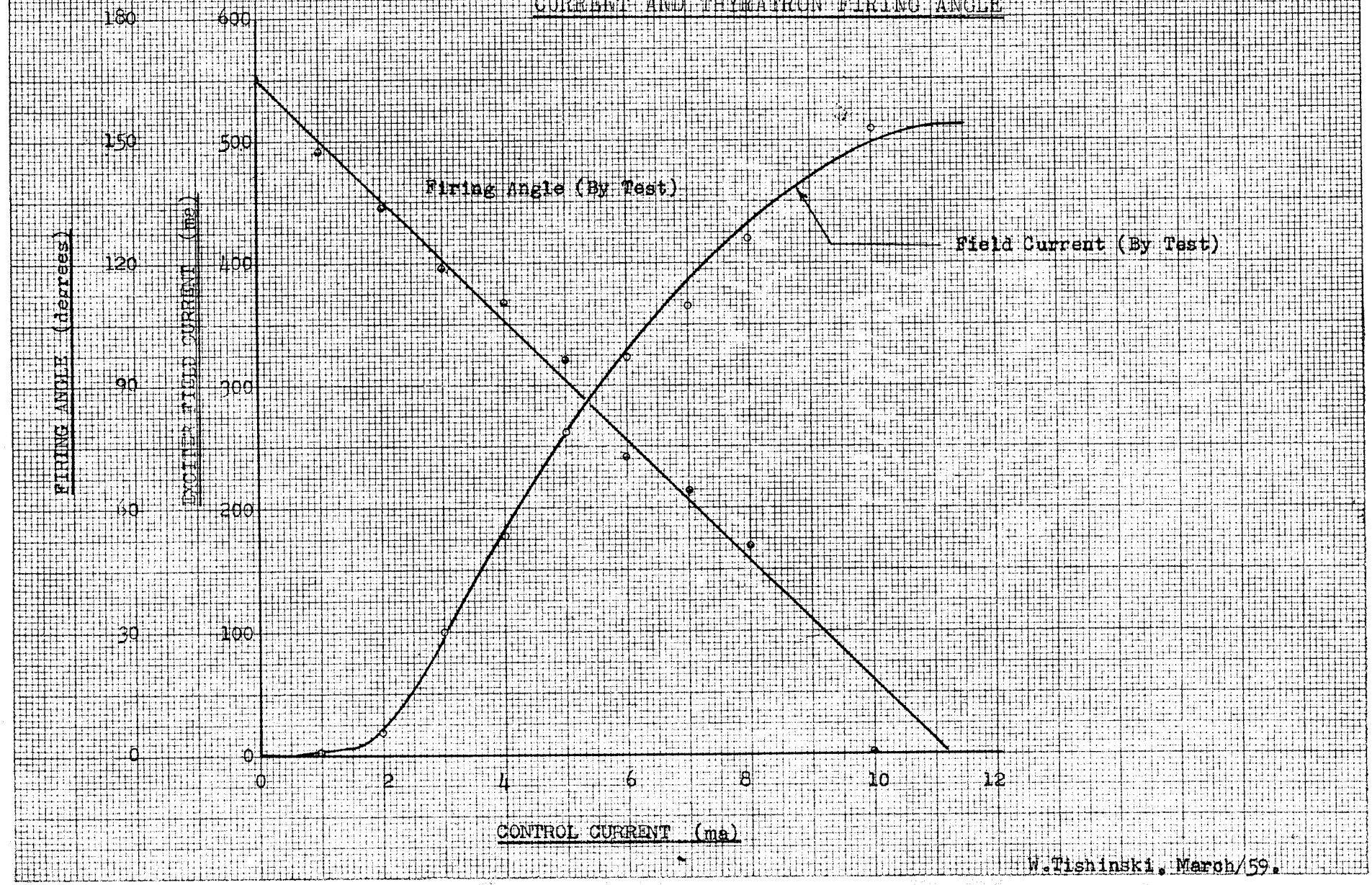

W.Tishinski, March/59.

MANUFACTURED BY RENOUF PUBLISHING CO., MONTREAL

FORM 100

26

The angle β will be selected for increments of 1 ma control current from Graph25. Tube drop must now be considered and if taken as 10 volts, the remaining $2^{o}30'$ ($\sin^{-1}$ 10/340) of the sine wave will not contribute any d-c voltage. This amount is negligible and will not enter the calculations, but the decrease in E_M will be considered.

A sample calculation is shown for $\beta = 119^{o}$,

$$E_{dc} = \frac{(340 - 10)}{2\pi} (1 + \cos 119^{o}) = 18.8 \text{ volts}$$

A plot of the curves, as determined by the above two methods, is shown on Graph26. The curve evaluated by the IR relation, would be the more precise of the two curves since no assumptions were made in its evaluation. For the curve determined from the above equation, utilizing the firing angle as the variable, an assumption was made in that the inductance was assumed constant for all magnitudes of current; hence, a constant rate of decay through the back-rectifier. The assumption is not valid due to the reason indicated in Appendix C.

The amplification K_s, which is the increase in the average exciter field voltage per ma of control current can now be evaluated from Graph26.

$$K_s = \frac{39.0}{3.6} = 10.8 \text{ volts/ma}$$

The next step in the design procedure is to devise a scheme which will enable the actuating error voltage to control the saturable reactor d-c current. A vacuum tube fulfills this requirement quite capably, with the control winding in the load circuit and the actuating error applied to the grid[1], Fig. 2.10 (a). This vacuum tube should have the following properties:

(1) A high gain ~~(m)~~ (g_m).

(2) A normal current-carrying capacity of at least 15 ma.

(3) A high plate resistance. This is in order to increase the transient response.[2]

(4) ~~Possess~~ Linear transfer characteristics. This will help to decrease the steady-state error as well as facilitate the theoretical analysis.[3]

---

1. H.J. Bichsel, Circuits for Industrial Control, Westinghouse Industrial Electronics Reference Book, pp. 284, J.Wiley and Sons, 1948.
2. See p. 36 of thesis.
3. See p. 31 and p. 130 of thesis.

MANUFACTURED BY RENOUF PUBLISHING CO., MONTREAL

THIS DRAWING IS RESERVED FOR DIMENSIONS.
IF SHEET IS READ THE OTHER WAY (VERTICALLY), THIS MUST BE LEFT-HAND SIDE.

GRAPH 2.6 RELATION BETWEEN SATURABLE REACTOR CONTROL CURRENT AND EXCITER FIELD VOLTAGE

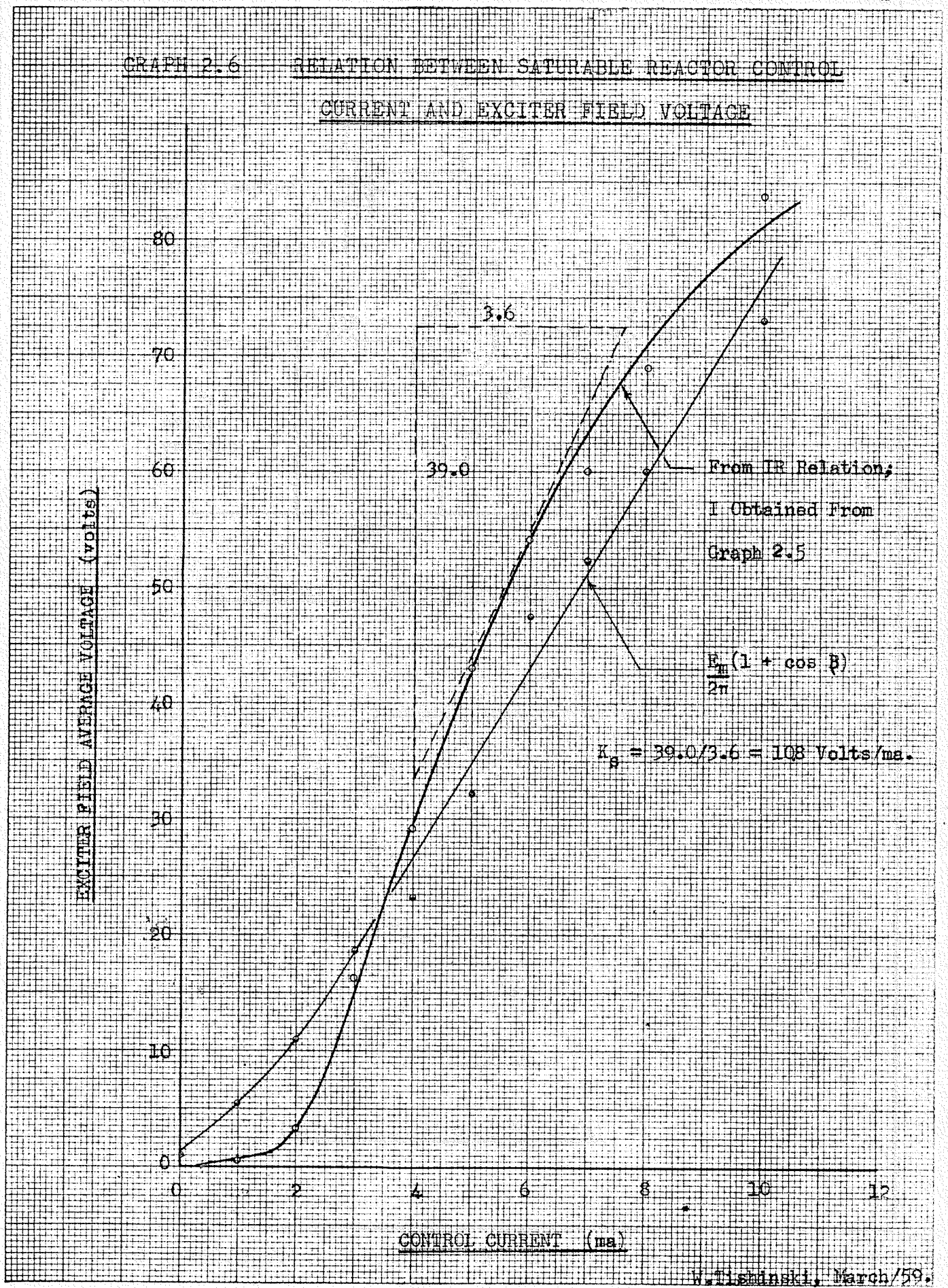

W.Tishinski, March/59.

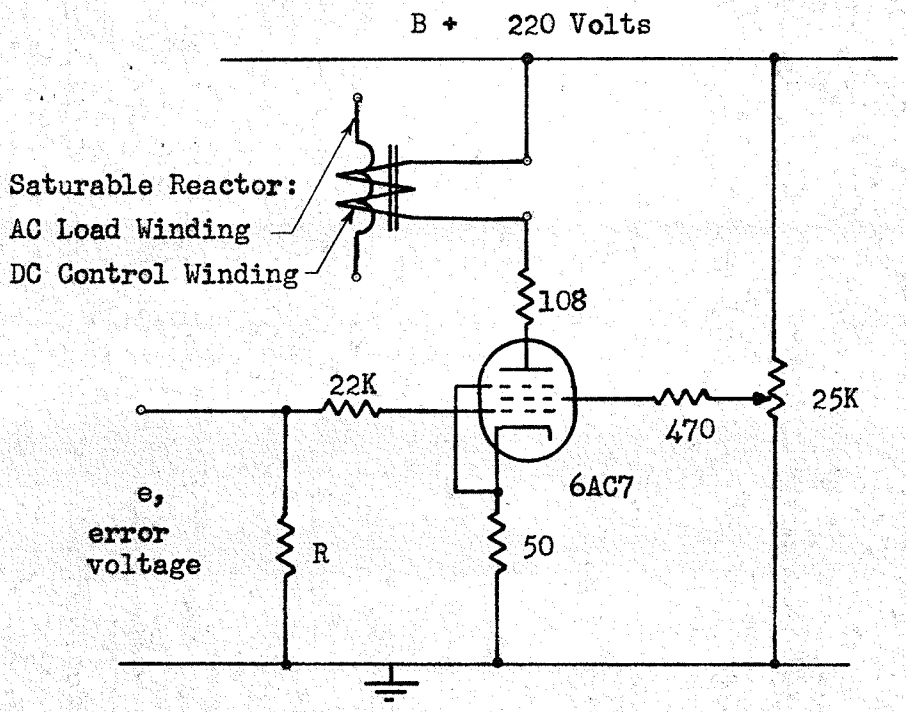

(a) SCHEMATIC OF ERROR-AMPLIFYING CIRCUIT

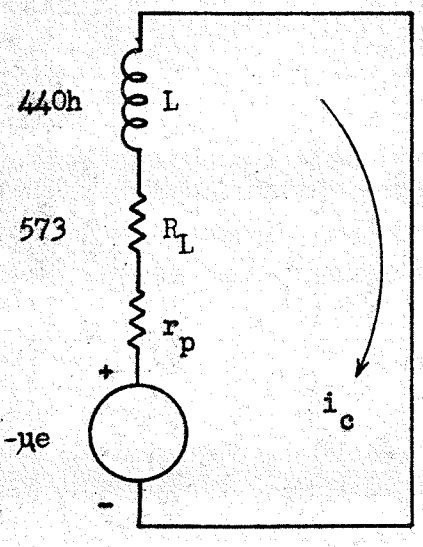

(b) EQUIVALENT CIRCUIT OF (a)

FIG. 2.10 ERROR-VOLTAGE CONTROL OF SATURABLE REACTOR DC CURRENT

The tube which met the given specifications was a 6AC7 sharp cut-off pentode. It is noted that this tube may be used as an oscillator in low-frequency applications. Thus, this property could produce local sustained oscillations. If the actuating error was a pure d-c potential with no ripple signal, no such oscillations could be feared. However, if the ripple is of sufficient magnitude, the tube could start to oscillate.

It might now be advantageous to comment on this oscillation phenomenon as it occurred with the actual completed circuit. Sustained oscillations were experienced whenever the settings of the regulator were such that a large ripple from the exciter was fed back to the grid. Readjusting the settings to attenuate the exciter ripple was not the solution here, since this action introduced other undesirable effects. Nevertheless, these oscillations were damped by inserting small resistors in the load circuit, a 105-ohm resistor close to the plate and a 48-ohm resistor close to the cathode. An original attempt of placing only a 15-ohm resistor in the plate circuit was unsuccessful in damping these oscillations. A 470-ohm resistor was inserted in the screen circuit for the same purpose.

Tests were conducted on the 6AC7 pentode to determine its dynamic transfer characteristics at constant plate voltage, with screen voltage as a parameter. The obtained data were plotted on Graph 27.

The curve with a screen voltage of 124 volts gives a lengthy linear portion of operation and this would be the most desirable setting. The amplification K_p provided by this pentode is

$$K_p = \frac{7.3}{2.7} = 2.7 \text{ ma/volts}$$

This amplification coupled with the previously determined amplification K_s, gives an over-all amplification of

$$K_a = K_p K_s$$

or $$K_a = 2.7 \text{ ma/volt} \times 10.8 \text{ volts/ma}$$

$$= 29.2 \text{ volts/volt}$$

Therefore, an actuating error of 1 volt will provide 29.2 volts at the exciter field.

MANUFACTURED BY RENOUF PUBLISHING CO., MONTREAL FORM 100

IF SHEET IS READ THE OTHER WAY (VERTICALLY), THIS MUST BE LEFT-HAND SIDE.

GRAPH 2.7 DYNAMIC TRANSFER CHARACTERISTICS OF 6AC7 PENTODE WITH CONTROL WINDING OF SATURABLE REACTOR AS LOAD E_{bb}=220Volts

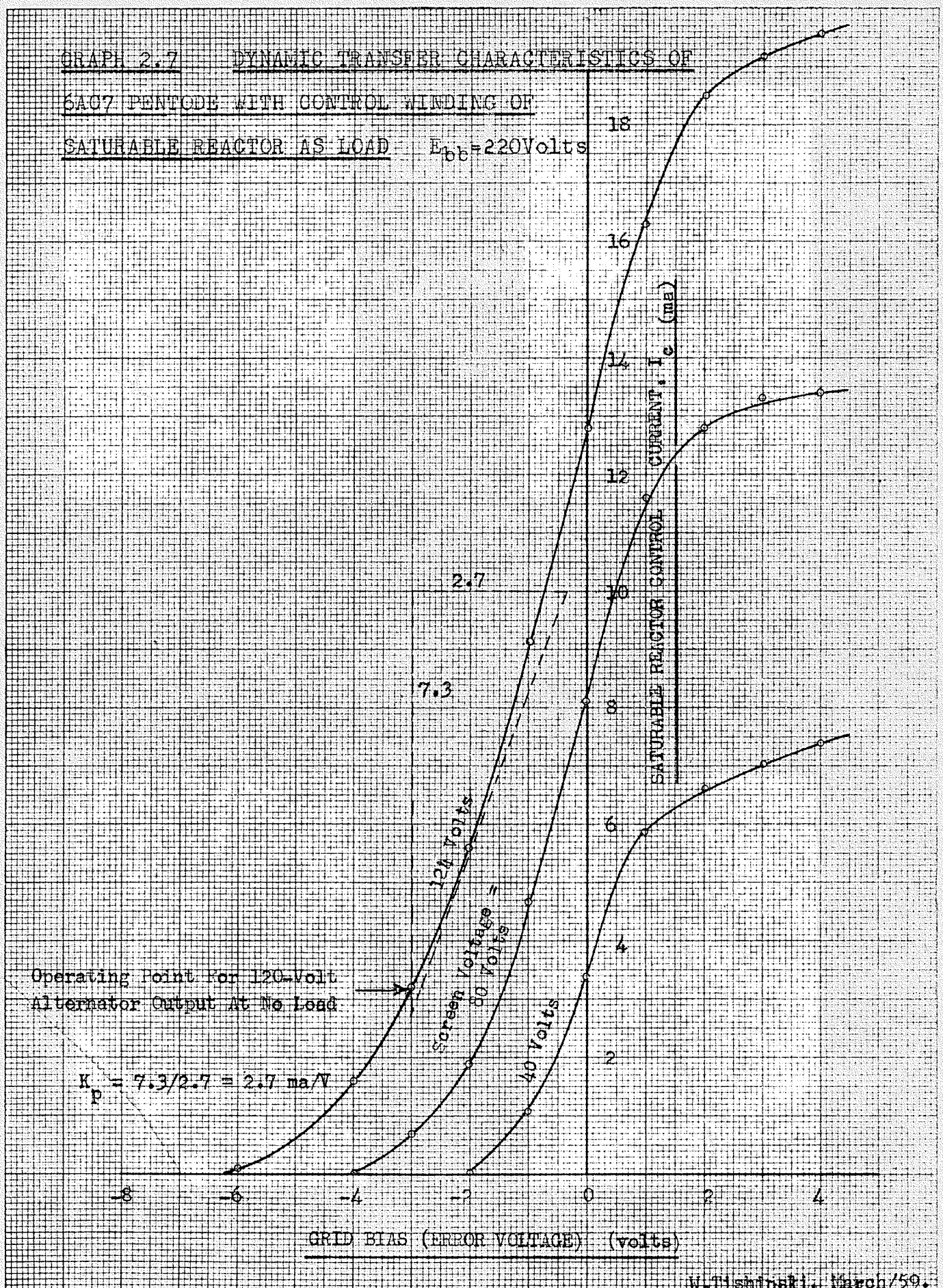

W.Tishinski, March/59.

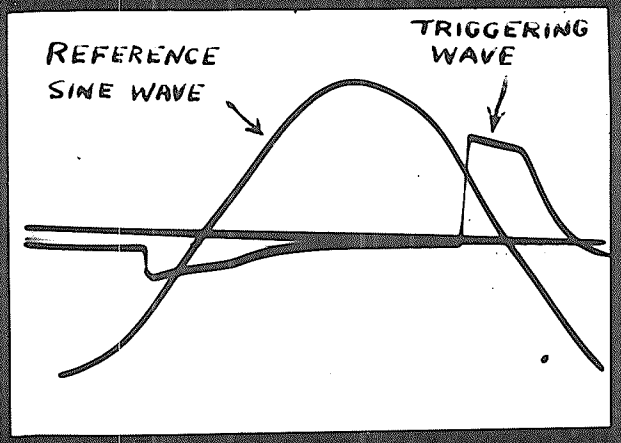

FIG. 2.11 MAXIMUM PHASE SHIFT POSSIBLE

I_c = 0 ma

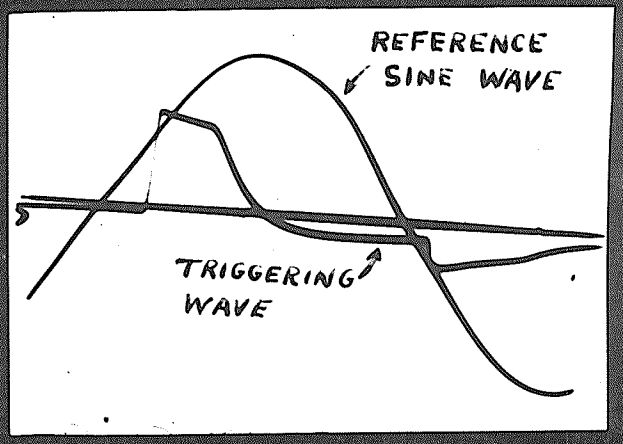

FIG. 2.12 MINIMUM PHASE SHIFT POSSIBLE

I_c = 13.0 ma

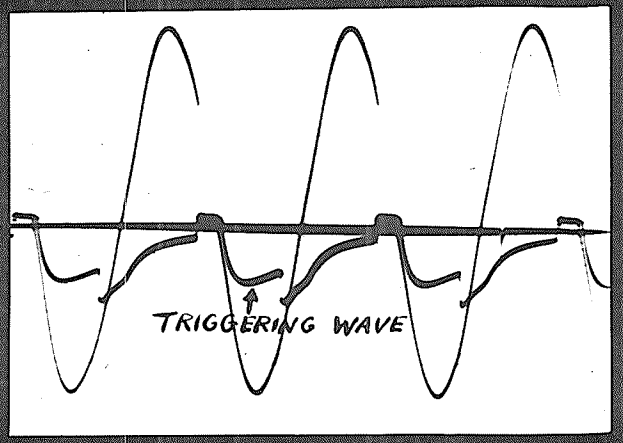

FIG. 2.13 VOLTAGE ACROSS THYRATRON FOR SMALL FIELD CURRENT

I_c = 1.5 ma β = 140° I_L = 10 ma

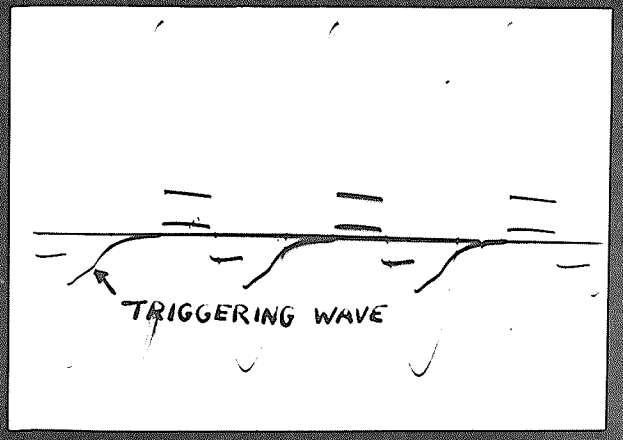

FIG. 2.14 VOLTAGE ACROSS THYRATRON FOR LARGE FIELD CURRENT

I_c = 5.0 ma β = 97° I_L = 262 ma

Figs. 2.11 and 2.12 illustrate the phase-shifting properties of the saturable reactor and of the associated wave-forming circuit. Figs. 2.13 and 2.14 show the action of the controlled rectifier on the voltage applied to the exciter field.

2.7 The Transfer Function of the Forward Elements

In all practical systems non-linearities exist in varying degrees. For a preliminary study all elements will be considered as linear. For a more precise analysis the elements departing largely from linear performance must be treated separately. This will be done later.

If a servomechanism system is already completed, it is possible to determine the transfer characteristics by means of a frequency response test. This fundamentally consists of injecting a sine wave into the circuit and comparing the phase angle and magnitude of the output with that of the input. Such a scheme would undoubtedly provide an interesting study, but since all the necessary equipment was not readily available, it is questionable whether the results obtained would warrant the time invested in preparing the test arrangement.

Nevertheless, the transfer function can be obtained analytically by determining the constants of the forward control elements. By inspection of Figs. 2.1 and 2.3, it can be seen that there are three time constants involved in the forward control elements:

(1) Time constant of the alternator field.

(2) Time constant of the exciter field.

(3) Time constant of the saturable reactor control windings.

The self-inductances of the exciter and alternator fields are found in Appendix B.2. The resistances associated with the fields will be taken as the values at room temperature ($23^{\circ}C$) rather than the corrected values to $75^{\circ}C$, because smaller resistances present larger time constants. Larger time constants invite instability, hence, the most critical cases must be treated.

Appendix D presents data on the control winding of the saturable reactor.

Referring to Fig. 2.1(a), the instantaneous loop equations can be written as

$$e_o(t) = R_f i_f + L_f \frac{di_f}{dt}$$

$$e_e = K_v i_f$$

$$e_e(t) = (R_g + R_a)\, i_g + L_a \frac{di_g}{dt} + L_g \frac{di_g}{dt}$$

$$E_g = K_g\, i_g$$

Where e_o = Average voltage impressed on the exciter field (provided by the controlled rectifier).

i_f = Exciter field current.

L_f = Exciter field inductance.

R_f = Exciter field resistance.

e_e = Exciter generated voltage.

L_a = Exciter armature inductance.

R_a = Exciter armature resistance.

e_g = Alternator generated voltage.

L_g = Alternator field inductance.

R_g = Alternator field resistance.

Kv = Exciter generator constant, Graph B.3.

K_g = Alternator generator constant, Graph B.1.

All other machine constants are found in Appendix B.

Substituting numerical values for the constants, the above equations can be written as

$$e_o(t) = 165\, i_f + 19.0 \frac{di_f}{dt}$$

$$e_e = 280\, i_f$$

$$e_e(t) = 46.2\, i_g + 15.2 \frac{di_g}{dt}$$

$$e_g = 100\, i_g$$

The transfer function of any element is obtained by taking the Laplace transform of the differential equations and equating the initial conditions to zero.

The preceding equations can now be rewritten:

$$E_o(s) = (165 + 19.0\ s)\ I_f(s)$$

$$E_e(s) = 280\ I_f(s)$$

$$E_e(s) = (46.2 + 15.2\ s)\ I_g(s)$$

$$E_g(s) = 100\ I_g(s)$$

The transfer function of the exciter becomes:

$$\frac{E_e(s)}{E_o(s)} = \frac{280}{(165 + 19.0s)}$$

and that of the alternator,

$$\frac{E_g(s)}{E_e(s)} = \frac{100}{(46.2 + 15.2s)}$$

Rewriting the above equations in terms of time constants:

$$\frac{E_e(s)}{E_o(s)} = \frac{1.70}{(1 + 0.115s)}$$

and

$$\frac{E_g(s)}{E_e(s)} = \frac{2.22}{(1 + 0.338s)}$$

Negligible delays will be experienced with the cathode - coupled clipper and with the power amplifier, since vacuum tubes may be considered to act instantaneously when considering delays not less than a cycle of power frequency. However, a time delay will be caused by the saturable reactor. Hence, a transfer function must be determined between the error voltage and the d-c control current. A change in control current produces a simultaneous change in the phase shift, so the phase-shifting response is completely specified by the d-c control current. An average value of inductance as evaluated in Appendix D can be taken as 440 henries. Then by writing Kirchhoff's voltage law equations around the loop consisting of the error-amplifier and its load, Fig. 2.10 (b), the transfer function for this part of the circuit can be obtained.

$$\mu e = (r_p + R_L)\ i_c + L\ \frac{di_c}{dt}$$

where e = the error voltage applied to the grid of the 6AC7 vacuum tube.

r_p = plate resistance of the vacuum tube.

R_L = load resistance; consists of the control windings and the damping resistors.

L = inductance of the control windings.

i_c = control current.

By taking Laplace transforms,

$$\mu E(s) = (r_p + R_L + sL)\, I_c(s)$$

or
$$\frac{I_c(s)}{E(s)} = \frac{g_m \cdot r_p}{(r_p + R_L)(1 + Ts)}$$

where
$$T = \frac{L}{r_p + R_L}$$

now since $r_p \gg R_L$,

$$\frac{r_p}{r_p + R_L} \simeq 1$$

and
$$\frac{I_c(s)}{E(s)} = \frac{g_m}{(1 + Ts)}$$

Now g_m is defined as the change in plate current for a unit change in grid voltage. This is identical to the amplification factor, K_p, determined in section 2.6.

Therefore, $\frac{I_c(s)}{E(s)} = \frac{2.7}{(1 + Ts)}$

The next constant in question is r_p. From Graph 27, it can be seen that to maintain a terminal voltage of 120 volts, e will be approximately - 3.0 volts. The plate resistance for the 6AC7 tube at this bias is approximately 1 megohm, Graph 28, for which $T = \frac{440}{10^6} = 0.00044$ sec $\frac{\text{cycles}}{}$, or 0.0264 ~~cps~~. A record was made of the response of the a-c current in the saturable reactor when the grid voltage of the 6AC7

IF SHEET IS READ THE OTHER WAY (VERTICALLY), THIS MUST BE LEFT-HAND SIDE.

GRAPH 2.8 LOAD LINE OF ERROR-AMPLIFYING 6AC7 PENTODE

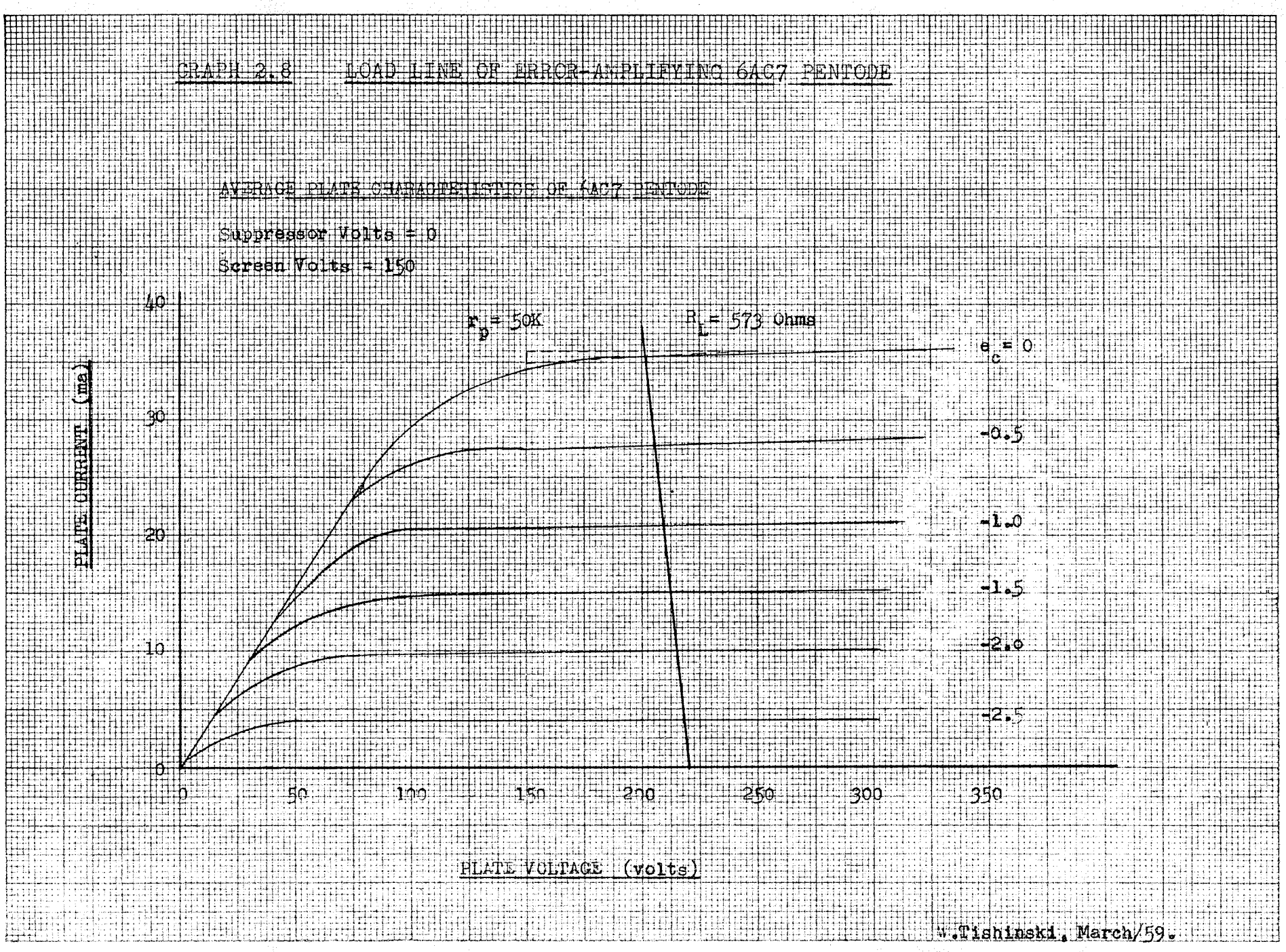

W.Tishinski, March/59.

MANUFACTURED BY RENOUF PUBLISHING CO., MONTREAL
001 FROM

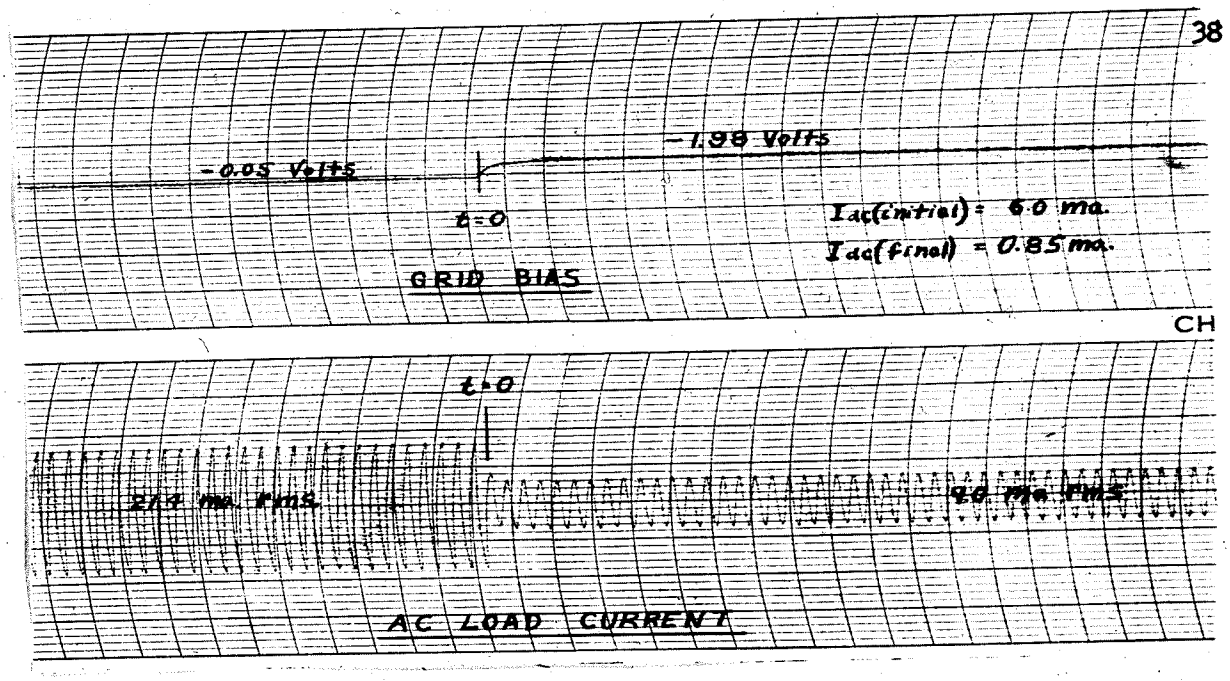

(a) INCREASING NEGATIVE BIAS

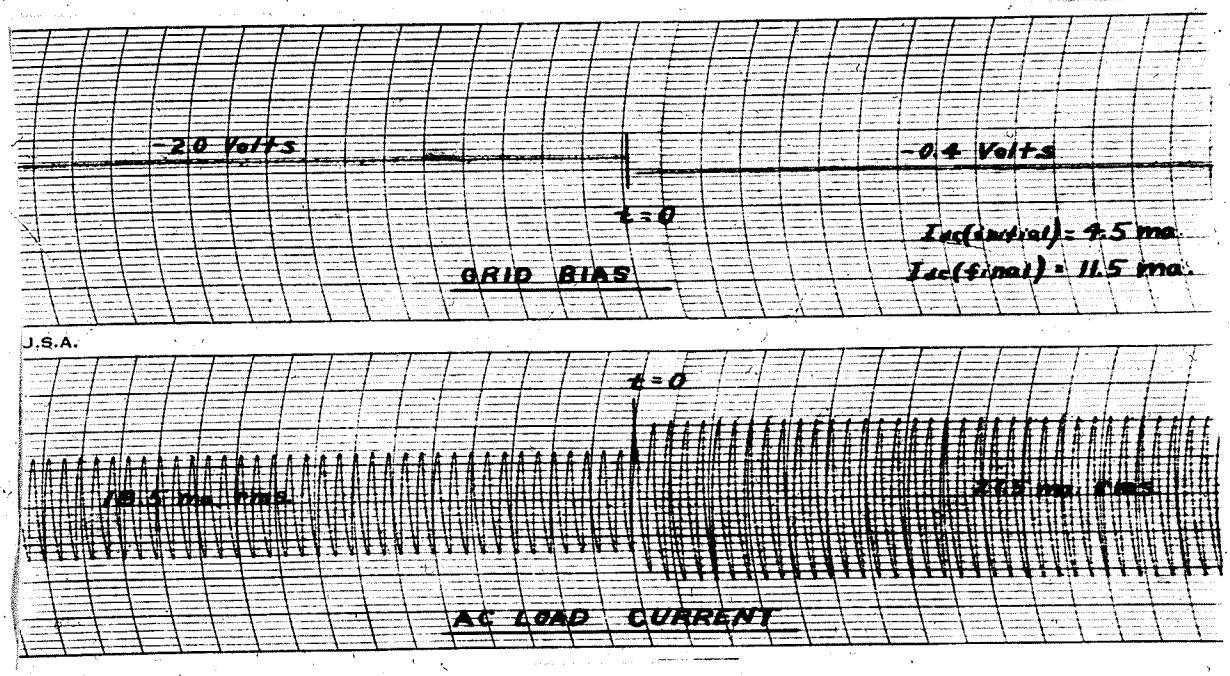

(b) DECREASING NEGATIVE BIAS

FIG. 2.15 TRANSIENT RESPONSE OF SATURABLE REACTOR WITH CONTROL WINDING IN LOAD CIRCUIT OF 6AC7 PENTODE

vacuum tube was suddenly changed from -0.05 volts to -1.98 volts, comparable to the calculated value Fig. 2.15(a). It is seen that the response is ~~almost instantaneous~~.

Now r_p for this vacuum tube is approximately 50K when the grid bias is 0 volts. However, r_p must be taken at the final bias voltage (-1.98 volts) and not at the initial bias. By the same token, if the bias change was such that the final bias was 0 volts, then r_p as determined at this bias should be used. In this case

$$T = \frac{440}{50,000}$$

$$= 0.0088 \text{ sec}, \text{ or } 0.53 \frac{\text{cycles}}{\text{sec}}$$

Fig. 2.15(b) shows a record of the saturable reactor current response when the grid bias was raised from -2.0 volts to -0.4 volts. A delay is noticeable here and the time constant is in the order of half a cycle per second.

Thus, if the error voltage swings in a negative direction, no transfer function need be considered for this element, but if it swings in a positive direction the following transfer function will be present:

$$\frac{I_c(s)}{E_g(s)} = \frac{2.7}{(1 + 0.0088s)}$$

CHAPTER III

DESIGN OF THE FEEDBACK ELEMENT

3.1 Filtering Qualities of the Detector Circuit

In order to discern any deviation of the alternator terminal voltage from a predetermined value, a system must be devised which will report to the reference voltage of any such deviations. This system, or detecting element must contain the following properties:

(1) Change the output a-c voltage of the alternator to a d-c value.

(2) Have a relatively short delay between an a-c change and the corresponding d-c change.

The first requirement can be fulfilled by a rectifier and filter, but in order to comply with the second, a few stringent conditions are imposed on the type of rectifier and filter to be used. An L-C filter is out of the question if a quick response network is required. This restricts the filter to an R-C type. The R-C components should be small enough to create short time constants in the network and yet be large enough to achieve the desired degree of filtering. Fundamental filter theory[1] states that the higher the order of fundamental ripple frequency that can be attained, the more thorough is the filtering. Thus, a 360-cps fundamental ripple will be filtered to a higher degree than a 60-cps fundamental ripple.

The most suitable rectifier for a three-phase supply is a three-phase wye, double-way rectifier[2]. This rectifier takes a three-phase a-c input to a delta-connected primary transformer bank. The secondary is wye-connected and supplies the selenium rectifiers as shown in Fig. 3.1(a). The operation of the rectifier can be understood by reference to Fig. 3.1(a) and (b). When phase A is positive rectifier 2 cannot start conduction until $\pi/6$ is reached. Then the anode of rectifier 2

---

1. W.L. Davies and H.R. Weed, Industrial Electronic Engineering, Ch. III, Prentice Hall, 1953.

2 H.J. Bichsel, Three Phase Wye, Double-Way Rectifier, Westinghouse Industrial Electronics Reference Book, 3rd. Ed., p. 241, Wiley, 1950.

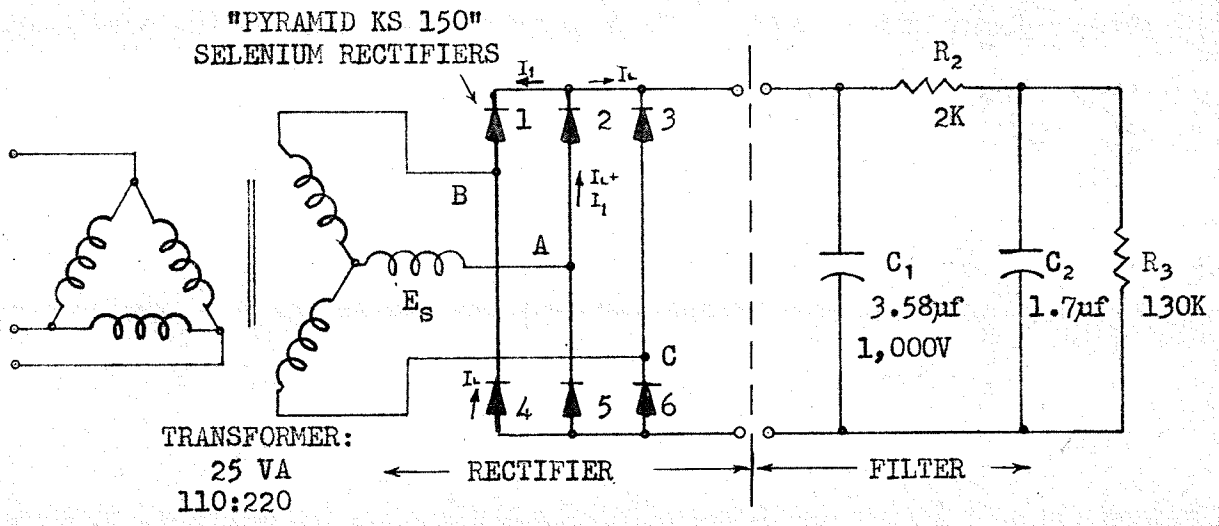

(a) THREE-PHASE WYE, DOUBLE-WAY RECTIFIER AND R-C FILTER

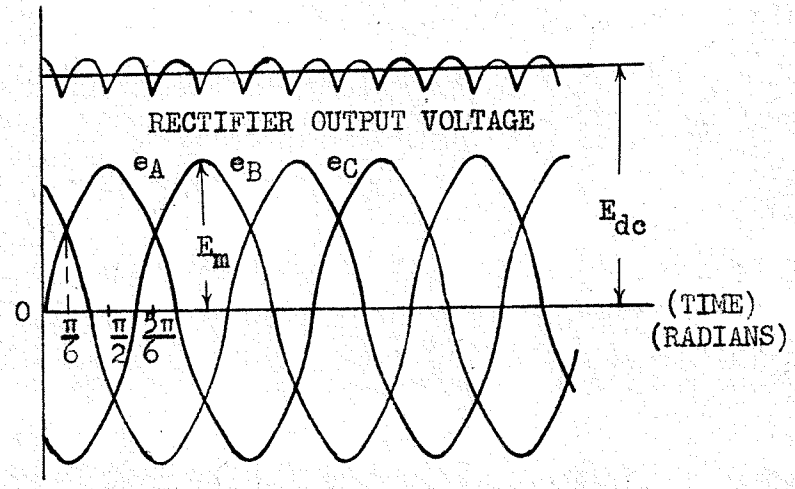

(b) RECTIFIER VOLTAGES

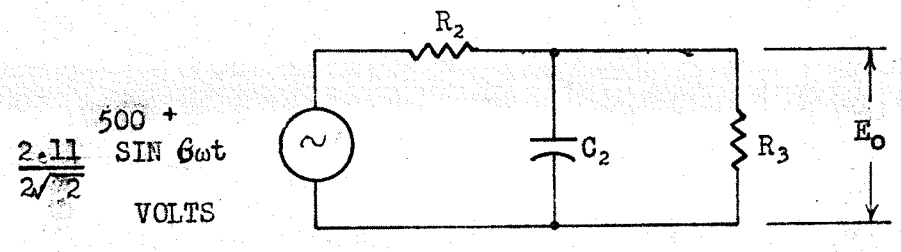

(c) EQUIVALENT GENERATOR

THE UNIVERSITY OF MANITOBA LIBRARY

FIG. 3.1 RECTIFIER AND FILTER IN FEEDBACK CIRCUIT

becomes positive and the rectifier conducts current through the load, providing that either rectifier 4 or 6 can conduct. At time $\pi/6$, the cathode of rectifier 4, which is connected to phase B, is negative. Current now flows through rectifier 2, through the load, and returns to the transformer through rectifier 4. The voltage appearing across the load, while these rectifiers are conducting, is

$$E = e_A - e_B$$

where e_A = instantaneous voltage from phase A

and e_B = instantaneous voltage from phase B

At time $\pi/2$, the voltage of phase C becomes more negative than phase B, and the load current transfers from rectifier 4 to rectifier 6. Thus, each rectifier carries current for 120 degrees; a commutation occuring every 60 degrees, which results in a fundamental ripple frequency of 360 cps. Higher order of ripple harmonics are also present. For a three-phase double - way rectifier the ripple frequency can be broken up into the following components[1]:

Component	Peak to Peak Value of Ripple
fundamental (360 cps)	5.7 %
2nd harmonic	1.4 %
3rd harmonic	0.6 %

The above factors are a percentage of the d-c output voltage, and are present in those proportions only for a resistive load.

If a capacitor is placed across the output, the ripple is cut down drastically; being negligible if no load is present. However, with selenium rectifiers the backward resistance is not infinite and some leakage does occur. Beyond the initial capacitor of the filter, any number of RC sections could be cascaded to cut down the ripple to a desired value, but as mentioned before the transient response places a limitation on this number.

---

1. H.J. Scott, Rectifier Filter Design, Electronics, Vol. II, pp. 28, June, 1938.

Several tests were conducted on a capacitor input filter and one R-C section. Various combinations of R and C were tested to determine the components that would produce an acceptable d-c output. The final values chosen were those shown in Fig. 3.1(a).

For an analytical treatment, the actual components of the rectifier circuit must be replaced by an equivalent rectifier circuit. Thus, the delta-wye transformer bank and the rectifiers can be replaced by a source in series with an impedance, Fig. 3.2(b).

Appendix E.1 gives the primary resistance of the 25-VA transformer as 320 ohms and of the secondary as 730 ohms. Since no neutral current flows in the wye side, the same current must flow in two secondary windings during the conduction period. At this same instant the third transformer carries no current. While a transformer is supplying current the amp-turns relation must hold for the primary and secondary windings. This means that the primary impedance will be reflected into the secondary side. With a one to two ratio, the secondary impedance is

$$R_{o_2} = a^2 R_p + R_s$$

$$= 4 \times 320 + 730$$

$$= 2{,}010 \text{ ohms}$$

However, at any instant of conduction, two secondary windings are in series and

$$R_1 = 2 \times 2{,}010$$

$$= 4{,}020 \text{ ohms}$$

It can be noted from Appendix E.1 that the reactance is negligible in these transformers.

The volt-ampere characteristics, of two samples of the "Pyramid KS 150" selenium rectifiers, were obtained in order to determine the forward and backward resistances, Graph 3.1. The dynamic resistance was obtained as the inverse of the slope of the tangent at the operating point on the curve.

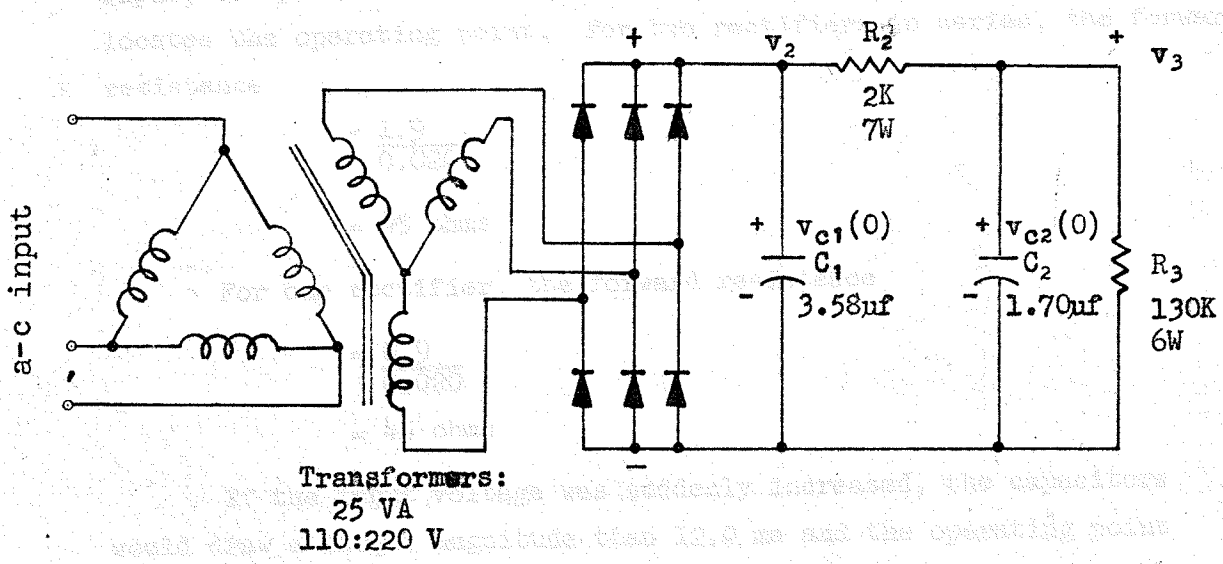

(a) DETECTOR CIRCUIT

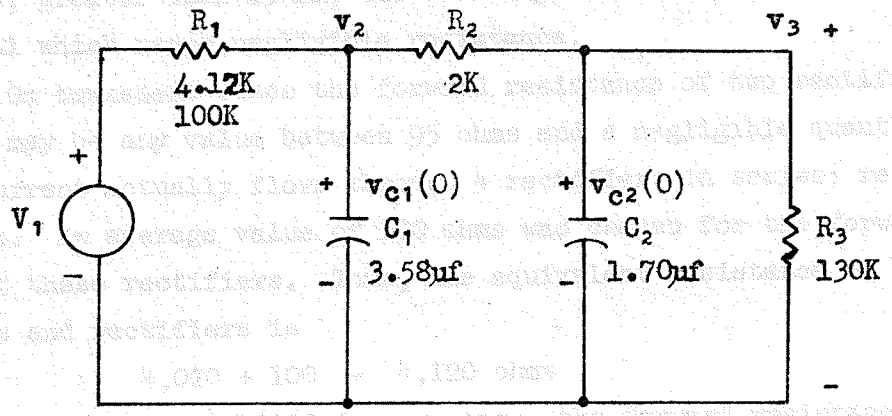

(b) EQUIVALENT DETECTOR CIRCUIT

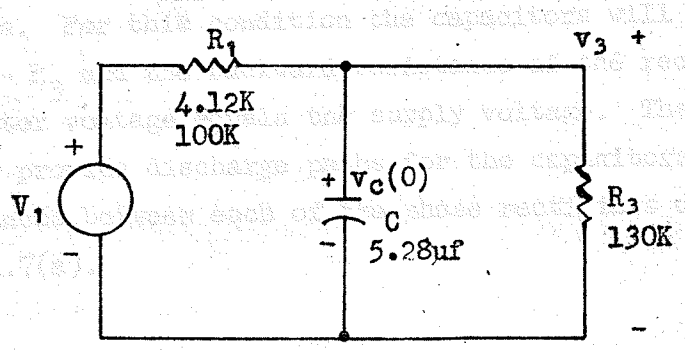

(c) SIMPLIFIED EQUIVALENT CIRCUIT

FIG. 3.2 SCHEMATIC AND EQUIVALENT CIRCUIT OF DETECTOR

Fig. 3.3 shows that under normal conditions, with a 120-volt input, the peak current through the rectifiers is 12.0 ma. This locates the operating point. For two rectifiers in series, the forward resistance

$$= \frac{1.9}{0.020}$$

$$= 95 \text{ ohms}$$

For one rectifier, the forward resistance

$$= \frac{0.9}{0.020}$$

$$= 45 \text{ ohms}$$

If the input voltage was suddenly increased, the capacitors would draw a larger magnitude than 12.0 ma and the operating point would be higher up on the rectifier curve. For high values of currents, that is, greater than 25 ma, the volt-amp characteristics are almost vertical which means negligible resistance.

On transient rises the forward resistance of two rectifiers in series may be any value between 95 ohms and a negligible quantity. The load current actually flows through 4 rectifiers in series; rectifiers 2 and 4. An average value of 100 ohms was chosen for the forward resistance of these rectifiers. Thus, the equivalent resistance of the transformers and rectifiers is

$$4{,}020 + 100 = 4{,}120 \text{ ohms}$$

For a voltage build-down process, the forward resistance of the rectifiers is no longer of concern nor is the resistance of the transformers. For this condition the capacitors will discharge through two paths - R_3 and the backward resistance of the rectifiers - until the capacitor voltage equals the supply voltage. The transformer windings do not provide discharge paths for the capacitors since they act as mere impedances between each of the phase rectifiers during this period, Fig. 3.7(a).

MANUFACTURED BY RENOUF PUBLISHING CO., MONTREAL

IF SHEET IS READ THE OTHER WAY (VERTICALLY), THIS MUST BE LEFT-HAND SIDE.

THIS MATERIAL IS COPYRIGHTED AND MAY BE PROTECTED BY PUBLISHING.

GRAPH 3.1 VOLT-AMPERE CHARACTERISTICS OF SELENIUM RECTIFIERS, TYPE "PYRAMID KS 150"

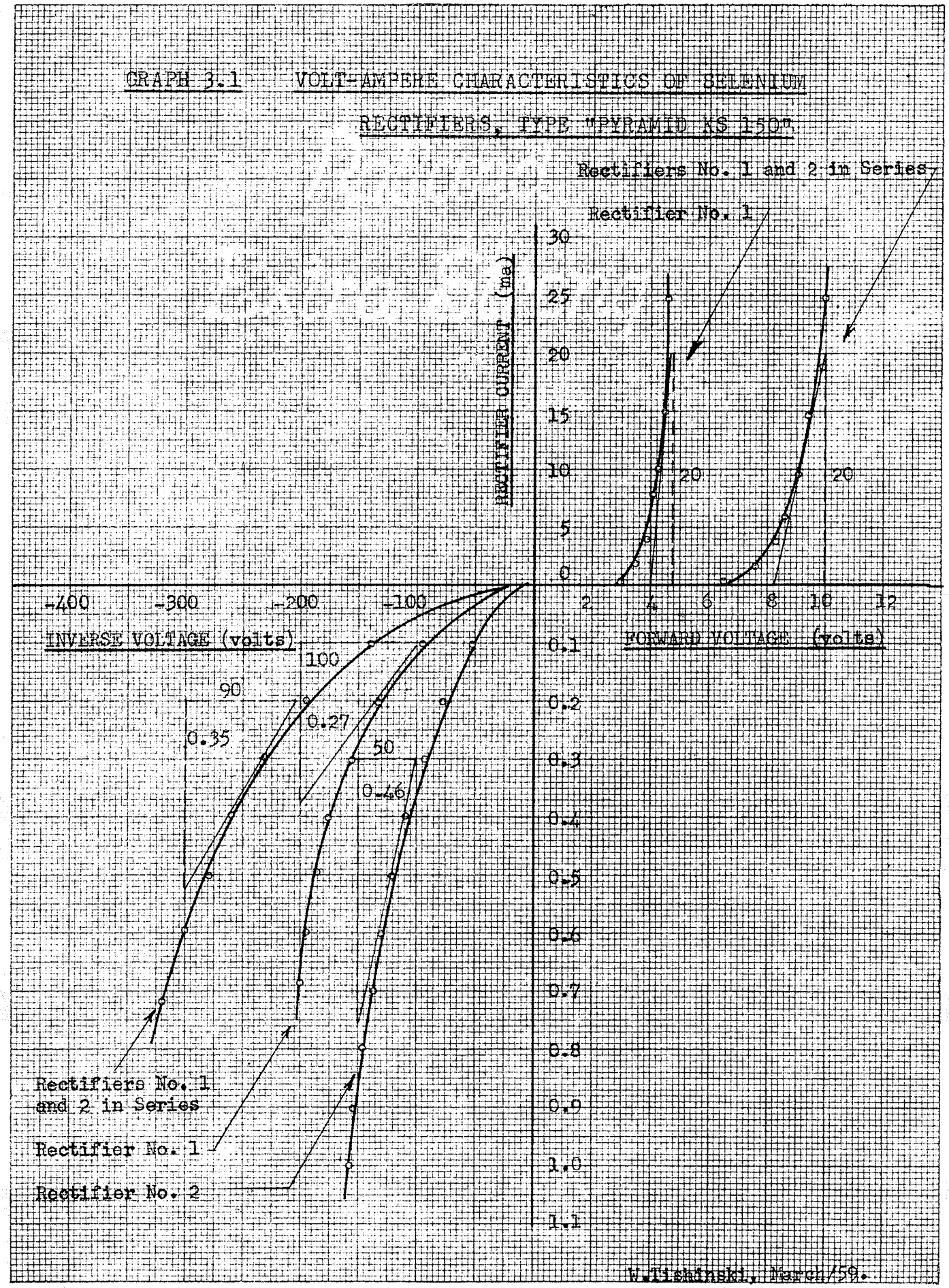

W.Tishinski, March/59.

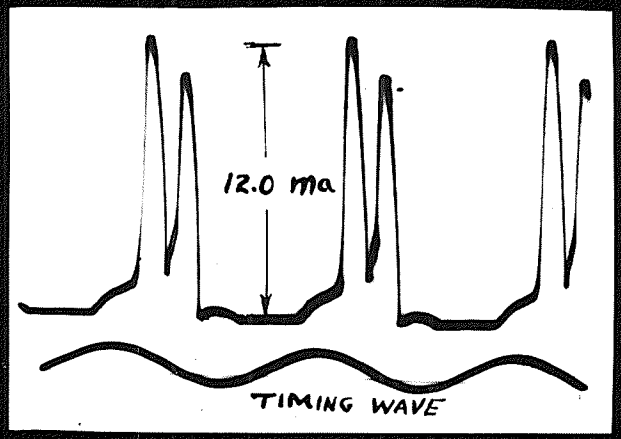

FIG. 3.3 RECTIFIER CURRENT FOR 120-VOLT INPUT

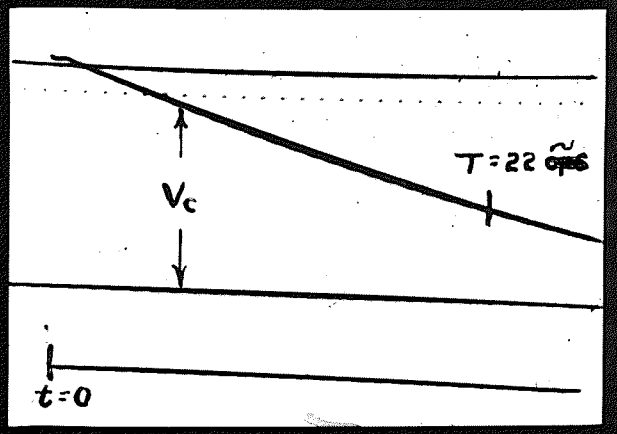

FIG. 3.4 CAPACITOR DISCHARGE THROUGH BACK-RESISTANCE OF RECTIFIERS

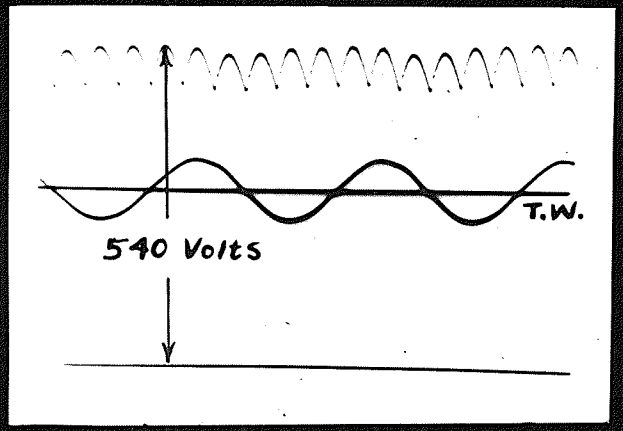

FIG. 3.5 RIPPLE VOLTAGE AT RECTIFIER OUTPUT WITH NO FILTER SECTION AND 120-VOLT INPUT

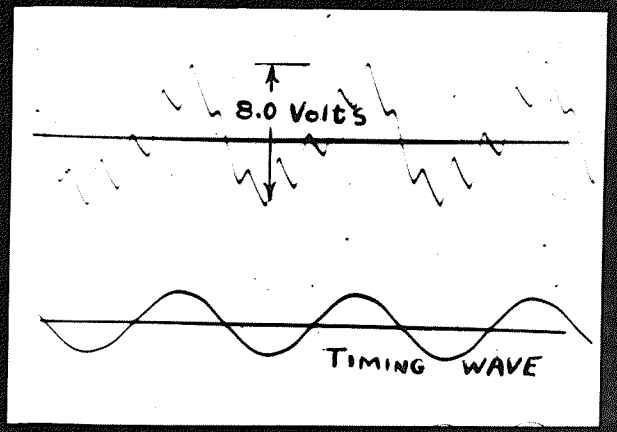

FIG. 3.6 RIPPLE VOLTAGE AT RECTIFIER OUTPUT WITH FILTER SECTION CONNECTED AND 120-VOLT INPUT

The backward resistance could be obtained by the same method as for the forward resistance. However, it is noted from Graph 31 that two samples of rectifiers, presumably identical, have very differing characteristics. The operating point on these reverse curves is determined by the voltage impressed across one rectifier.

If the supply voltage suddenly dropped and if the voltage across C_1 was, say, 500 volts, it is very unlikely that the voltage distribution would be 125 volts per rectifier for each phase. However, if forced to make this assumption (125 volts per rectifier), for lack of more exact information, an erroneous quantity is obtained, as will be shown.

From Graph 31 the inverse of the slope of the tangent at the 125-volt point on rectifier No. 2 curve

$$= \frac{50}{0.00046}$$

$$= 108K.$$

The backward resistance for rectifier No. 1 at the same operating voltage of 125 volts

$$= \frac{100}{0.00027}$$

$$= 370K.$$

The backward resistance of the two rectifiers in series at an operating voltage of 250 volts

$$= \frac{95}{0.00035}$$

$$= 270K.$$

The sum of the individual resistances is 108K + 370K = 478K, which is far from 270K.

Assuming that the resistance of 270K for two rectifiers in series is more exact, the backward resistance of one phase will be 2 x 270K, or 540K. However, since there are three paths in parallel the equivalent total backward resistance will be

$$\frac{540}{3} = 180K.$$

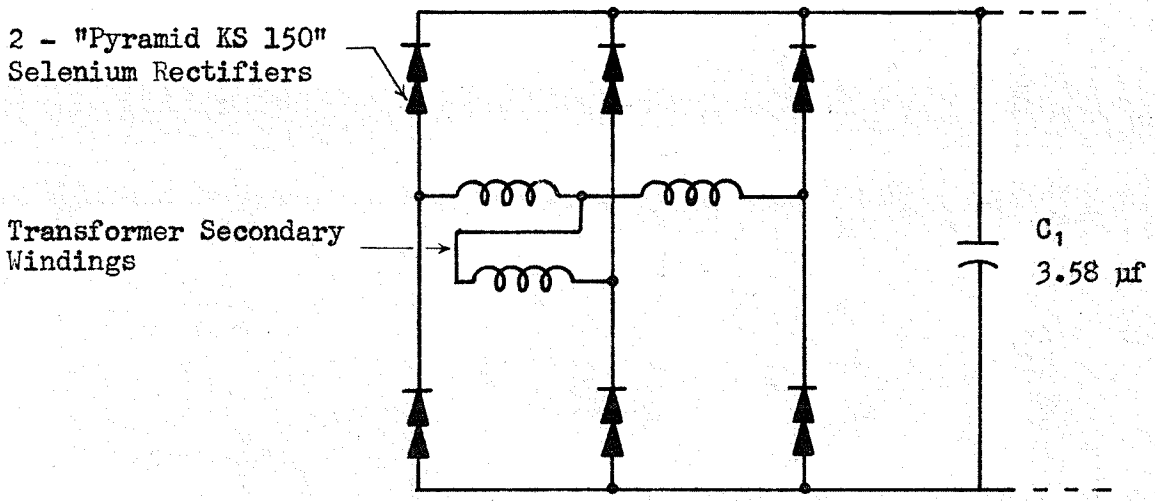

(a) INDIVIDUAL RECTIFIER ARRANGEMENT IN THE DETECTOR CIRCUIT

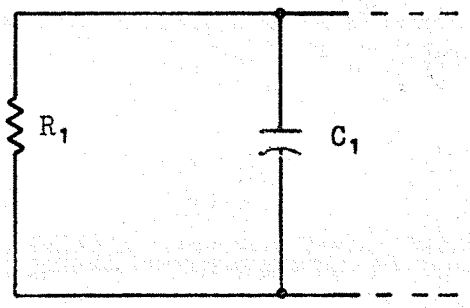

(b) EQUIVALENT CIRCUIT OF (a)

FIG. 3.7 INDIVIDUAL RECTIFIER ARRANGEMENT IN THE DETECTOR CIRCUIT

This value was checked experimentally by using the portion of the detector circuit shown in Fig. 3.7(a). For a build-down condition only one time constant T is involved and if C is known, R can be evaluated. The oscillograph tracing, Fig. 3.4, shows the decay of the voltage across capacitor C_1 through the rectifiers. C_1 was initially charged to 260 volts; the supply voltage was instantaneously dropped to 150 volts which initiated the discharging process. The voltage on the capacitor is given by

$$v_{c_1} = 150 + (260 - 150)\, e^{-t/RC}$$

When the capacitor reaches 63.2% of its steady-state voltage,

$$t/RC = 1$$

From Fig. 3.4, it is noted that v_{c_1} drops to 63.2% of its steady-state value at t = 22 cps.

Hence, $$R = \frac{22}{60} \times \frac{10^6}{3.58}$$

$$= 102.5K,$$

or 100K for calculating purposes; the difference being within the experimental accuracy.

The actual output voltage recorded from the rectifier on open-circuit conditions, with no filter section attached is shown in Fig. 3.5. The theoretical d-c output of this type of rectifier[1] for a 120-volt a-c input is

$$E_{dc} = E_{sm} \times 1.65$$

$$= 240\sqrt{2} \times 1.65$$

$$= 558 \text{ volts}$$

However, the actual wave ~~shape~~ had a peak value of 540 volts, and the average value will be somewhat lower. The ~~poor~~ regulation of the transformers is responsible for this discrepancy. From Fig. 3.1(b), it can be seen that the peak value of the output is given by

$$E_{dcm} = E_s \sqrt{2}\sqrt{3}$$

---

1. W.L. Davis and H.R. Weed, Industrial Electronic Engineering, pp. 129, Prentice - Hall, 1953.

hence, actual $E_s = 540/\sqrt{2}\sqrt{3}$

$= 221$ volts

Also, $E_{dc} = 221\sqrt{2} \times 1.65$

$= 516$ volts

The backward resistance (100 K) of the rectifiers as evaluated from Fig. 3.4 should be more accurate than the values obtained from Graph 3.1, which were determined by considering the slopes of the tangents at the operating points on the characteristic curves. This is because the former method (utilizing Fig. 3.4) treats the whole rectifier assembly in its completed state while the latter method treats the individual units, thus being subject to a cumulative error.

It is evident now that it is difficult to obtain an accurate value for the backward resistance of the rectifier since it is a non-linear element. However, the 100 K value obtained previously, should be close to the average value throughout the entire operating range of the rectifiers.

With the filter section connected to the rectifier, the effective d-c load is 132 K. However, another factor arises here concerning the d-c load, which is merely a discharge path for capacitor C_1, and that is the leg of the rectifier which is inactive during any instant of conduction. Thus, as rectifiers 2 and 4 conduct and have a governed amount of current flowing through them, rectifiers 3 and 6 are viewed by capacitor C_1 as a discharge path.

Taking the experimental value of 100 K as the back-resistance of the 3 legs of rectifiers in parallel, one leg will have a back-resistance of 300 K. The total d-c resistance as viewed by C_1 is

$$\frac{132 \times 300}{132 + 300} = 92 \text{ K}$$

At this stage it is necessary to adjust the d-c voltage level at the input to the filter. Connecting the filter to the rectifier draws an additional

$$\frac{516}{136 \text{ K}} = 3.8 \text{ ma}$$

This current creates an additional transformer IR drop of

$$3.8 \times 4.12 = 15.7 \text{ or } 16 \text{ volts}$$

Therefore, the rectifier terminal voltage with the rectifier connected is

$$E_{dc} = 516 - 16$$

$$= 500 \text{ volts}$$

If the ripple at the input to the capacitor is assumed to be a saw-tooth wave, the peak to peak value is given by

$$E_r = \frac{E_{dc}}{2 f RC}$$

$$= \frac{500}{2 \times 360 \times 92{,}000 \times 3.58 \times 10^{-6}}$$

$$= 2.11 \text{ volts (peak to peak)}$$

The voltage at C_1 now consists of a d-c component and a 360 cps ripple, neglecting all higher harmonics:

$$V_{c_1} = 500 + 2.11/2\sqrt{2} \sin 6\omega t \text{ volts}$$

With the above voltage at C_1, all the components to the left of C_1 can be replaced by a special generator delivering the above voltage, Fig. 3.1(c).

The output voltage, E_o can be determined by the superposition principle. The d-c component of E_{dc} views a resistive path and the output d-c voltage is

$$E_{odc} = \frac{500}{132} \times 130$$

$$= 493 \text{ volts}$$

The 360-cps ripple views R_2 in series with C_2.

$$X_{c_2} = \frac{1}{2\pi \times 360 \times 1.70 \times 10^{-6}}$$

$$= 260 \text{ ohms}$$

R_3 can be neglected since X_{c_2} is much less than R_3. The R_2 -C_2 combination acts as a potential divider with the voltage across C_2 also present across R_3.

$$E_{or} = \frac{2.11}{2{,}000 - j260} \times 260$$

$$= 0.27 \text{ volts (peak to peak)}$$

Therefore, for an a-c input of 120 volts, 60 cps, the output voltage of the detector is

$$493 + 0.27/2\sqrt{2} \sin 6\omega t \text{ volts}$$

Fig. 3.6 is a record of the ripple across C_1. The unexpected fact here is that the predominant ripple is not 360 cps, as was expected, but 60 cps. Closer examination of Fig. 3.5 reveals the fact that the output from the rectifiers, with no filter sections connected, contained a small 60-cps ripple. The filter would be only one-sixth as effective in eliminating this ripple as it would in eliminating the 360-cps component. Therefore, a fair portion of the 60-cps ripple still remained.

The peak to peak value of 8.0 volts, which is the ripple at the rectifier output, is far in excess of the calculated 2.11 volts.

Also, the output ripple is a fundamental 60-cps wave with a peak to peak value of 1.25 volts, which is much greater than the calculated peak to peak 360-cps ripple of 0.27 volts.

There are two possible reasons for the presence of this 60-cps ripple.

(1) The alternator terminal voltages between phases are not equal. A check was made with the alternator open-circuited and the following voltages were recorded:

$$V_{ab} = 120.0 \text{ volts}$$

$$V_{bc} = 119.0 \text{ volts}$$

$$V_{ca} = 120.3 \text{ volts}$$

(2) The non-matching back-resistance values of the rectifiers in each phase leg. Leakage currents through the back-resistances will not be equal and the capacitor at the rectifier output will discharge more over one portion of the 60-cps wave than over another.

3.2 Transfer Function of the Feedback Circuit

A transfer function of a network can be found by first writing out the differential equations for the system applying Kirchhoff's current or voltage law. Then the Laplace transforms of the above equations are taken, letting initial conditions equal zero. A check will be made on the accuracy of such calculations by impressing a unit-step input and recording the response at the output. This response will be compared with the wave form of the calculated response to a similar unit - step input.

In analysing this circuit for its transient response, the output voltage from the rectifiers and filter will be considered as pure d-c, neglecting the small ripple.

Referring to Fig. 3.2(b) the node-pair equations may be written as follows:

At node 2,

$$(G_1 + G_2)\, v_2(t) + C_1 \frac{d\, v_2(t)}{dt} - G_2 v_3(t) = G_1\, v_1(t)$$

and at node 3,

$$(G_2 + G_3)\, v_3(t) + C_2 \frac{d\, v_3(t)}{dt} - G_2 v_2(t) = 0$$

Taking the Laplace transform of the above two equations and noting that

$$L\, f'(t) = sF(s) - f(o^+)$$

the result becomes

$$(G_1 + G_2)V_2(s) + C_1\, sV_2(s) - C_1 v_{c1}(o) - G_2 V_3(s) = G_1 V_1(s)$$

and

$$(G_2 + G_3)V_3(s) + C_2\, sV_3(s) - C_2 v_{c2}(o) - G_2 V_2(s) = 0$$

The sign of the initial voltages, $v_{c1}(o)$ and $v_{c2}(o)$ are such that they will aid the driving voltage on the right hand side of the equation.

Placing the constants on the right hand side and combining, the results become

$$(G_1 + G_2 + C_1 s)\, V_2(s) - G_2 V_3(s) = G_1 V_1(s) + C_1 v_{c1}(o)$$

and

$$(G_2 + G_3 + C_2 s)V_3(s) - G_2 V_2(s) = C_2 v_{c2}(o)$$

If the input is a unit step then

$$V_1(s) = \frac{V_1}{s}$$

The transient output voltage $v_3(t)$, can be evaluated by solving for $V_3(s)$ and then taking the inverse Laplace transform.

By Cramer's Rule,

$$V_3(s) = \frac{\begin{vmatrix} G_1 + G_2 + C_1 s & G_1 \frac{V_1}{s} + C_1 v_{c1}(o) \\ -G_2 & C_2 v_{c2}(o) \end{vmatrix}}{\begin{vmatrix} G_1 + G_2 + C_1 s & -G_2 \\ -G_2 & G_2 + G_3 + C_2 s \end{vmatrix}}$$

$$V_3(s) = \frac{(G_1C_2 + G_2C_2)\, v_{c2}(o) + C_1C_2 s v_{c2}(o) + G_1G_2\, V_1/s + G_2C_1 v_{c1}(o)}{G_1G_2 + G_1G_3 + G_1C_2 s + G_2^2 + G_2G_3 + G_2C_2 s + G_2C_1 s + G_3C_1 s + C_1C_2 s^2 - G_2^2}$$

$$V_3(s) = \frac{G_1G_2V_1 + \left(G_1C_2\, v_{c2}(o) + G_2C_2\, v_{c2}(o) + G_2C_1\, v_{c1}(o)\right)s + C_1C_2 v_{c2}(o) s^2}{(G_1G_2 + G_1G_3 + G_2G_3)s + (G_1C_2 + G_2C_2 + G_2C_1 + G_3C_1)s^2 + C_1C_2 s^3}$$

let:

$$C_1C_2 = A$$

$$G_1G_2 + G_2C_2 + G_2C_1 + G_3C_1 = B$$

$$G_1G_2 + G_1G_3 + G_2G_3 = C$$

then,

$$V_3(s) = \frac{C_1C_2 v_{c2}(o) s^2 + \left(G_1C_2 v_{c2}(o) + G_2C_2 v_{c2}(o) + G_2C_1 v_{c1}(o)\right)s + G_1G_2V_1}{s(As^2 + Bs + C)}$$

Due to the lengthy expressions for A, B, and C, it would be rather hopeless to solve the above quadratic equation in this form. Hence, numerical values will be introduced at this stage of the solution.

If a relation for the build-up condition[15] desired, R_1 = 4,120 ohms; if an equation for build-down is desired, R_1 = 100K.

The build-up case will be considered first;

$$G_1 = \frac{1}{4,120}$$

$$= 24.3 \times 10^{-5} \text{ mhos}$$

$$G_2 = \frac{1}{2,000}$$

$$= 50.0 \times 10^{-5} \text{ mhos}$$

$$G_3 = \frac{1}{130,000}$$

$$= 0.77 \times 10^{-5} \text{ mhos}$$

$$C_1 = 3.58 \ \mu f$$

$$C_2 = 1.70 \ \mu f$$

Using the above,

$$A = 6.10 \times 10^{-12}$$

$$B = 30.8 \times 10^{-10}$$

$$C = 12.72 \times 10^{-8}$$

The characteristic equation of the system is

$$s^2 + \frac{B}{A} s + \frac{C}{A}$$

or $$s^2 + 505s + 20,900$$

The roots are

$$s_1, s_2 = \frac{-505 \pm \sqrt{(505)^2 - 4 \times 20,900}}{2}$$

$$= -45.5, -459.5$$

The following terms are also necessary for determining $v_3(t)$:

$$G_1G_2 = 12.15 \times 10^{-8}$$

$$G_1C_2 = 4.13 \times 10^{-10}$$

$$G_2C_2 = 8.5 \times 10^{-10}$$

$$G_2C_1 = 17.9 \times 10^{-10}$$

$$C_1C_2 = 6.10 \times 10^{-12}$$

Substituting in numerical values,

$$V_3(s) = \frac{12.15 \times 10^{-8} V_1}{6.10 \times 10^{-12} s(s + 45.5)(s + 459.5)} + \frac{12.63 \times 10^{-10} v_{c2}(o) + 17.9 \times 10^{-10} v_{c1}(o)}{6.10 \times 10^{-12} (s + 45.5)(s + 459.5)} + \frac{6.10 \times 10^{-12} v_{c2}(o)s}{6.10 \times 10^{-12} (s + 45.5)(s + 459.5)}$$

Now by taking the inverse Laplace transform,

$$v_3(t) = \frac{1.99 \times 10^4 V_1}{414} \int_0^t \left(e^{-45.5\,t} - e^{-459.5\,t} \right) dt + \frac{207 v_{c2}(o) + 293 v_{c1}(o)}{414} \left(e^{-45.5t} - e^{-459.5t} \right) + \frac{v_{c2}(o)}{414} \left(-45.5e^{-45.5t} + 459.5e^{-459.5t} \right)$$

$$v_3(t) = V_1 \left(1.060 \left(1 - e^{-45.5t}\right) - 0.105 \left(1 - e^{-459.5t}\right) \right) + 0.391 v_{c2}(o) e^{-45.5t} + 0.609 v_{c2}(o) e^{-459.5t} + 0.711 v_{c1}(o) \left(e^{-45.5t} - e^{-459.5t}\right) \quad - - - - - - \quad (3.1)$$

At $t = 0^+$

$$v_3 = (0.391 + 0.609)\, v_{c2}(o) = 1.000\, v_{c2}(o)$$

which is what would be expected.

As $t \rightarrow \infty$

$$v_3 = V_1 (1.06 - 0.105) = 0.955\, V_1$$

The preceding expression can be checked from fundamental considerations. Under steady-state conditions, the capacitors act as open-circuits. The output voltage is determined by the voltage divider arrangement of the resistances,

$$v_3 = \frac{130{,}00\ V_1}{130{,}000 + 2{,}000 + 4{,}120}$$

$$= 0.955\ V_1$$

Fig. 3.9 shows the response of the detector circuit to a unit-step input with zero initial conditions. The output rose from 0 to 250 volts which means that V_1 rose from 0 to $\frac{250}{0.955}$ = 262 volts.

With initial conditions equal to zero, the developed relation simply becomes

$$v_3(t) = V_1\left(1.060\ (1-e^{-45.5t})-0.105(1-e^{-459.5t})\right)$$

The following is a tabulation giving the rise in output voltage as measured directly off the oscillograph tracing:

TABLE 3.1

RECORDED VOLTAGE RISE OF DETECTOR CIRCUIT

Time (sec)	Unit Rise	Output Voltage 250 x Unit Rise (volts)
1/120	0.21	53
1/ 60	0.48	120
3/120	0.67	167
4/ 60	0.78	195
3/ 60	0.90	225
4/ 60	0.96	240
5/ 60	0.99	247

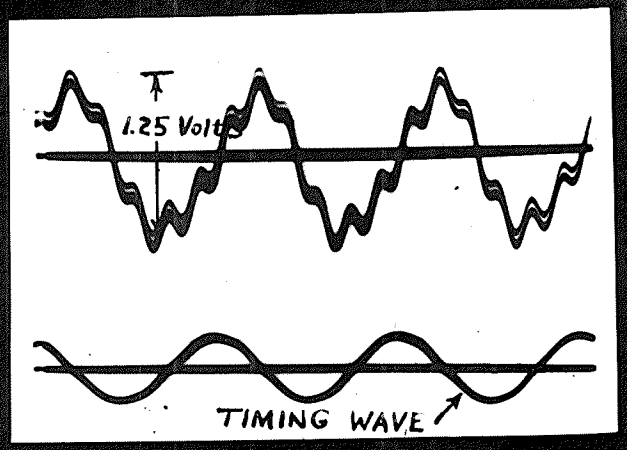

FIG. 3.8 RIPPLE VOLTAGE AT FILTER OUTPUT WITH 120-VOLT INPUT

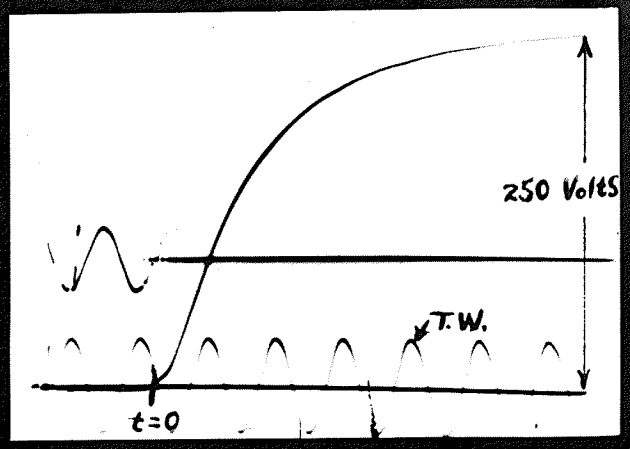

FIG. 3.9 RESPONSE OF DETECTOR TO A UNIT-STEP INPUT

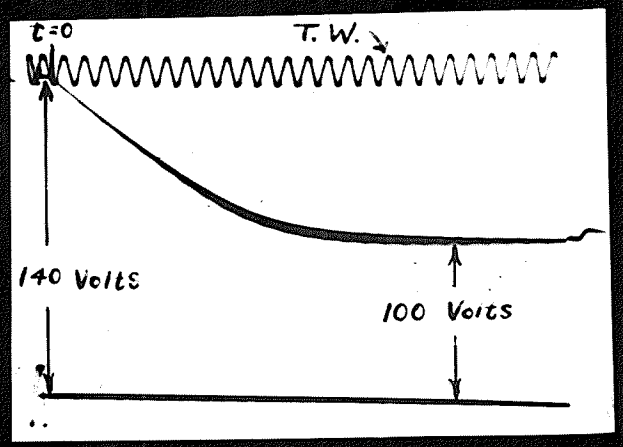

FIG. 3.10 DECAY OF DETECTOR VOLTAGE WITH A STEP INPUT

Graph 32 shows a remarkably good comparison between the measured and calculated responses.

In developing an expression for the voltage build-down of the circuit, one must realize that a rather unique action takes place at R_1. When the driving voltage suddenly drops, the capacitors discharge through R_3 and the rectifiers. However, it is obvious that in steady-state the rectifiers must be conducting in a forward direction. Thus, at some time during the discharging process, R_1 changes from a value of 100K to 4,120 ohms. This transition takes place just as $v_2(t)$ equals V_1. Normally, during a build-down case, $v_2(t)$ is initially equal to $v_{c2}(o)$ and will decay towards a steady-state value of

$$\frac{130K + 2K}{130K + 2K + 100K} V_1 = 0.568V_1$$

But $v_2(t)$ will never reach this value, for as soon as it equals V_1, backward conduction first ceases and then forward conduction takes place. $v_2(t)$ will then attain a steady-state value of

$$\frac{132K}{136.12K} V_1 = 0.970V_1$$

To develop an expression for $v_2(t)$ the node-pair simultaneous equations must first be solved for $v_2(s)$,

$$V_2(s) = \frac{\begin{vmatrix} \frac{G_1V_1}{s} + C_1v_{c1}(o) & -G_2 \\ C_2v_{c2}(o) & G_2 + G_3 + C_2s \end{vmatrix}}{\begin{vmatrix} G_1 + G_2 + C_1s & -G_2 \\ -G_2 & G_2 + G_3 + C_2s \end{vmatrix}}$$

MANUFACTURED BY RENOUF PUBLISHING CO., MONTREAL

IF SHEET IS READ THE OTHER WAY (VERTICALLY), THIS MUST BE LEFT-HAND SIDE.

THIS MATERIAL IS COPYRIGHTED AND PROTECTED BY RENOUF PUBLISHING CO.

GRAPH 3.2 RESPONSE OF DETECTOR CIRCUIT TO A UNIT-STEP INPUT

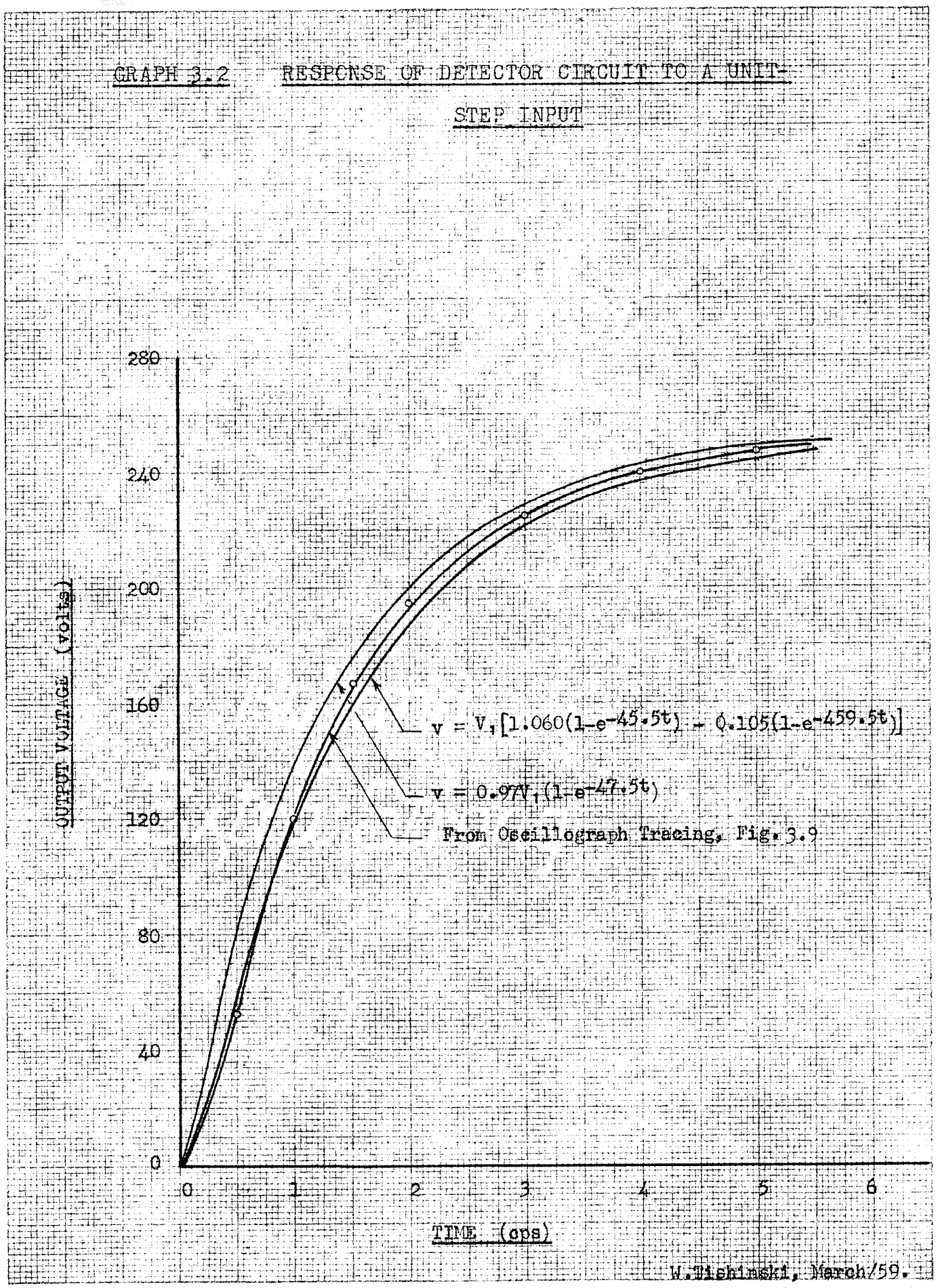

W. Tiehinski, March/59.

$$V_2(s) =$$

$$\frac{G_1G_2\ V_1/s + G_1G_3\ V_1/s + G_1G_2V_1 + C_1G_2v_{c1}(o) + C_1G_3v_{c1}(o) + C_1C_2sv_{c1}(o)}{(G_1G_2 + G_1G_3 + G_2G_3) + (\ G_1C_2 + G_2C_2 + G_2C_1 + G_3C_1)s}$$

$$+ \frac{G_2C_2v_{c2}(o)}{+\ C_1C_2\ s^2}$$

Now, $G_1 = 1/100K$

$= 1 \times 10^{-5}$ mhos

G_2, G_3, C_1, C_2 are the same values as before.

Let,

$$D = C_1C_2 = 6.10 \times 10^{-12}$$

$$E = G_1C_2 + G_2C_2 + G_2C_1 + G_3C_1 = 26.84 \times 10^{-10}$$

$$F = G_1G_2 + G_1G_3 + G_2G_3 = 89.27 \times 10^{-10}$$

The characteristic equation now becomes

$$Ds^2 + Es + F$$

or

$$6.10 \times 10^{-12}\ (s^2 + 440s + 1{,}463)$$

The roots of the above equation are s_1, $s_2 = -3.35, -436.5$.

$$V_2(s) = \frac{(G_1G_2 + G_1G_3)\ V_1}{Ds(s + 3.35)(s + 436.5)}$$

$$+ \frac{G_1C_2V_1 + (C_1G_2 + C_1G_3)v_{c1}(o) + G_2C_2v_{c2}(o)}{D(s + 3.35)(s + 436.5)}$$

$$+ \frac{s\ C_1C_2v_{c1}\ (o)}{D(s + 3.35)(s + 436.5)}$$

Substituting XX numbers for the remaining terms and taking the inverse Laplace transform,

$$v_2(t) = \frac{50.77 \times 10^{-10} V_1}{6.1 \times 10^{-12} \times 433} \int_o^t \left(e^{-3.35t} - e^{-436.5t} \right) dt$$

$$+ \frac{\left(17 \times 10^{-12} V_1 + 18.17 \times 10^{-10} v_{c1}(o) + 8.5 \times 10^{-10} v_{c2}(o)\right)\left(e^{-3.35t} - e^{-436.5}\right)}{6.1 \times 10^{-12} \times 433}$$

$$+ \frac{v_{c1}(o)}{433} \left(-3.35e^{-3.35t} + 436.5e^{-436.5t} \right)$$

$$v_2(t) = V_1 \left(0.5686 - 0.56658e^{-3.35t} - 0.00252e^{-436.5t}\right)$$

$$+ v_{c1}(o)\left(0.6781e^{-3.35t} + 0.322e^{-436.5t}\right)$$

$$+ v_{c2}(o)\left(0.321e^{-3.35t} - 0.321e^{-436.5t}\right)$$

- - - - - - - - (3.2)

At $t = 0^+$,

$$v_2 = 1.0001\, v_{c1}(o)$$

which gives one check.

As $t \rightarrow \infty$

$v_2 = 0.5686 V_1$, which agrees with the result obtained by treating the circuit as a simple potential divider, that is,

$$v_2(t) = \frac{132K\, V_1}{232K}$$

$$= 0.568\, V_1$$

An expression for the output voltage, $v_3(t)$ must also be obtained for the build-down case. This will be of similar form as for the build-up case except for a different characteristic equation in the denominator and a different value of G_1.

$$v_3(s) = \frac{G_1G_2\frac{V_1}{s} + (G_1C_2 + G_2C_2)v_{c2}(o) + G_2C_1v_{c1}(o) + C_1C_2\, sv_{c2}(o)}{D(s + 3.35)(s + 436.5)}$$

Substituting in numerical values, taking the inverse Laplace transform and simplifying, yields

$$v_3(t) = V_1(0.560 - 0.564\, e^{-3.35t} + 0.00439\, e^{-436.5t}) + 0.319v_{c2}(o)\, e^{-3.35t} + 0.681v_{c2}(o)\, e^{-436.5t} + 0.676v_{c1}(o)(e^{-3.35t} - e^{-436.5t}) \quad - - - - - \quad (3.3)$$

An oscillograph tracing, Fig. 3.10 shows a record of the response of the detector circuit as the input was decreased by a unit step. The output voltage decreased from 140 volts to 100 volts.

Under steady-state conditions, when v_3 = 140 volts,

$$V_1 = \frac{136.12\ K}{130\ K} \times 140$$

$$= 145 \text{ volts}$$

and $$v_2 = \frac{136.12}{132} \times 140$$

$$= 142 \text{ volts}$$

When v_3 = 100 volts,

$$V_1 = \frac{136.12}{130} \times 100$$

$$= 105 \text{ volts}$$

and $$v_2 = \frac{136.12}{132} \times 100$$

$$= 101.5 \text{ volts}$$

The analytical method of solution will be as follows:

(1) v_2 will be calculated for increasing values of t, using equation 3.2.

(2) A time t_1 will be found when $v_2 = V_1(\infty)$, (105V).

(3) v_3 will be calculated at incremental steps of t until t_1 is reached, using equation 3.3.

(4) At time t_1, the transition takes place, R_1 changes from 100 K to 4,120 ohms and calculations for v_3 can be completed by using equation 3.1, with initial conditions as at t_1.

The calculated values are arranged in tabular form.

$$v_2(t) = V_1(0.5686 - 0.56658\, e^{-3.35t} - 0.00252\, e^{-436.5t}) + v_{c1}(o)(0.6781\, e^{-3.35t} + 0.322\, e^{-436.5t}) + v_{c2}(o)(0.321\, e^{-3.35t} - 0.321\, e^{-436.5t}) \quad - - - - - \quad (3.2)$$

$V_1 = 105$ volts

$v_{c1}(o) = 142$ volts

$v_{c2}(o) = 140$ volts

TABLE 3.2

VOLTAGE DECAY AT CAPACITOR C_1 WITH A STEP INPUT

Time (sec)	$v_2(t)$(volts)
0	140.0
1/60	136.6
3/60	128.5
5/60	121.3
8/60	110.9
10.6/60	105.1

Time t_1 = 10.6/60 sec

$v_3(t)$ will be calculated up to time, 10.6/60 sec, using equation 3.3 with the following initial conditions:

$V_1 = 105$ volts

$v_{c1}(o) = 142$ volts

$v_{c2}(o) = 140$ volts

TABLE 3.3

VOLTAGE DECAY AT OUTPUT WITH A STEP INPUT

Time (sec)	$v_3(t)$(volts)
0	140.0
1/60	134.7
3/60	127.6
5/60	120.3
8/60	110.8
10.6/60	104.7

Now equation 3.1 will be used with the following initial conditions:

V_1 = 105 volts

$v_{c1}(o)$ = 105.1 volts

$v_{c2}(o)$ = 104.7 volts

TABLE 3.4

VOLTAGE DECAY AT OUTPUT AFTER TRANSITION TAKES PLACE

Time (sec)	$v_3(t)$(volts)
0 (10.6/60)	104.7
1.4/60 (12/60)	101.5
4.4/60 (15/60)	100.1

The following is a tabulation giving the decay in output voltage measured directly off the oscillograph tracing, Fig. 3.10:

TABLE 3.5

RECORDED VOLTAGE DECAY WITH A STEP INPUT

Time (sec)	Unit Fall	Voltage Drop (volts)	Output Voltage (volts)
0	0	0	140.0
1 /60	0.105	4.2	135.8
3 /60	0.293	11.7	128.3
6 /60	0.577	23.1	116.9
10/60	0.853	34.1	105.9
13/60	0.966	38.6	101.4
15/60	1.000	40.0	100.0

Practically perfect agreement exists between the calculated and experimental results as shown on Graph 3.3.

From Tables 3.2 and 3.3 it can be seen that $v_2(t)$ and $v_3(t)$ are very close to being equal for all values of t during the build-down process. Therefore, R_2 can be replaced by a short and C_1 and C_2 can be replaced by a single capacitor C without affecting the output to any considerable extent. This is done in order to avoid lengthy and awkward computations which will occur if any additional load is connected to the detector. Very little accuracy is sacrificed because of this simplification, as will be shown by the following computations.

Applying Kirchhoff's current law at node 3, Fig. 3.2(c), and using Laplace transforms gives:

$$V_3(s)(G_1 + G_3 + Cs) = V_1(s)G_1 + v_c(o)C \qquad - - - - \quad (3.4)$$

If $V_1(s) = V_1/s$,

$$V_3(s) = \frac{V_1 G_1}{Cs\left(s + \frac{G_1 + G_3}{C}\right)} + \frac{v_c(o)}{\left(s + \frac{G_1 + G_3}{C}\right)}$$

By taking the inverse Laplace transform,

$$v_3(t) = \frac{V_1 G_1}{G_1 + G_3}\left(1 - e^{-\frac{(G_1 + G_3)t}{C}}\right) + v_c(o)\, e^{-\frac{(G_1 + G_3)t}{C}}$$

For build-up conditions,

$R_1 = 4{,}120$ ohms

$G_1 = 24.3 \times 10^{-5}$ mhos

$R_3 = 130K$

$G_3 = 0.77 \times 10^{-5}$ mhos

$C = 5.28\ \mu f$

$$v_3(t) = 0.97\, V_1(1 - e^{-47.5t}) + v_c(o)\, e^{-47.5t}$$

With $V_1 = 262$ volts,

and $v_c(o) = 0$,

a plot of the above equation on Graph 3.2, shows that the simplified equivalent circuit can replace the actual equivalent circuit, with a negligible amount of error.

THIS MARGIN RESERVED FOR BINDING.

IF SHEET IS READ THE OTHER WAY (VERTICALLY), THIS MUST BE LEFT-HAND SIDE.

GRAPH 3.3 VOLTAGE DECAY AT DETECTOR OUTPUT WITH A STEP INPUT

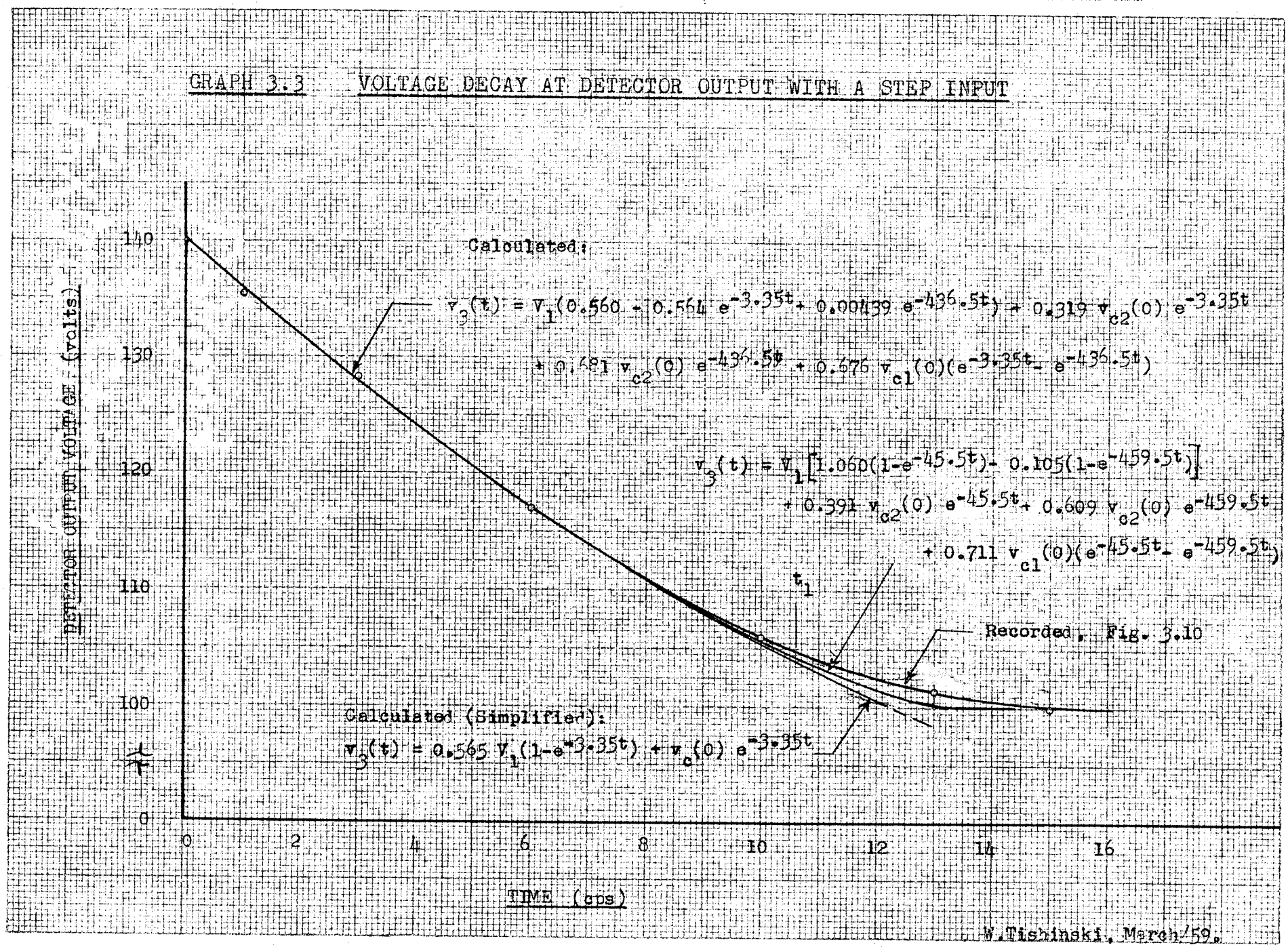

W.Tishinski, March'59.

FORM 160 KEUFFEL & ESSER CO. MANUFACTURED BY INTERNATIONAL

A similar test is made for the build-down process.

$R_1 = 100K$

$G_1 = 10^{-5}$ mhos

$R_3 = 130K$

$G_3 = 0.77 \times 10^{-5}$ mhos

$C = 5.28\ \mu f$

$$v_3(t) = 0.565V_1 (1 - e^{-3.35t}) + v_c(o)\, e^{-3.35t}$$

with $V_1 = 105$ volts

$v_c(o) = 140$ volts

The above equation, when plotted on Graph 3.3 coincides to a large extent with the original calculated curve.

Now, the transfer function of the detector circuit can be taken as

$$\frac{V_3(s)}{V_1(s)} = \frac{G_1}{C\left(s + \frac{G_1 + G_3}{C}\right)}$$

$$= \frac{G_1}{G_1 + G_3\left(1 + \frac{C}{G_1 + G_3}\, s\right)}$$

where $G_1 = 24.3 \times 10^{-5}$ mhos for a build-up process and 10^{-5} mhos for a build-down process.

Therefore, for a build-up process,

$$\frac{V_3(s)}{V_1(s)} = \frac{B(s)}{C(s)} = H(s) = \frac{0.97}{(1 + 0.021s)}$$

and for a build-down process,

$$H(s) = \frac{0.565}{(1 + 0.298s)}$$

CHAPTER IV

DESIGN OF THE REFERENCE SUPPLY CIRCUIT

4.1 Required Voltage Output

Since the detector circuit was designed to give a 500-volt d-c output for a 120-volt a-c input, the reference supply should be made approximately 500 volts d-c to keep the actuating error low.

Thus, if a larger output is desired, R(reference) must be increased proportionately - assuming linear operation, and decreased if a smaller C is desired.

Because the load on the supply transformer of the reference circuit will be constant, regulation will pose no problem here so a capacitor input filter can be utilized. A capacitor input filter has poorer regulation characteristics than a choke input, but on the other hand it produces a higher output voltage.

If a 5V4-G full-wave vacuum rectifier is selected to rectify the a-c voltage, then, from the operation characteristic curves for the above tube[1], it is noted that an output d-c voltage of 500 volts can be obtained with a 4-μf capacitor input filter and a supply of 375 volts rms per plate, when delivering 25 ma load current. Hence, the supply transformer must have a voltage ratio of 115:750 with the secondary centre-tapped. A 5-volt filament supply must also be present.

The remaining portion of the filter was designed to smooth out the ripple by introducing a large choke and large shunt capacitor. Fig. 4.1 shows the schematic of the reference supply.

With a 110 K bleeder resistor the current supplied by the filter would be $\frac{500}{110K} = 4.5$ ma.

At this stage of the development the output voltage was checked by a meter and found to be 465 volts and not 500 volts as predicted by preliminary calculations. The difference could be due to the resistance

---

1. R C A Receiving Tube Manual, p. 99, Radio Corporation of America, 1954.

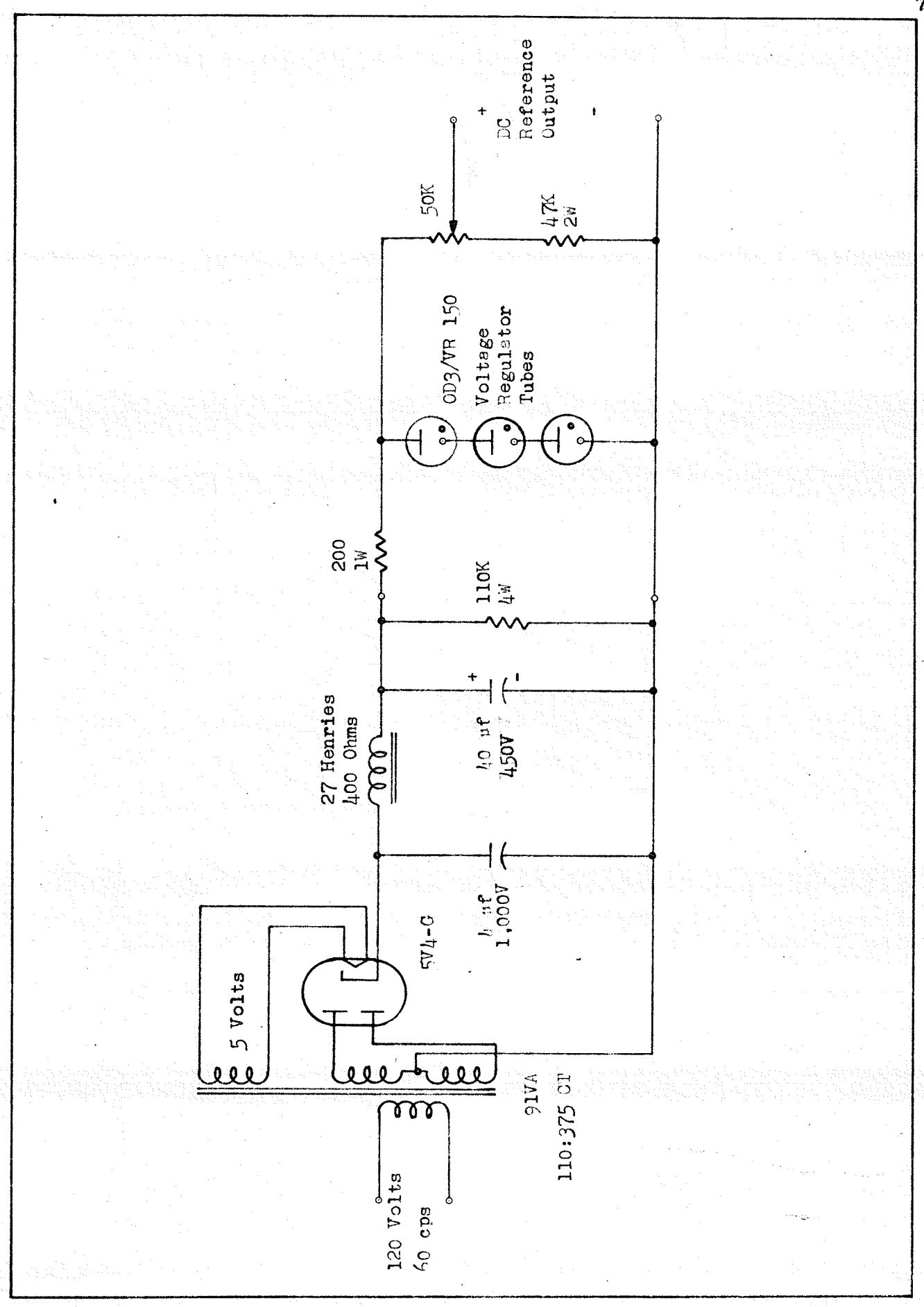

FIG. 4.1 REFERENCE SUPPLY CIRCUIT

of the transformer windings and of the choke which were not accounted for by the operation characteristic curve. The aforementioned curve assumed only an effective plate supply impedance of 100 ohms which is even lower than the 160-ohm resistance of one half of the secondary winding. A 120-cps ripple, with a 0.05-volt, peak to peak value, was also measured at the filter output.

With a 465-volt output from the filter, three-OD3/VR150 voltage regulator tubes can be arranged in series to provide a constant voltage output of 450 volts. A dropping resistor must also be placed in series with the gas tubes to limit the current to a safe value.

A variable reference supply can be obtained by merely connecting a potentiometer across the gas tubes.

If the desired controllable range of the alternator output voltage is from 130 volts to 65 volts, the potentiometer of the reference supply must be capable of covering a proportional range of voltages.

If the forward gain constant G is relatively high, then a simple relation exists between the reference, output and feedback gain constant,[1]

$$\frac{C}{R} = \frac{1}{H} \qquad - - - - - - - - - - - - (4.1)$$

If a maximum open-circuit voltage of 130 volts is desired, which is 146 volts on the air gap line, R can be at its maximum of 450 volts and then H should be

$$\frac{R}{C} = \frac{450}{146} = 3.08$$

This may require some adjusting on the detector circuit output. The voltage transformation ratio between the a-c input and the d-c output of the detector circuit rectifiers is

$$\frac{500}{120} = 4.16 \qquad \text{(section 3.1)}$$

The actual output will be somewhat lower due to the drop across the filter resistors. Therefore the gain constant, as stands, is

$$H = 0.97 \times 4.16$$
$$= 4.03$$

---

1. H. Chestnut and R. Mayer, Servomechanism and Regulating System Design, pp. 7, J. Wiley and Sons, Inc., 1951.

In order to reduce the feedback gain constant, the 130 K bleeder resistor of the detector circuit must be arranged as a voltage divider. Since the gain constant must be reduced from 4.03 to 3.08, a similar ratio must exist for the resistors comprising the voltage divider,

$$\frac{4.03}{3.08} = \frac{130\ K}{x}$$

$$x = 100\ K$$

In the actual circuit x was made 105 K.

Now with the gain constant fixed for the detector circuit, another voltage divider must be introduced in the reference supply between the potentiometer resistance and a series resistor. It would be undesirable to have an arrangement whereby R could be decreased to zero. This is prevented by the inclusion of a series resistor.

Using equation 4.1,

$$\frac{65}{R} = \frac{1}{3.08}$$

$$R = 200 \text{ volts}$$

A 50 K potentiometer in series with a 47 K resistor will produce the required voltage - divider ratio in the reference circuit, Fig. 4.1.

When the a-c power supply was 120 volts, the gas-tube current was metered and found to be 13 ma, which provides a comfortable margin of safety above the 5 ma required to maintain conduction.

CHAPTER V

BLOCK DIAGRAM OF THE CLOSED - LOOP UNCOMPENSATED REGULATING SYSTEM

5.1 Connection of Control Elements to Form a Closed Loop

In the general servomechanism system outlined in Chapter I, the various signals around the loop could have been speed, pressure, voltage or any other such variable. In the voltage-regulating system considered here, the actuating error is a voltage which is the difference in voltages produced by the reference and feedback elements. This signal is fed to the forward elements and thus controls the output voltage of the alternator.

All of the necessary components have now been designed and all that remains to be done is to arrange these components to form a closed loop.

Starting at the controlled output, which is the alternator terminal voltage, the forward control element will be treated first; then the actuating error and finally the feedback element will complete the loop for the system. The schematic of the system is shown on Fig. 5.1.

The supply for the saturable reactor, which is the source of the wave triggering the grid-controlled rectifier, is taken from a standard 120-volt 60-cycle source. A polarized receptacle is used for the supply to the thyratron so that the triggering wave will appear at the proper half cycle of the thyratron supply sine wave. Should the equipment be dismantled and then set up again, this polarized receptacle prevents the possibility of a phase reversal in the thyratron supply.

Since the output of the reference supply is a d-c voltage, as is the output of the detector circuit, these two supplies are merely connected in opposition so that the difference voltage or actuating error can be obtained. At this stage it must be decided upon whether the positive terminals or the negative terminals of the two circuits should be tied together. From Graphs 2.5 and 2.7 it is seen that a higher exciter field current will result if the grid voltage of the 6AC7 error-

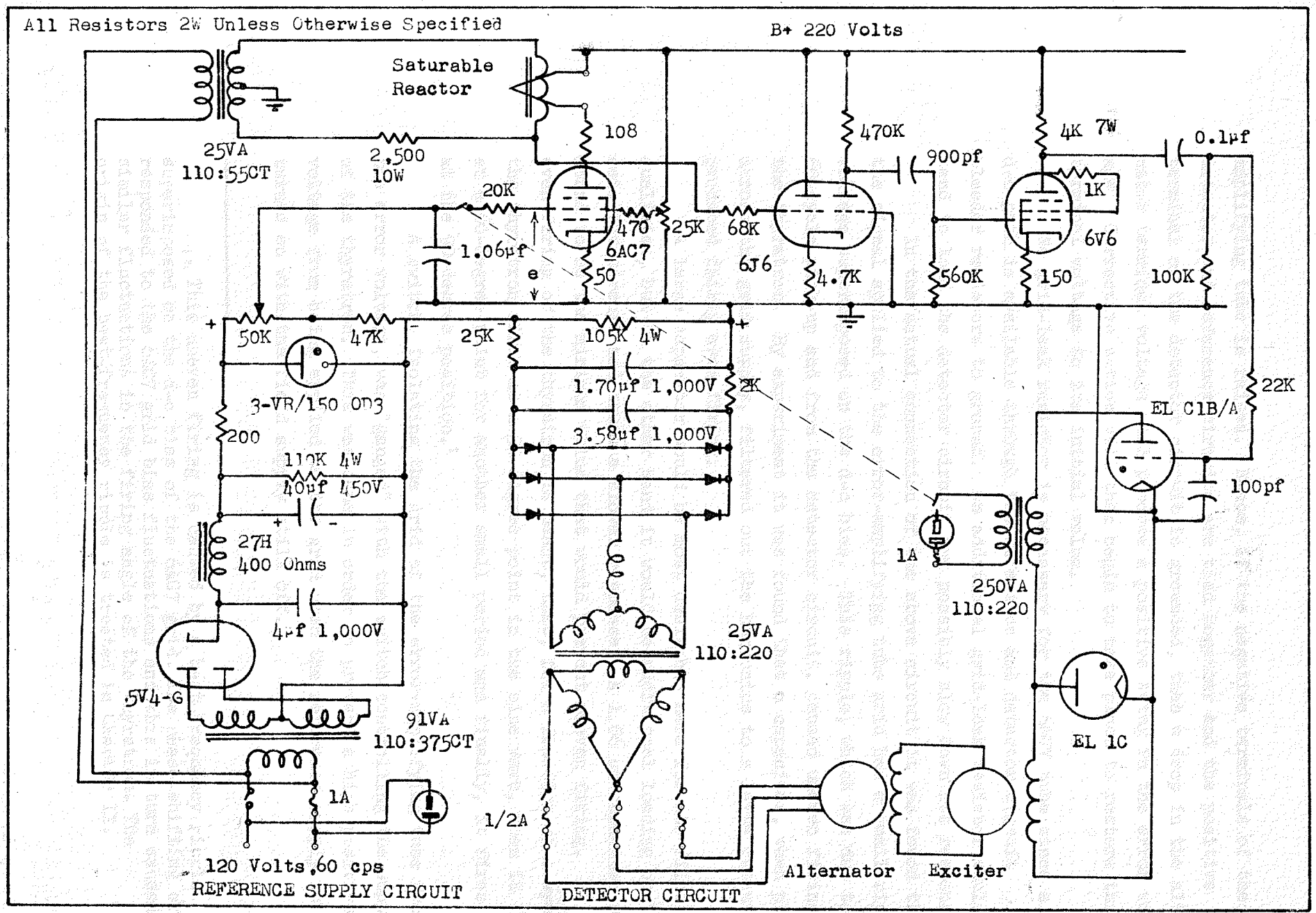

FIG. 5.1 SCHEMATIC OF UNCOMPENSATED VOLTAGE-REGULATING SYSTEM

amplifying tube is raised. Hence, if the negative terminals of the detector and reference circuits are tied together and the positive terminal of the detector circuit is grounded, then a drop in the alternator terminal voltage will produce a positive swing in the error voltage. Corrective action will then begin to take place to restore the terminal voltage to its initial value.

No grid-leak resistor is necessary for the 6AC7 tube since a d-c path is available through the reference and detector circuit bleeder resistors to ground. An additional grid-leak resistor would tend to load the detector circuit and possibly slow down its response.

In the actual connection of the above circuit it was found that the signal applied to the error-amplifying tube grid had a small ripple voltage superimposed on the d-c bias. This ripple, which was due to 60-cycle pick-up and from the detector circuit, caused uneven firing of the thyratron. By experiment it was found that a capacitor, when placed across the grid supply, filtered out the harmonics to a large extent and produced fairly even firing.

A large capacitor would be most desirable here for its filtering qualities, but on the other hand it would be additional loading on the detector circuit and cause a slower response. A 1.06 μf capacitor was found to be the minimum value that would prevent uneven firing. By uneven firing of the thyratron is meant, that, for a fraction of a ~~cycle~~ second the thyratron fires at a 90-degree point in the sine wave, then it fires at a 60-degree point for another small period and finally, it fires back at the 90-degree position.[1]

A switch, isolating the grid of the error-amplifying tube from the error voltage, was "ganged" with the switch controlling the supply of the thyratron. This was done in order to prevent a high positive voltage from being applied to the grid when the reference supply is turned on with the field supply still off.

---

1. This uneven firing is caused by a beat-frequency ripple superimposed on the d-c bias of the 6AC7 grid. The phase-shifting circuit responded to the 6AC7 grid bias fluctuations and this in turn caused similar fluctuations in the firing angle of the thyratron. The origin of the beat-frequency ripple is treated in Chapter IX.

5.2 Loading On the Detector Circuit

From Fig. 5.1 it can be seen that if a transient occurs on the input side of the detector circuit, current on the d-c side, will flow through an additional loop, namely, through the resistance of the reference circuit and the 1.06 μf capacitor to ground. Hence, another transfer function must be evaluated for the detector circuit. The potential of the reference supply does not contribute in any manner to the transfer function since its potential is constant and changes only are of interest.

Fig. 5.2 (a) shows the equivalent circuit of the detector with the transformers and rectifiers replaced by an equivalent generator. Fig. 5.2(b) shows the same circuit as in (a) except for a simplification which was treated in Section 3.2. It is obvious that the simplification performed has dispensed with a great deal of tedious calculations.

Applying Kirchhoff's current law, the equations can be written directly using Laplace transforms,

At node 1; $(G_1 + G_2 + C_1 s)\, V_1(s) - G_2 V_2 = E_1(s)\, G_1$

At node 2; $-G_2 V_1(s) + \left(G_2 + G_3 + \dfrac{G_4 C_2 s}{G_4 + C_2 s}\right) V_2(s) = 0$

from which

$$V_2(s) = \frac{\begin{vmatrix} G_1 + G_2 + C_1 s & E_1(s)\, G_1 \\ -G_2 & 0 \end{vmatrix}}{\begin{vmatrix} G_1 + G_2 + C_1 s & -G_2 \\ -G_2 & G_2 + G_3 + \dfrac{G_4 C_2 s}{G_4 + C_2 s} \end{vmatrix}}$$

Expanding,

$$v_2(s) = \frac{E_1(s)\, G_1 G_2 (G_4 + C_2 s)}{(G_1 + G_2 + C_1 s)(G_2 G_4 + G_2 C_2 s + G_3 G_4 + G_3 C_2 s + G_4 C_2 s) - G_2^2 G_4 - G_2^2 C_2 s}$$

Units of G's are mhos

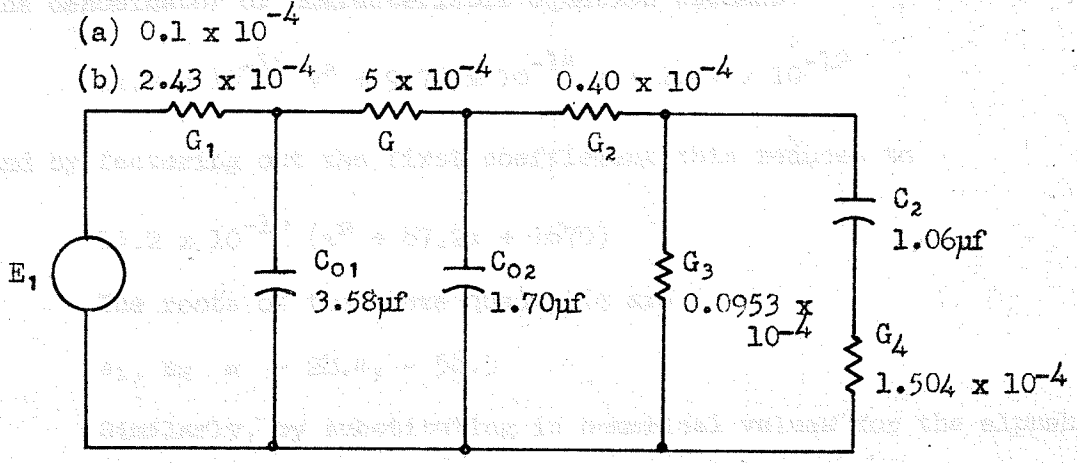

(a) EQUIVALENT DETECTOR CIRCUIT WITH LOADING

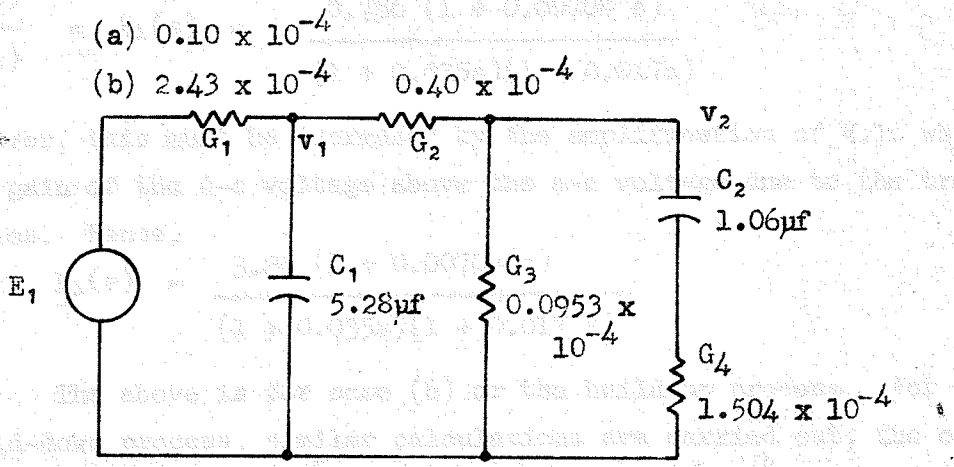

(b) SIMPLIFIED EQUIVALENT CIRCUIT WITH LOADING

FIG. 5.2 DETECTOR CIRCUIT WITH LOADING

Substituting in numerical values for case (b), the build-up process, the denominator or characteristic equation becomes

$$11.2 \times 10^{-16}\, s^2 + 9.77 \times 10^{-14}\, s + 1.87 \times 10^{-12}$$

and by factoring out the first coefficient this reduces to

$$11.2 \times 10^{-16}\, (s^2 + 87.2s + 1670)$$

The roots of the above quadratic are

$$s_1,\ s_2 = -28.4,\ -58.5$$

Similarly, by substituting in numerical values for the alphabetical terms, the numerator becomes

$$E_1(s)(146.5 \times 10^{-14} + 103 \times 10^{-16} s)$$

By factoring out the coefficient of s in the numerator,

$$V_2(s) = \frac{E_1(s)\ 1.03 \times 10^{-14}\ (s + 142)}{11.2 \times 10^{-16}\ (s + 28.4)(s + 58.5)}$$

and the transfer function for the feedback element or detector circuit becomes

$$\frac{V_2(s)}{E_1(s)} = H_1(s) = \frac{0.786\ (1 + 0.00704\ s)}{(1 + 0.035s)(1 + 0.017s)}$$

However, this must be increased by the amplification of 4.16 which is the gain of the d-c voltage above the a-c voltage due to the transformer ratios. Hence,

$$H_1(s) = \frac{3.26\ (1 + 0.00704\ s)}{(1 + 0.035s)(1 + 0.017\ s)}$$

The above is for case (b) or the build-up process. For the build-down process, similar calculations are carried out, the only change being that $G_1 = 1 \times 10^{-5}$ mhos instead of 2.43×10^{-4} mhos.

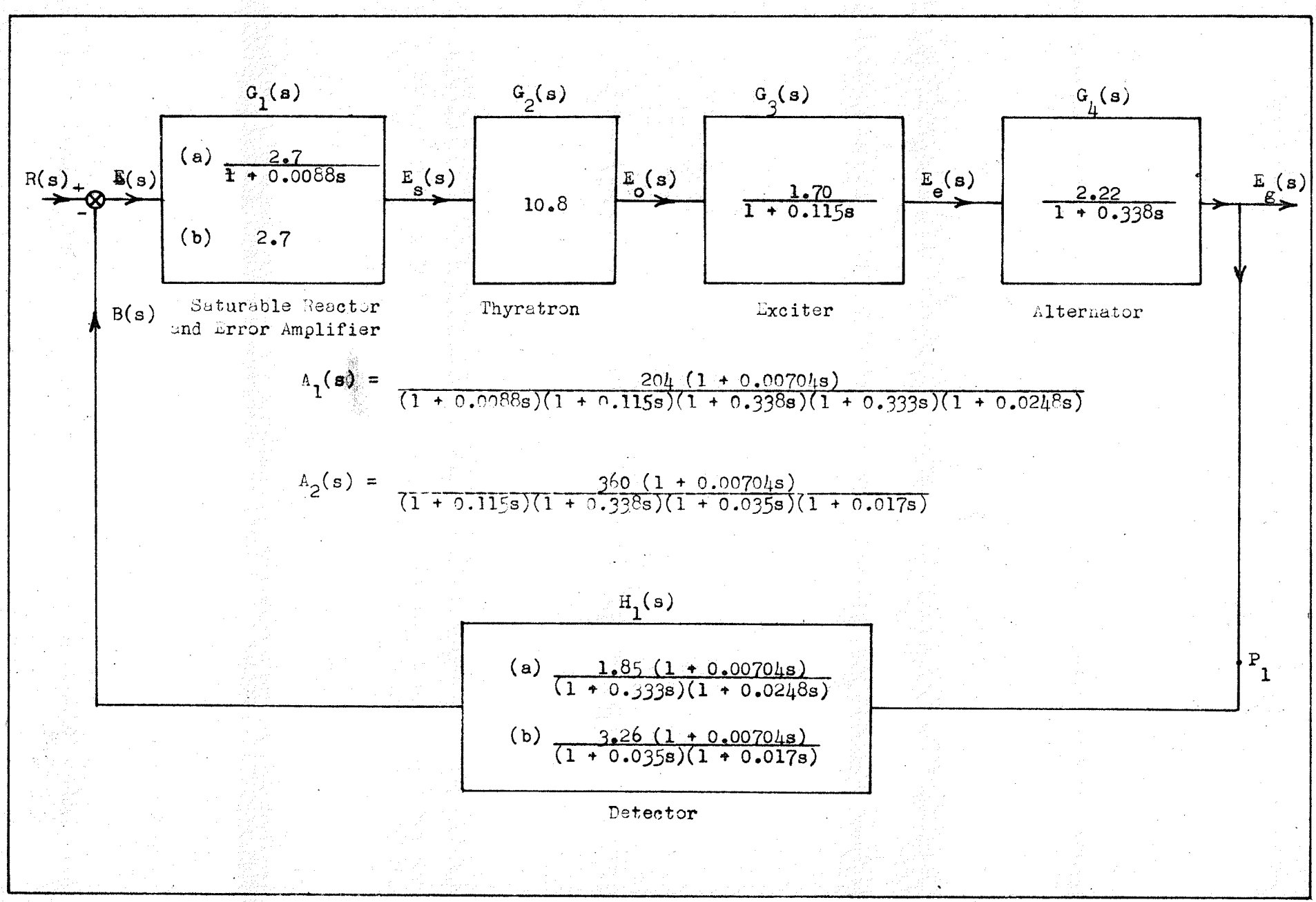

FIG. 5.3 BLOCK DIAGRAM OF UNCOMPENSATED VOLTAGE-REGULATING SYSTEM

The characteristic equation is

$$11.2 \times 10^{-16}(s^2 + 43.2\ s + 118.8)$$

for which the roots are

$$s_1,\ s_2 = -3.00,\ -40.2$$

The numerator becomes

$$E_1(s)\ (6.02 \times 10^{-14} + 4.24 \times 10^{-16} s)$$

and

$$V_2(s) = \frac{E_1(s)\ 4.24 \times 10^{-16}(s + 142)}{11.2 \times 10^{-16}(s + 3)(s + 40.2)}$$

Introducing the amplification of 4.16 and with further manipulation the transfer function for the build-down process becomes

$$\frac{V_2(s)}{E_1(s)} = H_1(s) = \frac{1.85(1 + 0.00704s)}{(1 + 0.333s)(1 + 0.0248s)}$$

Henceforth, the build-down process of the detector will be associated with the application of load on the alternator since it is under this condition that the alternator terminal voltage drops, initiating the build-down process. Similarily, the build-up process will be associated with the dropping of load off the alternator. The block diagram of the uncompensated voltage-regulating system is shown in Fig. 5.3.

CHAPTER VI

STABILITY OF THE UNCOMPENSATED REGULATING SYSTEM

6.1 The Nyquist Diagram

Instability in a servomechanism system is associated with poles of the system transfer function in the right half of the s plane[1]. The general transfer function is

$$\frac{C(s)}{R(s)} = \frac{G(s)}{1 + A(s)}$$

where $G(s)$ = forward transfer function

$A(s) = G(s)\,H(s)$ = open-loop transfer function

Hence, if the zeroes of $1 + A(s)$, which are the poles of the closed-loop transfer function, can be tested then the stability of the system can be established.

The Nyquist criterion states that if a frequency response plot of $A(j\omega)$ is made, then, the number of net clockwise encirclements establishes the difference between the number of zeroes and poles in the right half plane. However, it is the zeroes of $A(s)$ that are of interest and not the poles. Inspection of the open-loop transfer function, Fig. 5.3 reveals the fact that no poles exist in the right half plane, which means that the system is open-circuit stable. Thus, the $A(j\omega)$-plane plot will give the number of zeroes in $1 + A(j\omega)$ directly by the number of clockwise encirclements of the critical point, $-1 + j0$.

As shown previously, two separate open-loop transfer functions exist for the voltage-regulating system and both must be tested separately for stability. The polar plots of $A_1(j\omega)$ and $A_2(j\omega)$, Graph 6.1, encircle the critical point indicating an unstable system.

---

1. J.L. Bower and P.M. Schultheiss, Introduction to the Design of Servomechanisms, Ch. V, p. 118, J. Wiley and Sons, 1958.

TABLE 6.1

TABULATION OF POINTS FOR POLAR PLOT OF

$$A_1(j\omega) = \frac{204(1 + j\omega 0.00704)}{(1 + j\omega 0.0088)(1 + j\omega 0.115)(1 + j\omega 0.338)(1 + j\omega 0.333)(1 + j\omega 0.0248)}$$

ω (radians/sec)	$\lvert A_1(j\omega)\rvert$	Phase Shift (degrees)
0	204	0
1	182	$-\ 44^\circ 33'$
2	137	$-\ 83^\circ 25'$
3	96	$-\ 113^\circ 20'$
4	67	$-\ 137^\circ 0'$
5	46	$-\ 156^\circ 10'$
7	24	$-\ 182^\circ 40'$
10	11	$-\ 210^\circ 50'$
12	6.70	$-\ 223^\circ 50'$
15	3.70	$-\ 237^\circ 40'$
17	2.56	$-\ 247^\circ 40'$
20	1.57	$-\ 257^\circ 50'$
25	0.79	$-\ 271^\circ 40'$
30	0.44	$-\ 282^\circ 10'$

GRAPH 6.1 POLAR PLOT OF TRANSFER FUNCTION FOR UNCOMPENSATED VOLTAGE-REGULATING SYSTEM

$$A_2(j\omega) = \frac{360\ (1+j\omega 0.00704)}{(1+j\omega 0.115)(1+j\omega 0.338)(1+j\omega 0.035)(1+j\omega 0.017)}$$

$$A_1(j\omega) = \frac{204\ (1+j\omega 0.00704)}{(1+j\omega 0.0088)(1+j\omega 0.115)(1+j\omega 0.338)(1+j\omega 0.333)(1+j\omega 0.048)}$$

ω increasing

Critical Point

50

100

150

200

250

0

-180°

210° -150°

200° -160°

190° -170°

170° -190°

160° -200°

150° -210°

220° -140°

230° -130°

240° -120°

250° -110°

260° -100°

270° -90°

280° -80°

290° -70°

300° -60°

310° -50°

320° -40°

140° -220°

130° -230°

120° -240°

110° -250°

100° -260°

90° -270°

80° -280°

70° -290°

60° -300°

50° -310°

40° -320°

330° -30°

340° -20°

350° -10°

10° -350°

20° -340°

30° -330°

W.Tishinski, March 59.

TABLE 6.2

TABULATION OF POINTS FOR POLAR PLOT OF

$$A_2(j\omega) = \frac{360\ (\ 1 + j\omega 0.00704)}{(1 + j\omega 0.115)(1 + j\omega 0.338)(1 + j\omega 0.035)(1 + j\omega 0.017)}$$

(radians/sec)	$\lvert A_2(j\omega)\rvert$	Phase Shift (degrees)
0	360	0
3	240	- 60°10'
4	190	- 91°30'
5	158	- 105°0 '
7	128	- 127°0 '
10	63	- 151°30'
15	30	- 180°0 '
25	9.60	- 208°0 '
30	6.18	- 220°0'
36.1	3.80	- 230°30'
45	2.00	- 242°50'
60	0.83	- 255°50'

The gains of the two transfer functions at a phase angle of 180° are 24 and 30. Stability could be attained by decreasing the open-loop gain by a factor of 30. However, this is undesirable since such an adjustment would produce slow transient response after a load disturbance and poor regulation. Other methods of stabilization must be tried and these will be presented shortly.

Fig. 6.1 shows a record of the performance of the alternator at no load when controlled by the unstable voltage regulator. The oscillations would be much more violent if saturation was not present in the alternator and exciter fields.

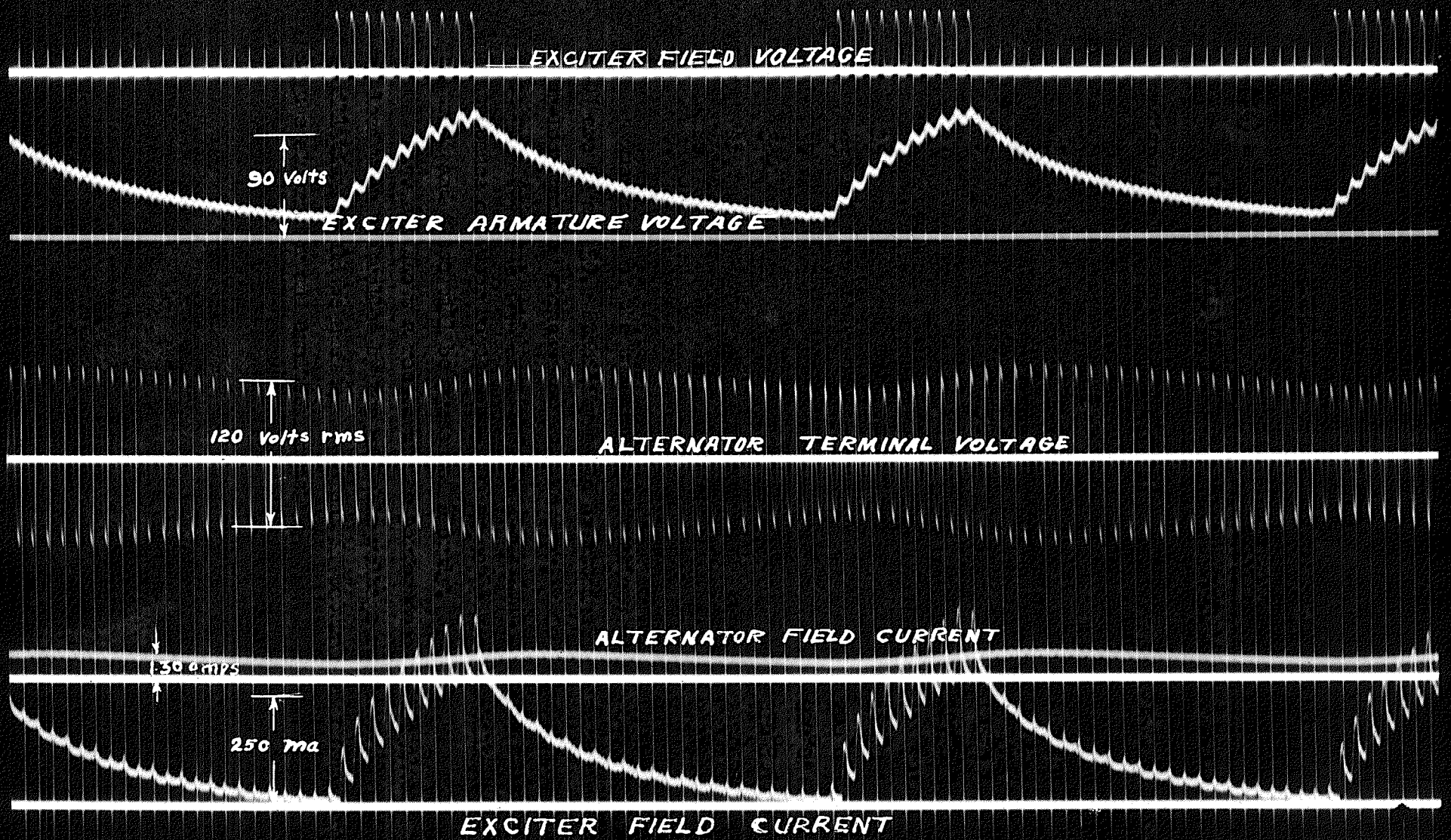

FIG. 6.1 PERFORMANCE OF UNSTABLE VOLTAGE-REGULATING SYSTEM

6.2 The Bode Diagram

The Nyquist diagram presents a simple method of analysing a regulator system but it does not lend itself to aid in design work other than by trial and error. On the other hand, the Bode diagram[1] enables one to easily calculate the phase shift of the harmonic response function at the crossover frequency. The crossover frequency is the frequency at which the plot of the harmonic response function intersects the unity circle on the Nyquist diagram. Hence, the design is confined to the task of modifying the circuit so that the phase margin at the crossover frequency is positive or that the phase lag is less than 180 degrees.

There are certain stipulations in using the Bode diagram, these being that the open loop transfer function must be of the minimum-phase type and must have negative feedback. A minimum-phase function has no poles or zeroes in the right half of the s plane.

An examination of the transfer functions, $A_1(j\omega)$ and $A_2(j\omega)$, shows that all of the roots of the numerator and denominator lie in the left half of the s plane. The feedback circuit and reference were connected so that negative feedback was present; hence, Bode's diagram is applicable.

From the Bode diagram, Graph 6.2, for the aforementioned two transfer functions, the following crossover frequencies were graphically located:

$$\omega_{c1} = 25.5 \text{ rad/sec}$$

$$\omega_{c2} = 63.0 \text{ rad/sec}$$

The crossover frequencies could have been calculated beginning with the gain at unity frequency, however, the graphical determination is sufficiently accurate.

---

1. J. M. Bower and P.M. Schultheiss, Introduction to the Design of Servomechanisms, Ch. VI, pp. 162, J. Wiley and Sons, 1958.

Having located the crossover frequencies, the phase shift at these points may be found, using the arc tan approximation[2].

$$\beta_{c1} = -\left(\frac{\pi}{2} - \frac{2.96}{25.5}\right) - \left(\frac{\pi}{2} - \frac{3.0}{25.5}\right) - \left(\frac{\pi}{2} - \frac{8.7}{25.5}\right) - \frac{25.5}{40.4} - \frac{25.5}{114} + \frac{25.5}{142}$$

$$= -4.81 \text{ rad/sec}$$

$$= -276^{\circ}$$

$$\beta_{c2} = -\left(\frac{\pi}{2} - \frac{2.96}{63}\right) - \left(\frac{\pi}{2} - \frac{8.7}{63}\right) - \left(\frac{\pi}{2} - \frac{28.6}{63}\right) - \left(\frac{\pi}{2} - \frac{59}{63}\right) + \frac{63}{142}$$

$$= -4.26 \text{ rad/sec}$$

$$= -244^{\circ}$$

For a stable system the phase ~~angle~~ lag at the crossover frequency must not exceed 180 degrees.

A phase margin of approximately 30 degrees (a phase shift of - 150 degrees) would provide a sufficient margin of safety to ensure an adequate degree of stability. Therefore, the system must be modified to possess this amount of phase margin.

---

2. Ibid., Ch. III, Xp. 84.

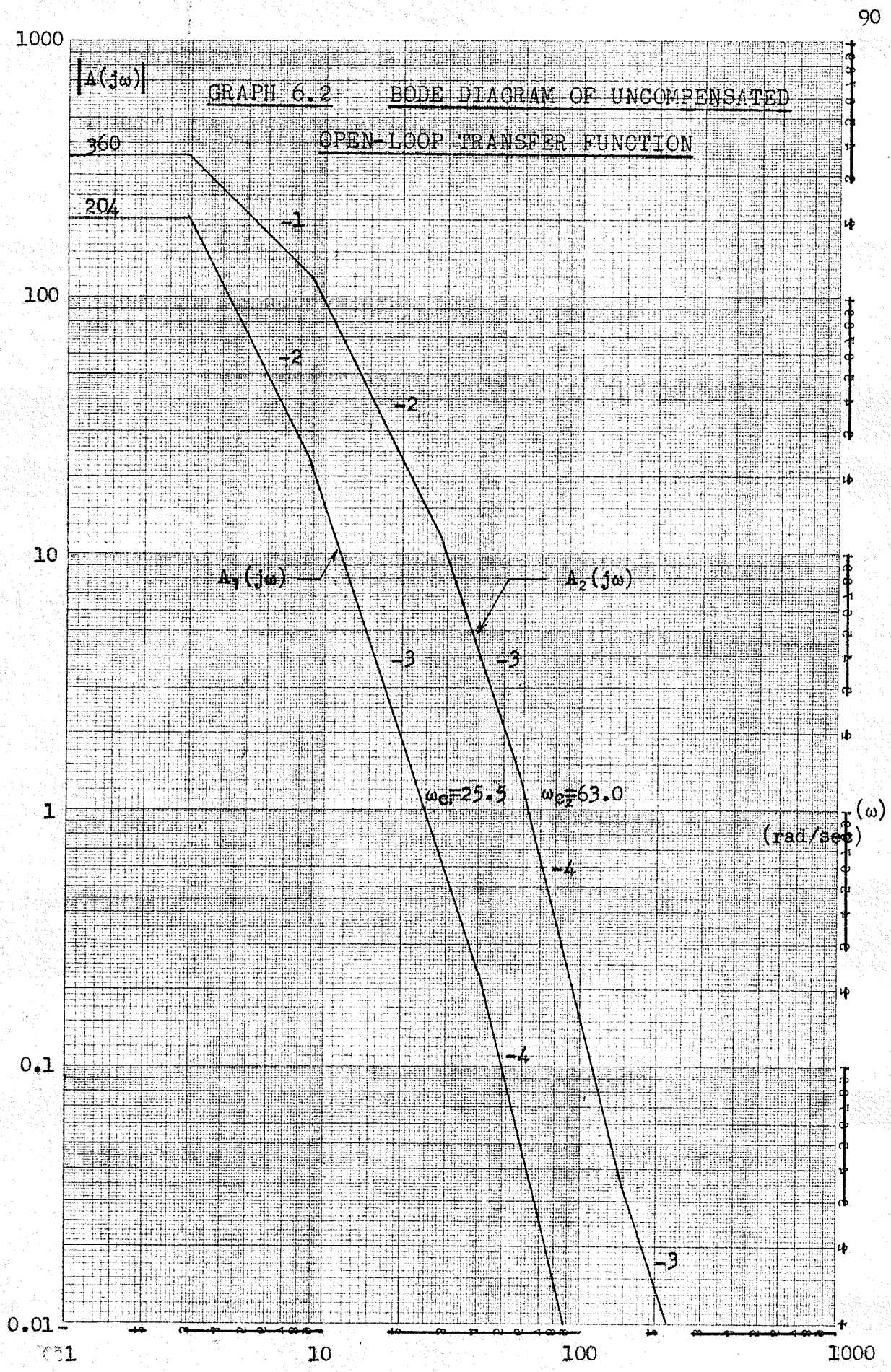

W.Tishinski, March/59.

CHAPTER VII

STABILIZING NETWORKS FOR THE REGULATING SYSTEM

7.1 The Lag and Lead Networks

There are several standard series equalizer networks which may be used to attain stability. One of these is the lag network equalizer, Fig. 7.1(a). This network has a distinct disadvantage of attenuating the gain of the higher frequencies. However, this may not be serious and if stability can be attained, this network may be introduced into the system.

Before proceeding with the design of the lag network, it would be beneficial to know what attenuation or decrease in gain at all frequencies should be present to give a specified phase margin. If the required phase margin is + 30 degrees, $\beta_c = -2.62$ rad/sec.

In using the arc tan approximation it is necessary to know between which two break-points ω_c lies. For the initial calculation this will be assumed and then checked back against the calculated result.

Since $A_2(j\omega)$ requires less phase correction than $A_1(j\omega)$ it will be considered first. If ω_c is assumed to be less than 8.7 rad/sec but greater than 2.96 rad/sec the phase shift equation may be written as

$$-2.62 = -\left(\frac{\pi}{2} - \frac{2.96}{\omega_c}\right) - \frac{\omega_c}{8.7} - \frac{\omega_c}{28.6} - \frac{\omega_c}{59} + \frac{\omega_c}{142}$$

$$-1.05 = \frac{2.96}{\omega_c} - \omega_c\left(0.115 + 0.035 + 0.017 - 0.007\right)$$

or

$$0.16\,\omega_c^2 - 1.05\,\omega_c - 2.96 = 0$$

The roots of the above equation are

$$\omega_{c1},\ \omega_{c2} = 1.39 \text{ rad/sec},\ -0.34 \text{ rad/sec}$$

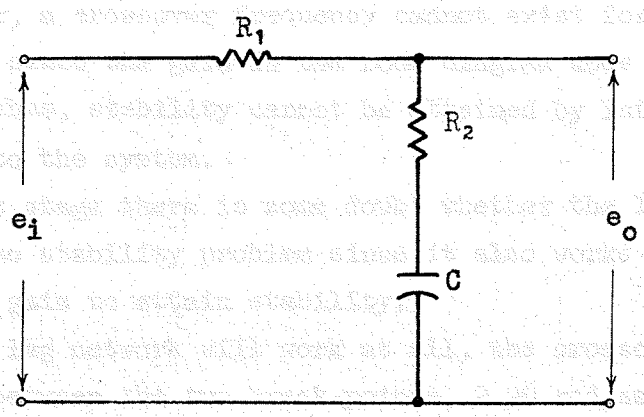

(a) LAG NETWORK

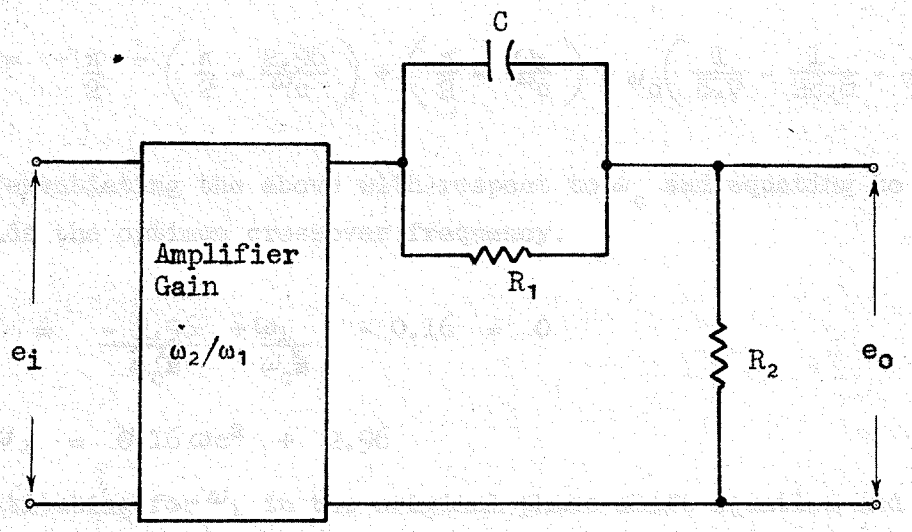

(b) LEAD NETWORK

FIG. 7.1 EQUALIZER NETWORKS

Positive values only are of interest. The preceding assumption appears to be incorrect since ω_c in the above calculation lies below 2.96 rad/sec.

However, a crossover frequency cannot exist for values less than 2.96 rad/sec, since the gain in the Bode diagram does not rise beyond this point. Thus, stability cannot be attained by introducing a simple attenuator into the system.

At this stage there is some doubt whether the lag network is the solution to the stability problem since it also works on the principle of decreasing gain to attain stability.

If the lag network will work at all, the crossover frequency will probably lie between the two break-points, 2.96 rad/sec and 8.7 rad/sec. The second break-point ω_1 of the lag network will be assumed to occur between ω_c and 2.96 rad/sec, Graph 7.1. The first break-point ω_o of the lag network will be small so it can be neglected in any phase shift calculations.

With two unknowns ω_1 and ω_c, the phase shift equation can be written as

$$\beta_c = -\frac{\pi}{2} - \left(\frac{\pi}{2} - \frac{2.96}{\omega_c}\right) + \left(\frac{\pi}{2} - \frac{\omega_1}{\omega_c}\right) - \omega_c\left(\frac{1}{8.7} - \frac{1}{28.6} - \frac{1}{59} + \frac{1}{142}\right)$$

Differentiating the above with respect to ω_c and equating to zero yields the optimum crossover frequency.

$$\frac{d\beta_c}{d\omega_c} = \frac{-2.96}{\omega_c^2} + \frac{\omega_1}{\omega_c^2} - 0.16 = 0$$

or $\omega_1 = 0.16\omega_c^2 + 2.96$

Substituting for ω_1 in the original phase shift equation and assigning the permissible phase shift to β_c,

$$-2.62 = -\frac{\pi}{2} - \left(\frac{\pi}{2} - \frac{2.96}{\omega_c}\right) + \left(\frac{\pi}{2} - \frac{0.16\omega_c^2 + 2.96}{\omega_c}\right) - \omega_c\,(0.16)$$

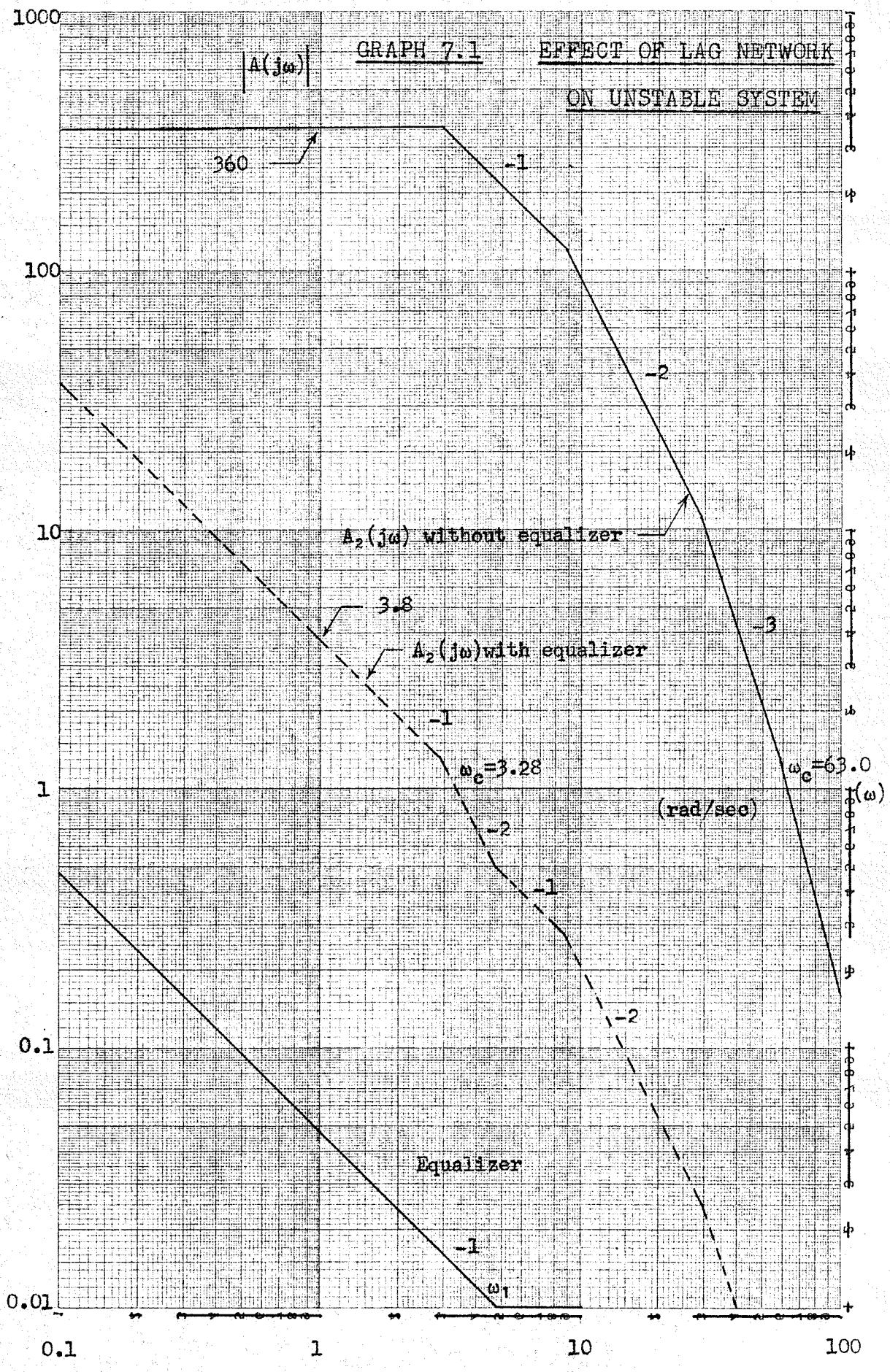

W.Tishinski, March '59.

from which ω_c = 3.28 rad/sec

and ω_1 = 4.69 rad/sec

It is noted that ω_1 is greater than ω_c and not as previously assumed. Calculations could be repeated with this correction. However, it is evident now that the gain of the corrected system is much too low for a practical system ~~and the components comprising the lag network would place a large load on the preceding transfer elements~~ causing other complications to arise.

It has been shown that the lag network can not produce stability so the next step will be to test the lead network, Fig. 7.1(b). This network introduces phase lead into the system and also transmits a wider range of input frequencies.

If a phase margin of 20 degrees is specified, the lead network must have a maximum phase lead of 20 + 64 or 84 degrees if $A_2(s)$ is considered. Then by the arc tan approximation

$$\beta_o = 1.46 = \frac{\pi}{2} - \frac{\omega_1}{\omega_o} - \frac{\omega_o}{\omega_2}$$

Since $\frac{\omega_1}{\omega_o} = \frac{\omega_o}{\omega_2}$ maximized for a lead network

$$1.46 = \frac{\pi}{2} - \frac{2\omega_o}{\omega_2}$$

and $$\frac{\omega_o}{\omega_2} = 0.055$$

But $$\frac{\omega_2}{\omega_1} = \left(\frac{\omega_2}{\omega_o}\right)^2$$

$$= \left(\frac{1}{.055}\right)^2$$

$$= 320$$

Therefore, $\frac{T_1}{T_2} = 320$

A mere glance at the above figure immediately informs one that the lead network is not the solution to the stability problem. If forced to use such a network an amplifier with a gain of 320 must be introduced into the loop. Even if an amplifier could be inserted into the loop as specified, the input impedance of the equalizer would be so low that this would load the preceding stage to the point where it would not be effective.

7.2 Feedback Stabilization

Since the lead and lag networks have been useless in stabilizing the system, the last resort is the feedback method of stabilization. This involves the insertion of a minor loop around one or a few of the forward elements. The closed-loop transfer function of the modified forward elements would then be

$$\frac{C}{R} = \frac{G}{1 + GH}$$

H, of course, must be a frequency sensitive element so that the gain G of the uncompensated forward elements could be modified at different range of frequencies. The above equation can be rewritten as

$$\frac{C}{R} = \frac{1}{H}\left(\frac{GH}{1 + GH}\right)$$

For best performance of the closed - loop transfer function H must be small at low frequencies and large at intermediate frequencies. Thus at low frequencies

$$\frac{C}{R} = G$$

and the control elements retain the transfer characteristics of the original control elements without feedback. In the intermediate range of frequencies

$$\frac{C}{R} = \frac{1}{H}$$

and the resultant function is almost entirely dependent on the characteristics of the feedback network. This means that large phase shifts caused by the forward elements in a certain range of frequencies could be minimized or even eliminated.

The largest time constant in the forward elements is present in the alternator field and a feedback loop around this element would be desirable. However, problems with rectifying and filtering the a-c voltage create more difficulties so the feedback loop must be taken around the remaining forward element, which is the exciter field.

Since there are two feedback loops in the system, it is necessary to differentiate between the two when referring to feedback.

The larger loop, which rectifies the alternator voltage and compares it with the reference shall be called the major loop and the one around the exciter as the minor loop.

Feedback networks or anti-hunt circuits for voltage regulating systems are standard depending on whether a voltage or current component is used as the feedback signal. With a d-c signal feeding the amplifier preceding the exciter it is more convenient to feed back a voltage rather than a current signal. Thus, a portion of the exciter d-c voltage will be used as the feedback signal. This is accomplished by the anti-hunt circuit[1] shown in Fig. 7.2(a).

The time constant of the R-C combination for the minor-loop feedback element is usually taken to equal the time constant of the forward elements within the minor loop[2]. With the time constant of the exciter field being 0.115 sec, a time constant of 0.100 sec for the anti-hunt circuit should be satisfactory.

The treatment of the stability problem will shift now from the synthesis approach to one of analysis. With the anti-hunt circuit established it remains to be shown that the selection of components and type of feedback circuit was correct.

---

1. W. Osbon and V. Baker, Regulation, Westinghouse Industrial Electronics Reference Book, p. 589, J. Wiley and Sons, 1948.

2. Ibid., p. 589.

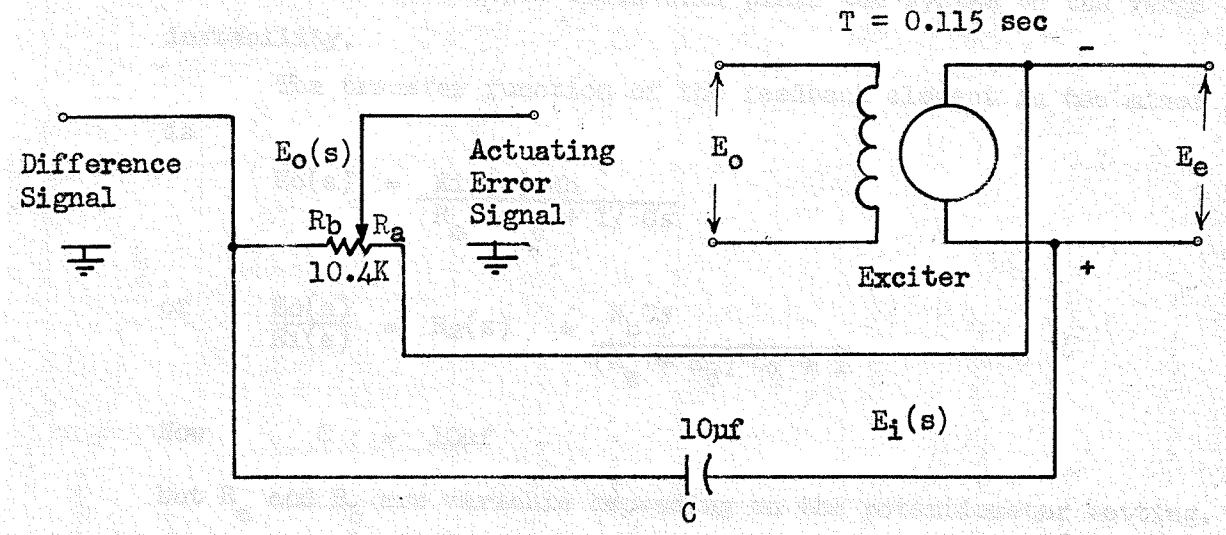

(a) ANTI-HUNT OR MINOR-FEEDBACK CIRCUIT

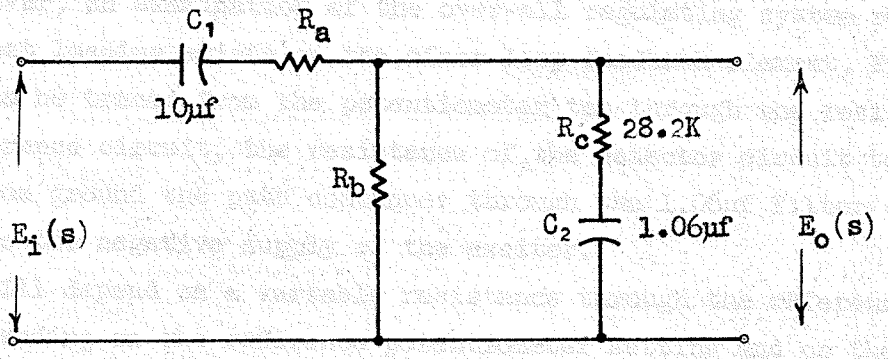

(b) LOADING ON MINOR-FEEDBACK CIRCUIT

FIG. 7.2 MINOR-LOOP FEEDBACK CIRCUIT

A 10K potentiometer and a 10 μf capacitor were chosen to give the selected 0.10 sec time constant. The purpose of the potentiometer, rather than a fixed-valued resistor, was for test work. By this arrangement the amount of feedback in the minor loop can be varied and thus a situation can be reached which will place the system on the verge of instability.

The transfer function of the feedback element in the minor loop is

$$Eo(s) = \frac{Ei\ (s)\ Rb}{R_a + R_b + 1/\ Cs}$$

or $$\frac{Eo(s)}{Ei(s)} = H_2(s) = \frac{R_b Cs}{(R_a + R_b)\ Cs + 1}$$

Now $C = 10\mu f$

but R_a and R_b are variable depending on the potentiometer setting. The measured value of $R_a + R_b$ was found to be 10.4K.

For a preliminary calculation the following resistive values will be selected:

$R_a = 2.4K$

$R_b = 8.0K$

Then $H_2(s) = \frac{0.08s}{(1 + 0.104s)}$

However, an examination of the over-all regulating system reveals the fact that loading exists on the minor-loop feedback element, Fig. 7.3. The load can be traced from the potentiometer tap through the resistance of the reference circuit, the resistance of the detector circuit to ground. From ground the path continues through the 1.06μf filter capacitor back to the negative supply of the exciter.

R_c will depend on a variable resistance through the reference supply, depending on the reference potentiometer setting and on the direction of current flow through the rectifier due to the exciter voltage.

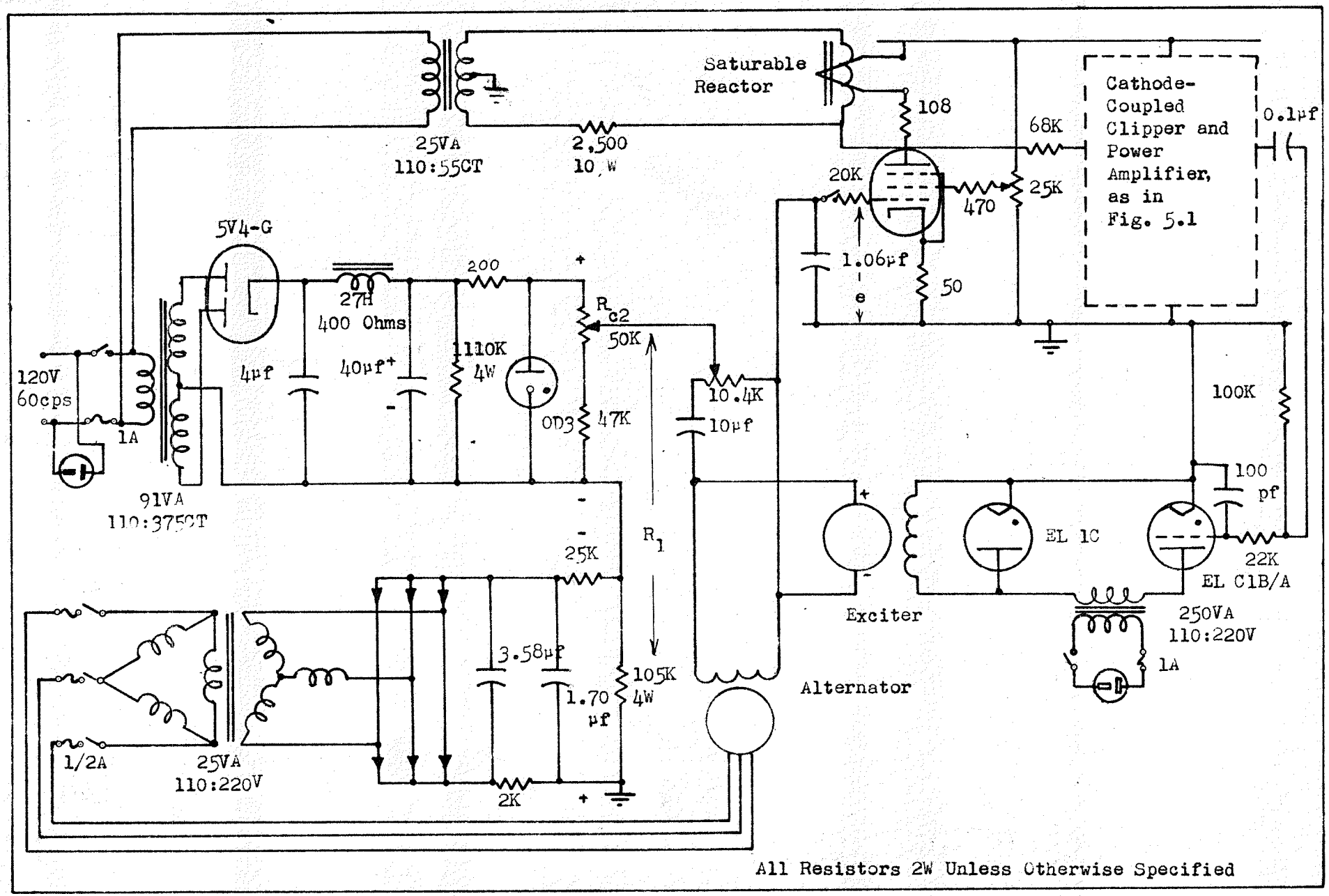

FIG. 7.3 SCHEMATIC OF COMPENSATED VOLTAGE-REGULATING SYSTEM

The case posing the greatest load will be considered and that is when the current flows through the rectifiers in a forward direction. The rectifiers then act as a short and the detector circuit resistance consists of two branches in parallel,

$$R_{c1} = \frac{(25K + 2K)\ 105K}{25K + 2K + 105K} = 21.5\ K$$

If current from the exciter was flowing in the opposite direction through the rectifiers, the back resistance would be considerably larger and the loading effect would be greatly diminished.

A gas tube has a dynamic resistance of approximately 40 ohms, which for practical purposes can be considered as a short in the reference supply circuit. By measurement, the portion of the potentiometer shorted to the negative side through the gas tubes, for a 120-volt setting was found to be:

$$R_{c2} = 6{,}670 \text{ ohms}$$

Thus
$$R_c = R_{c1} + R_{c2}$$

$$= 21.5K + 6.67K$$

$$= 28.2K$$

Using the nodal method of solution, the following equation can be written from Fig. 7.2(b)

$$E_o(s)\left(\frac{G_a C_1 s}{G_a + C_1 s} + G_b + \frac{G_c C_2 s}{G_c + C_2 s}\right) = E_i(s)\left(\frac{G_a C_1 s}{G_a + C_1 s}\right)$$

from which

$$\frac{E_o(s)}{E_i(s)} = \frac{G_a G_c C_1 s + G_a C_1 C_2 s^2}{G_a G_c C_1 s + G_a C_1 C_2 s^2 + G_a G_b G_c + (G_b G_c C_1 + G_a G_b C_2)s + G_b C_1 C_2 s^2 + G_a G_c C_2 s + G_c C_1 C_2 s^2}$$

At this stage it is advantageous to substitute in numerical values,

$$G_a = \frac{1}{2.4K} = 4.16 \times 10^{-4} \text{ mhos}$$

$$G_b = \frac{1}{8.0K} = 1.25 \times 10^{-4} \text{ mhos}$$

$$G_c = \frac{1}{28.2K} = 0.335 \times 10^{-4} \text{ mhos}$$

The solution then simplifies to

$$\frac{E_o(s)}{E_i(s)} = \frac{14.75 \times 10^{-14} s\ (1 + 0.0294\ s)}{61.11 \times 10^{-16} s^2 + 26.27 \times 10^{-14} s + 1.85 \times 10^{-12}}$$

or

$$\frac{E_o(s)}{E_i(s)} = \frac{23.1\ s\ (1 + 0.0294\ s)}{s^2 + 43.0\ s + 303}$$

Factoring the denominator yields,

$$\frac{E_o(s)}{E_i(s)} = H_3(s) = \frac{23.1s\ (1 + .0294s)}{(s + 34.1)(s + 8.9)}$$

Rewriting the denominator so that it will possess time constants,

$$H_3(s) = \frac{23.1s\ (1 + .0294s)}{8.9 \times 34.1(1 + 0.0293s)(1 + 0.112\ s)}$$

A term in the numerator and in the denominator conveniently cancel to give

$$H_3(s) = \frac{0.076s}{(1 + 0.112s)}$$

$H_3(s)$, which is the transfer function taking loading into account, does not deviate considerably from the transfer function which disregarded loading,

$$H_2(s) = \frac{0.08s}{(1 + 0.104s)}$$

Since it may at times be desirable to change the amount of feedback in the minor loop by adjusting the potentiometer, a new transfer function must be calculated for each setting. $H_2(s)$ can be recalculated with little difficulty whereas the evaluation of $H_3(s)$ involves much more labor. Hence, $H_2(s)$ will be taken as the minor-loop feedback element, Fig. 7.4.

Before proceeding with the analysis of the effect of the minor feedback loop $G_1G_2G_3H_2$ on the system, the open-loop transfer function should be checked for stability. The minor-loop transfer function is of the minimum-phase type (contains no poles or zeroes in the right half of the s plane) and was connected so as to supply negative feedback at the summing point. Once again the Bode diagram may be utilized to determine the crossover frequency and phase margin. If the potentiometer setting on the anti-hunt circuit is left unchanged so that $R_b = 8K$, Graph 7.2, shows that the crossover frequency for this setting is 340 rad/sec.

Thus $$\beta_c = \frac{\pi}{2} - \left(\frac{\pi}{2} - \frac{8.7}{340}\right) - \left(\frac{\pi}{2} - \frac{9.6}{340}\right)$$

$$= -87^\circ$$

indicating a stable loop.

To obtain the major-loop transfer function the minor loop must be closed and the over-all transfer function be determined,

$$\frac{E_e}{R_1} = \frac{G_1G_2G_3}{1 + G_1G_2G_3H_2}$$

Then the corrected major loop becomes

$$A_M = \frac{G_1\ G_2\ G_3}{1 + G_1G_2G_3H_2} \times G_4H_1$$

To represent the above transfer function asymptotically, two special cases will be considered.

(1) When the minor-loop gain,

$| A_m | \ll 1$

$$\frac{E_e}{R_1} = G_1G_2G_3$$

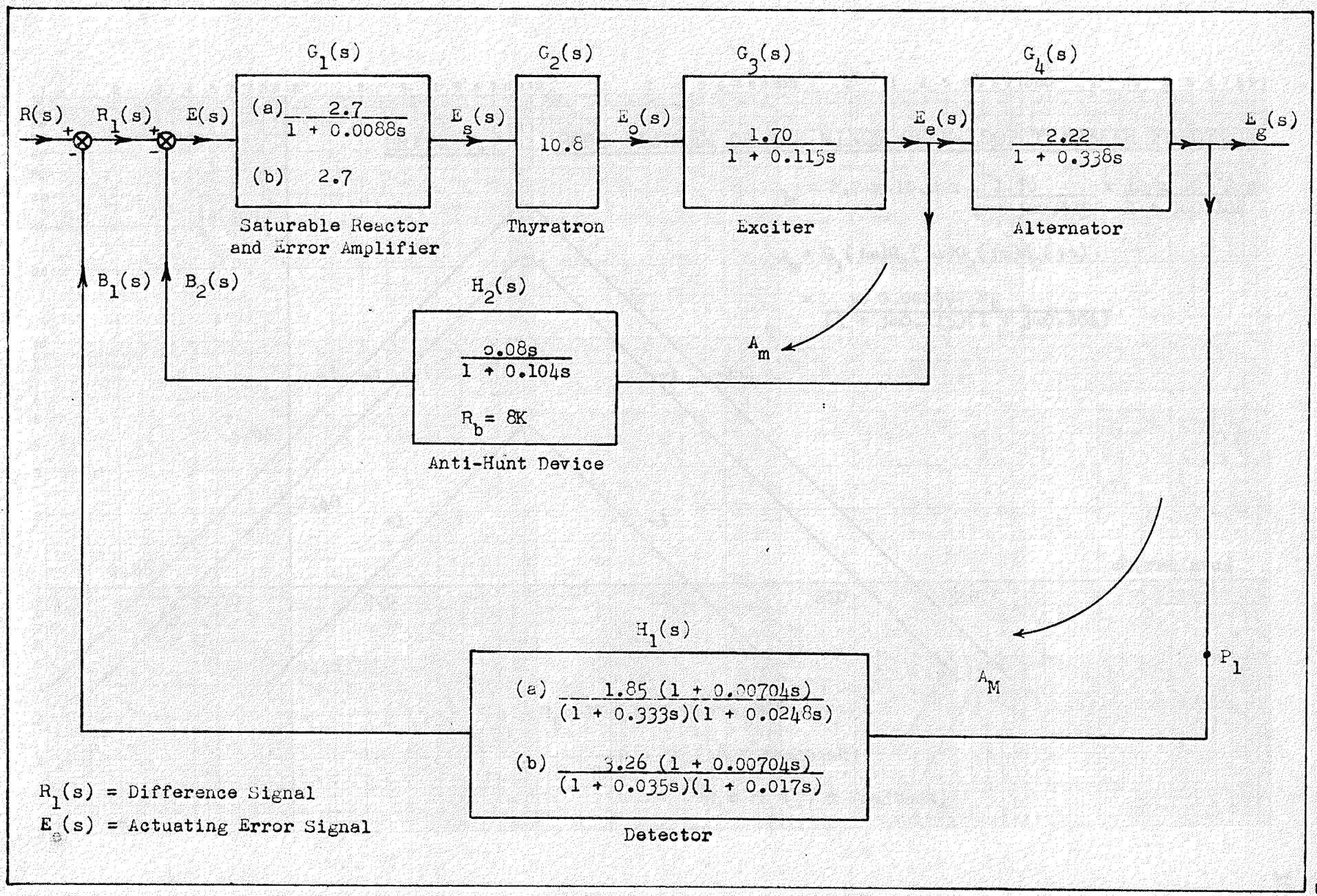

FIG. 7.4 BLOCK DIAGRAM OF COMPENSATED VOLTAGE-REGULATING SYSTEM

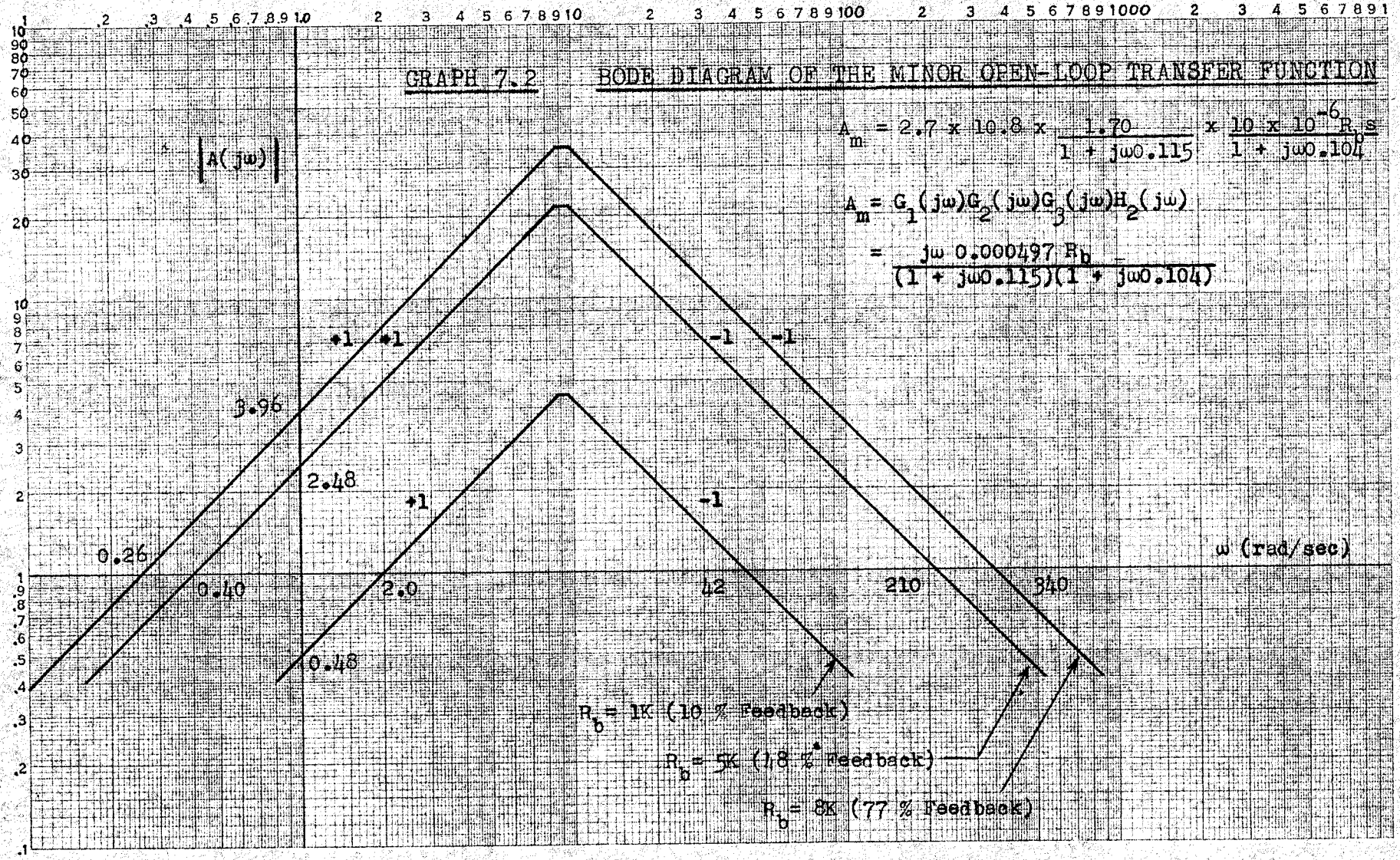
GRAPH 7.2 BODE DIAGRAM OF THE MINOR OPEN-LOOP TRANSFER FUNCTION
$A_m = 2.7 \times 10.8 \times \frac{1.70}{1 + j\omega 0.115} \times \frac{10 \times 10^{-6} R_b s}{1 + j\omega 0.104}$
$A_m = G_1(j\omega)G_2(j\omega)G_3(j\omega)H_2(j\omega)$
$= \frac{j\omega\, 0.000497\, R_b}{(1 + j\omega 0.115)(1 + j\omega 0.104)}$
$|A(j\omega)|$
+1
+1
-1
-1
3.96
2.48
+1
-1
0.26
0.40
2.0
42
210
340
0.48
ω (rad/sec)
R_b = 1K (10 % Feedback)
R_b = 5K (18 % Feedback)
R_b = 8K (77 % Feedback)

(2) When $|A_m| \gg 1$

$$\frac{E_e}{R_1} = \frac{1}{H_2}$$

The same conditions will hold for the corrected major loop,

(1) When $|A_m| \ll 1$

$$A_M = G_1G_2G_3G_4H_1 \qquad \text{- - - - - - - - (7-1)}$$

(2) When $|A_m| \gg 1$

$$A_M = \frac{G_4H_1}{H_2} \qquad \text{- - - - - - - - (7-2)}$$

Therefore, in order to plot the corrected major loop asymptotically, two ranges of frequencies must be considered. Whenever the gain of A_m is greater than one, the transfer function as specified by equation 7-2 will be plotted and similarly where the gain of A_m is less than one the transfer function in equation 7-1 will be plotted.

It is immediately obvious that considerable error may exist where the gain of A_m is equal to unity, however this error is small if there are no break-points in this vicinity.

Graph 7.3 shows the Bode diagram for the corrected major loop of $A_2(j\omega)$ with three settings of the anti-hunt circuit, R_b = 1K, 5K and 8K. With R_b = 8K, the minor loop gain becomes greater than one at ω = 0.26 rad/sec. Beyond this point the transfer function becomes

$$A_{M2} = \frac{G_4(j\omega)\, H_1(j\omega)}{H_2(j\omega)}$$

$$= \frac{90.5\,(1 \mp j\omega 0.00704)(1 + j\omega 0.104)}{j\omega(1 + j\omega 0.338)(1 + j\omega 0.035)(1 + j\omega 0.017)}$$

This transfer function remains unchanged until ω = 340 rad/sec or when the gain of A_m falls below one. The crossover frequency for an anti-hunt circuit setting of 8K is 28.6 rad/sec.

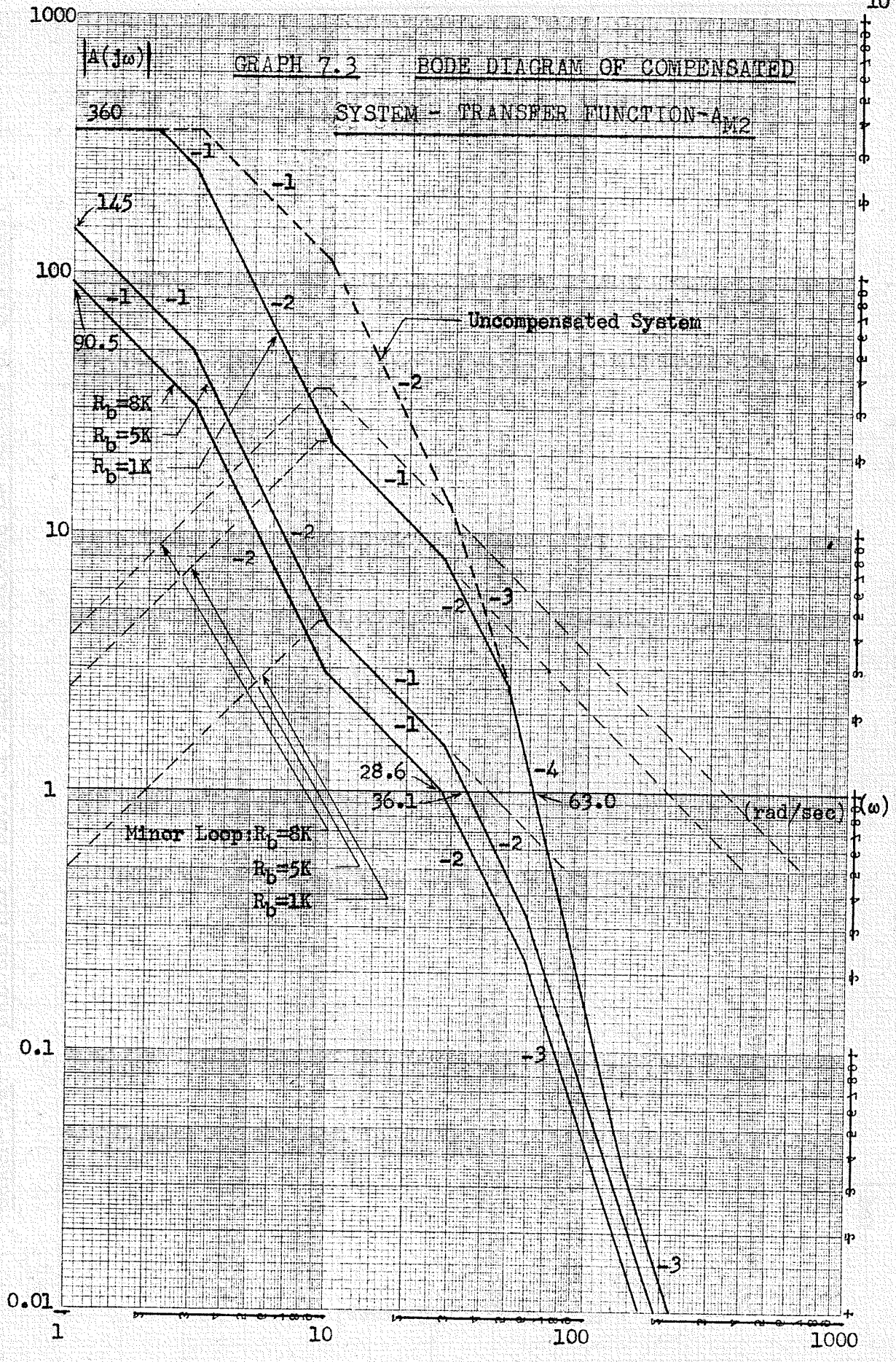

W.Tishinski, March/59.

THIS MARGIN RESERVED FOR BINDING

IF SHEET IS READ THE OTHER WAY (VERTICALLY), THIS MUST BE LEFT-HAND SIDE.

GRAPH 7.4 CALCULATED EFFECT OF FEEDBACK SIGNAL ON DEGREE OF STABILITY

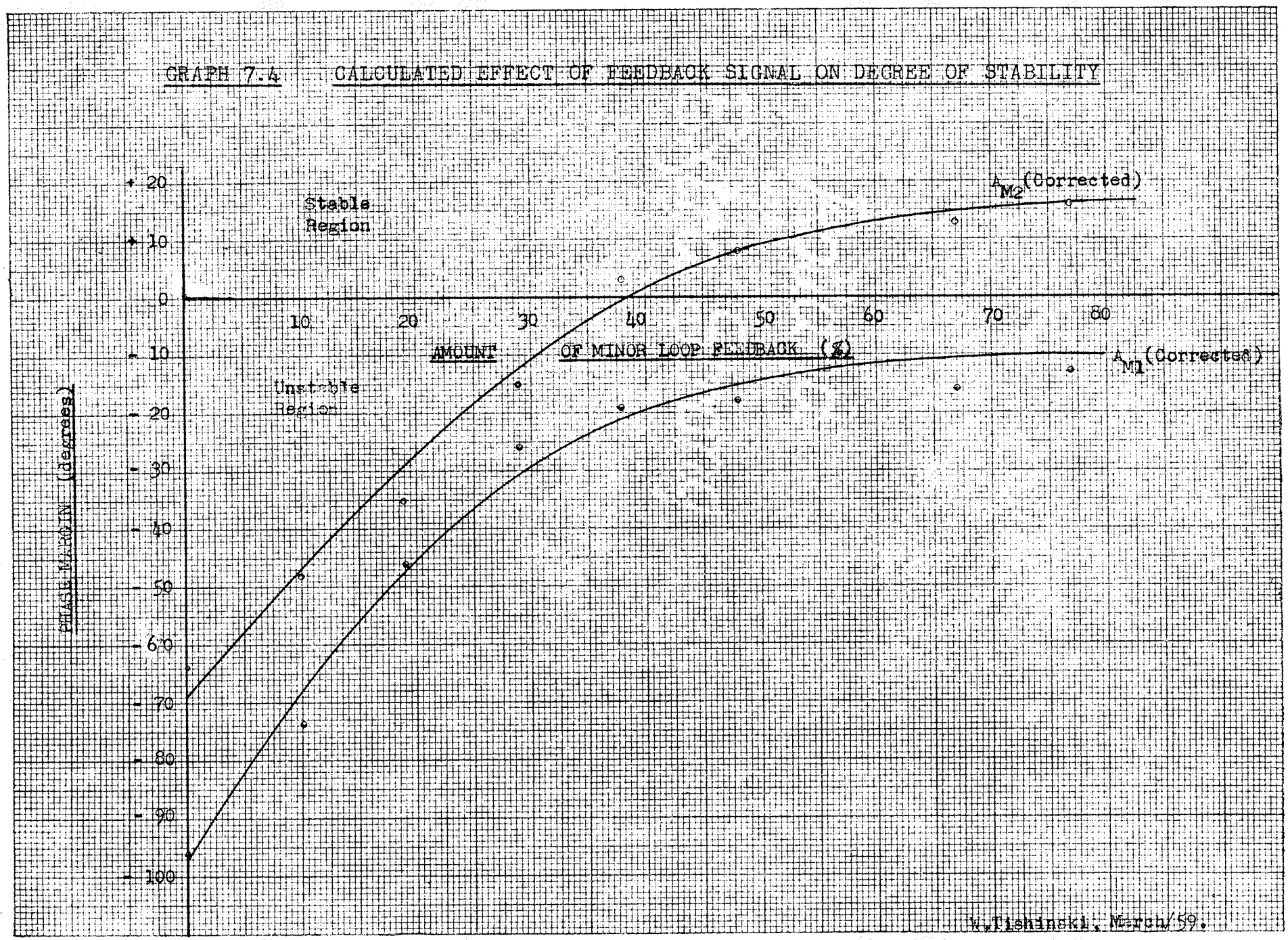

W. Tishinski, March/59.

MANUFACTURED BY RENOUF PUBLISHING CO., MONTREAL FORM 100

Then

$$\beta_c = \frac{-\pi}{2} - \left(\frac{\pi}{2} - \frac{2.96}{28.6}\right) + \left(\frac{\pi}{2} - \frac{9.6}{28.6}\right) - \tan^{-1}\frac{28.6}{28.6} - \frac{28.6}{59} + \frac{28.6}{142}$$

$$= -2.86 \text{ rad/sec}$$

$$= -164^\circ$$

This amount of phase shift indicates that the system is stable. The arc tan approximation is not accurate if ω_c/ω_1 is greater than one half. In this case the phase shift must be evaluated by the inverse tangent relation.

If R_b is decreased to 1K, $\omega_c = 63$ rad/sec and

$$\beta_c = -\frac{\pi}{2} - \left(\frac{\pi}{2} - \frac{2.96}{63}\right) + \left(\frac{\pi}{2} - \frac{9.6}{63}\right) - \left(\frac{\pi}{2} - \frac{28.6}{63}\right) - \tan^{-1}\frac{63}{59} - \frac{63}{114} + \frac{63}{142}$$

$$= -3.715 \text{ rad/sec}$$

$$= -213^\circ$$

which indicates instability.

Some intermediate setting will yield a 0-degree phase margin and place the system on the verge of instability. The phase shift will be calculated for other R_b settings and a curve plotted to show the effect of the variation of this control on stability, Graph 7.4.

If $R_b = 5K$

$$H_2(j\omega) = \frac{j\omega\, 0.05}{1 + j\omega 0.104}$$

and

$$\frac{G_4(j\omega)\, H_1(j\omega)}{H_2(j\omega)} = \frac{145(1 + j\omega\, 0.00704)(1 + j\omega\, 0.104)}{j\omega\,(1 + j\omega\, 0.338)(1 + j\omega 0.035)(1 + j\omega 0.017)}$$

If R_b is changed, the only change in $G_4(j\omega)H_1(j\omega)/\ H_2(j\omega)$ will be in the gain. With $R_b = 8K$ the gain of $G_4(j\omega)\ H_1(j\omega)/\ H_2(j\omega) = 90.5$.

Therefore, for the setting of $R_b = 5K$, A_{M2} will lie above the plot with the setting of $R_b = 8K$, by a gain of 145/90.5 or 1.60. This ratio permits the evaluation of the crossover frequency for any setting of R_b without plotting the whole curve, provided that no break-points

cross the unity axis as the total plot moves upwards, and that the second crossover frequency of $H_2(j\omega)$ is greater than the evaluated ω_c.

By similar triangles, Graph 7.3,

$$\frac{\log 1.60}{\log \omega_c/28.6} = -2$$

or $$\log \sqrt{1.60} = \log \left(\frac{\omega_c}{28.6}\right)$$

and $$\omega_c = \sqrt{1.60} \times 28.6$$

$$= 36.1 \text{ rad/sec}$$

which is the crossover frequency for A_{M2} when R_b = 5K.

Similar calculations were carried out for other settings of R_b. The amount of feedback can also be expressed on a percentage basis of the total available feedback from the anti-hunt circuit. This is evaluated as

$$\frac{R_b}{10.4 \text{ K}} \times 100 \%$$

TABLE 7.1

RELATION BETWEEN R_b AND PHASE SHIFT OF TRANSFER FUNCTION A_{M2} $(j\omega)$

R_b	Feedback (%)	ω_c (rad/sec)	β_c (degrees)	Phase Margin (degrees)
8K	77	28.6	- 164	+ 16
7K	67	30.4	- 167	+ 13
5K	48	36.1	- 172	+ 8
4K	38	40.4	- 177	+ 3
3K	29	47.0	- 195	- 15
2K	19	59.0	- 215	- 35
1K	10	63.0	- 228	- 48
0K	0	63.0	- 244	- 64

A Bode diagram of $A_{M1}(j\omega)$ with an R_b setting of 8K, Graph 7.5, indicates a crossover frequency of 7.6 rad/sec.

Thus,

$$\beta_c = -\frac{\pi}{2} - 2\left(\frac{\pi}{2} - \frac{2.98}{7.6}\right) + \frac{7.6}{9.6} - \frac{7.6}{40.4} + \frac{7.6}{142}$$

$$= -3.373 \text{ rad/sec}$$

$$= -193^{\circ}$$

For other settings of R_b the phase shift was evaluated and tabulated.

TABLE 7.2

RELATION BETWEEN R_b and PHASE SHIFT OF TRANSFER FUNCTION $A_{M1}(j\omega)$

R_b	Feedback (%)	ω_c(rad/sec)	β_c(degrees)	Phase Margin (degrees)
8K	77	7.6	- 193	-13
7K	67	7.9	- 196	-16
5K	48	8.9	- 198	-18
4K	38	9.5	- 199	-19
3K	29	11.5	- 206	-26
2K	19	14.1	- 226	-46
1K	10	19.0	- 254	-74
0	0	25.8	- 276	-96

The Bode diagram has presented a vivid picture of how $H_2(s)$ modifies the major loop. The transfer function from R_1 to E_e becomes almost independent of the time constants in G_1 and G_3 for the entire frequency range where the minor-loop gain exceeds unity. Therefore, all lags in G_1 and G_3 have been eliminated from the major loop. A minor feedback around G_4 would have been more effective due to the larger time constant in this transfer element. However, as mentioned previously, rectifying problems would have entered here.

Had the time constant of $H_2(s)$ been made larger, a larger leading effect would be present in the minor open-loop, but a larger lag effect would exist in the over-all transfer function. This is because $H_2(s)$ appears in the denominator of E_e/R_1, thus contributing a negative angle

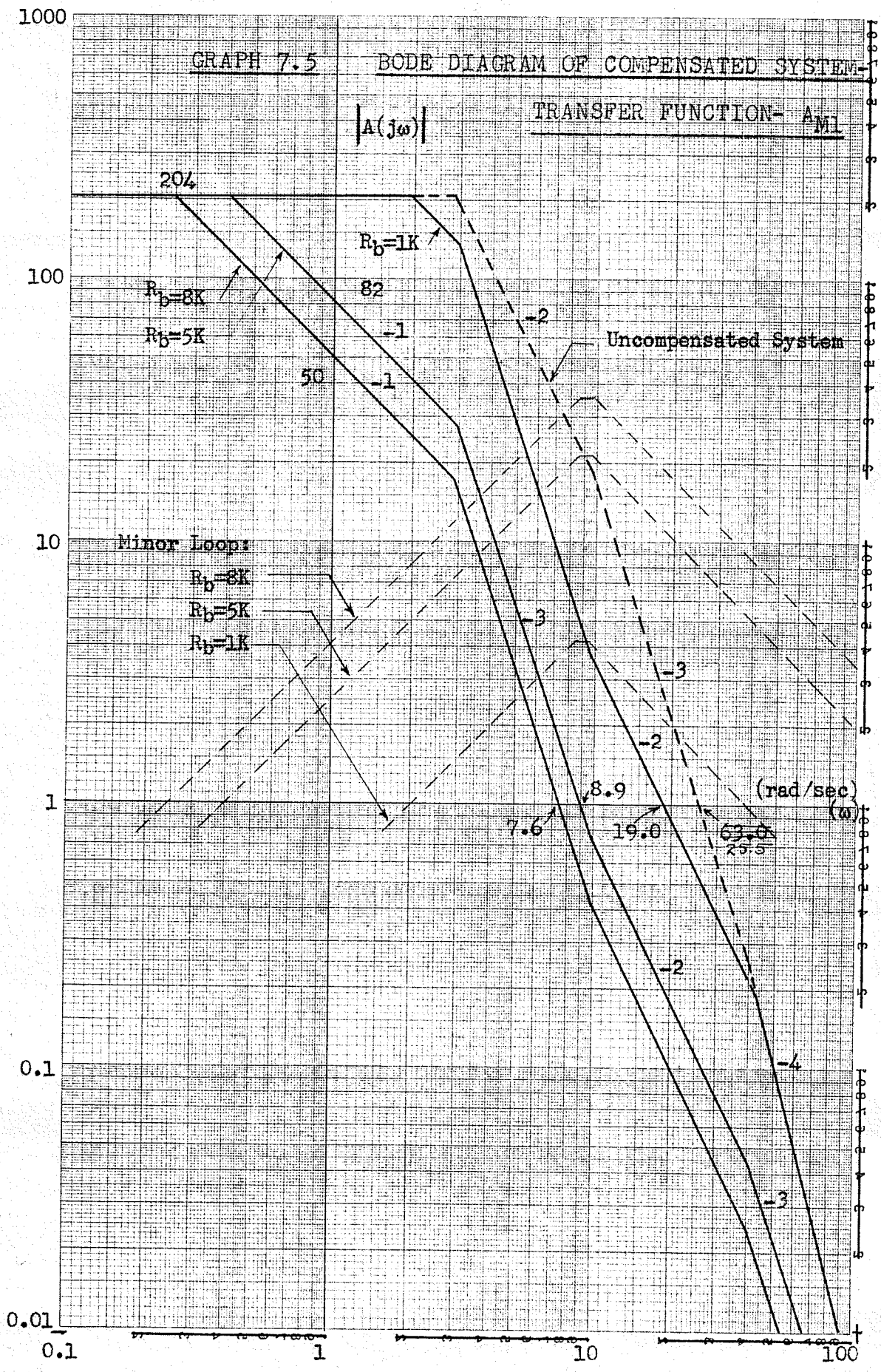

W.Tishinski, March/59.

to the phase shift. So even if a greater degree of stability is achieved it is done so at the sacrifice of gain.

Decreasing the value of R_b in the anti-hunt or minor feedback circuit has two effects on the major-loop transfer function:

(1) It narrows the frequency range in which $H_2(s)$ is effective.

(2) It contributes less correction and thus moves the crossover frequency closer to the uncorrected unstable value of crossover frequency.

In the actual physical arrangement this type of feedback stabilization proved to be the answer to the stability problem. The setting of R_b at which no-load oscillations began to occur was not a definite value but depended on the voltage output of the alternator. A test was conducted to determine at what R_b settings the system would begin to oscillate for various alternator terminal voltages, Graph 7.6.

TABLE 7.3

MINIMUM AMOUNT OF ANTI-HUNT SIGNAL THAT WILL MAINTAIN STABILITY AT VARIOUS ALTERNATOR TERMINAL VOLTAGES.

Alternator is at no load.

Alternator Terminal Voltage (volts)	Feedback Signal (%)
133	28
126	34
120	36
110	42
100	47
90	50
80	55
70	58
66	59

No direct correlation can be obtained between Graphs 7.4 and 7.6. Calculations show only one value of R_b for which the phase shift of the system becomes 180 degrees - placing the system on the verge of instability. Test results show that the setting of R_b, which determines the amount of feedback signal, does not alone determine stability. Saturation as well, is a vital factor in determining the degree of stability. It can be seen from Graph 7.6 that as the terminal voltage increases, saturation is more pronounced and less feedback signal is necessary for stabilization. This effect will be analyzed in the next section.

The Bode diagram indicates that with the selected time constant of 0.104 sec for $H_2(s)$ it is possible to attain stability when considering $A_2(s)$ but not with $A_1(s)$. It was noted in section 3.2 that $A_1(s)$ existed whenever the input voltage of the detector circuit decreased. For this case, a large time constant, due to the back resistance of the of the rectifiers, resulted in $H_1(s)$. However, the normal current flow is in the forward direction which is associated with the build-up process of the detector circuit and thus $A_2(s)$ is applicable. Since the Bode diagram has shown that stability was attained by considering $A_2(s)$, with the feedback element $H_2(s)$, and this was proven by test to be true, then it can safely be concluded that $A_2(s)$ is the proper transfer function for the uncorrected major loop.

With an external disturbance, such as the application of load to the alternator, the input voltage to the detector circuit falls by a considerable extent, forcing the transfer function $A_1(s)$ to exist.

The Nyquist diagram is a more exact indication of the system's stability than the Bode diagram. Hence, calculations will be carried out to determine the points for the polar plot with an R_b setting of 5K and considering both, $A_1(j\omega)$ and $A_2(j\omega)$.

However, first of all it is necessary to check the minor loop, $G_1G_2G_3H_2$ for any encirclements of the critical point in the Nyquist diagram.

MANUFACTURED BY RENOUF PUBLISHING CO., MONTREAL

GRAPH 7.6 EFFECT OF ALTERNATOR TERMINAL VOLTAGE AND FEEDBACK ON SYSTEM STABILITY

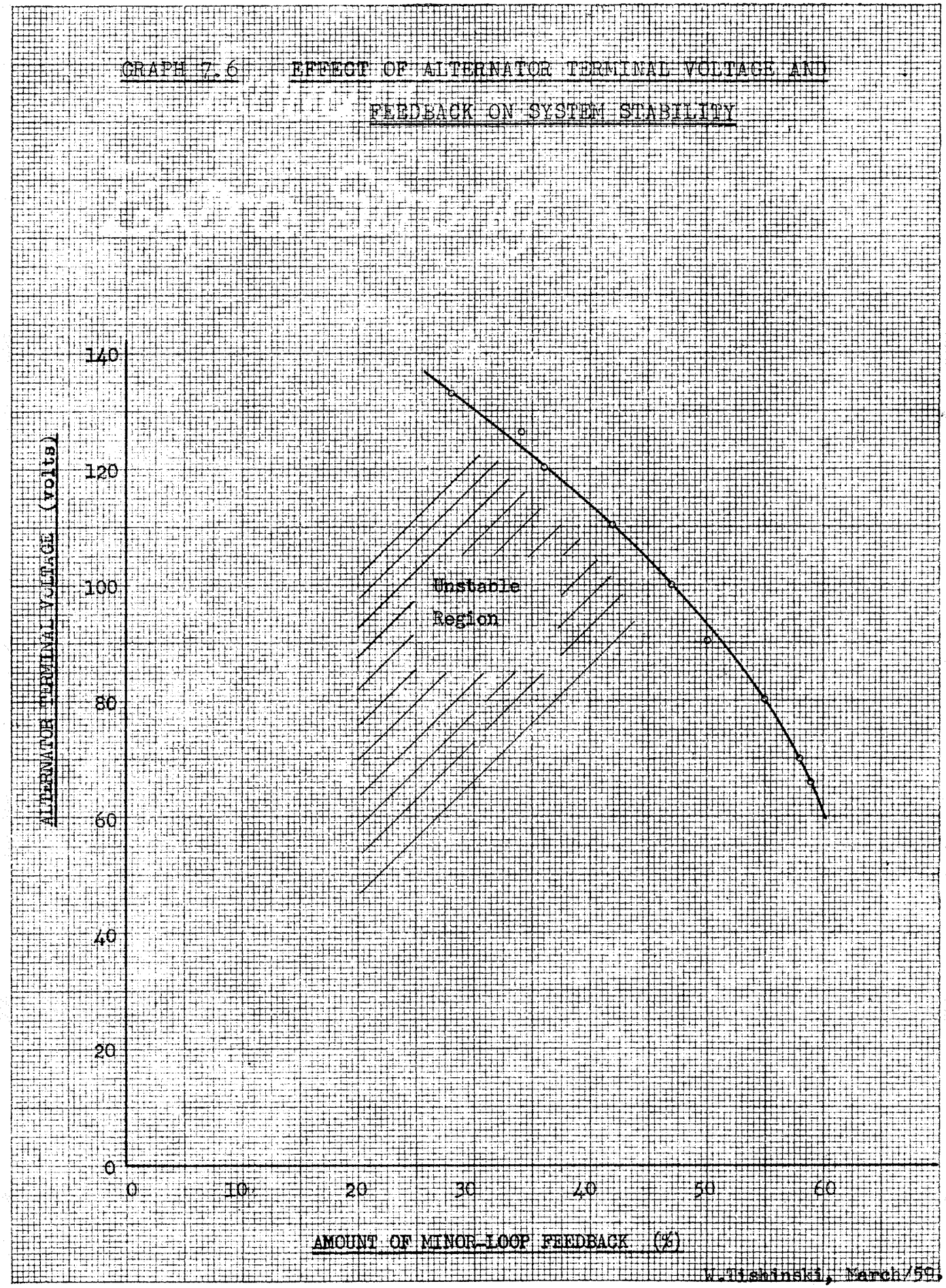

W.Tiskinski, March/59.

IF SHEET IS READ THE OTHER WAY (VERTICALLY), THIS MUST BE LEFT-HAND SIDE.

TABLE 7.4

TABULATION OF POINTS FOR POLAR PLOT OF

$$A_m(j\omega) = G_1(j\omega)G_2(j\omega)G_3(j\omega)H_2(j\omega)$$

$$= \frac{j\omega\, 2.48}{(1 + j\omega\, 0.115)(1 + j\omega 0.104)}$$

ω (rad/sec)	$\lvert A_m(j\omega) \rvert$	Phase Shift (degrees)
0	0	0
1	2.4	$77^\circ 30'$
2	4.8	$65^\circ 20'$
3	6.7	$57^\circ 40'$
5	9.6	$32^\circ 30'$
7	10.9	$15^\circ 20'$
10	11.3	$-5^\circ 10'$
15	10.0	$-27^\circ 20'$
20	8.6	$-40^\circ 50'$
30	6.3	$-56^\circ 0'$
45	4.7	$-67^\circ 10'$
100	2.1	$-79^\circ 30'$
500	0.4	$-87^\circ 50'$

Graph 7.7 shows that the polar plot of the minor-loop transfer function has no encirclements of the critical point - 1 + jo.

Therefore, number of zeroes - number of poles = 0 in the right half s plane for $1 + A_m(s)$. Since no poles of the open-loop function exist in the right half plane, the number of zeroes must also be zero. Therefore, there are no poles in the closed-loop forward transfer function of $A_m(s)$. Further examination reveals no poles in the right half of the s plane for the remaining transfer elements in the major loop. Thus, any encirclements of the critical point by the corrected major open-loop function will indicate the presence of zeroes, hence instability.

GRAPH 7.7 POLAR PLOT OF MINOR LOOP

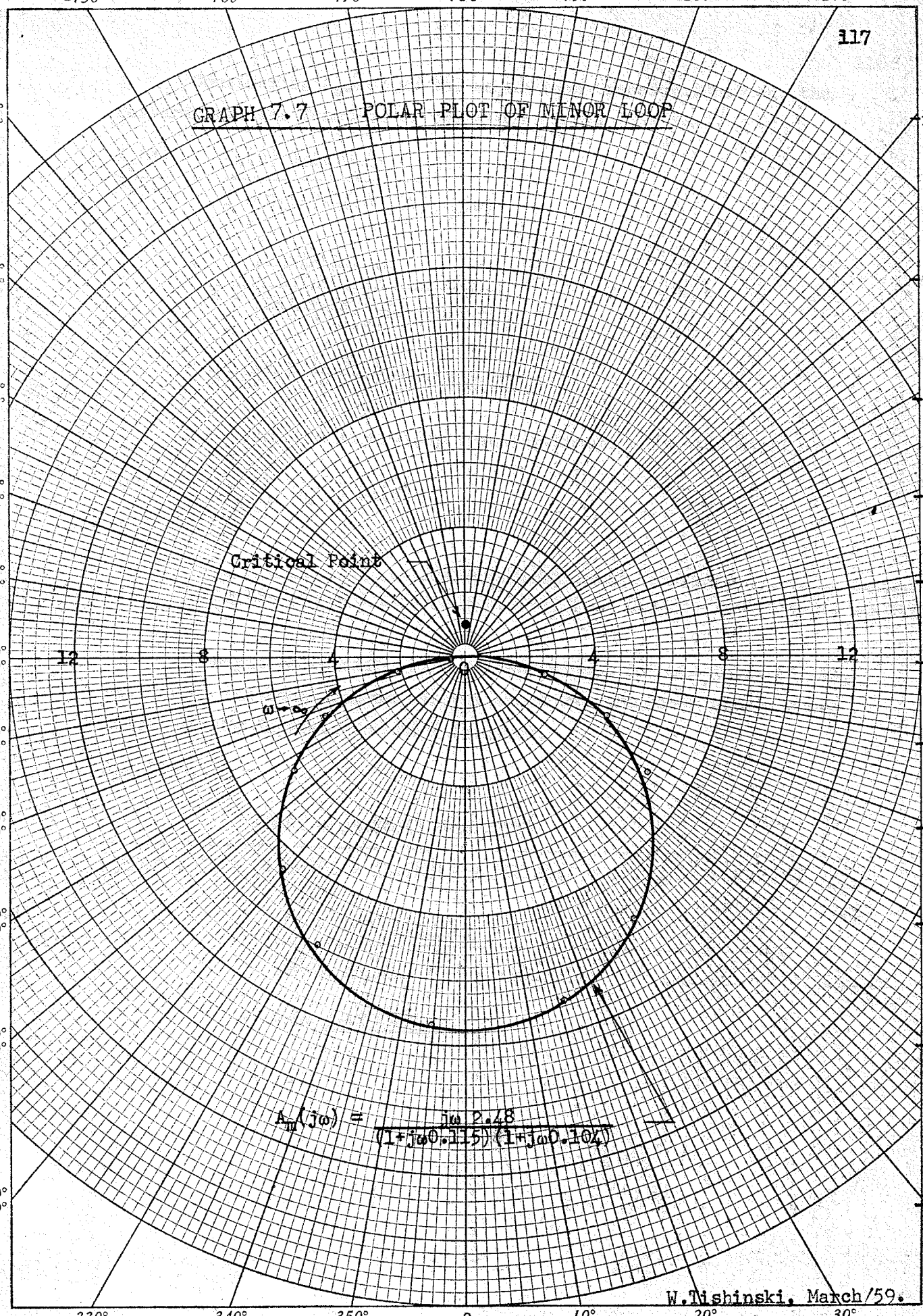

W.Tishinski, March/59.

Considering $A_{M2}(s)$ as the major-loop transfer function, the forward transfer function of the minor closed loop is

$$\frac{E_e(s)}{R_1(s)} = \frac{G_1(s)\, G_2(s) G_3(s)}{1 + G_1(s) G_2(s) G_3(s)\, H_2(s)}$$

$$= \frac{\dfrac{49.7}{(1 + 0.115\, s)}}{1 + \dfrac{49.7 \times 0.05\, s}{(1 + 0.115s)(1 + 0.104s)}}$$

$$= \frac{49.7(1 + 0.104s)}{2.48s + (1 + 0.115s)(1 + 0.104s)}$$

The corrected major-loop transfer function is then simply

$$A_{M2} = \frac{E_e(s)}{R_1(s)}\, G_4(s)\, H_1(s)$$

$$= \frac{360(1 + 0.104s)(1 + 0.00704s)}{\Big(2.48s + (1 + 0.115s)(1 + 0.104s)\Big)(1 + 0.338s)(1 + 0.035s)(1 + 0.017s)}$$

A sample calculation will be carried out for $\omega = 36.1$ rad/sec, which from the Bode diagram was the crossover frequency with a phase shift of -172 degrees, for 48 % feedback.

$$A_{M2}(j36.1) =$$

$$\frac{360(1 + j3.78)(1 + j0.254)}{\Big(j89.6 + (1 + j4.16)(1 + j3.78)\Big)(1 + j12.2)(1 + j1.26)(1 + j0.614)}$$

$$= \frac{360 \times 3.89\, \underline{/75^\circ 05'} \times 1.03\, \underline{/14^\circ 15'}}{(98.5\, \underline{/98^\circ 30'})\, 12.2\, \underline{/85^\circ 20'} \times 1.60\, \underline{/51^\circ 30'} \times 1.17\, \underline{/31^\circ 30'}}$$

$$= 0.64\, \underline{/-179^\circ 40'}$$

TABLE 7.5

TABULATION OF CALCULATED POINTS FOR POLAR PLOT OF A_{M^2}

ω (rad/sec)	$\lvert A_{M^2}(j\omega) \rvert$	Phase Shift (degrees)
7.0	8.78	$-137^{\circ}40'$
10.0	5.12	$-142^{\circ}10'$
15.0	2.74	$-150^{\circ}\ 0'$
20.0	1.76	$-158^{\circ}10'$
30.0	0.89	$-170^{\circ}50'$
36.1	0.64	$-179^{\circ}40'$
45.0	0.41	$-196^{\circ}30'$

If the original transfer function $A_1(s)$ is considered then the corrected major-loop transfer function becomes

$$A_{M^1}(s) = \frac{204(1 + 0.104s)(1 + 0.00704s)}{\Big(2.48s + (1 + 0.115s)(1 + 0.104s)\Big)(1 + 0.338s)(1 + 0.333s)(1 + 0.0248s)}$$

TABLE 7.6

TABULATION OF CALCULATED POINTS FOR POLAR PLOT OF A_{M^1}

ω(rad/sec)	$\lvert A_{M^1}(j\omega) \rvert$	Phase Shift (degrees)
4	7.57	$-174^{\circ}50'$
5	4.60	$-182^{\circ}20'$
7	2.04	$-193^{\circ}40'$
10	0.87	$-200^{\circ}40'$
15	0.33	$-207^{\circ}10'$
20	0.17	$-212^{\circ}10'$
30	0.06	$-218^{\circ}20'$
45	0.02	$-225^{\circ}50'$

The Nyquist diagram, Graph 7.8, shows that A_{M^2} is stable, but A_{M^1} is not. This agrees with the result obtained from the Bode diagram.

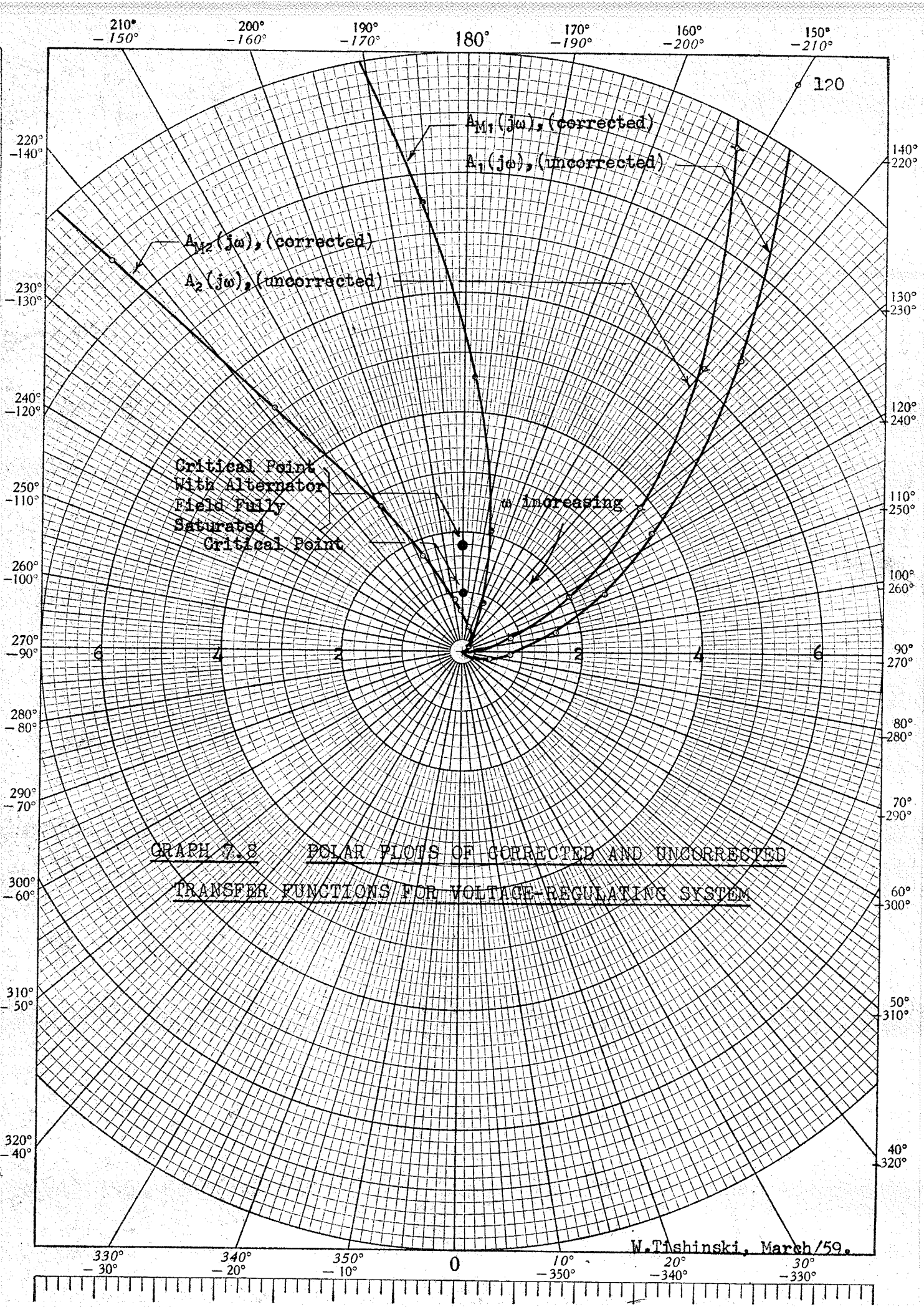

GRAPH 7.8 POLAR PLOTS OF CORRECTED AND UNCORRECTED TRANSFER FUNCTIONS FOR VOLTAGE-REGULATING SYSTEM

7.3 Effect of Saturation on Stability

In the preceding sections, the regulating system was treated with the assumption that no saturation was present. Saturation, in varying degrees, is present in all of the iron-core control elements. The saturable reactor, Graph 2.1, is linear in the normal operating range but if the d-c control current swings to an extreme positive direction the iron core saturates and no additional phase shift can occur. Similarily, with the exciter and alternator saturation curves, if the field current is increased the generated voltage begins to depart from the linear relation at a certain point. It is readily seen that additional saturation provides the system with greater stability since, beyond the saturating point the gain is decreased and a decrease in gain is always associated with a more stable system.

When dealing with saturable control elements, the input over the output relation is referred to as the "describing function." In the study of non-linear control systems the basic assumption made is that if the input to the non-linear element is sinusoidal and constant in amplitude, the output will be periodic of the same frequency. For a step input to the saturated element, the above assumption is in error if only the fundamental component of the sine wave input is selected[1]. However, for conditions where sustained oscillations are maintained, the input amplitude tends to be nearly sinusoidal and the use of the assumed sinusoidal input is quite valid. Where sustained oscillations are not maintained and the system tends to be stable, the use of the assumed sinusoidal input indicates a value of gain for the saturated element that predicts an initial performance comparing favourably with the actual system performance.

To provide a means for simplifying the analysis of the saturation problem, it is assumed that the actual output-input curve can be approximated by an ideal saturation curve, Graph B.1 and Fig. 7.5(a). Thus, for a sinusoidal input, Fig. 7.5(b), the output will be linear until the saturating point O_s is reached beyond which there is no additional output for an increase in input.

---

1. H. Chestnut and R. Mayer, Servomechanisms and Regulating Systems, Vol. II, pp. 279, J. Wiley and Sons, 1955.

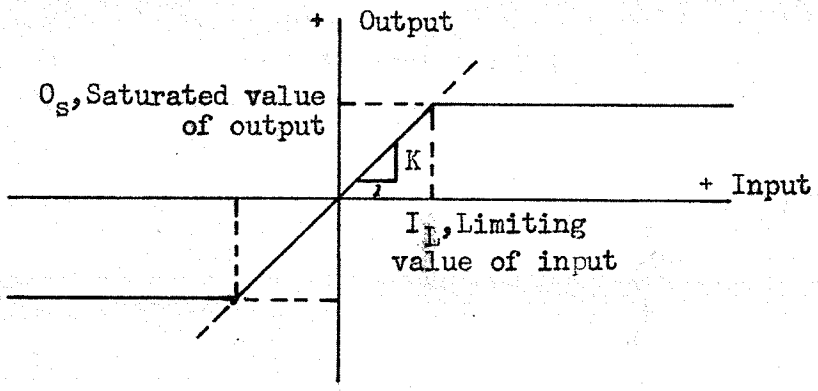

(a) IDEALIZED SATURATION CHARACTERISTIC

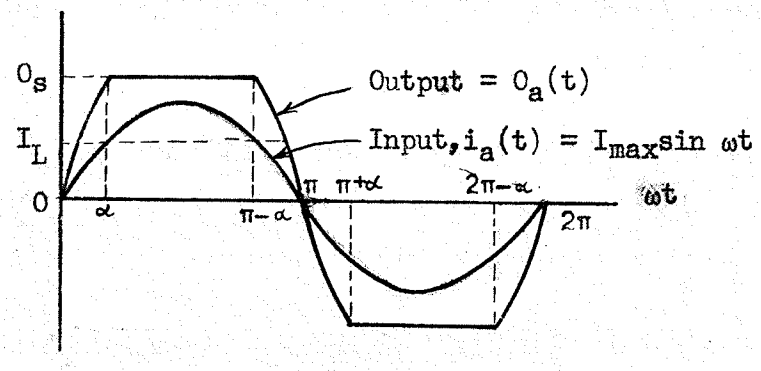

(b) OUTPUT $O_a(t)$ AS A FUNCTION OF TIME FOR INPUT, $i_a(t) = I_{max} \sin \omega t$, TO A SATURATED ELEMENT WITH $I_{max} > I_L$, THE LIMITING VALUE OF THE INPUT QUANTITY

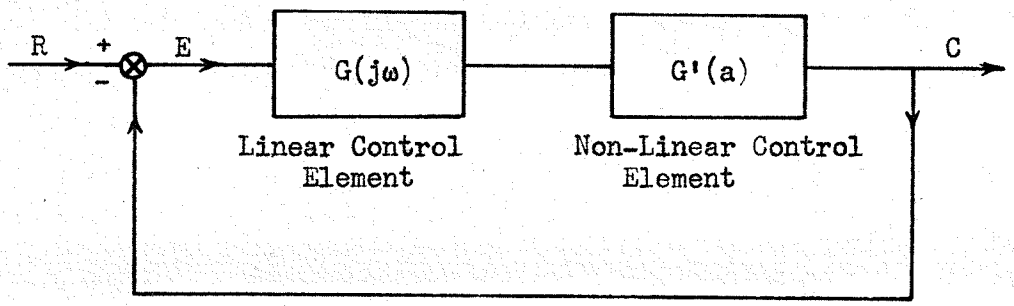

(c) SIMPLE CONTROL SYSTEM HAVING LINEAR AND NON-LINEAR CONTROL ELEMENTS

FIG. 7.5 TREATMENT OF NON-LINEAR ELEMENTS

If the input to the saturating element is given by

$$i_a(t) = I_m \sin\omega t$$

three regions must be considered for the output.

(a) $o < \omega t < \alpha$; $\quad o_a(t) = KI_m \sin\omega t$

(b) $\alpha < \omega t < \pi - \alpha$; $\quad o_a(t) = KI_L = KI_m \sin\alpha$

(c) $\pi - \alpha < \omega t < \pi$; $\quad o_a(t) = KI_m \sin\omega t$

- - - - - - - (7.1)

where $\alpha = \sin^{-1} I_L/I_m$

The actual output to the sinusoidal input can be represented by a Fourier series as

$$o_a(t) = \frac{1}{2} \sum_{n=-\infty}^{n=+\infty} o_{an}\, e^{jn\omega t}$$

where o_{an} is a complex number having both magnitude and phase at each frequency and is given by

$$o_{an} = \frac{1}{\pi} \int_{-\pi}^{+\pi} o_a(t)\; e^{-jn\omega t}\; d(\omega t)$$

- - - - - - - (7.2)

Since there is no phase shift between the output and input for the saturation case, only the fundamental component of the output need be considered. By utilizing equations 7.1 and 7.2, one obtains

$$o_{a1} = \frac{2KI_m}{\pi} \left(2\int_o^{\alpha} \sin^2\omega t\; d(\omega t) + \int_{\alpha}^{\pi-\alpha} \sin\alpha \sin\omega t\; d(\omega t) \right.$$

from which

$$o_{a1} = \frac{KI_m}{\pi} (2\alpha + \sin 2\alpha)$$

The describing function is defined as [1]

$$G'(a) = \frac{o_{a1}}{I_m}$$

---

1. H. Chestnut and R. Mayer, Servomechanisms and Regulating System Design, Vol. II, pp. 244, J. Wiley and Sons, 1955.

thus,

$$G'(a) = \frac{K}{\pi} (2\alpha + \sin 2\alpha)$$

If the above equation is applied to the alternator, K = 100 and

$$G'(a) = \frac{100}{\pi} (2\alpha + \sin 2\alpha)$$

By test, Appendix B.3, it has been found that the maximum current, I_m that can be supplied to the alternator field is 3.66 amps. From the construction on Graph B.1, I_L was found to 1.70 amps.

Hence,

$$\alpha = \sin^{-1} \frac{1.70}{3.66}$$

$$= 0.475 \text{ radians}$$

from which

$$G'(a) = \frac{100}{\pi} \left(2 \times 0.475 + \sin (2 \times 0.475)\right)$$

$$= 100 \times 0.56$$

Essentially, the gain is reduced by 0.56, due to the saturation of the alternator field, if the alternator is operating at its maximum available voltage. Normally, operation would not take place at full saturation but at some intermediate region. The above results must be interpreted on either the Nyquist or Bode diagram to indicate what extent saturation contributes to the stabilization of the system.

If a linear and a non-linear element compose a servomechanism system, Fig. 7.5(c), the closed-loop transfer function can be written as

$$\frac{C}{R} = \frac{G'(a)\, G(j\omega)}{1 + G'(a) G(j\omega)}$$

In the above, G'(a) is independent of the frequency of the sinusoidal input, but is a function only of the amplitude.

Instability will result when the denominator in the above equation becomes zero or when

$$G(j\omega) = -\frac{1}{G'(a)}$$

As noted before, no phase shift is associated with the describing function when considering saturation. Thus, the factor -1/G'(a) establishes another critical point on the 180-degree axis of the Nyquist diagram. Had phase shift been associated with G'(a), as it must be when considering hysteresis, -1/G'(a) would not be located on the 180-degree axis.

Returning to the calculated example and transferring the constant K to the linear elements

$$\frac{-K}{G'(a)} = \frac{-1}{0.56} = -1.78$$

It is obvious that the critical point as now located, Graph 7.8, provides the system with greater stability. The same effect could have been represented on the Bode diagram by a straight line parallel to the frequency axis and of a magnitude dictated by -K/G'(a).

The saturation due to the exciter and to the saturable reactor would be treated in a similar manner - each element contributing a term to move the critical point outwards along the 180-degree line on the Nyquist diagram.

The actual recorded effect of saturation on the stability of the voltage - regulating system is shown on Graph 7.6. At lower alternator voltages the system becomes more unstable indicating less saturation. From the alternator open-circuit saturation curve, it can be seen that non-linear performance begins to occur at 100 volts. But Graph 7.6 indicates that saturation is still present below this value, so the saturation at this stage must be attributed to the exciter and to the saturable reactor.

CHAPTER VIII

STEADY-STATE AND TRANSIENT PERFORMANCE OF ALTERNATOR WITH REGULATING SYSTEM

8.1 Alternator Regulation

Although a fast transient response is an important item in a voltage-regulating system the regulation must not be disregarded. Thus far the forward and feedback components have been designed with as high a gain as was feasible. A higher gain means that the system is more sensitive to a change than a system with low gain, thus, larger corrective measures will be introduced to attempt to restore the output to its original level.

Fig. 8.1 shows the steady-state vector diagram for the regulated alternator when fully loaded with an 80 % pf, lagging load. The procedure for constructing this diagram will be outlined[1].

(1) The current is laid off from the terminal voltage at the proper power factor angle $\theta = \cos^{-1} 0.80 = 36^{\circ}52'$.

(2) To the terminal voltage is added the internal resistance drop and the vector $X_q I$, which give E_{qd} the voltage behind the quadrature-axis reactance.

$$E_{qd} = 1.0 + 0.05 \cos 36^{\circ}\,52' + 0.519 \sin 36^{\circ}52' - j\ 0.05 \sin 36^{\circ}52' + j\ 0.519 \cos 36^{\circ}52'$$

$$= 1.41 \angle 15^{\circ}50' \quad \text{p/u}$$

(3) The excitation voltage E_q is determined by adding to the terminal voltage the internal resistance drop and the synchronous reactance drop. A perpendicular from this resultant vector to the quadrature axis gives E_q.

$$E_q = E_{qd} + (0.985 - 0.519) \cos 37^{\circ}18'$$

$$= 1.78 \text{ p/u}$$

---

1. E.W. Kimbark, Power System Stability, Vol. III, Synchronous Machines, pp.77, J. Wiley and Sons, 1956.

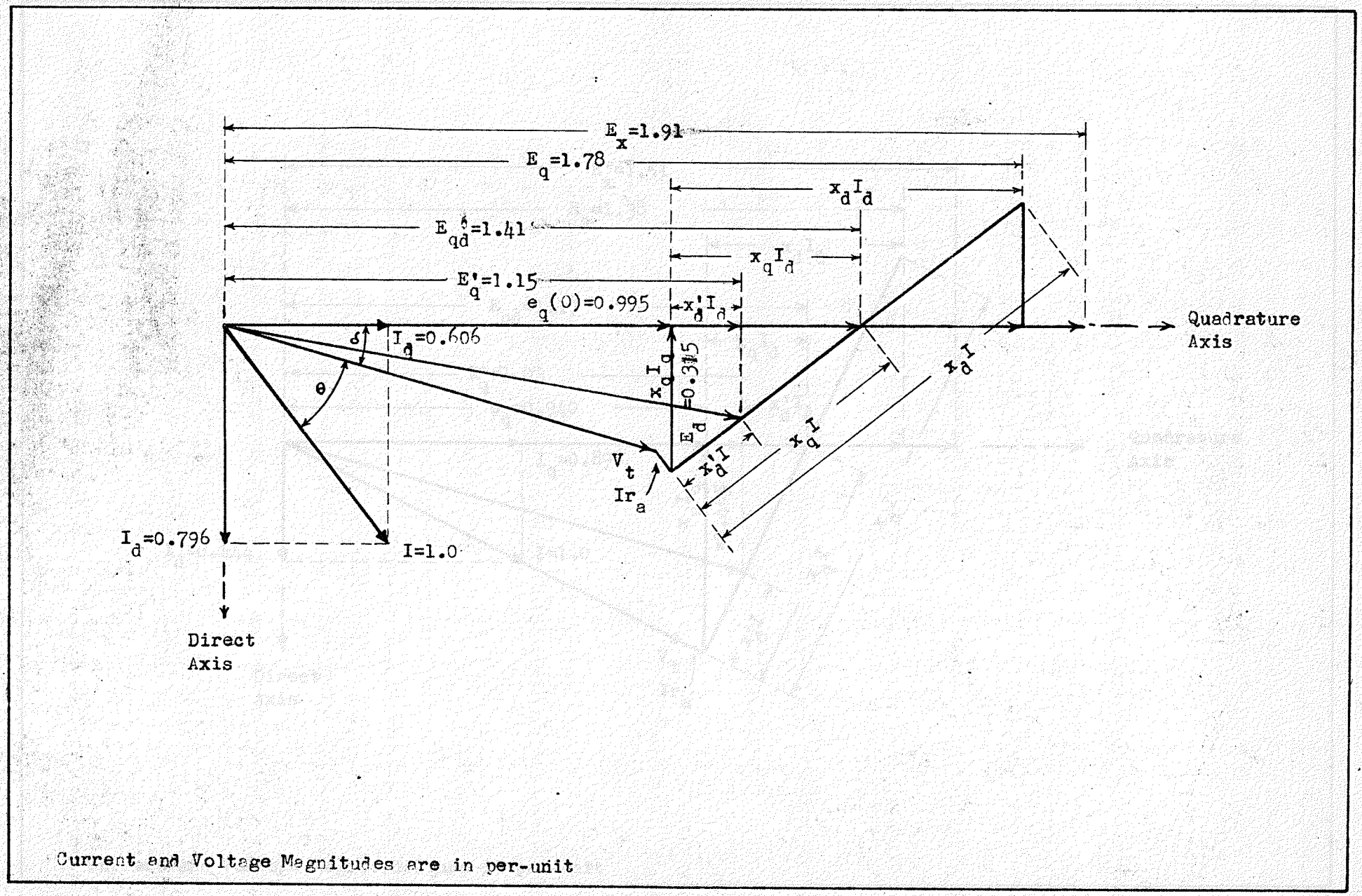

FIG. 8.1 VECTOR DIAGRAM FOR FULL LOAD AT 80 % PF, LAGGING

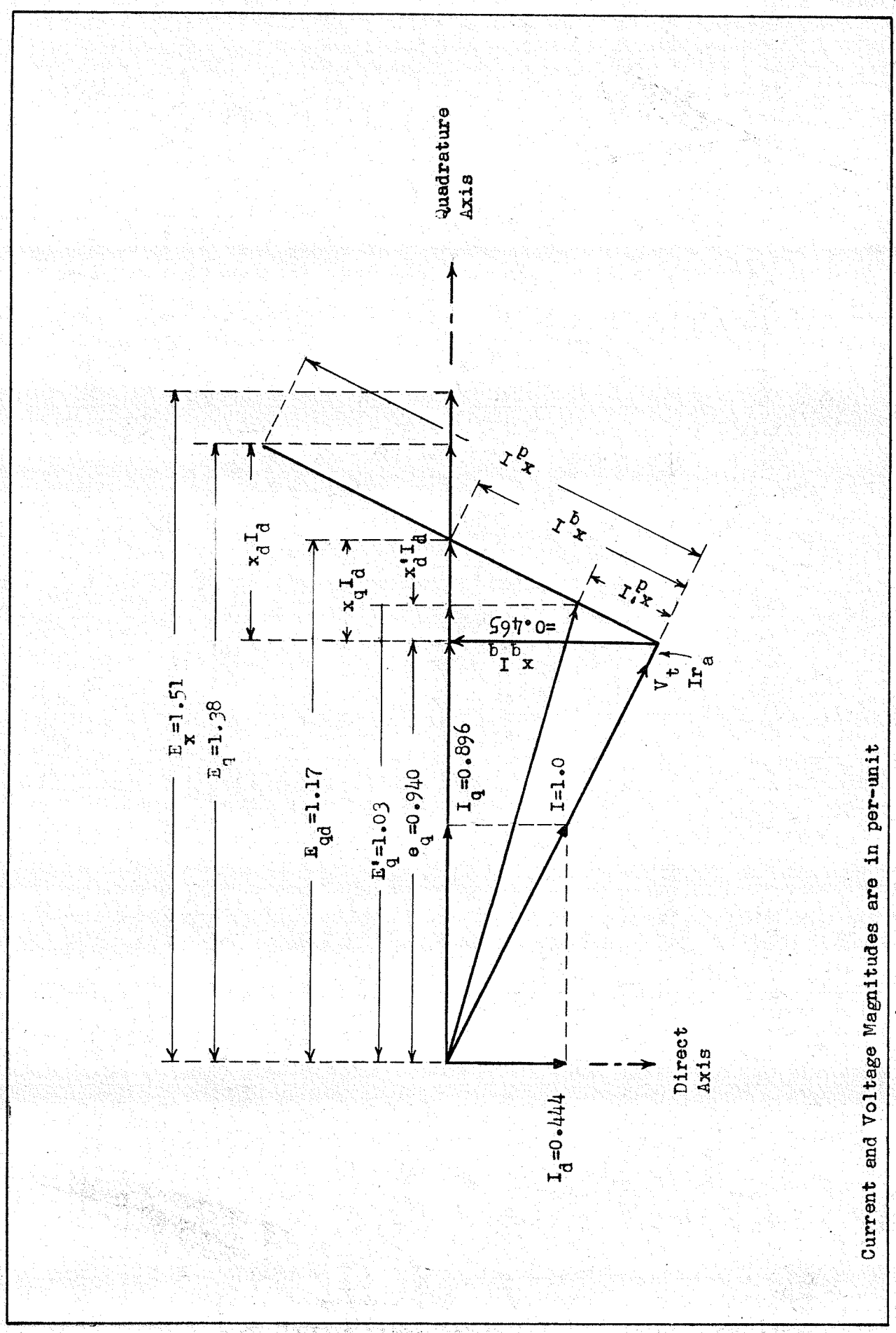

Current and Voltage Magnitudes are in per-unit

FIG. 8.2 VECTOR DIAGRAM FOR FULL LOAD AT UNITY POWER FACTOR

(4) The exciter voltage is found by adding saturation to E_q. Saturation at rated voltage and no load = 0.13, Graph B.1.

$$E_x = E_q + 0.13$$
$$= 1.91 \text{ p/u}$$

(5) Having δ and θ the direct axis and quadrature axis currents can now be determined.

$$I_q = 1.0 \cos 52^{\circ}42' = 0.606 \text{ p/u}$$
$$I_d = 1.0 \sin 52^{\circ}42' = 0.796 \text{ p/u}$$

(6) E_d can now be evaluated

$$E_d = X_q I_q$$
$$= 0.519 \times 0.606$$
$$= 0.315 \text{p/u}$$

(7) E_q', the quadrature axis component of the internal voltage back of the transient reactance is

$$E_q' = E_{qd} - I_d (X_q - X_d')$$
$$= 1.41 - 0.796 (0.519 - 0.194)$$
$$= 1.151 \text{ p/u}$$

The vector diagram indicates an exciter voltage of 1.91 p/u. Therefore, the field current necessary under these loaded conditions is 1.91 base field current, or

1.91 x 1.20 = 2.30 amps.

Under actual conditions the alternator field current was metered at 2.50 amps. The additional 0.20 amps was due to the fact that the alternator speed decreased from the rated 1800 r p m to 1700 r p m when under load. A higher field current was necessary to maintain the required voltage.

Nevertheless, assuming that speed was constant after load was applied, the exciter voltage must rise from 48.0 volts (1.0p/u) to 1.91 x 48.0 or 91.5 volts.

Since the gain of the exciter (loaded) is 225 volts/amp, Graph B.4, the exciter field current must rise by

$$\frac{91.5 - 48.0}{225} = 193 \text{ ma.}$$

Thus the field current must rise from 107 ma at no load to 107 + 193 = 300 ma at full load. From Graphs 2.5 and 2.7 it can be seen that the error voltage must shift from a -3.0-volt bias to a -2.0-volt bias to produce the necessary exciter field current. This 1.0-volt shift at the 6AC7-grid means that the output of the detector circuit must be 1.0 volts lower. With the gain of the detector circuit being 3.26, a drop of 1/3.26 or 0.3 volts at the alternator terminal will produce the required bias change.

Thus, theoretically if full-load at 80% pf, lagging was applied to the alternator, the terminal voltage should drop from 120.0 volts to 119.7 volts.

The terminal voltages of the alternator as measured at no load and full load were found to be as follows:

TABLE 8.1

TEST DATA FOR FULL LOAD AT 80% PF, LAGGING

Terminal Voltage	No load (volts) #1DW3	Full Load (volts) #1DW3
V_{ab}	120.0	119.0
V_{bc}	119.0	119.0
V_{ca}	120.3	119.2

I_a (#DK3) = 36.0 amps
I_b (#DK6) = 36.1 amps
I_c (#DK1) = 35.8 amps

W_A (# 38) = 1.65 kw
W_B (# 39) = 4.15 kw

N (no load) = 1800 rpm
N (full load) = 1700 rpm

Averaging the line voltages at no load and full load, the voltage regulation for full load, 80% pf, lagging is

$$V.R. = \frac{0.7}{120.0} \times 100 = 0.58\%$$

The regulation is not affected to any large extent by the drop in speed. This causes more field current to be forced through both the alternator and exciter to maintain the required voltage. Some of the components will be forced to work at greater saturation where the gain is lower, thus increasing the regulation slightly.

A test was also conducted on a unity power factor load and on a 94% pf, leading load.

TABLE 8.2

TEST DATA FOR FULL LOAD AT 100% PF

Full Load (volts)

#1DW3

V_{ab}	119.5	I_a (#DK3)	=	36.8 amps
V_{bc}	118.5	I_b (#DK6)	=	36.8 amps
V_{ca}	119.5	I_c (#DK1)	=	36.2 amps

W_A (#38) = 3.66 kw

W_B (#39) = 3.65 kw

N (no Load) = 1800 rpm

N (full load)= 1700 rpm

$$V.R. = \frac{0.5}{120} \times 100 = 0.41\%$$

TABLE 8.3

TEST DATA FOR FULL LOAD AT 94% PF,LEADING

Full Load (volts)

V_{ab} = 119.8
V_{bc} = 118.9
V_{ca} = 119.8

I_a (#DK3) = 35.5 amps
I_b (#DK6) = 35.5 amps
I_c (#DK1) = 34.6 amps

W_A (# 38) = 3.12 kw
W_C (# 39) = 3.85 kw

N (no load) = 1800 rpm
N (full load)= 1700 rpm

$$VR. = \frac{0.3}{120} \times 100 = 0.25\ \%$$

Graph 8.1 illustrates the effectiveness of the voltage regulator for two types of loads. A single line represents the same regulation for 100% pf, 80% pf, lagging and 94% pf, leading, loads. The variation in regulation among these three types of loads was notwithin the accuracy of the recording voltmeter.

8.2 Transient Response with Suddenly-Applied Loads

The treatment thus far has been entirely concerned with the stability of the voltage-regulating system under no-load conditions. This is a prerequisite to transient response study with either applied or dropped loads.

THIS MARGIN RESERVED FOR BINDING.

IF SHEET IS READ THE OTHER WAY (VERTICALLY), THIS MUST BE LEFT-HAND SIDE.

GRAPH 8.1 VOLTAGE REGULATION OF ALTERNATOR WITH AND WITHOUT REGULATOR

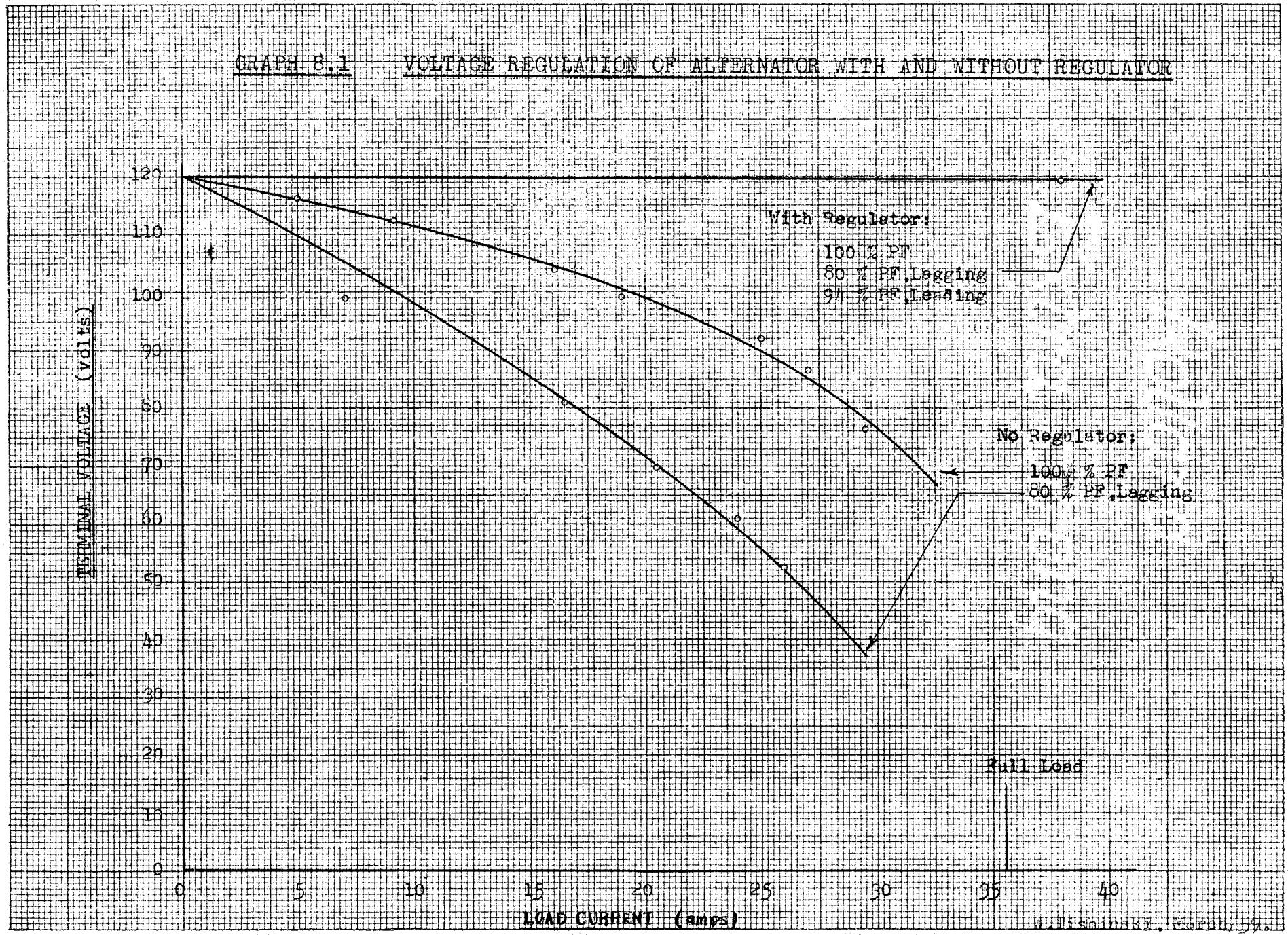

MANUFACTURED BY RENOUF PUBLISHING CO., MONTREAL

FORM 100

For an accurate treatment of the alternator terminal voltage response, the servomechanism basis must be discarded to some extent and the problem confined solely to the exciter, alternator and load. This is due to the fact that the reactance of the alternator under sudden changes is not constant but follows two consecutive exponential curves before reaching a steady-state value. Since the theory evolved for the treatment of these reactances can be found in many texts it will not be discussed here.

With the existence of the variable reactance in the alternator upon sudden load changes, an analytical expression for the closed-loop regulating system would involve lengthy expressions which would require a great deal of tedious calculations. However, this approach need not be taken since the prime concern with a voltage regulator is the maximum drop in the voltage and the time required for the voltage to reach normal value. Overshoots are of lesser importance as far as operation is concerned since they will not exceed the initial dip. This is true provided the system is stable. As a matter of fact, if load is applied to the machine, all of the saturable components will operate higher up on the saturation curve, thus greater stability is attained than under the no-load case.

Since the subtransient time constant for this alternator is 0.0108 sec, which is small compared with the transient time constant and exciter time constant, it can be neglected in all further calculations.

When load is suddenly applied to an alternator, the terminal voltage suffers a sudden initial transient drop, followed by a gradual drop from the transient towards the synchronous value. In the meantime, regulator action raises the exciter voltage, halting further drop and restoring the voltage to its normal value. As the voltage approaches normal, the anti-hunt device takes effect slowing the rise. This does not usually have any effect on the minimum voltage reached during the dip.

The build-up of the exciter voltage is considered to rise exponentially, Appendix B.3. Further assumptions are that speed is constant and a constant fixed excitation S is required to overcome saturation. The initial voltage of the machine back of the transient reactance, namely e_q', is associated with the flux linkages which remain constant when load is suddenly changed. Since this quantity does not undergo an instantaneous change there are no discontinuities in the formula representing it. This makes the flux linkage relation rather convenient to analyse when considering the effect of loading on the terminal voltage. The terminal voltage e_t is related to e_q' by the following relationship[1]:

$$e_t = \frac{\sqrt{(X_{qt}^2 + r_t^2)(X_e^2 + r_e^2)}}{X_{dt}' X_{qt} + r_t^2} \quad e'_q \quad - - - - - - (8.1)$$

where $X_{qt} = X_q + X_e$

X_q = quadrature - axis synchronous reactance

X_e = external reactance

$X_{dt}' = X_d' + X_e$

X_d' = direct-axis transient reactance

$r_t = r_a + r_e$

r_a = alternator armature resistance

r_e = external resistance

Other terms appearing in this section will be listed now as well.

e_q' = quadrature - axis transient internal voltage

$e_{q(o)}$ = quadrature - axis component of terminal voltage in steady-state before load is removed.

$e_f = e_X$ = voltage applied to the alternator field terminals

e_{X1} = initial exciter terminal voltage

e_c = exciter ceiling voltage

---

1. C.F. Wagner, Machine Characteristics, Westinghouse Electrical Transmission and Distribution Reference Book, Ch. VI, pp. 171, 1950.

$i_d(o)$ = direct-axis component of armature current in steady-state before load is removed

i_f = generator field current

h = regulator operating time

ψ_d = direct-axis armature flux linkages

ψ_q = quadrature-axis armature flux linkages

ψ_f = field winding flux linkages

r_f = resistance of the field winding

X_d = direct-axis synchronous reactance

X_{ad} = direct-axis armature reactance

X_{ff} = reactance of field winding

T_{do} = alternator open-circuit transient time constant

T_d' = alternator loaded transient time constant

T_e = build-up time constant of loaded exciter

S = per unit excitation required to overcome saturation at no-load, rated voltage

t = time

All equations, henceforth, will be on a per-unit basis. Thus, an alternator field current of 1.20 amps, which produces a rated-120 volts at the armature terminals at no load, is considered to be 1.0 p/u.

The differential equation for the alternator field with the armature open-circuited is given by

$$L\frac{di}{dt} + ri = e_\chi$$

Dividing through by r, and replacing L/r by T_{do}', which is the open-circuit time constant of the field, the equation can be rewritten as

$$T_{do}'\frac{di}{dt} + i = \frac{e_\chi}{r}$$

On a per-unit basis $i = e_q$. Also e_χ/r is per-unit field current and e_χ is the exciter voltage required to force unit field current through r. If saturation S is considered now, the effective per-unit

current must be decreased on a linear basis. The equation now becomes

$$T_{do}' \frac{de_q}{dt} + e_q = e_\chi - S$$

Since it is necessary to express the above equation in terms of e_q', the following relationship proves useful[2]:

$$\frac{T_{do}'}{T_d'} = \frac{e_q}{e_q'} \qquad \text{- - - - - - - - - - - - (8.2)}$$

If the armature circuit is closed by means of a load, the open-circuit transient time constant T_{do}' is changed to the closed-circuit transient time constant T_d', the relation being

$$T_d' = \frac{X_{dt}' X_{qt} + r_t^2}{X_{dt} X_{qt} + r_t^2} T_{do}' \qquad \text{- - - - - - - - - - - - (8.3)}$$

The closed-circuit field equation now becomes

$$T_d' \frac{de_q}{dt} + e_q = e_\chi - S \qquad \text{- - - - - - - - - - - - (8.4)}$$

Now if a certain delay h exists, which is the time taken by the thyratron to conduct for 180 degrees after the load is applied, two equations will be applicable for the exciter voltage

(1) If $0 \leq t \leq h$, $\quad e_\chi - S = e_{\chi 1} - S$

(2) If $t \geq h$,

$$e_\chi - S = (e_{\chi 1} - S) + (e_c - e_{\chi_1})(1 - e^{-(t-h)/T_e})$$

Since the field circuit differential equation is desired in terms of e_q', equation 8.4 can be rewritten using the relation given in equation 8.2,

$$T_{do}' \frac{de_q'}{dt} + \frac{T_{do}'}{T_d'} e_q' = e_\chi - S$$

---

2. Ibid., pp. 169.

Substituting for $(e_{\chi_1} - S)$ from (1) and (2), the final differential equation can be written as

$$\frac{de_q'}{dt} + \frac{e_q'}{T_d'} = \frac{1}{T_{do}'}\left((e_{\chi 1} - S)\, U(t) + (e_c - e_{\chi 1})(1 - e^{-(t-h)/T_e})\, U(t-h) \right) \quad - - - - - - \quad (8.5)$$

where U(t-h) is the Heaviside notation for a delayed unit function, that is, up to time h only $(e_{\chi 1} - S)$ contributes to the exciter voltage, but after time h, the equivalent exciter voltage is given by (2).

Equation 8.5 must be solved for e_q'! By taking Laplace transforms it can be written as

$$s\, E_q'(s) - e_q'(o) + \frac{E_q'(s)}{T_d'} = \frac{1}{T_{do}'}\left(\frac{e_{\chi 1} - S}{s} + \frac{(e_c - e_{\chi_1})e^{-hs}}{s\, T_e(s + T_e)} \right)$$

Isolating $E_q'(s)$ the above becomes

$$E_q'(s) = \frac{1}{T_{do}'}\left(\frac{(e_{\chi_1} - S)}{s(s + 1/T_d')} + \frac{(e_c - e_{\chi_1})e^{-hs}}{T_e s(s + 1/T_d')(s + 1/T_e)} \right) + \frac{e_q'(o)}{(s + 1/T_d')}$$

Now by taking the inverse Laplace transform

$$e_q'(t) = \frac{(e_{\chi_1} - S)T_d'\,(1 - e^{-t/T_d'})}{T_{do}'} + e_q'(o)e^{-t/T_d'}$$

$$+ \frac{(e_c - e_{\chi_1})T_d'}{T_{do}'(T_d' - Te)} \int_0^t \left(e^{-t/T_d'} - e^{-t/Te} \right) dt$$

One must take care not to insert the delay factor h until the inverse transform operation has been completed.

$$e_q'(t) = \left((e_{\chi_1} - S)\, \frac{T_d'}{T_{do}'}\, (1 - e^{-t/Td'}) + e_q'(o)\, e^{-t/Td'} \right) U(t)$$

$$+ \frac{(e_c - e_{\chi 1})T_d'}{T_{do}'(T_d' - T_e)} \left(T_e\, (e^{-(t-h)/Te} - 1) - T_d'\, (e^{-(t-h)/T_d'} - 1) \right) U(t-h)$$

$$- - - - \quad (8.6)$$

In the preceding equation the following terms are constant for the alternator irregardless of the type or size of load applied:

e_c = 2.80 p/u
e_{x_1} = 1.13 p/u
S = 0.13 p/u
T_{do}' = 0.234 sec
T_e = 0.080 sec
$e_q'(o)$ = 1.00 p/u, if the machine in operating at no load prior to any load changes.

The above constants are evaluated in Appendix B. The remaining terms will vary depending on the type of load.

If full load at 80% pf, lagging is suddenly applied to the alternator,

x_e = 0.60 p/u
r_e = 0.80 p/u

Then from equation 8.3

$$T_d' = \frac{(0.194 + 0.60)(0.519 + 0.60) + (0.80 + 0.05)^2}{(0.985 + 0.60)(0.519 + 0.60) + (0.80 + 0.05)^2} \times 0.234$$

$$= 0.152 \text{ sec}$$

The value of h is rather an indefinite quantity since the effective d-c voltage applied to the exciter field, after a load change, is not a step function, but rather a function of the alternator output voltage and the transfer function of the detector circuit. If load is suddenly applied, the alternator voltage drops instantaneously before beginning its exponential decay. This drop is related to e_q' by equation 8.1. Since e_q' can not change instantaneously its value will be 1.0 p/u just after load is applied and thus e_t can be found as

$$e_t = \frac{\sqrt{\left((0.519 + 0.60)^2 + (0.80 + 0.05)^2\right)}\,(1)}{(0.194 + 0.60)(0.519 + 0.60) + (0.80 + 0.05)^2}\, e_q'$$

$$= 0.872\, e_q' \qquad = 0.872 \text{ p/u}$$

In absolute terms $e_t = 0.872 \times 120 = 105$ volts. From Graphs 2.6 and 2.7 it is noted that a positive swing of 2.5 volts at the grid of the 6AC7 error-amplifying tube will raise the exciter field voltage from 20 volts to a maximum value of 82 volts. This rise is not instantaneous but gradual. A 15-volt drop at the alternator will be reproduced at the 6AC7 grid by the function $1.82\ (1 - e^{-3.0t})$ which is an approximate weighting function of the detector circuit for a build-down case. As soon as the change in the alternator voltage is represented by 2.5 volts at the 6AC7 grid, the thyratron will be firing for 180 degrees, and 82 volts will be impressed across the exciter field. The delay caused by the saturable reactor is sufficiently small that it can be neglected.

Thus for the above condition

$$2.5 = 15 \times 1.82\ (1 - e^{-3.0t})$$

from which

$$t = 0.032 \text{ sec}$$

Now h is not equal to t but some value between zero and t because the exciter field voltage is raised gradually until t is reached. For an approximation h can be taken as t/2 or 1 cps. If h is neglected, equation 8.6 reduces to

$$e_q'(t) = (e_c - S)\frac{T_d'}{T_{do}'} - \left(\frac{(e_c - e_{\chi_1})T_d'^2}{T_{do}'(T_d' - T_e)} + \frac{(e_{\chi_1} - S)T_d'}{T_{do}'} - e_q'(o)\right) e^{-t/T_d'} + \frac{(e_c - e_{\chi_1})T_d' T_e}{T_{do}'(T_d' - T_e)} e^{-t/T_e} U(t) \quad - - - - \quad (8.7)$$

In order to show the effect of the delay factor h in equation 8.6, calculations for e_q' and e_t will be carried out using both equations 8.6 and 8.7. A sample calculation for e_t will be shown utilizing equation 8.6 at t = 2 cycles or 0.0333 sec.

$$e_q' = \left((1.13 - 0.13)\frac{0.152}{0.234}\left(1 - e^{-0.0333/0.152}\right) + 1.00\, e^{-0.0333/0.152} \right) U(t)$$

$$+ \frac{(2.80 - 1.13)0.152}{0.234(0.152 - 0.080)} \left(0.080 \left(e^{-(0.0333 - 0.0167)/0.08} - 1 \right) \right.$$

$$\left. - 0.152\left(e^{-(0.0333 - 0.0167)/0.152} - 1\right) \right) U(t - 0.0167)$$

$$= 0.941 \text{ p/u}$$

$$e_t = 0.872\, e_q'$$

$$= 0.820 \text{ p/u}$$

$$= 120 \times 0.820$$

$$= 98.7 \text{ volts}$$

TABLE 8.4

COMPUTATIONS OF e_t FOR FULL LOAD AT 80% PF, LAGGING, FROM EQUATIONS 8.6 AND 8.7

Time(cps)	e_q'(p/u) Eq.8.7	e_q'(p/u) Eq.8.6	e_t(volts) Eq. 8.7	e_t(volts) Eq. 8.6
0	1.000	1.000	104.8	104.8
1	0.975	0.963	102.0	101.5
2	0.972	0.941	101.8	98.7
3	- - -	0.941	- - -	98.7
4	1.007	- - -	105.2	- - -
5	- - -	0.994	- - -	104.2
6	1.073	- - -	112.2	- - -
7	- - -	1.056	- - -	110.8
8	1.154	- - -	120.8	- - -
9	- - -	1.138	- - -	119.2
10	1.237	- - -	128.2	- - -

These calculated results are plotted, along with the recorded responses, on Graph 8.2, Two records of transient responses were taken for the same load conditions, Fig. 8.4 and 8.5, but with different settings of the anti-hunt circuit. More feedback by means of the anti-hunt circuit provides the regulating system with a greater degree of stability. However, as can be seen on the graph, it slows down the response slightly as rated voltage is approached. This is of minor consequence for this particular regulating system, since an increase from 71% to 100% of the total available anti-hunt signal, delayed the rise of the terminal voltage back to normal by only a fraction of a cycle.

The most interesting item on Graph 8.2 is the comparison between the calculated and recorded results. This comparison is valid only for the initial part of the curve since the calculated curve is based on the assumption that the terminal voltage would continue to rise until the ceiling voltage of the exciter was reached. The discrepancy between the curves immediately after load is applied is due to the assumption that the reactance at this instant is the transient value and not the sub-transient value as is in the actual case. Thus, it can be seen from equation 8.1, that if X_d'' was substituted for X_d', e_t would be larger, bringing it closer to the recorded value. The calculated minimum voltage of 98.7 volts occuring at 3 cps is comparable to the recorded 102.0 volts occuring at 4.5 cps.

It is rather difficult to get perfect agreement because of the small time constants involved. The developed formula, equation 8.6, is most accurate for constants which are large, since then an error in the evaluation of either T_e or T_d' causes a smaller percentage error for e_q'. As a matter of fact, as soon as T_e and T_d' are equal, equation 8.6 is not valid because several of the terms approach infinity.

If full load at 100% pf is suddenly applied to the alternator a different relationship will exist between e_t and e_q'. Now,

$$X_e = 0$$

$$r_e = 1.0 \text{ p/u}$$

THIS MARCIN RESERVED FOR BINDING.

IF SHEET IS READ THE OTHER WAY (VERTICALLY), THIS MUST BE LEFT-HAND SIDE.

GRAPH 8.2 CALCULATED AND RECORDED ALTERNATOR TERMINAL VOLTAGES FOR SUDDEN APPLICATION OF FULL LOAD AT 80 % PF. LAGGING

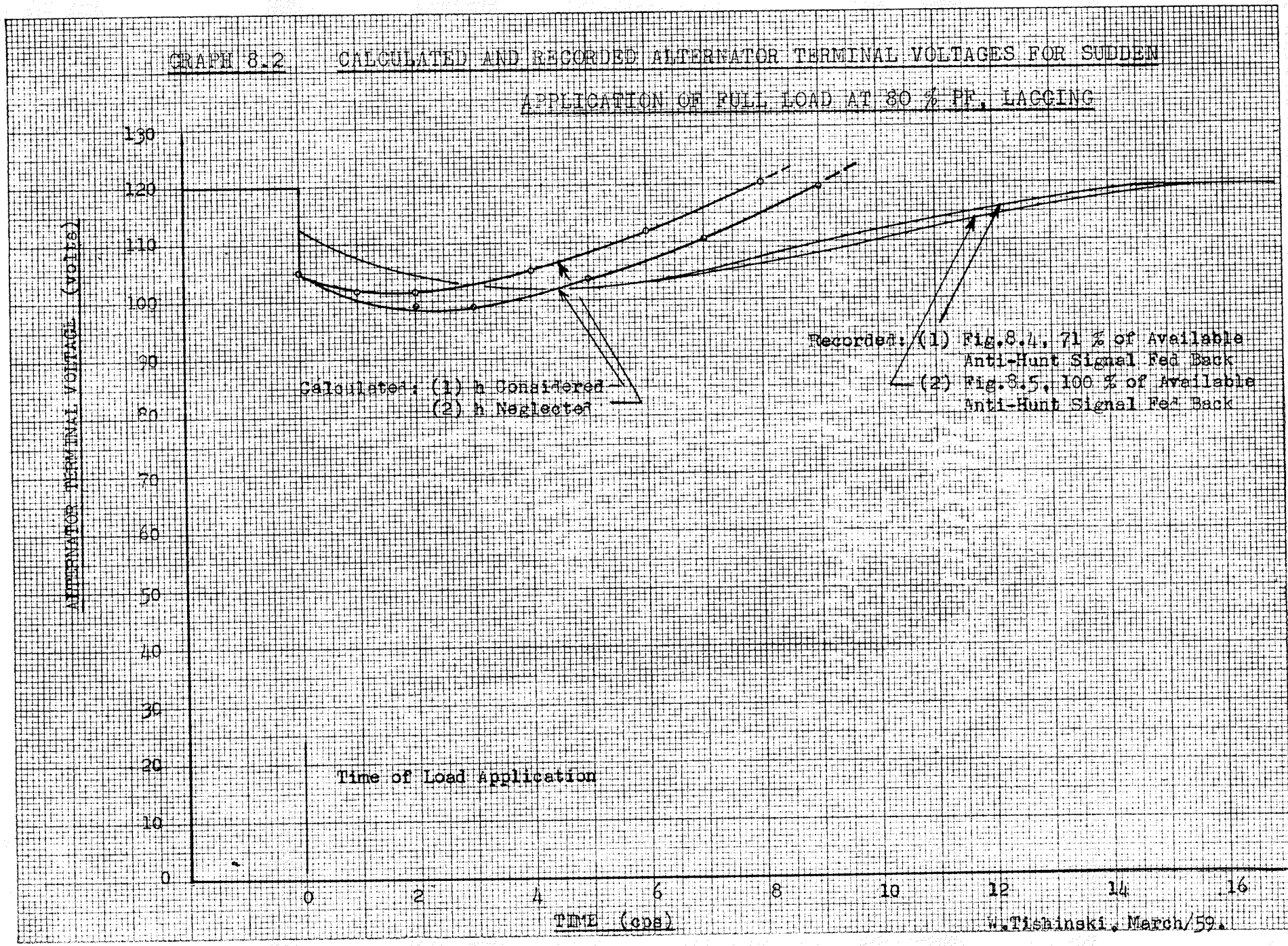

W.Tishinski, March/59.

MANUFACTURED BY RENOUF PUBLISHING CO., MONTREAL

FORM 1000

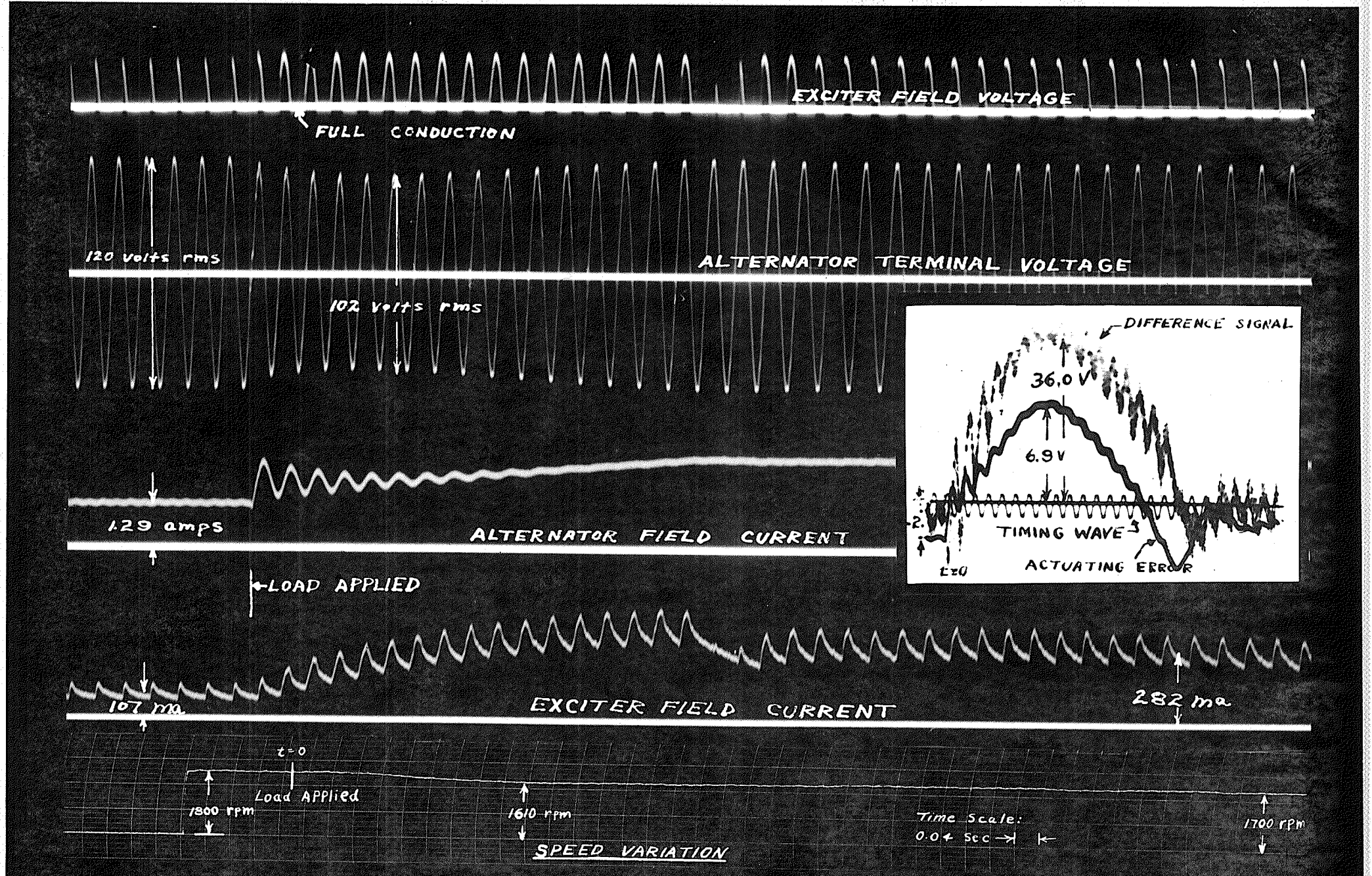

FIG. 8.3 TRANSIENT RESPONSE OF ALTERNATOR UPON SUDDEN APPLICATION OF FULL LOAD AT 80 % PF, LAGGING AND WITH 71 % FEEDBACK

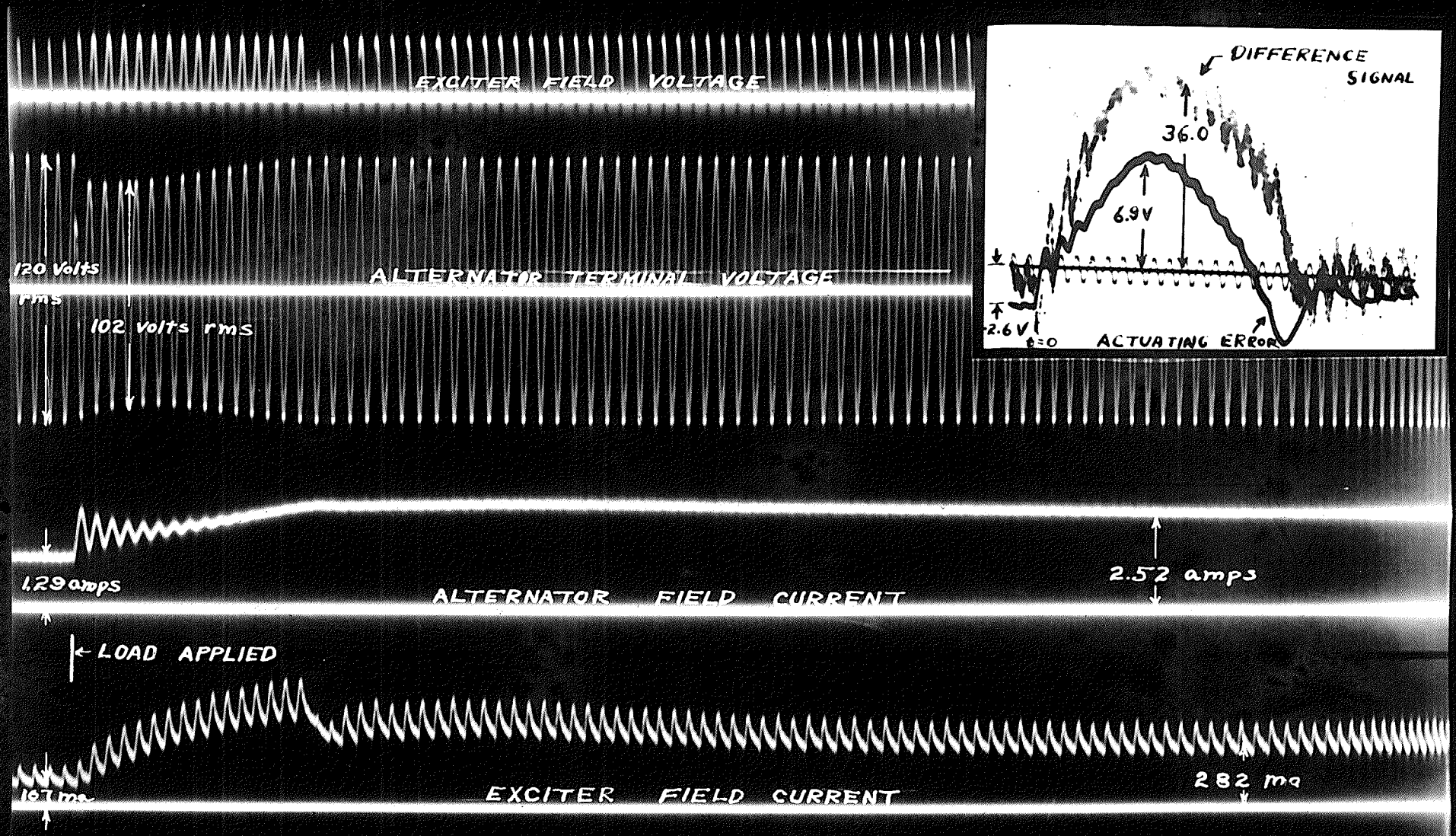

FIG. 8.4 TRANSIENT RESPONSE OF ALTERNATOR UPON SUDDEN APPLICATION OF FULL LOAD AT 80 % PF, LAGGING AND WITH 71 % FEEDBACK

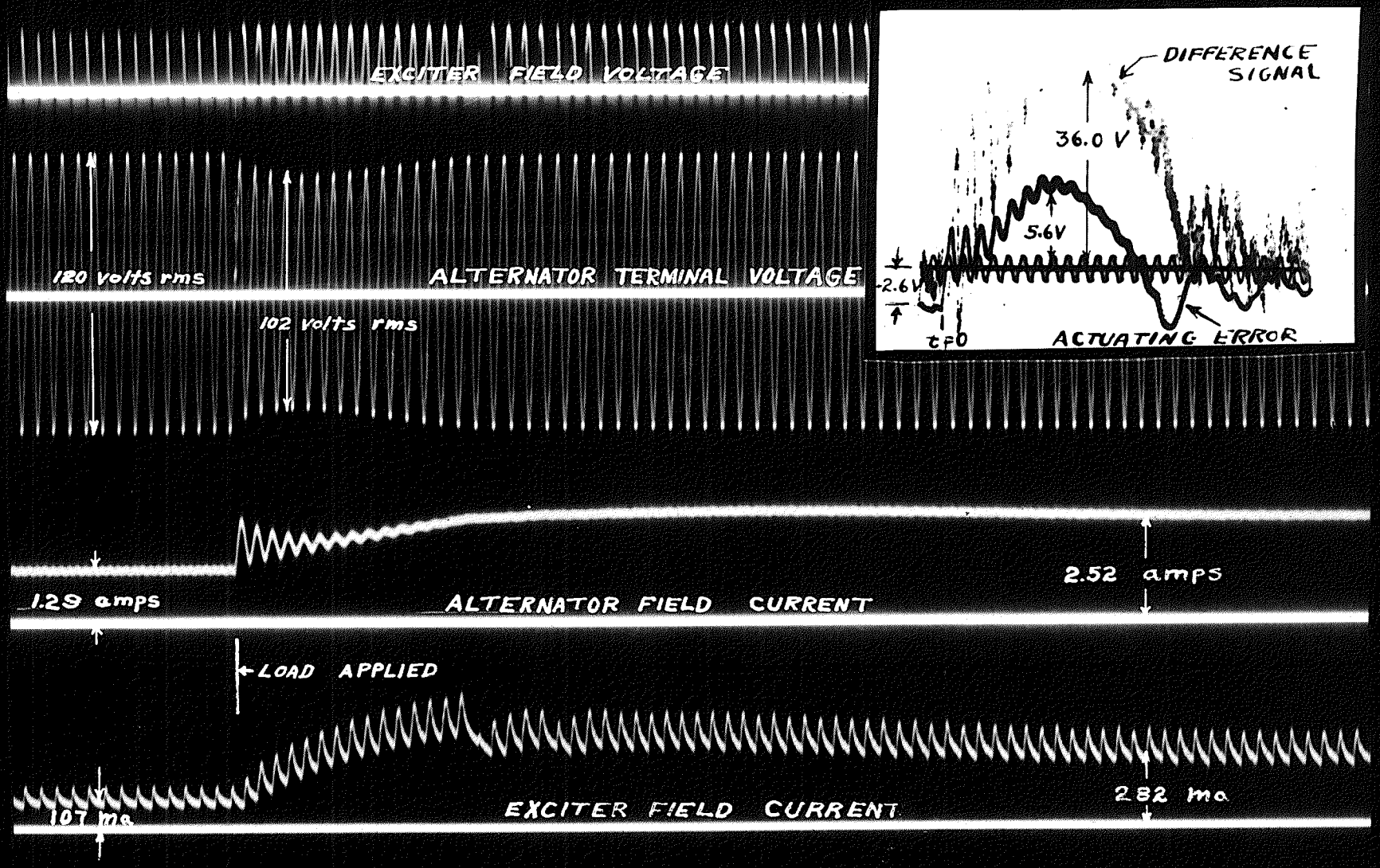

FIG. 8.5 TRANSIENT RESPONSE OF ALTERNATOR UPON SUDDEN APPLICATION OF FULL LOAD AT 80 % PF, LAGGING AND WITH 100 % FEEDBACK

and from equation 8.1

$$e_t = \frac{\sqrt{\left((0.519)^2 + (1.05)^2\right)(1)}}{0.194 \times 0.519 + (1.05)^2} \; e_q'$$

$$= 0.972 \; e_q'$$

Thus, the terminal voltage will drop to 0.972 or 116.5 volts when load is applied. The delay factor h will be determined in a fashion similar to that for the 80% pf, lagging case.

$$2.5 = 3.5 \times 1.82(1 - e^{-3.0t})$$

from which

$$t = 0.165 \text{ sec or } 10 \text{ cps}$$

The above figure means that if the terminal voltage remained constant at 116.5 volts, the delay of the detector circuit is of such duration that it would take 0.165 sec. for the thyratron to conduct for the maximum duration. Because t is relatively long, considerable error may exist if h is selected to be t/2 or 5.0 cps. By the time 5.0 cps have elapsed, the maximum dip of the alternator voltage may have been reached and the recovery begun. Furthermore, there is no reason to believe that the thyratron must conduct for the complete 180-degrees during any portion of the transient response. However, since equation 8.6 had been derived for conditions of a maximum available step-input voltage to the exciter field, this criterion will be carried through for the calculations for this type of load.

Since h, for the 80% pf, lagging case was taken as 1 cps, it will be somewhat longer for the less severe terminal voltage disturbance, as with the unity power factor case, and will be arbitrarily taken as 2 cps or 0.0333 sec.

From equation 8.3

$$T_d' = \frac{0.194 \times 0.519 + (1.05)^2}{0.985 \times 0.519 + (1.05)^2} \times 0.234$$

$$= 0.176 \text{ sec}$$

All other terms in equation 8.6 are the same as for the 80% pf, lagging case. Calculations once again will be carried out using the formula considering the delay factor h. Equation 8.7, which neglects h, will not be used for further calculations since it yields a curve with greater error than does equation 8.6. A sample calculation is worked out for e_q' at t = 3 cps or 0.05 sec.

$$e_q' = \left((2.80 - 0.13)\frac{0.176}{0.234}(1 - e^{-0.05/0.176}) + 1.00\, e^{-0.05/0.176}\right) U(t)$$

$$+ \frac{(2.80 - 1.13)0.176}{0.234(0.176 - 0.080)}\left(0.08\,(e^{-(0.05 - 0.0333)/0.08} - 1)\right.$$

$$\left. - 0.176\,(e^{-(0.05 - 0.0333)/0.176} - 1)\right) U(t - 0.0333)$$

$$= 0.949 \text{ p/u}$$

Then $e_t = 0.949 \times 0.972$

$= 0.921$ p/u

$= 110.5$ volts

TABLE 8.5

COMPUTATIONS OF e_t FOR FULL LOAD, 100% POWER FACTOR FROM EQUATION 8.6

Time (cps)	e_q' (p/u)	e_t (volts)
0	1.000	116.5
1	0.978	114.0
2	0.957	111.5
3	0.949	110.5
4	0.961	112.0
5	0.989	115.1
7	1.073	125.1

The calculated and recorded responses for the above loading condition are shown on Graph 8.3. Due to the fact that the subtransient reactance was neglected the calculated initial drop can be expected to be greater. A slower decay is indicated by the recorded curve. This is attributed to the fact that the thyratron began to increase its

THIS MARGIN RESERVED FOR BINDING.

IF SHEET IS READ THE OTHER WAY (VERTICALLY), THIS MUST BE LEFT-HAND SIDE.

GRAPH 8.3 CALCULATED AND RECORDED ALTERNATOR TERMINAL VOLTAGE FOR SUDDENLY APPLIED LOAD AT 100 % PF

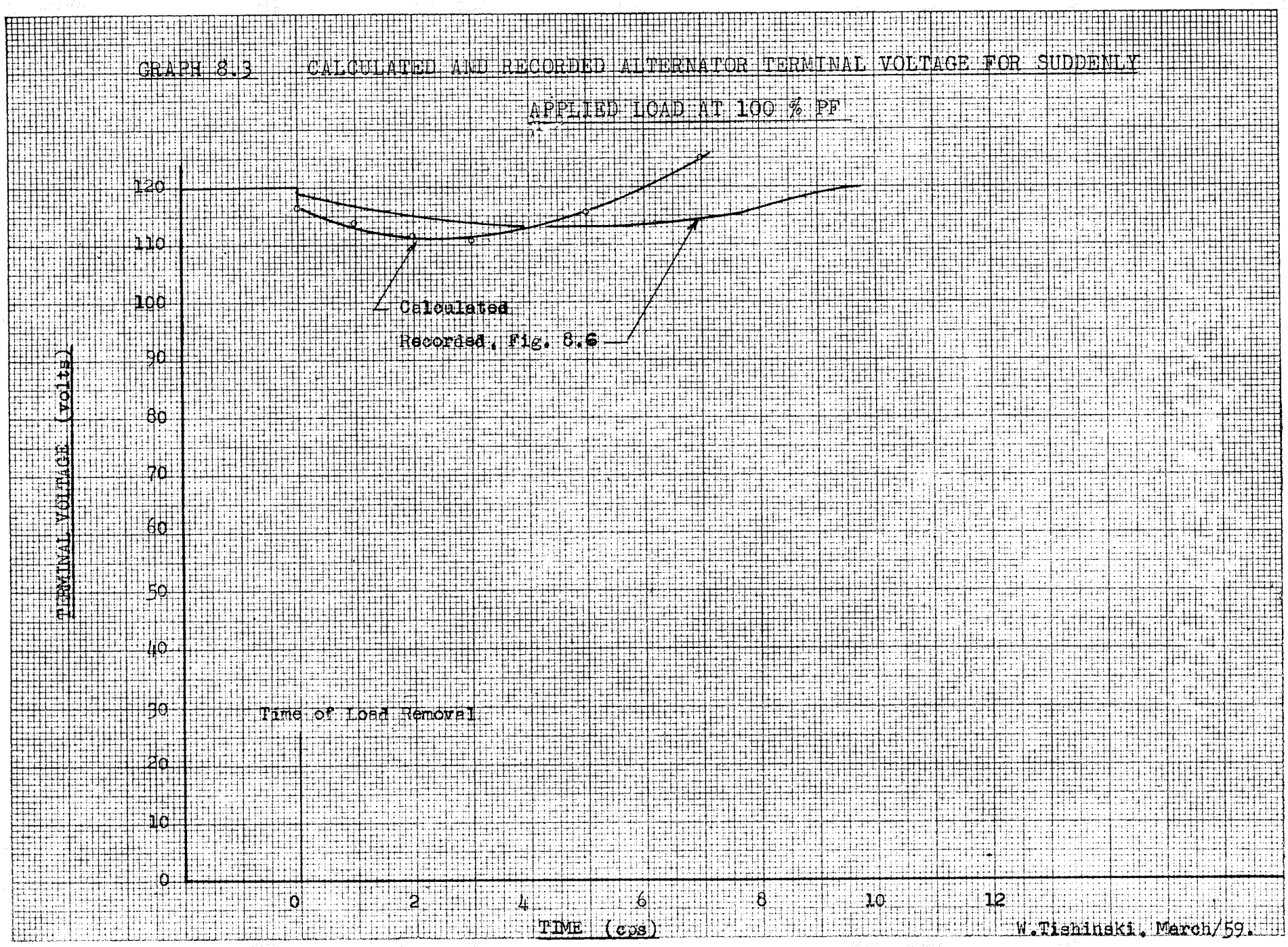

W.Tishinski, March/59.

MANUFACTURED BY RENOUF PUBLISHING CO., MONTREAL

FORM 1300

149

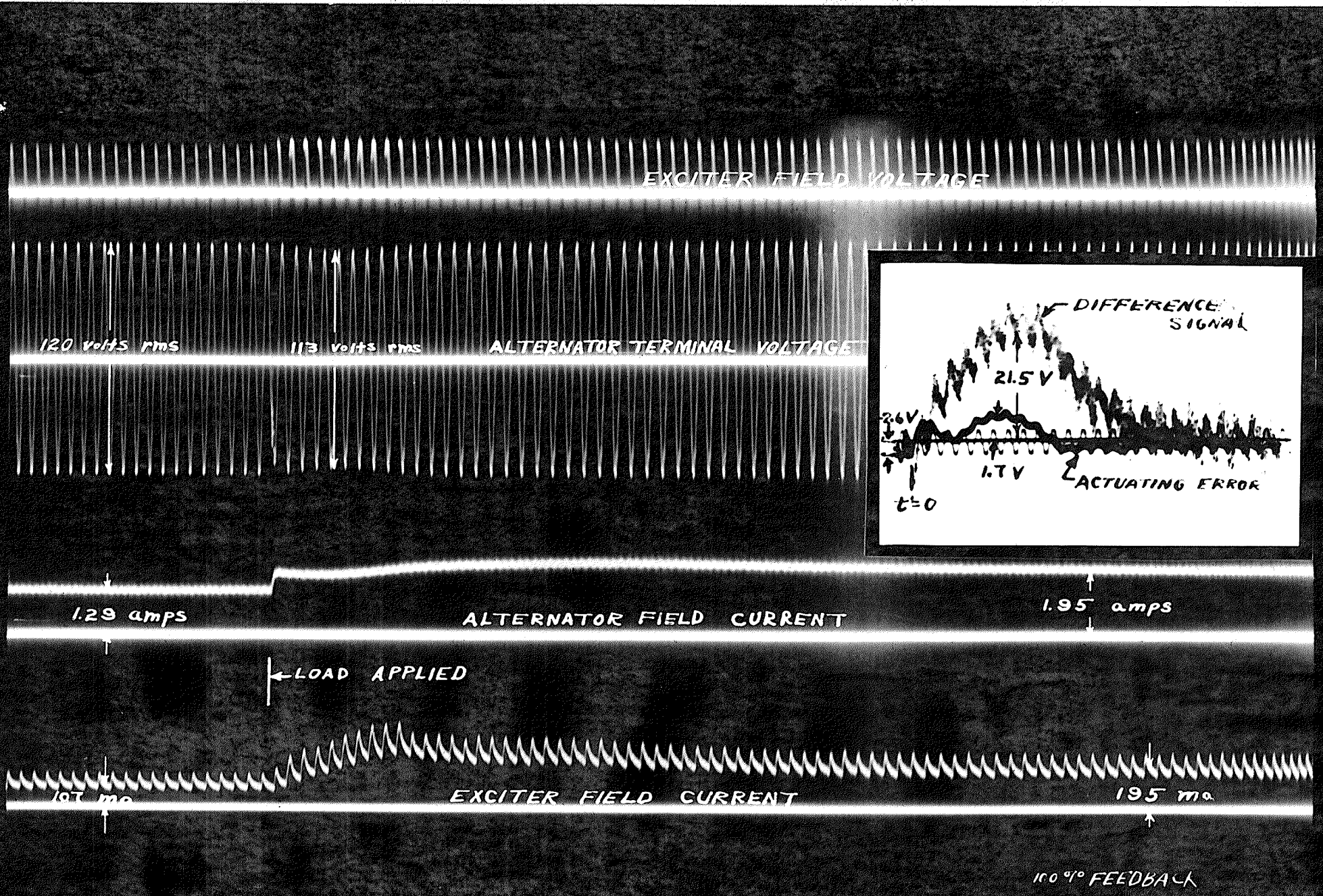

FIG. 8.6 TRANSIENT RESPONSE OF ALTERNATOR UPON SUDDEN APPLICATION OF FULL LOAD AT 100 % PF

firing angle even for the first cycle after load application, Fig. 8.6, and not after a delay h, (2cps) which was assumed in the calculations. The recorded recovery is slower for two reasons:

(1) The oscillogram shows that during no portion of the transient did the thyratron fire for a full 180 degrees. This is not what was assumed and hence a slower response can be expected.

(2) The anti-hunt circuit, which provides a negative feedback, makes the actuating error less severe during the recovery stage, thus the thyratron's firing angle eases gradually into the steady-state position.

A study of the recorded oscillograms enables one to view the physical aspects of the various components in the voltage - regulating system.

Figs. 8.3 and 8.4 are records for the same loading condition; the only change being the speed of the recording paper. From the exciter field voltage trace, it can be seen that the thyratron conducts for the full 180 degrees in a matter of 2 cps, which corresponds to the calculated value. The thyratron continues to conduct for the maximum range until the actuating error signal falls below - 0.5 volts at which time the thyratron triggering wave begins to shift its phase position. A small overshoot in the negative direction is seen to take place in the actuating error signal beginning at 16 cps and lasting for a duration of 2 cps. This overshoot affects the firing angle of the thyratron for the same duration. There is no delay between the overshoot of the actuating error signal and the change in the firing angle of the thyratron. This confirms a previous statement which said that if the bias of the 6AC7 pentode swings in a negative direction, r_p is large, giving a negligible time constant in the saturable reactor control winding.

On the other hand, if the bias of the 6AC7 pentode swings in a positive direction, r_p is relatively small and then the time constant of the saturable reactor control winding is appreciable. From Fig. 8.4, the actuating error signal is seen to jump immediately, after load application, to give a 0-volt bias to the pentode grid. In steady-state, a 0-volt bias produces maximum conduction of the thyratron. However, in

this case, several cycles lapsed before the thyratron attained this situation.

As a result of the small overshoot in the actuating error signal, the exciter field current suffers a slight irregularity for the same duration. No overshoot is noted in the alternator field current indicating the fact that sufficient inductance was present in the field circuit to smooth out the oscillatory effect. With a uniform alternator field current, no overshoot will be experienced in the alternator terminal voltage.

The difference signal, which is merely the difference between the reference circuit and the detector circuit, is seen to contain many harmonic components. These are mostly due to the exciter voltage but some may be attributed to the ripple from the detector circuit and to stray pick-up. Practically all of the harmonics are filtered out by the 1.06 μf capacitor.

The difference signal minus the actuating error signal represents the feedback signal due to the minor loop. The numerical quantities are illustrated on all of the photographs. Care must be taken not to misinterpret the feedback signal as the physical distance between the two signals recorded on the photograph. The calibration is different for each wave.

When the feedback signal is increased from 71% to 100%, Figs. 8.4 and 8.5, several changes in component signals can be noted. First of all, a longer time is necessary for the thyratron to reach its full-conduction period. The additional negative feedback retards the response of the actuating error signal as well as decreasing its magnitude. However, this has no effect on the alternator response after the first few cycles, since a 0-volt bias on the 6AC7 pentode is sufficient to cause the thyratron to conduct for a full 180 degrees. The actuating error swings into the positive region for both settings of the anti-hunt circuit.

As a matter of fact, the exciter field circuit response is identical for both settings of the anti-hunt circuit. Fifteen peaks can be counted on the exciter field current for each condition during the rising portion, before a small overshoot is experienced. The additional feedback appears to be less desirable for load applications since the actuating error signal is more oscillatory as normal alternator voltage is approached. This is contrary to the theory which states that a larger feedback signal provides the system with more damping. The additional magnitude of the harmonic content from the exciter could be responsible for this unpredictable occurrence.

Many of the comments stated previously with regard to the physical aspect of the system, will apply for the case where full load at 100% pf, is suddenly applied, Fig. 8.6. This type of load is less severe than the previous type as can be seen from the magnitudes of the field currents, thus the transient response of the alternator voltage is faster. It is noted that at no time does the thyratron conduct for a full 180 degrees. This occurrence was predicted in the calculations for h, where the fully-conducting period was found to take place after 10 cps. It can also be noted that the actuating error signal approaches its steady-state value after only 10 cps, whereas the difference signal requires approximately 18 cps. Beyond the 10 cps point, the minor loop feedback must be equal to the incremental value of the difference signal since

$$R_1 - B_2 = E$$

and in steady-state, the incremental value of E is equal to zero.

When full load at 94% pf, leading is suddenly applied to the alternator, Fig. 8.7, a small jump is noted in the terminal voltage. This is because the capacitive reactance is greater than the inductive subtransient reactance causing a negative regulation. As the machine reactance increases the total impedance becomes inductive causing positive regulation. This jump could have been predicted by the use of equation 8.1.

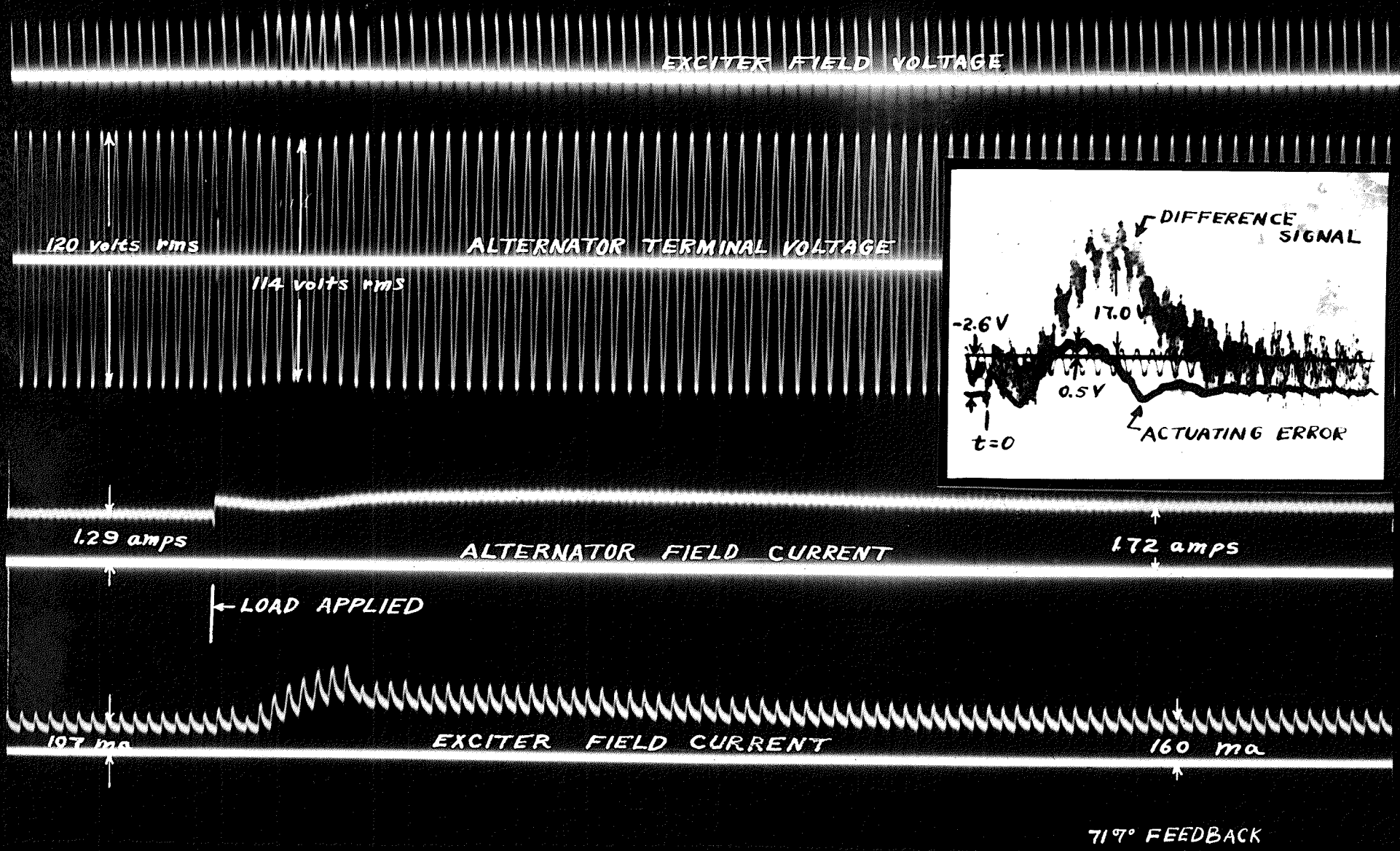

FIG.8.7 TRANSIENT RESPONSE OF ALTERNATOR UPON SUDDEN APPLICATION OF FULL LOAD AT 94 % PF, LEADING

For a 94% pf, leading load

$$X_e = -0.342 \text{ p/u}$$

$$r_e = 0.940 \text{ p/u}$$

$$e_t = \frac{\sqrt{(0.519 - 0.342)^2 + (0.94 + 0.05)^2}}{(0.194 - 0.342)(0.519 - 0.342) + (0.94 + 0.05)^2} e_q'$$

$$= 1.06\, e_q'$$

where

$$e_q(o)' = 1.00$$

It would have been desirable to test the operation of the regulating system on a load with a higher leading power factor. However, sufficient power capacitors were not available to carry out such a test.

Fig. 8.8 illustrates the effect of applying a single-phase load at 100% pf across two of the alternator phases. Oscillations were experienced in all of the components in the regulating system. The following voltages and load current were recorded:

I_a (#DK6) = 30.0 amps

Voltmeter: # 1DT8

V_{ab} = 89.5 volts (load across these phases)

V_{bc} = 113.5 volts

V_{ca} = 113.0 volts

The regulator did not function with the above load, the fault being with the detector circuit. Fig. 5.1 shows that the primary sides of the transformers constituting the rectifier are connected in delta. If the voltage between two lines fails, the output of the transformers will decrease by a small amount. In the above, one line voltage dropped to 89.5 volts, the other two decreased only slightly. Although the rms value of line voltages V_{bc} and V_{ca} dropped, the peak values were still at approximately 120 volts.

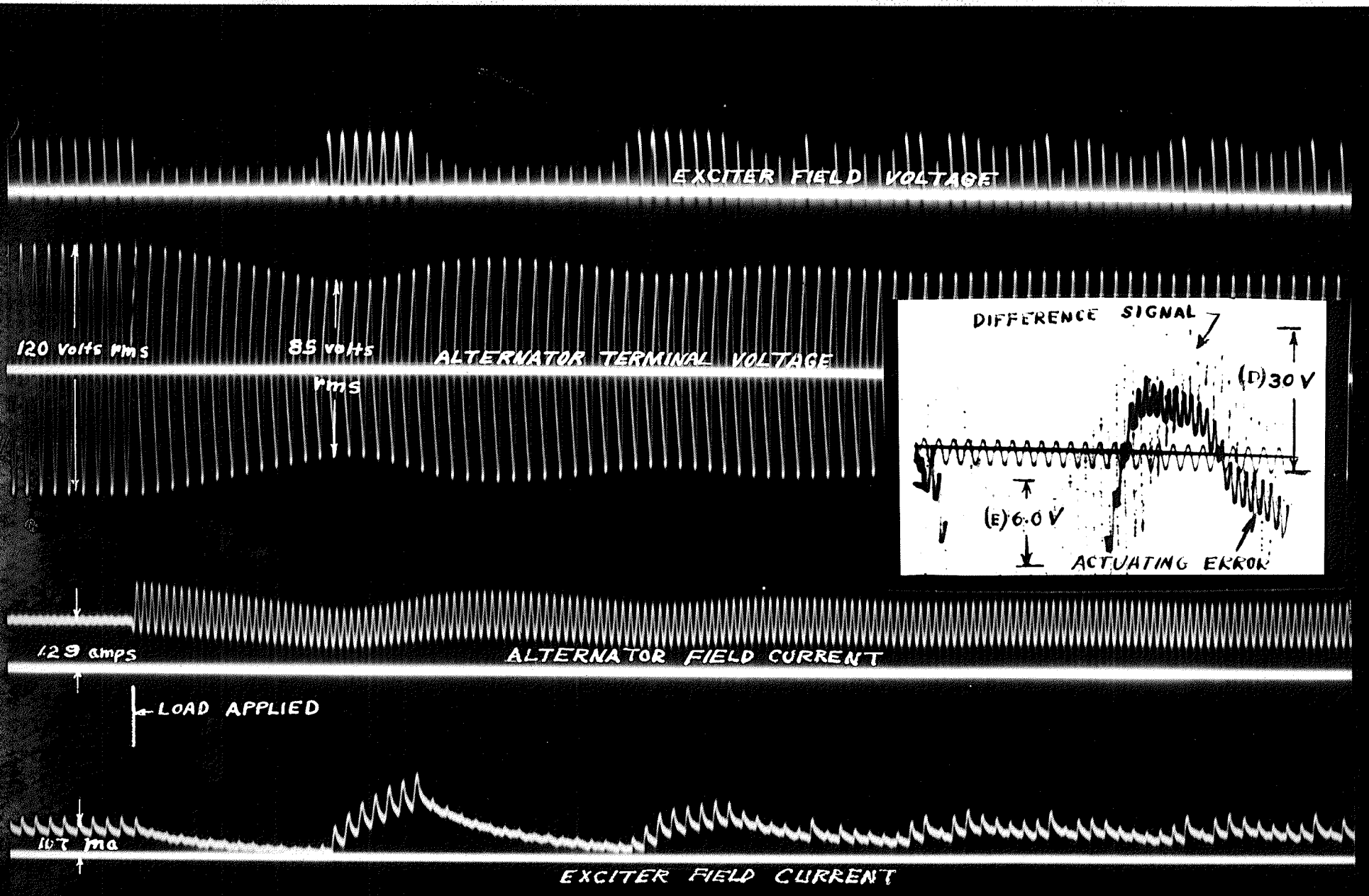

FIG. 8.8 TRANSIENT RESPONSE OF ALTERNATOR UPON APPLICATION OF A SINGLE-PHASE LOAD AT 100 % PF

Thus, two of the transformers maintained a normal voltage at the output of the rectifiers in the detector circuit, thereby preventing an actuating error to exist. A similar problem would exist if the load was applied across phase and neutral. This test was not carried out because the neutral was not accessible.

In order to utilize this regulator for a single-phase load, a single-phase detector must be used, which would be placed across the loaded lines.

Fig. 8.9 illustrates the effectiveness of the regulator when starting a wound rotor induction motor. The nameplate data of the test motor is as follows:

General Electric Induction Motor

Type MT 45A - 1800
Form 0
Amps 27 Sec. Amps 15
Volts 110
Speed NL 1800
Resistance in rotor circuit 2.5 ohms per phase
NL speed with resistance in rotor circuit 1680 rpm

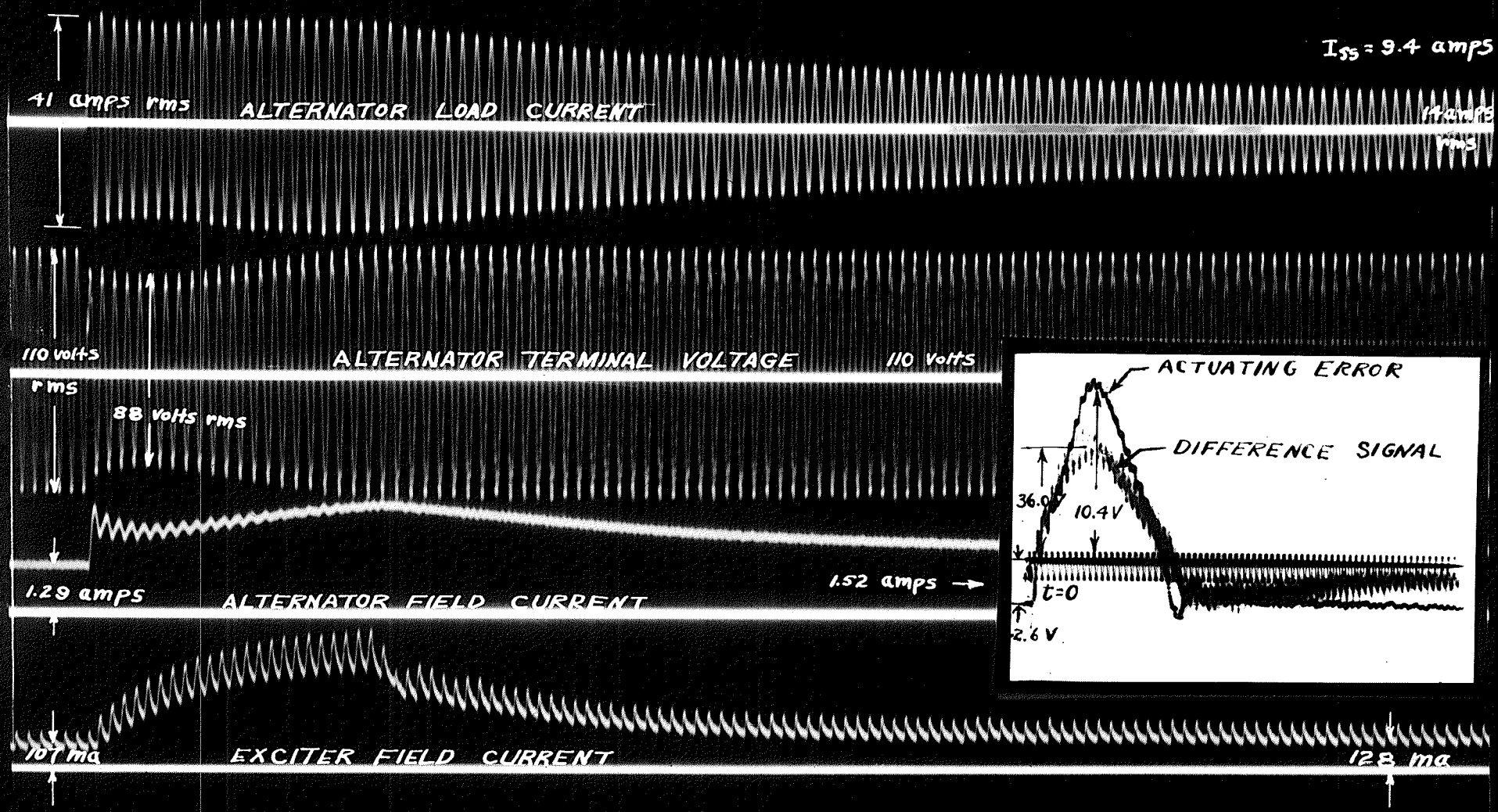

FIG. 8.9 TRANSIENT RESPONSE OF ALTERNATOR UPON STARTING A WOUND ROTOR INDUCTION MOTOR

8.3 Maximum Voltage Rise Upon Removal of Load

When load is suddenly removed from an alternator, the voltage will first rise to some maximum value and then reduce to the initial value due to the regulator action. Rather than include a complete closed-loop system in the analysis, a given voltage, as a function of time, will be applied to the exciter field. As with the case in which load was suddenly applied, armature transients, speed changes and subtransient effects are neglected.

In the previous section it was noted that e_q', the quadrature component of the voltage behind the transient reactance, never experienced a sudden change with load changes. Therefore, as the stator circuit is opened the terminal voltage will immediately rise to the value of e_q'. From here the terminal voltage would rise exponentially with the alternator open-circuit time constant if the exciter voltage was constant. However, the regulator effect is in an opposite direction so that the voltage will rise only by a limited amount and then begin its downward trend. The solution for the transient response will consist of superimposing the following components which contribute to a change in terminal voltage:

(1) The direct-axis component of terminal voltage, e_d caused by opening the switch.

(2) The quadrature-axis component of terminal voltage, caused by opening the switch.

(3) The quadrature-axis voltage caused by a change in the excitation voltage.

Fig. 8.1 shows the first two components on the vector diagram.

From Park's equations[1]

$$e_d = \psi_q$$

$$e_q = \psi_d$$

$$e_f = p\psi_f + r_f i_f \qquad - - - - - - - \quad (8.8)$$

---

1. C. Concordia, Synchronous Machines, pp. 17, J. Wiley and Sons, Inc., 1951.

The flux linkages are

$$\psi_d = -\chi_d i_d + \chi_{ad} i_f \qquad \text{- - - - - - - (8.9)}$$

$$\psi_q = -\chi_q i_q$$

$$\psi_f = -\chi_{ad} i_d + \chi_{ff} i_f \qquad \text{- - - - - - - (8.10)}$$

Combining equations 8.8 and 8.10

$$e_f = -p\,\chi_{ad} i_d + (p\,\chi_{ff} + r_f) i_f$$

or $$i_f = \frac{e_f + p\,\chi_{ad} i_d}{p\,\chi_{ff} + r_f}$$

Substituting the above into equation 8.9

$$e_q = -\chi_d i_d + \chi_{ad}\left(\frac{e_f + p\,\chi_{ad} i_d}{p\,\chi_{ff} + r_f}\right)$$

$$= \frac{\chi_{ad}\, e_f}{\left(1 + p\,\frac{L_{ff}}{r_f}\right) r_f} - i_d\left(\chi_d - \frac{p\,\chi_{ad}^2}{p\,\chi_{ff} + r_f}\right)$$

$$= \frac{\chi_{ad}\, e_f / r_f}{1 + p\,T_{do}^1} - i_d\left(\frac{p\,\chi_{ff}(\chi_d - \chi_{ad}^2/\chi_{ff}) + \chi_d r_f}{r_f(1 + p\,T_{do}^1)}\right)$$

but $\chi_d - \chi_{ad}^2/\chi_{ff} = \chi_d'$

Therefore,

$$e_q = \frac{\chi_{ad}\, e_f / r_f}{1 + p\,T_{do}'} - i_d\left(\frac{\chi_d + \chi_d'\, p\,T_{do}'}{1 + p\,T_{do}'}\right)$$

$$= G(p)E - \chi_d(p) i_d$$

where $G(p) = \frac{1}{1 + p\,T_{do}'}$

$$E = \frac{\chi_{ad} e_f}{r_f}$$

$$\chi_d(p) = \frac{\chi_d + \chi_d' \, p \, T_{do}'}{1 + p \, T_{do}'}$$

$$T_{do}' = \frac{\chi_{ff}}{r_f}$$

Also from Park's equations,

$$e_d = \chi_q i_q$$

Having produced the preceding equations the various components contributing to the alternator terminal voltage can now be described analytically as functions of time:

(1) $e_d(t) = \chi_q i_q(t)$

(2) $e_{q1}(t) = -\chi_d(p) \, i_d(t)$

(3) $e_{q2}(t) = G(p) \, \Delta E \, (t)$

(1) Effect of opening the switch is given by

$$i_q(t) = i_q(o) - i_q(o) \, U(t)$$

Therefore

$$e_d(t) = \chi_q \Big(i_q(o) - i_q(o) \, U \, (t) \Big)$$

(2) The component of the incremental quadrature-axis voltage caused by opening the switch with the excitation voltage constant is

$$e_{q_1} \, (t) = -\chi_d(p) \, i_d(t) \qquad - - - - - - \quad (8.11)$$

and $i_d(t) = i_d(o) - i_d(o) \, U(t)$

Taking Laplace transforms of equation 8.11 yields

$$E_{q1}(s) = \chi_d(s)\,\frac{i_d(o)}{s}$$

$$= \frac{(\chi_d + \chi_d' T_{do}'s)}{1 + T_{do}'s}\;\frac{i_d(o)}{s}$$

since zero initial conditions apply.

Expanding the above into partial fractions yields

$$E_q'(s) = \left(\frac{\chi_d}{s} + \frac{(\chi_d' - \chi_d)}{s + 1/T_{do}'}\right) i_d(o)$$

By taking the inverse transform the above becomes

$$e_{q1}(t) = i_d(o)\left(\chi_d - (\chi_d - \chi_d')\, e^{-t/T_{do}'}\right) U(t)$$

(3) The component of the quadrature-axis voltage as caused by a change in excitation voltage is

$$e_{q2}(t) = G(p)\;\Delta E(t)$$

By taking the Laplace transforms this becomes

$$E_{q2}(s) = G(s)\;\Delta E(s)$$

Now E(t) denotes the excitation voltage which is identical to the excitation current in per-unit during steady-state conditions. The nature of response of the exciter voltage depends on the exciter field voltage supply. Upon load removal the supply to the detector circuit rises and this produces an actuating error which decreases the firing angle to the minimum possible value. It can be assumed that the thyratron acts as an open circuit during the period following the disturbance and that whatever current was present in the exciter

field, it will decay exponentially through the back rectifier, with the time constant of the field.

The time constant of the loaded exciter for a decaying process will be somewhat larger than T_e which was the time constant of the loaded exciter for a build-up process. This is due to the higher degree of saturation which the exciter field core experiences during a a build-up process. Saturation, of course, causes a smaller inductance and likewise time constant. For the decaying process a larger inductance will be present in the field circuit due to operation in the lower portion of the saturation curve. Two time constants have been evaluated experimentally for the exciter field, Appendix B:

(1) $T_f = 0.115$ sec, which is the time constant of the exciter field as determined over the linear portion of the saturation curve and with the exciter unloaded.

(2) $T_e = 0.080$ sec, which is the time constant of the exciter field as determined when the exciter voltage was increased from its no-load voltage to the ceiling voltage. The exciter was loaded during this test.

For the case at hand, the exciter operates over both the linear portion and the non-linear portion of the saturation curve, hence the time constant will lie between the above two values.

This value can be assumed to be the average,

$$T_f' = \frac{0.080 + 0.115}{2}$$

$$= 0.0975 \text{ sec}$$

The exciter voltage $E_e(t)$ will also decay with this time constant after a delay of h sec,

$$E_e(t) = E\, e^{-t/0.0975}\, U(t - h)$$

The exciter voltage when plotted, Graph 8.4, decays exponentially. This decay can be approximated by a straight line with a slope of -5.45t p/u/sec. Having this slope, the change in excitation voltage,

THIS MARGIN RESERVED FOR BINDING.

IF SHEET IS READ THE OTHER WAY (VERTICALLY), THIS MUST BE LEFT-HAND SIDE.

GRAPH 8.4 APPROXIMATE RATE OF DECAY OF EXCITER VOLTAGE UPON LOAD REMOVAL

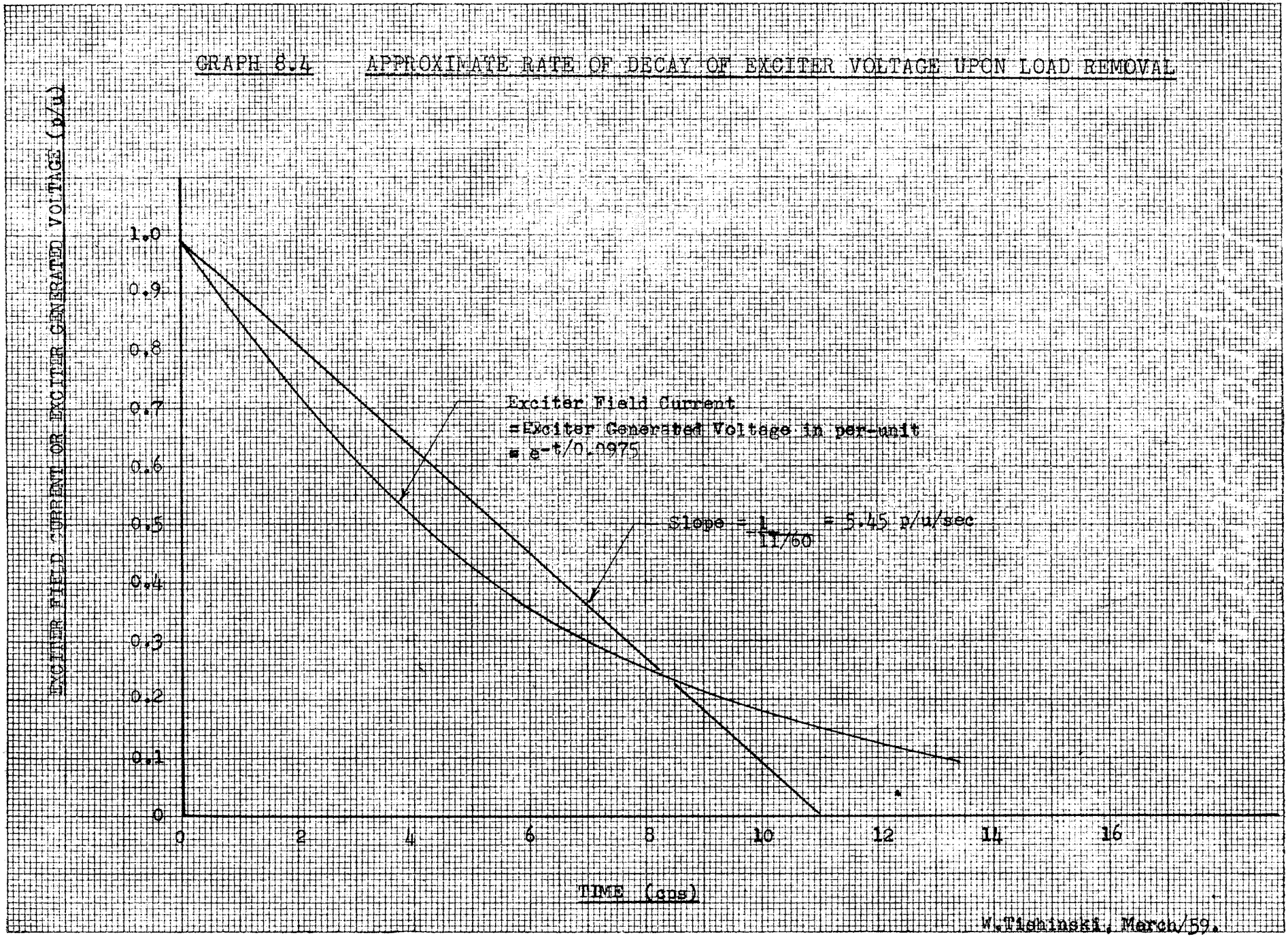

W.Tichinski, March/59.

MANUFACTURED BY REMOUF PUBLISHING CO., MONTREAL

FORM 100

E(t) can be expressed as

$$E(t) = -5.45t\ U(t-h)$$

or

$$E(s) = \frac{-5.45\ e^{-hs}}{s^2}$$

Then

$$E_{q2}(s) = G(s)\ \Delta E(s)$$

$$= \frac{1}{(1 + T_{do}'s)} \cdot - \frac{(5.45)\ e^{-hs}}{s^2}$$

Expanding the above into partial fractions yields

$$E_{q2}(s) = -5.45e^{-hs}\left(- \frac{T_{do}'}{s} + \frac{1}{s^2} + \frac{T_{do}'}{s + 1/T_{do}'} \right)$$

By taking the inverse transform this becomes

$$e_{q2}(t) = -5.45\left((t-h) - T_{do}'\ (1 - e^{-(t-h)/T_{do}'})\right) U(t-h)$$

The total quadrature-axis voltage is proportional to the field flux linkage. In section 8.1, this component of voltage was denoted by e_q'. Therefore, the total quadrature-axis voltage is

$$e_q'(t) = e_q(o) + e_{q1}(t) + e_{q2}(t)$$

$$= e_q(o) + i_d(o)\left(\chi_d - (\chi_d - \chi_d')e^{-t/T_{do}'} \right) U(t)$$

$$- 5.45\left((t-h) - T_{do}'\ (1 - e^{-(t-h)/T_{do}'}) \right)\ U\ (t-h)$$

- - - - - (8.12)

and the direct-axis component of terminal voltage is

$$e_d(t) = \chi_q\left(i_q(o) - i_q(o)\ U(t)\right) \qquad \text{- - - - - (8.13)}$$

Upon removal of load, that is, at $t = o^+$,

$$e_q'(t) = e_q(o) + i_d(o)\, X_d'$$

$$e_d(t) = 0$$

and since

$$|e_t| = \sqrt{e_d^2 + e_q'^2}$$

$$|e_t| = e_q(o) + i_d(o)\, X_d'$$

The above equation gives the same relation between e_t and e_q' as does equation 8.1.

If the removed load is full load at 80% pf, lagging, from Fig. 8.1,

$$e_q(o) = 0.995 \text{ p/u}$$

$$i_d(o) = 0.796 \text{ p/u}$$

$$i_q(o) = 0.606 \text{ p/u}$$

The delay factor h will be evaluated in a manner similar to that for the sudden application of load. If load is suddenly removed the predominant term in the transfer function of the detector circuit is

$$\frac{1}{(1 + 0.035s)}$$

The weighting function can be approximated by $3.26\ (1 - e^{-28.6t})$. If e_t prior to any load changes is 1.00 p/u, then

$$e_q' = \frac{1}{0.872}$$

$$= 1.15 \text{ p/u}$$

When the load is removed, the field flux linkages do not change instantaneously. Therefore e_q' remains constant immediately after the

switch is opened and the terminal voltage rises instantaneously to this value. This sudden rise in terminal voltage is 0.15 p/u or 18 volts. A negative swing of 2.5 volts in the grid bias of the 6AC7 error-amplifying tube will produce cut-off conditions in the thyratron. The time taken for this condition can be evaluated from the following relation:

$$2.5 = 18.0 \times 3.26 \left(1 - e^{-28.6t}\right)$$

or $$t = 0.0015 \text{ sec}$$

which is merely a fraction of a cycle. Hence, the delay factor h can be neglected when treating the sudden removal of loads.

A sample calculation will be shown for the evaluation of e_t at $t = 1$ cps.

$$e_d = 0$$

$$e_q' = 0.995 + 0.796 \left(0.985 - (0.985 - 0.194)e^{-0.0167/0.234}\right) - 5.45 \left(0.0167 - 0.234(1 - e^{-0.0167/.234})\right)$$

$$= 1.189 \text{ p/u}$$

$$e_t = 120 \times 1.189$$

$$= 142.2 \text{ volts}$$

TABLE 8.6

COMPUTATIONS OF e_t AFTER DROPPING FULL LOAD AT 80% PF, LAGGING

Time (cps)	e_q' (p/u)	e_t (volts)
0	1.149	137.5
1	1.189	142.2
2	1.221	146.5
3	1.243	149.0
5	1.267	152.0
7	1.263	151.5
9	1.262	151.4
11	1.186	142.0
13	1.122	135.0
16	1.027	123.0

Graph 8.5 shows a relatively good agreement between the calculated and recorded curves. The discrepancy during the initial part of the curves is due to the neglect of the subtransient reactance. This gives a calculated step-voltage somewhat larger than the actual.

The assumption that the delay factor h was negligible was correct as can be seen from Fig. 8.10. Upon load removal, the thyratron immediately began to fire at its minimum angle. This created the effect of a negative unit-step input applied to the exciter field. The exciter field is seen to decay exponentially with a time constant of approximately 0.10 sec, which corresponds to the equation of the field current, Graph 8.4.

Any error in the calculated results could be attributed to the transient reactance. For small machines the transient time constant is relatively small and this does not give many points on the graph used for evaluating the initial transient current, as can be seen from Graph B.6.

Thus, an inaccurate value of X_d' could be largely responsible for the discrepancy between the calculated and recorded curves. The deviation of the curves in the latter stages is due to the assumption of a linear characteristic of the exciter voltage. During this period, the exponential function has "flattened-out", which will tend to slow down the response as indicated by the recorded curve.

Figs. 8.10 and 8.11 show the effect of various amounts of stabilizing feedback on the transient response. With 100% of the total available anti-hunt signal being utilized for stability, little undershoot occurs in the terminal voltage. However, with 71% of the available anti-hunt signal being fed back, a definite undershoot occurs, followed by an overshoot. Optimum conditions exist with 100% of the signal fed back since it is seen that the anti-hunt setting does not affect the transient response to any noticeable extent. With 100% feedback the actuating error signal swings downward to a peak value of 40.0 volts, whereas with 71% feedback it reaches a maximum value of 51.0 volts. This difference between the actuating error

THIS MARGIN RESERVED FOR BINDING.

IF SHEET IS READ THE OTHER WAY (VERTICALLY), THIS MUST BE LEFT-HAND SIDE.

GRAPH 8.5 CALCULATED AND RECORDED ALTERNATOR TERMINAL VOLTAGE UPON SUDDEN REMOVAL OF FULL LOAD AT 80 % PF, LAGGING

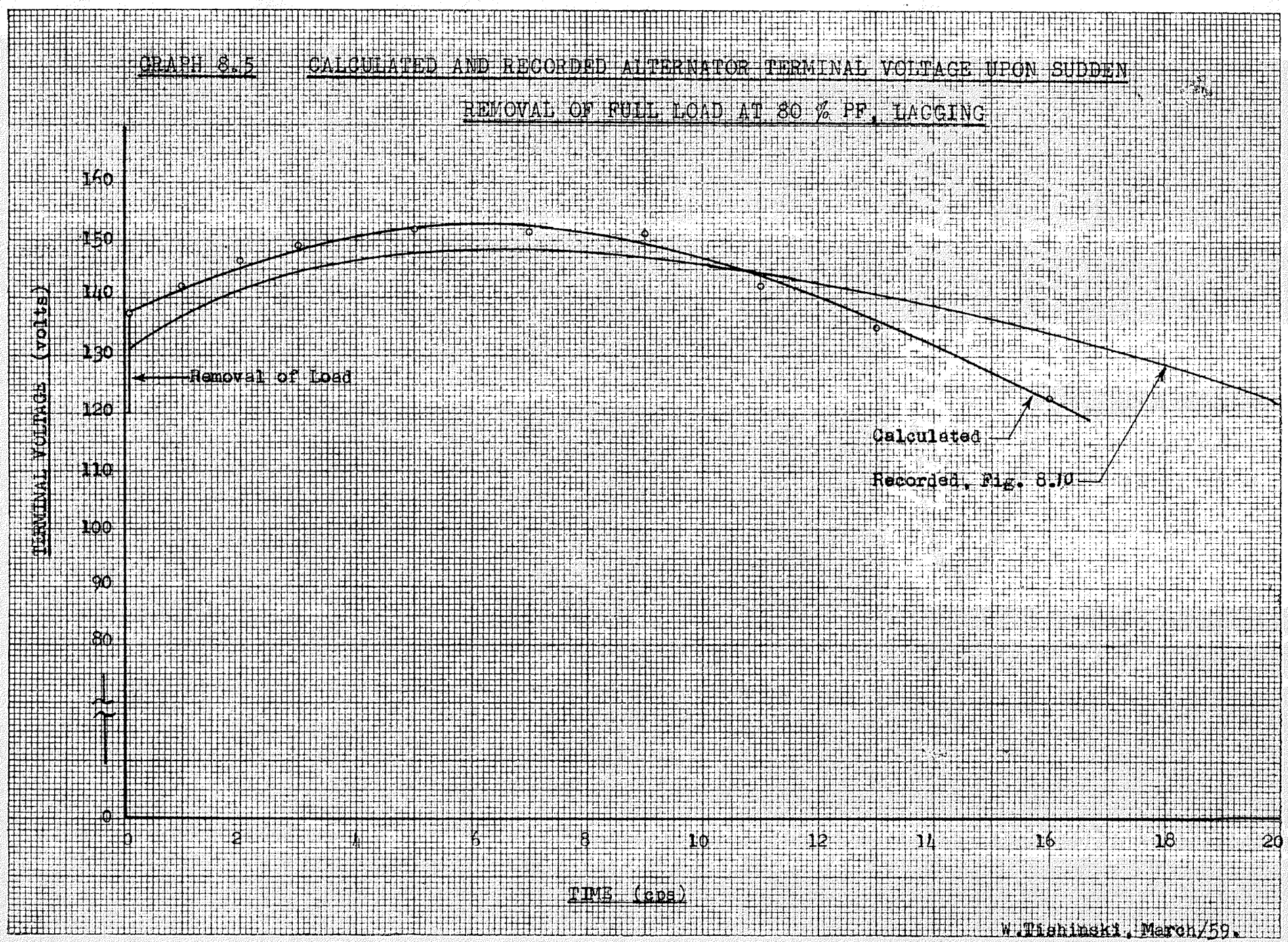

W.Tishinski, March/59.

MANUFACTURED BY REMOUF PUBLISHING CO., MONTREAL

FORM 100

LAGGING AND WITH 100 % FEEDBACK

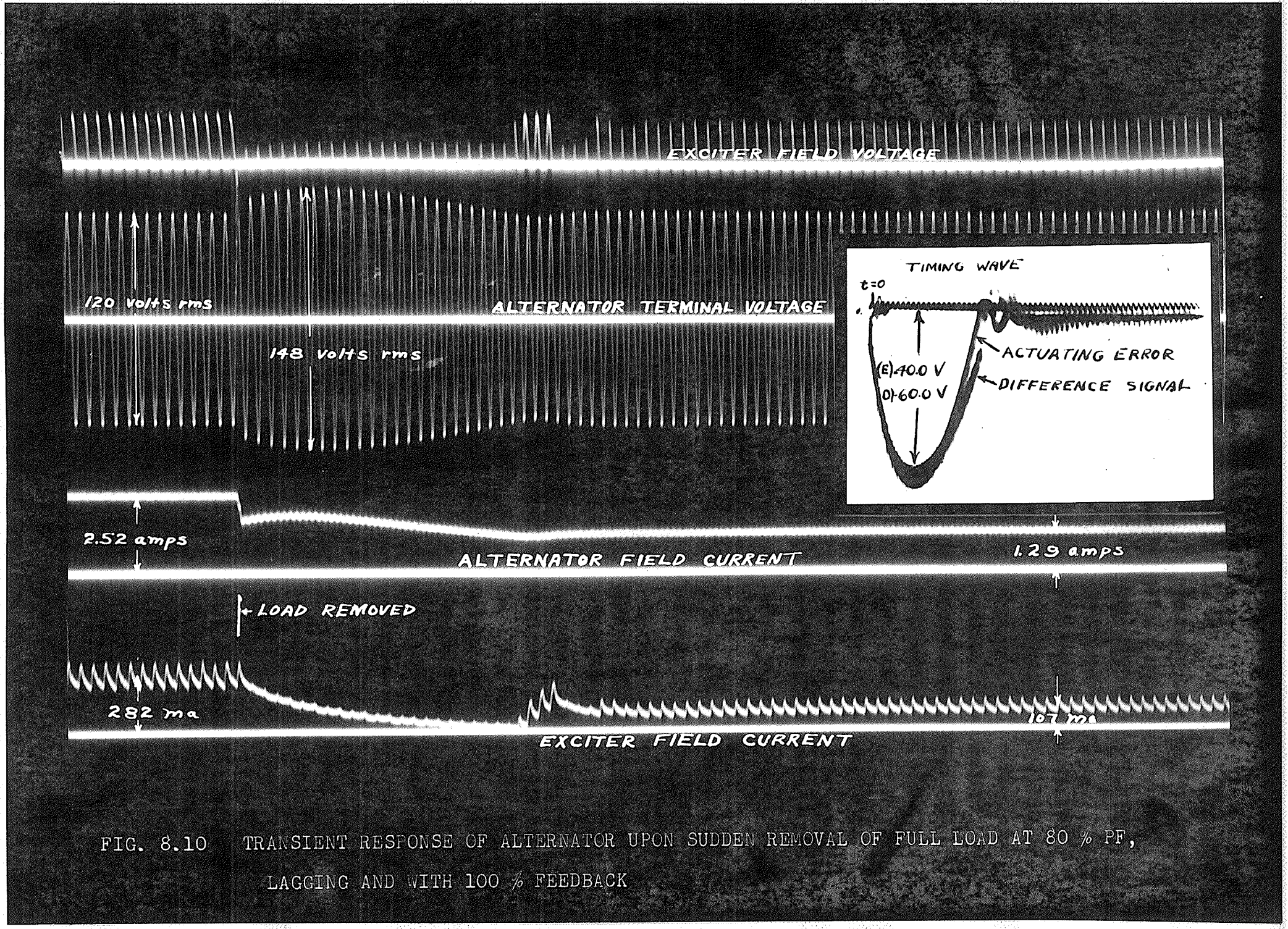

FIG. 8.10 TRANSIENT RESPONSE OF ALTERNATOR UPON SUDDEN REMOVAL OF FULL LOAD AT 80 % PF, LAGGING AND WITH 100 % FEEDBACK

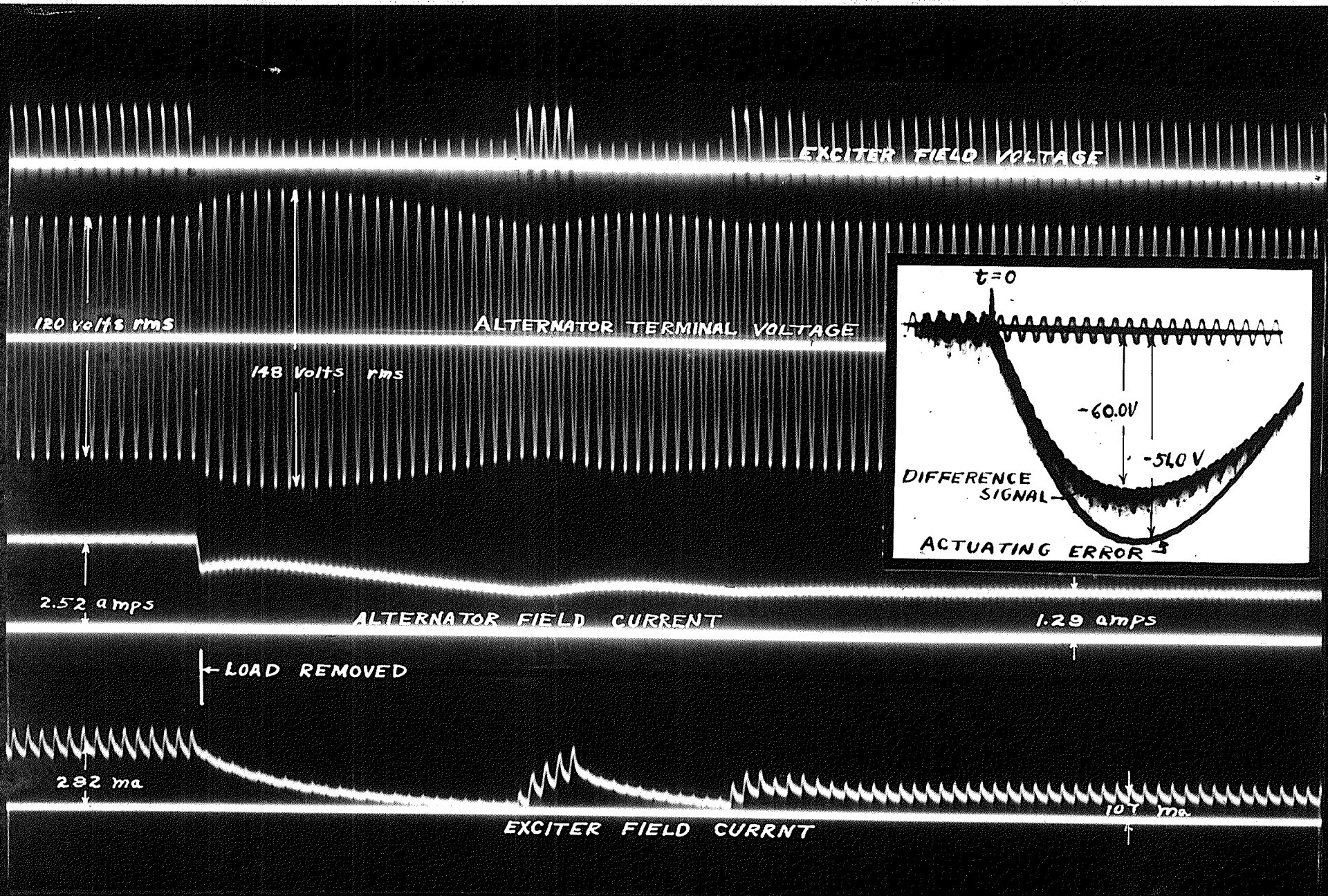

FIG. 8.11 TRANSIENT RESPONSE OF ALTERNATOR UPON SUDDEN REMOVAL OF FULL LOAD AT 80 % PF, LAGGING AND WITH 71 % FEEDBACK

signals does not affect the transient response since in this neighborhood both signals produce cut-off conditions on the 6AC7 pentode.

As with the application-of-load case, a unity power factor load is less severe than an 80% pf, lagging load. Fig. 8.12 shows the transient response upon removal of full load at 100% pf.

Equation 8.12 applies for the removal of all types of loads. If the removed load is full load at 100% pf, then from the steady-state vector diagram, Fig. 8.2,

$$e_q(o) = 0.940 \text{ p/u}$$

$$i_d(o) = 0.444 \text{ p/u}$$

$$i_q(o) = 0.896 \text{ p/u}$$

All other constants remain the same, and calculations can be repeated for the above loading.

TABLE 8.7

COMPUTATIONS OF e_t AFTER DROPPING FULL LOAD AT 100% PF

Time (cps)	e_q' (p/u)	e_t (volts)
0	1.026	123.0
1	1.047	125.5
2	1.061	127.3
3	1.067	128.0
5	1.061	127.3
7	1.031	123.9
9	1.011	121.5

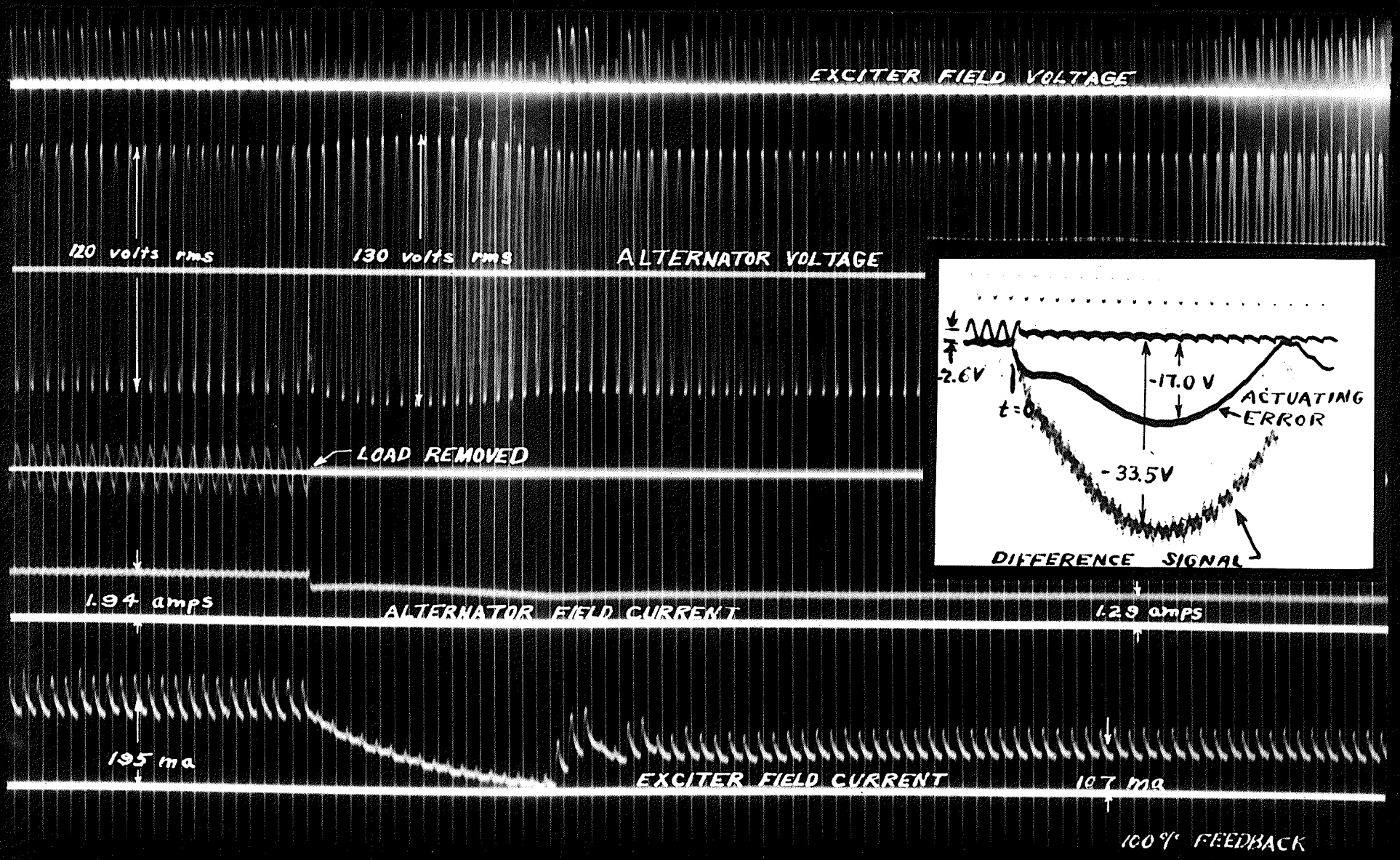

FIG. 8.12 TRANSIENT RESPONSE OF ALTERNATOR UPON SUDDEN REMOVAL OF FULL LOAD AT 100 % PF

The curves in Graph 8.6 follow the same trend as those in Graph 8.5, so any comments pertaining to the 80% pf, lagging case would also apply to the 100% pf case.

Having determined the relative performance of the voltage-regulating system for both the steady-state and transient conditions, the question that arises is methods of improving this performance.

Little is left to be desired of this system in its steady-state operation since regulation at full load is at worst 0.60%. However, should it be necessary to decrease the regulation, the following components could be modified:

(1) The saturable reactor. Operation did not take place entirely upon the linear region. If a reactor possessed a long linear region in its saturation characteristics, the gain could have been held constant throughout all regions.

(2) The detector circuit. If greater gain is provided by the detector circuit a smaller change at the alternator terminal voltage would create the necessary corrective measures. This step is not advisable due to practical limitations. The output from the detector rectifier is presently at 500 volts d-c and a larger output would demand higher-rated rectifier components.

(3) The reference circuit. An increase in gain for this circuit would be necessary to conform with the corresponding increase in the detector circuit.

One should take care not to over-emphasize the advantages of a large gain in a system, since systems with large gains are always more difficult to stabilize.

In attempting to increase the transient responses, reference should be made to equations 8.6 and 8.12. The only controlled variable in equation 8.6, which gives the transient response for the application of loads, is e_c, the ceiling voltage of the exciter. The remaining terms are constant, and are determined by the characteristics of the machine. The ceiling voltage of the exciter can be elevated by replacing the exciter field supply transformer with one containing a higher step-up ratio. The present ceiling exciter field current is

THIS MARGIN RESERVED FOR BINDING.

IF SHEET IS READ THE OTHER WAY (VERTICALLY), THIS MUST BE LEFT-HAND SIDE.

GRAPH 8.6 CALCULATED AND RECORDED ALTERNATOR TERMINAL VOLTAGE UPON SUDDEN REMOVAL OF FULL LOAD AT 100 % PF

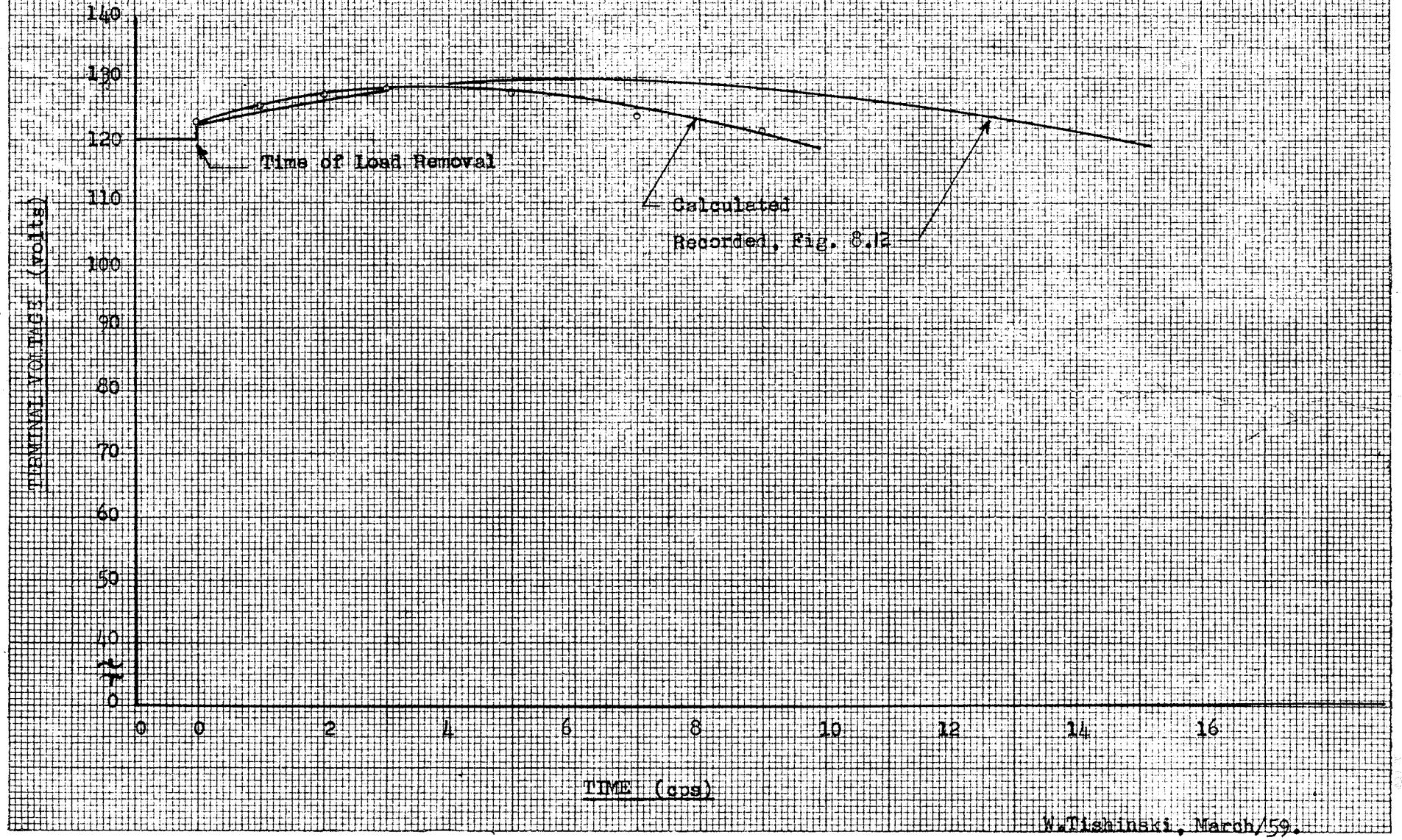

W.Tischinski, March/59.

MANUFACTURED BY RENOUF PUBLISHING CO., MONTREAL

FORM 1009

510 ma, which is 145% of the rated value of 350 ma. This could be increased to possibly 200%. This magnitude would exist only in transient state and would not cause excessive heating of the exciter field windings.

Equation 8.12 shows that there are no components which can readily be modified to increase the response of the alternator when load is dropped. All terms in the equation are determined by the characteristics of the machine.

CHAPTER IX

PRACTICAL DIFFICULTIES WITH CIRCUIT OPERATION

9.1 Ripple in the Actuating Error Signal

The designed circuit in its preliminary stages presented difficulties due to ripple from the following sources:

(1) A small ripple of 0.05 volts, peak to peak, existed across the voltage-regulating tubes in the reference circuit. This magnitude of ripple was almost insignificant compared to the other ripples present in the circuit.

(2) A ripple from the detector circuit was treated earlier, Fig. 3.8. Larger capacitors, which produced better filtering action, also produced a slower response, and for this reason were undesirable.

(3) Sixty-cycle-per-second ripple, due to electromagnetic induction, was experienced in the existing circuit. This was mainly caused by the wire-wound potentiometers. The recorded wave across points a and b, Fig. 9.1, is shown in Fig. 9.2. Point e and the detector circuit were physically disconnected from the reference supply. Since the ripple across the gas tubes was only 0.05 volts, peak to peak, the additional ripple must be due to pick-up. As the slider of the potentiometer was moved towards the positive end of the refernce supply, this ripple signal decreased proportionally. Fig. 9.3 shows a record of the wave across f and ground with the detector supply off and e disconnected. The magnitude of this ripple has decreased somewhat from that of Fig. 9.2. Fig. 9.4 is the trace across b and ground with the detector supply off and the reference supply on. The circuit is once again disconnected at e. The ripple magnitude in this case is 2.1 volts, peak to peak, which is larger than the 0.3 volt ripple across f to ground. It is practically impossible to predict what effect pick-up will have on the circuit.

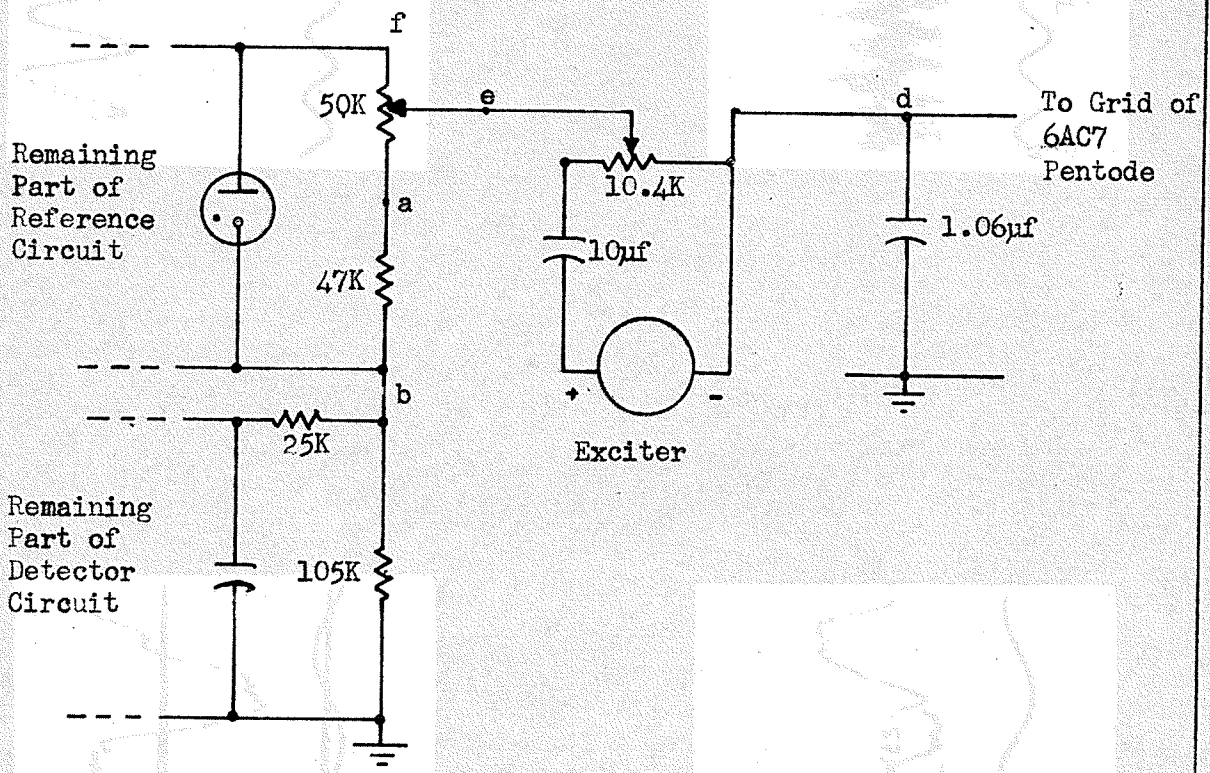

FIG. 9.1 PORTION OF REGULATING CIRCUIT CONTRIBUTING RIPPLE COMPONENTS

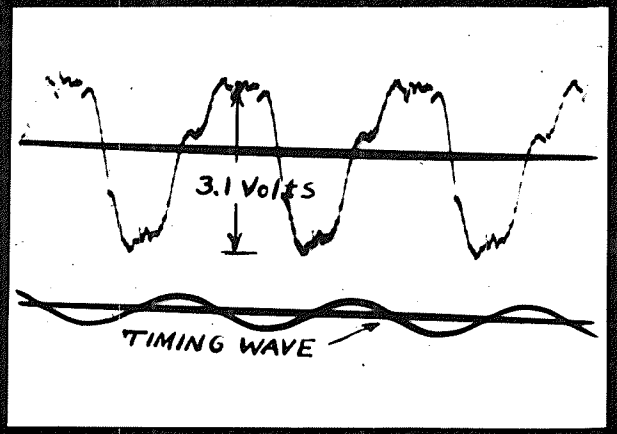

FIG. 9.2 RIPPLE ACROSS POINTS a AND b

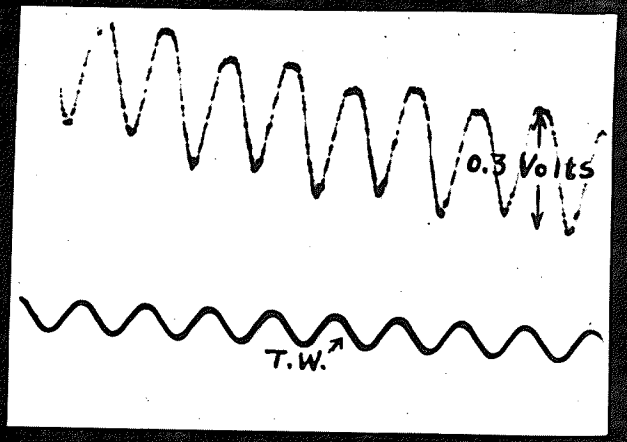

FIG. 9.3 RIPPLE ACROSS f AND ground

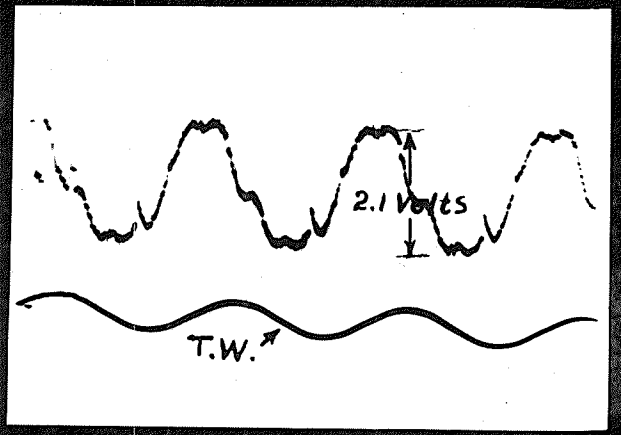

FIG. 9.4 RIPPLE ACROSS b AND ground

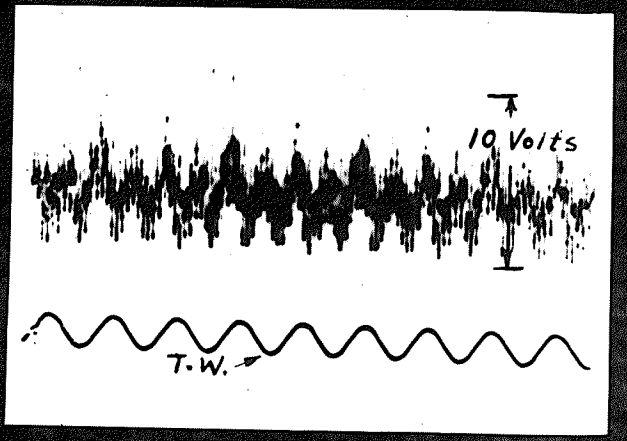

FIG. 9.5 ACTUATING ERROR SIGNAL WITH NO FILTER CAPACITOR

(4) The most serious source of ripple was from the exciter through the feedback circuit. Although the 10 μf capacitor blocked out the d-c component of the exciter voltage it easily by-passed most of the ripple. The harmonic content of the exciter voltage was analysed by means of a General Radio Co., Wave Analyzer, Type 736 - A, Serial No. 1276.

TABLE 9.1

HARMONIC CONTENT OF THE EXCITER AT VARIOUS D-C VOLTAGE LEVELS

(a) E_e (loaded) = 50 volts

N = 1800 rpm

Ripple Frequency (cps)	Magnitude (volts-rms)	Ripple Frequency (cps)	Magnitude (volts-rms)
27	0.13	780	0.40
56	0.30	1,000	0.20
120	0.75	1,025	0.14
188	0.09	1,100	0.12
240	0.09	1,150	0.14
300	0.07	1,200	0.16
330	0.07	1,300	0.22
360	0.05	1,350	0.25
420	0.06	1,520	0.60
450	0.10	1,610	0.26
480	0.15	1,680	0.23
510	0.17	1,800	0.20
530	0.26	2,000	0.10
600	0.17	Plus higher harmonics	

(b) E_e (loaded) = 100 volts
N = 1800 rpm

Ripple Frequency (cps)	Magnitude (volts-rms)	Ripple Frequency (cps)	Magnitude (volts-rms)
25	0.22	450	0.15
55	0.40	480	0.32
119	2.50	510	0.28
188	0.16	530	0.48
240	0.75	600	0.42
300	0.10	680	0.28
330	0.12	720	0.26
360	0.18	740	0.26
420	0.20	760	2.40
		800	0.60

plus all higher harmonics recorded in (a)

The difference signal when summed with the feedback signal, produced a wave as recorded in Fig. 9.5. This wave was recorded with the regulating system fully in operation and with the no-load alternator terminal voltage at 120 volts. The 1.06 μf capacitor had been disconnected for this test. A small pulsating signal was indicated by a d-c voltmeter applied across the 6AC7 pentode grid and ground. This was caused by all of the ripple frequencies superimposed on the grid bias.

The effect of several sizes of capacitors was tested across d and ground, Fig. 9.1. A large capacitor produced the best filtering effect but this caused instability. Increasing the feedback signal to stabilize the system introduced more undesirable effects in that a larger voltage drop was tapped off the 10K resistor. This meant that the magnitude of the ripple component was larger, thus partially nullifying the effect of introducing a larger filter capacitor. An optimum value of capacitor finally selected was 1.06 μf.

Figs. 9.6 and 9.7 show the effect of varying the feedback signal from 60% to 100%. A slightly larger magnitude in the ripple component is noticeable with more feedback.

When the speed of the alternator and exciter decreased below rated, as upon loading, another effect appeared. A ripple with a beat frequency of approximately 2 cps was produced by the exciter ripple and the detector circuit ripple. This beat-frequency ripple was determined by the speed of the exciter and became more frequent as the exciter speed decreased. If the exciter speed reached its rated value this beat-frequency ripple disappeared.

This beat frequency was more serious upon the firing angle of the thyratron than the higher harmonics, since it could not be smoothed out by the saturable reactor. Small fluctuations were noted in the exciter field current ammeter with the same frequency as the beat-frequency ripple, which was applied to the 6AC7 grid. Without any filter capacitor across the 6AC7 grid these fluctuations in the field current were estimated as being in the order of 2 to 3% in magnitude.

Figs. 9.6 and 9.8 illustrate the presence of this beat frequency. The harmonics in the wave in Fig. 9.8 are regular while those in Fig. 9.6 are not.

An attempt was made to eliminate this beat-frequency ripple. It was hoped that if a filter for a 60-cps signal was placed across the line, containing the actuating error signal, this component would be removed and thus eliminate the beat.

A parallel-T network, which has characteristics of fine tuning, was tested, but it imposed too great of a load on the preceding stages and caused no-load instability.

An L-C series filter was tested as well, but it was then realized that neither one of the components causing the beat was 60-cps, but both were variable depending on the speed of the machine.

Therefore, a simple capacitor filter was introduced, which decreased the magnitude of the ripple with the beat frequency but did

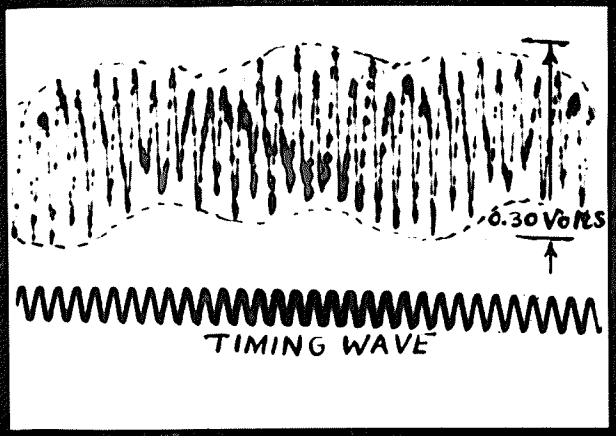

FIG. 9.6 RIPPLE IN ACTUATING ERROR SIGNAL WITH 60 % FEEDBACK, N=1720 rpm

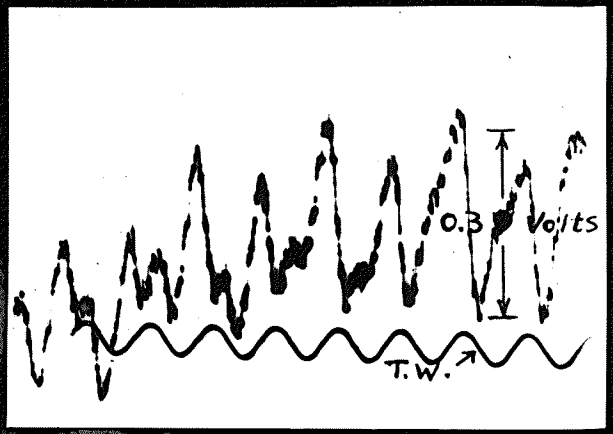

FIG. 9.7 RIPPLE IN ACTUATING ERROR SIGNAL WITH 100 % FEEDBACK, N=1720 rpm

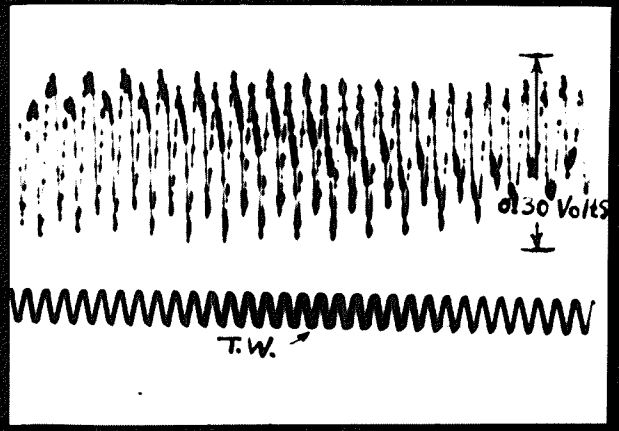

FIG. 9.8 RIPPLE IN ACTUATING ERROR WITH 60 % FEEDBACK, N=1800 rpm

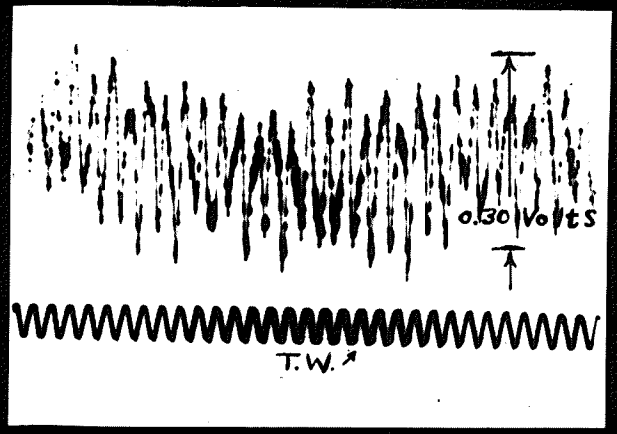

FIG. 9.9 RIPPLE IN ACTUATING ERROR WITH FULL LOAD AT 100 % PF APPLIED TO ALTERNATOR, N=1690 rpm

not completely eliminate it. The fluctuations, as noted on the exciter field current ammeter, were less than 1 %, which are of minor consequence.

Another technique used to decrease the pick-up in the system was to ground the chassis, containing the regulating components, to the frame of the alternator. This reduced the ripple magnitude by approximately 10 %.

CHAPTER X

CONCLUSIONS

An attempt had been made to design a voltage-regulating system and evaluate its performance from a purely theoretical basis. However, it was found that on numerous occasions, the calculated results deviated considerably from the test results. Therefore, occasional readjustments in the design figures had to be made. These complications were caused by the non-linear components, unequal alternator terminal voltages and by the ripple components in the exciter voltage. Because of these discrepancies, construction followed closely after component design work, in order that a test could be conducted on its performance before proceeding to the next stage.

The recorded transient performance of the alternator, upon sudden application of full load, agreed quite well with the theoretical curves. As mentioned previously, greater percentage errors can be expected in the evaluated constants of the machine due to their small magnitudes. This is a factor contributing largely to the discrepancy between the calculated and recorded curves. The results of the various recorded responses were discussed in their respective sections.

Due to the rise of many unforseen complications and to the lengthy computations involved in designing regulating systems, many industries have abandoned the purely theoretical approach and have resorted to the use of analog computers. However, in order to simulate a regulating system on a computer, one must be thoroughly familiar with the operation of the various components in the alternator. A thorough knowledge can be obtained only by a detailed theoretical treatment of such a system. Thus, the analysis, as presented in this thesis, may be considered to be the preliminary stage in a study of a servomechanism system on an analog computer.

APPENDICES

APPENDIX A

WAVE SHAPE RECORDING TECHNIQUE

A.1 The Phantastron Circuit

In order to make a thorough and accurate evaluation of the performance of electrical equipment, a record of the current and voltage wave shapes, produced by the various components within the apparatus, are required. Photographing the wave, as viewed on an oscilloscope, is one common form of recording. A recurrent wave poses no problem here since it can be synchronized or held stationary on the oscilloscope screen. However, when a transient or a pulse occurs, the problem of photographing becomes more complex. Since the wave to be recorded is not of the recurring type, the time base must be set for single sweep operation. The sweep is triggered just prior to the application of the transient wave signal to the oscilloscope input terminals.

Since the starting time of this wave can be anticipated the shutter of the camera can be opened a fraction of a second before the sweep begins. However, in this short interval the beam, which sits in wait to begin its sweep, causes an undesirable blot on the film by overexposure, thus obliterating the detail of the initial part of the wave. So for proper recording the beam and time base must both be triggered after the camera shutter is open and before the transient wave appears.

The oscilloscopes employed in this thesis were two Cossor Double Beam Oscilloscopes, Model 1049. All terminals mentioned will refer exclusively to this type of oscilloscope. For purposes of convenient notation the oscilloscope bearing Serial Number 01954 will be referred to as the Mark I Cossor and the one bearing the Serial Number 8428 as the Mark III Cossor.

The time base can be triggered from an external signal applied between the SYNC and COMMON terminals with the SYNC SELECTOR set on the "Triggered External" position. Before beam triggering can occur,

certain steps must first be taken to blank the beam. On the Mark III Cossor, when the INTENSITY MODULATION SELECTOR is set to the "Mech" position and the INTENSITY MOD terminal is shorted to the COMMON terminal, the beam will disappear. It can be made to reappear at the desired instant by open-circuiting the INTENSITY MOD and COMMON terminals.

The two Cossor oscilloscopes differ in the beam brightening phase of operation in that the Mark I Cossor requires a short-circuit between the BEAM TRIGGER and COMMON terminals to switch the beam on, whereas, the Mark III Cossor requires an open circuit between the INTENSITY MOD and COMMON terminals. The beam, of course, must be blanked or switched off after one sweep of the time base expires. This is to avoid any further blots on the film.

Hence, a device is necessary which will produce this switching action for a wide range of sweep speeds. This is attained with the use of the well-known phantastron - a simple electronic circuit which produces square pulses of variable duration. Since a thorough treatment of this circuit is given in numerous articles[1,2,3], only the basic operation will be outlined here.

The phantastron works on the same principle as the Miller sweep circuit, which produces a linear fall in plate voltage after an initiating trigger. A cathode-coupled phantastron circuit is shown in Fig. A.1. Under quiescent conditions the suppressor grid is biased to plate cut-off conditions, hence, the cathode current flows through the screen creating a low screen voltage V_b. Since the grid is connected to the positive supply through a large resistor (1.2M), which is much larger than the equivalent grid to cathode resistance, the grid is said to be clamped to the cathode. Before applying any triggering signal the measured quiescent voltages of the actual circuit were as follows:

---

1. Chance, Hughes, MacNichol, Sayre, Williams, Phantastron Type Circuits, MIT Radiation Laboratory Series, Vol. 19, pp. 195.

2. R.N. Close & M.T. Lebenbaum, Design of Phantastron Time Delay Circuits, Electronics, Vol. 21, pp. 101, April, 1948.

3. Millman & Taub, Pulse and Digital Circuits, McGraw - Hill, pp. 207, 1956.

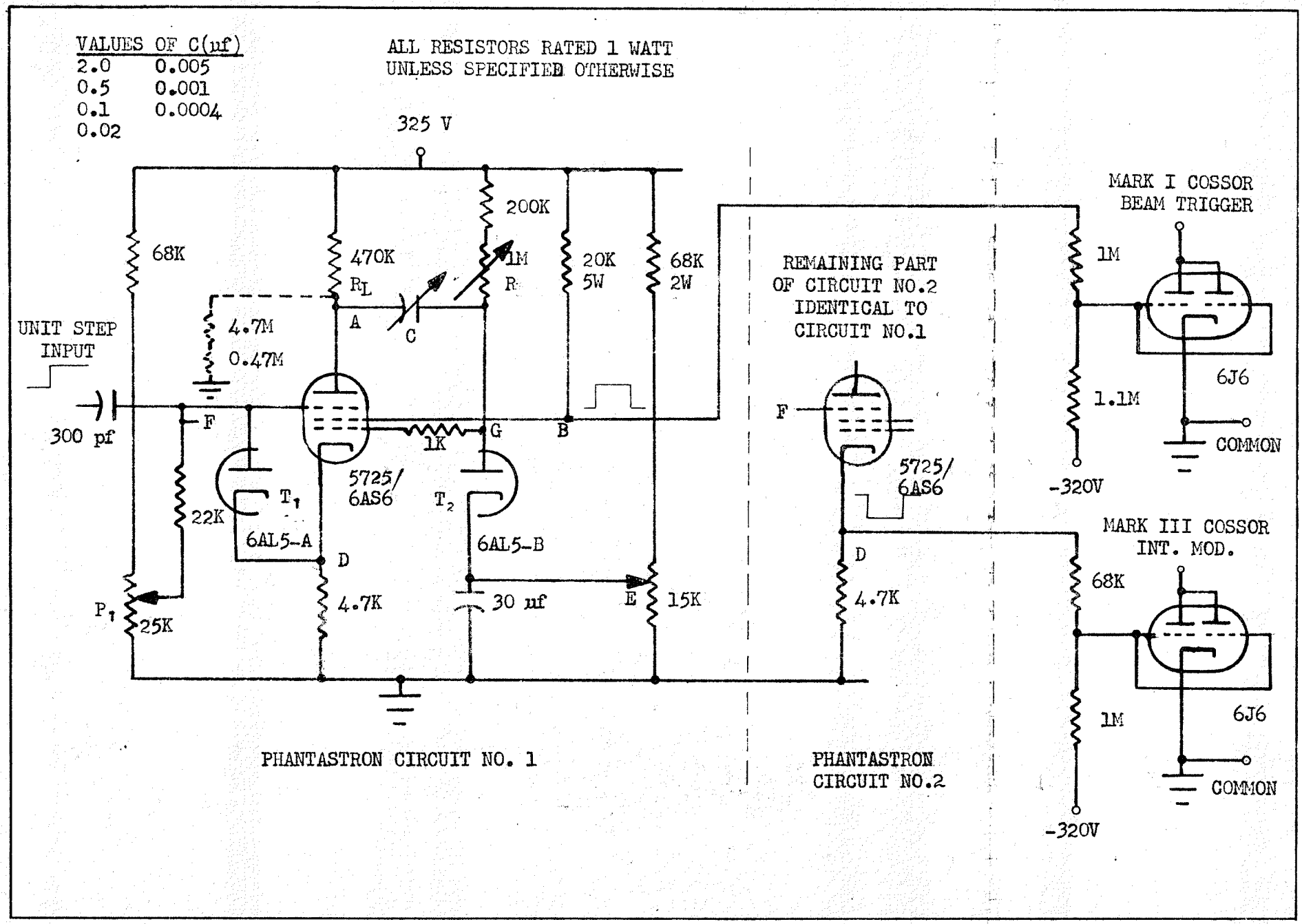

FIG. A.1 CATHODE-COUPLED PHANTASTRON CONTROLLING OSCILLOSCOPE BEAM

V_a (plate voltage) = 310.0 volts
V_b (screen voltage) = 180.0volts
V_d (cathode voltage)= 36.0 volts
V_e (potentiometer tap voltage) = 33.0 volts
V_f (suppressor voltage) = 5.0 volts
V_g (grid voltage) = 34.5 volts

To trigger the circuit a unit-step voltage is applied to the input terminal which produces a "spike" at f. This "spiked"-wave is due to the R-C differentiating circuit comprised of the 300 pf capacitor and the total resistance from f to ground. As the suppressor grid goes positive, plate current begins to flow and this causes a sudden drop in plate voltage. A chain of events take place at this moment. Since the voltage across capacitor C cannot change instantaneously, the grid voltage falls by the same amount as the plate voltage. This greatly reduces the current through the cathode biasing resistor, causing the cathode voltage V_d to drop. It also causes a large reduction in screen current and thus the screen voltage V_b rises. At this point the Miller action begins to take place. Since the plate side of capacitor C experienced a voltage drop, current will flow through R and C to the plate and the potential at A will drop at a rate of $\frac{E_{bb} + E_1}{RC}$ volts/sec.

This process continues, with the grid rising slightly to permit the plate to take the increasing current needed for the 470K resistor. While this run down of the plate voltage continues, the screen and cathode voltages remain constant at the values they had attained upon triggering.

When the plate voltage runs down to a value such that no potential difference exists across capacitor C, the grid side of C must rise with respect to ground. This ascent takes place with a time constant RC which may be relatively long compared to a vertical rise in screen voltage which occurred at the time the circuit was triggered.

Therefore, this might create some anxiety in that a true vertical edge may not exist for the drop in screen voltage. However, such is not the case, for a slight rise in the grid voltage produces a regenerative action. As cathode current increases, causing a rise in cathode potential, the suppressor potential falls, reducing the plate current. An increase in screen current also produces a drop in screen voltage at the same instant. A reduction in plate current means a rise in plate voltage, which in turn causes the grid to rise still further. Thus, the regenerative action drives the suppressor voltage rapidly negative and produces well defined vertical edges in the square pulses.

Upon cut-off, the plate recovers in voltage with a time constant, $t = R_L C$.

Grid voltage rises until diode T_2 conducts, catching the grid. This diode also serves the important role of stabilizing the initial level of the grid and the initial voltage across the timing capacitor C. Diode T_1 prevents the suppressor from being carried too high by the triggering impulse and "sticking", caused by secondary electron emission. On the other hand, if the triggering impulse is not of sufficient strength so as to bring the suppressor potential above cathode potential, the circuit will not fire. However, this is overcome by inserting potentiometer P_1 in the circuit. This enables the suppressor bias to be raised closer to the cathode potential. Such an arrangement requires a smaller triggering impulse. The 30 μf capacitor connected from ground to the cathode of diode T_2 gives a stabilizing effect by damping any voltage surges.

The theoretical wave forms[1] in a cathode-coupled phantastron are as shown in Fig. A.2. Actual recorded wave forms, Fig. A.3, compare favorably with the theoretical.

It can be noted that the potential at a, as recorded on the trace, is 285 volts and not 310 volts, as originally stated. This drop was due to a 5.17 M shunt which was temporarily added to enable the oscilloscope to record the wave form at a. The shunt increased the current

---

1. Millman and Taub, Pulse and Digital Circuits, McGraw - Hill, pp. 227, 1956.

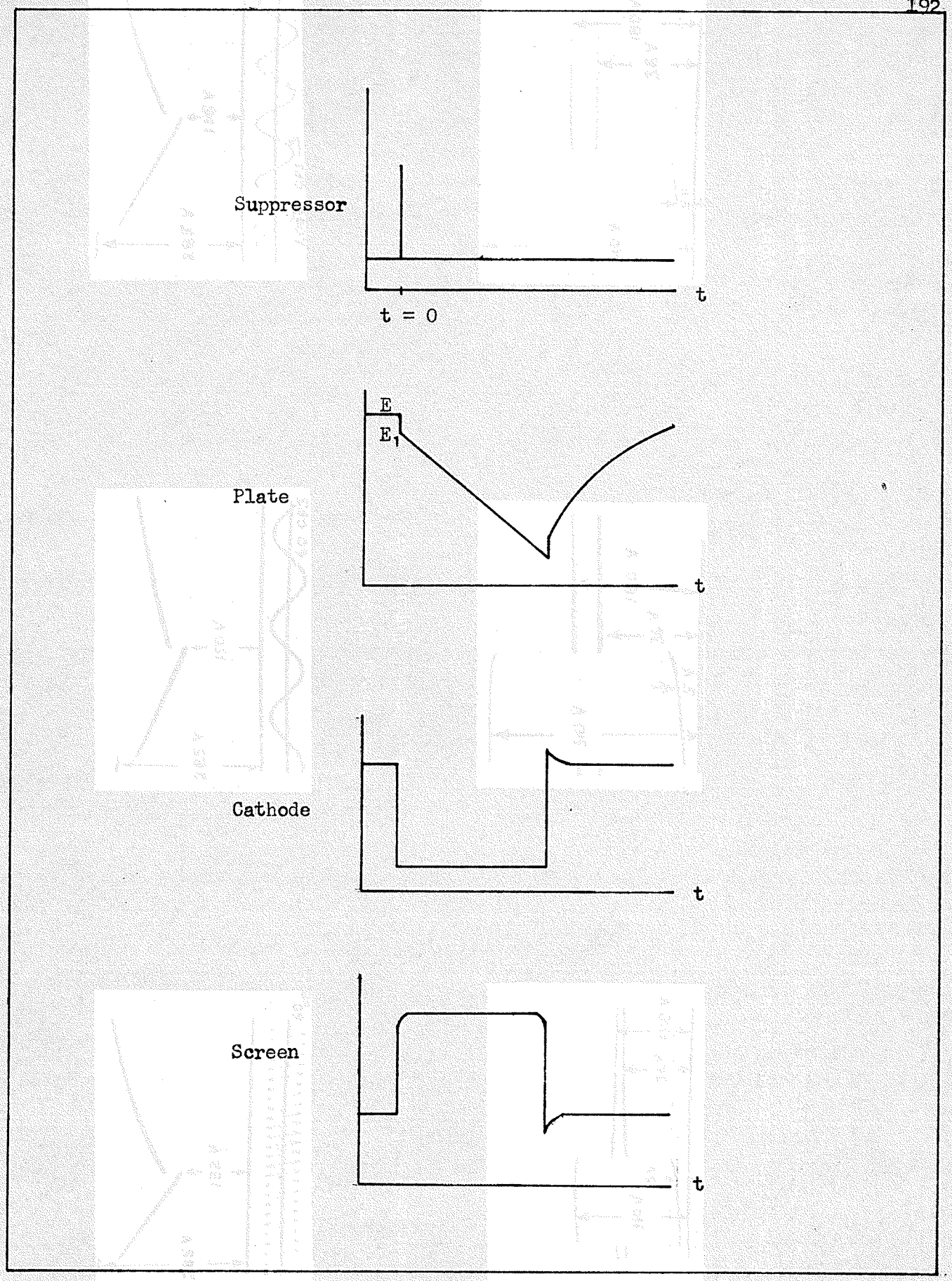

FIG. A.2 THEORETICAL VOLTAGE WAVEFORMS IN CATHODE-COUPLED PHANTASTRON

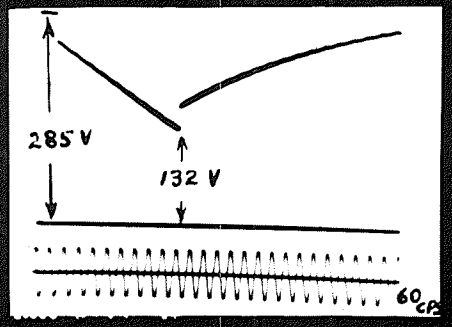

Upper Trace: Plate Output
Lower Trace: Timing Wave

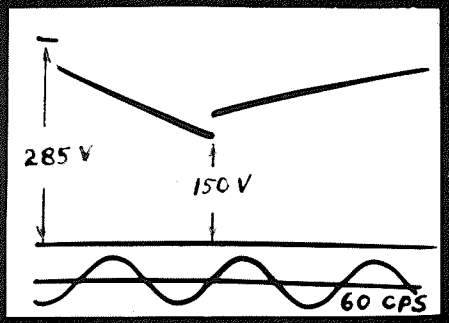

Upper Trace: Plate Output
Lower Trace: Timing Wave

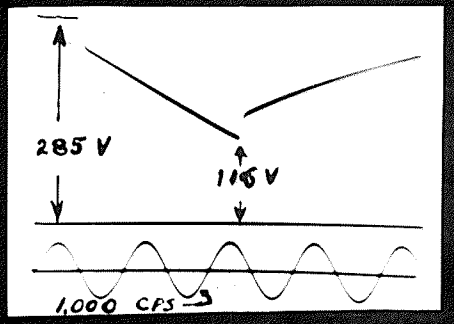

Upper Trace: Plate Output
Lower Trace: Timing Wave

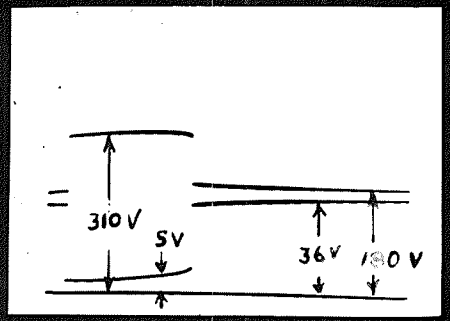

Upper Trace: Screen Output
Lower Trace: Cathode Output

(a) RC = 0.420 sec

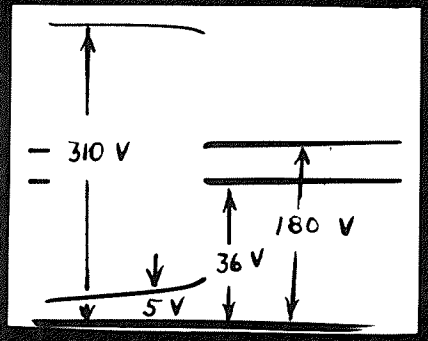

Upper Trace: Screen Output
Lower Trace: Cathode Output

(b) RC = 0.0660 sec

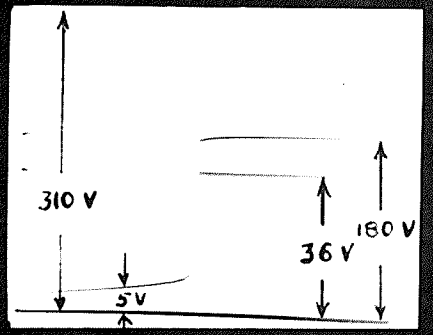

Upper Trace: Screen Output
Lower Trace: Cathode Output

(c) RC = 0.00446 sec

FIG. A.3 RECORDED WAVEFORMS IN CATHODE-COUPLED PHANTASTRON

through the 470 K resistor, thus lowering the voltage to 285 volts. When the oscilloscope (internal impedance of 0.5M) was connected directly to the plate, the voltage at a dropped so drastically that the circuit was unable to fire.

The duration of the output wave at the screen and at the cathode is proportional to the R-C product. For the traces shown in Fig. A.3 (a),

$$RC = 0.84 \times 10^{6} \times 0.5 \times 10^{-6}$$
$$= 0.420 \text{ sec}$$

The duration T of the square pulse was 8.5 cycles on a 60 cps base.

Therefore, $T = \frac{8.5}{60}$

$$= 0.142 \text{ sec}$$

Since $RC \propto T$,

a proportionality factor K can be introduced to form the equation,

$$RCK = T$$

Therefore,

$$K = \frac{T}{RC}$$

$$= \frac{0.142}{0.420}$$

$$= 0.338$$

K was also determined from traces in (b) and (c), with the following results:

Traces, Fig. A.3	RC (sec)	T (sec)	K
(a)	0.420	0.142	0.338
(b)	0.0660	0.0208	0.316
(c)	0.00446	0.00175	0.392

The average value of K = 0.350. Discrepancy in values of K can be attributed to errors in measurement of R; to errors in scaling T off the photograph; and to the fact that the value of C was taken as the nominal value.

Since K is known, R and C can be adjusted in any combination to give specific durations of T. Thus, coarse control for the square pulse is obtained by varying C and fine control is attained by varying R. The setting of d is normally left unchanged after the circuit has been adjusted for operating conditions. The largest RC product obtainable is

$$1.2 \times 10^{6} \times 2 \times 10^{-6} = 2.40 \text{ sec}$$

or $T = 0.35 \times 2.4$

$= 0.875$ sec.

The smallest RC product is

$$0.2 \times 10^{6} \times 0.0004 \times 10^{-6} = 80 \ \mu \text{ sec}$$

or $T = 0.35 \times 80$

$= 28 \ \mu$ sec.

Therefore, it is possible to obtain pulses of any duration within the above two T - limits.

A.2 Application of the Phantastron for Control of the Oscilloscope Beam.

Before proceeding with any further design work from the phantastron screen and cathode outputs, it was necessary to determine the firing characteristics of the oscilloscope's beam trigger. The BEAM TRIGGER dial on the Mark I Cossor was set to the "Mech" position. This operation blanked the beam and produced a 50-volt d-c potential between the BEAM TRIGGER and COMMON terminals. A test was conducted, using the circuit illustrated in Fig. A.4, to determine what conditions were necessary to brighten the beam.

In Fig. A.4, the triode acts as a variable resistor, whose resistance is controlled by the grid bias voltage. A relatively high negative bias produces cut-off conditions and the vacuum tube acts as a high impedance. Decreasing the negative bias will cause greater conduction through the tube, thus simulating the presence of a low-valued resistor. If the grid bias is driven sufficiently positive

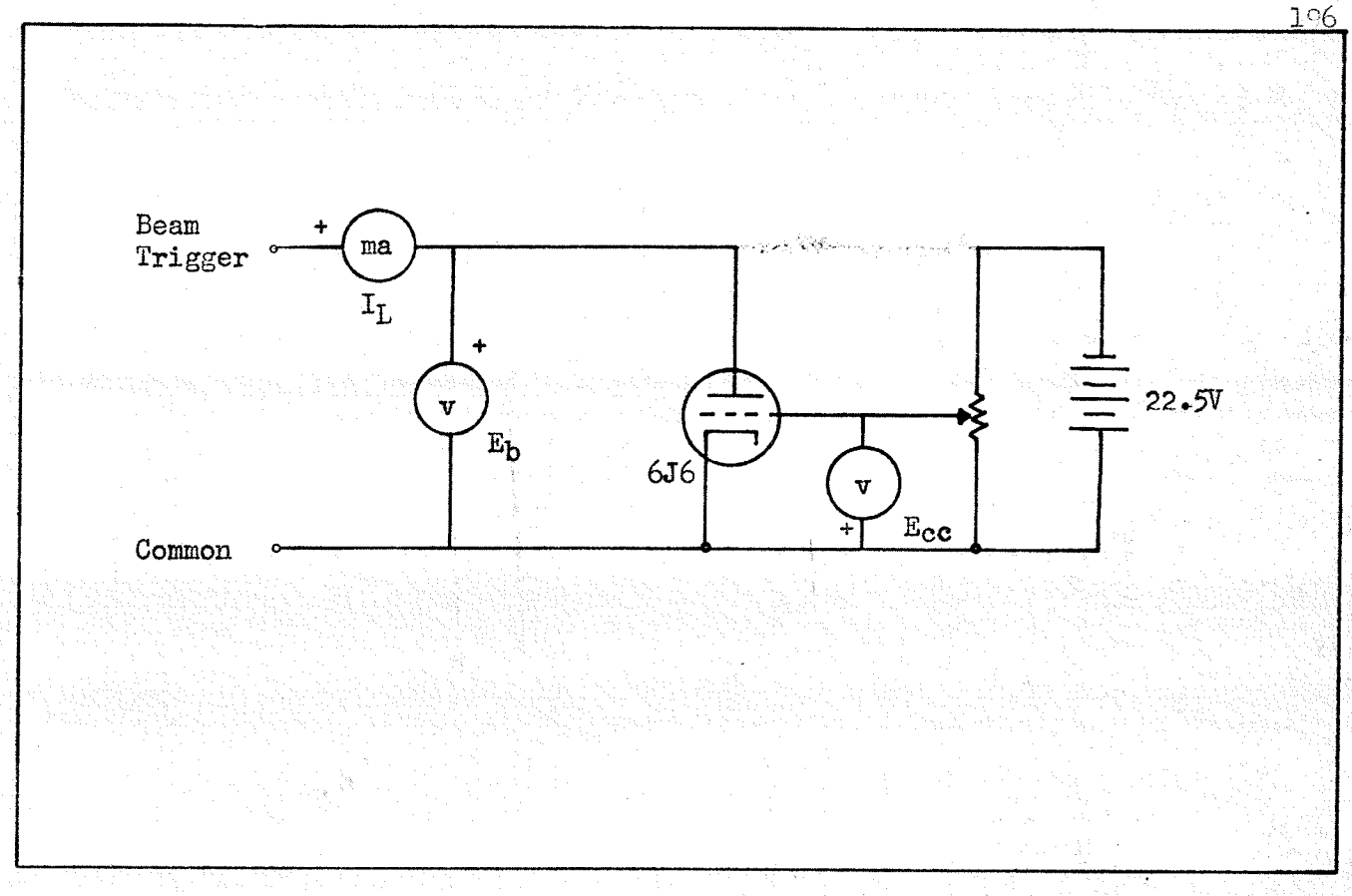

FIG. A.4 TEST CIRCUIT FOR DETERMINING BEAM TRIGGERING CHARACTERISTICS OF THE MARK I COSSOR

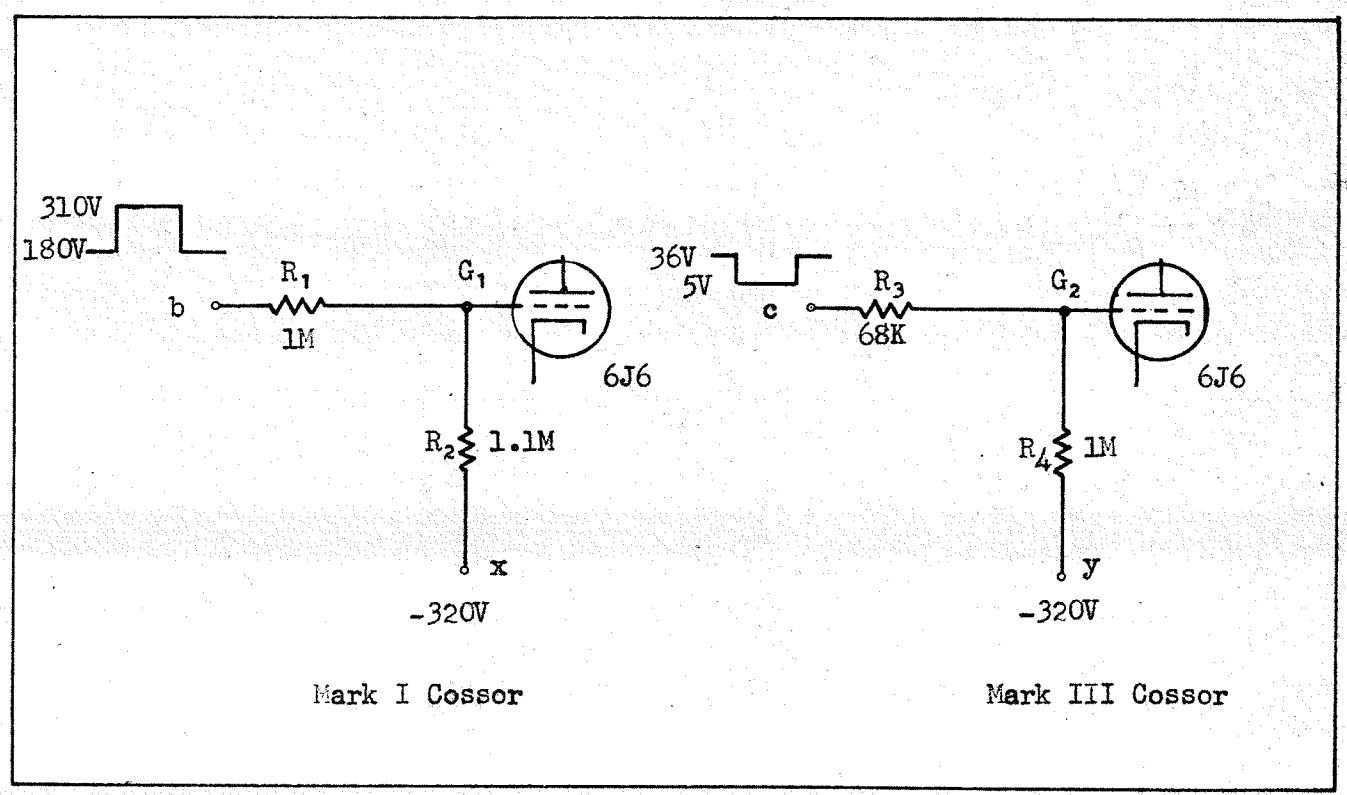

FIG. A.5 POTENTIOMETER ARRANGEMENT FOR BIAS VOLTAGES

the drop across the tube will be negligible, essentially creating a short across the BEAM TRIGGER and COMMON terminals. The vacuum tube, when operating in the above fashion, simulates a "mechanical switch."

TABLE A.1

BEAM-TRIGGERING CHARACTERISTICS OF THE MARK I COSSOR

E_b(volts) VTVM	I_L (ma) Simpson #R193	E_{cc}(volts) VTVM	Beam
47	0.10	-3.0	Not visible
39	0.40	-2.0	Visible
50	1.35	0	Visible
39	0.40	-2.0	Visible
47	0.10	-3.0	Visible
49	0.08	-3.2	Not visible

TABLE A.2

BEAM-TRIGGERING CHARACTERISTICS OF THE MARK III COSSOR

E_b(volts) VTVM	I_L(ma) Simpson #R193	E_{cc}(volts) VTVM	Beam
61	0.20	-3.0	Visible
47	0.55	-2.0	Visible
24	1.10	-0.6	Not visible
2.0	1.70	0	Not visible
17	1.40	-0.5	Visible

From the test data pertaining to the Mark I Cossor it is noted that a grid voltage of below -3.2 volts was necessary for complete blanking and above -2.0 volts for definite triggering. On the other hand, a grid bias voltage of less than -0.6 volts was necessary for triggering and above -0.5 volts for blanking of the beam on the Mark III Cossor.

Upon triggering the phantastron circuit, the positive rise of the square wave, obtained from the screen, was used to raise the grid bias of the 6J6 triode. This closed the "mechanical switch," and triggered the beam of the Mark I Cossor. Blanking occurred during the vertical fall in the square wave which opened the "mechanical switch". The cathode square wave output was used in a similar manner to trigger and blank the beam of the Mark III Cossor.

As the unit-step input was applied to the suppressor grid, a similar signal was applied to the SYNC terminal to begin the time base line sweep, thus, eliminating over-exposure blots on the film.

The grid bias voltage for the 6J6 triode was derived from a simple potentiometer arrangement. A 320-volt negative bias was available and the total resistance of the potentiometer was connected between this voltage and the output square wave. After running a few tests the components, as shown in Fig. A.5, were selected to give optimum operating conditions.

At quiescent conditions the potential of the screen from circuit No. 1 is 180 volts. Thus,

$V_{x-B} = 320 + 180 = 500$ volts

The drop across

$R_1 = \frac{1 \times 500}{2.1} = 238$ volts

Therefore, the potential at

$G_1 = 180 - 238 = -58$ volts

The measured value at G_1 was also -58 volts.

During the triggered period, V_b rises to 310 volts, (Fig. A.3).

The drop across

$R_1 = 1/2.1 \times 630 = 300$ volts

Therefore, the potential at

$G_1 = 310 - 300 = 10$ volts

Under quiescent conditions the grid potential of -58 volts is well below the required value of -3.2 volts. The +10 volts indicates that a sufficient positive bias is present to ensure proper triggering.

In circuit No. 2 the quiescent voltage at the cathode is 36 volts. Hence, the total voltage across the potentiometer is

$36 + 320 = 356$ volts

The drop across $R_3 = \frac{0.068}{1.068} \times 356 = 23$ volts

Therefore, the potential at

$G_2 = 36 - 23 = 13$ volts

The measured value at G_2 was found to be 0.4 volts - discrepancy arising from the fact that the grid current was neglected in the calculation.

During the brightening period, V_d drops to 5 volts.

Therefore, the drop across

$R_3 = \frac{0.068}{1.068} \times (320 + 5) = 21$ volts

And the potential at

$G_2 = 5 - 21 = -16$ volts

The grid voltage is well below and above the critical voltage of -0.60 volts during the blanking and brightening periods respectively.

APPENDIX B

MACHINE CONSTANTS

Nameplate of Alternator

American Custom Built Motors

KVA	7.5	RPM	1800
Volts	120	Model	1284 - 6
Amps	36.0	Type	OG
PF	1.0	Temp.	50°C
Rating	Cont.	Serial #	22703

Nameplate of Exciter

Exciter Voltage 125 volts

Field amps 0.350

Graphs B.1 and B.2 present the usual information on the alternator's regulation and characteristics.

Graphs B.3 and B.4 present some information on the exciter characteristics. A loaded exciter refers to the alternator field as being the load.

B.1 Three Phase Short-Circuit Current Analysis

Direct-axis reactances and time constants can be evaluated by an analysis on the oscillogram of a no-load three phase fault on an alternator. The procedure is standard[1], hence only the data and computations will be presented here.

---

1. E.W. Kimbark, Power System Stability, Vol. III, J. Wiley and and Sons, Inc., pp. 40, 1956.

MANUFACTURED BY RENOUF PUBLISHING CO., MONTREAL

IF SHEET IS READ THIS WAY (HORIZONTALLY), THIS MUST BE TOP.
IF SHEET IS READ THE OTHER WAY (VERTICALLY), THIS MUST BE LEFT-HAND SIDE.
THIS MARGIN RESERVED FOR BINDING.

GRAPH B.1 ALTERNATOR VOLTAGE CHARACTERISTICS

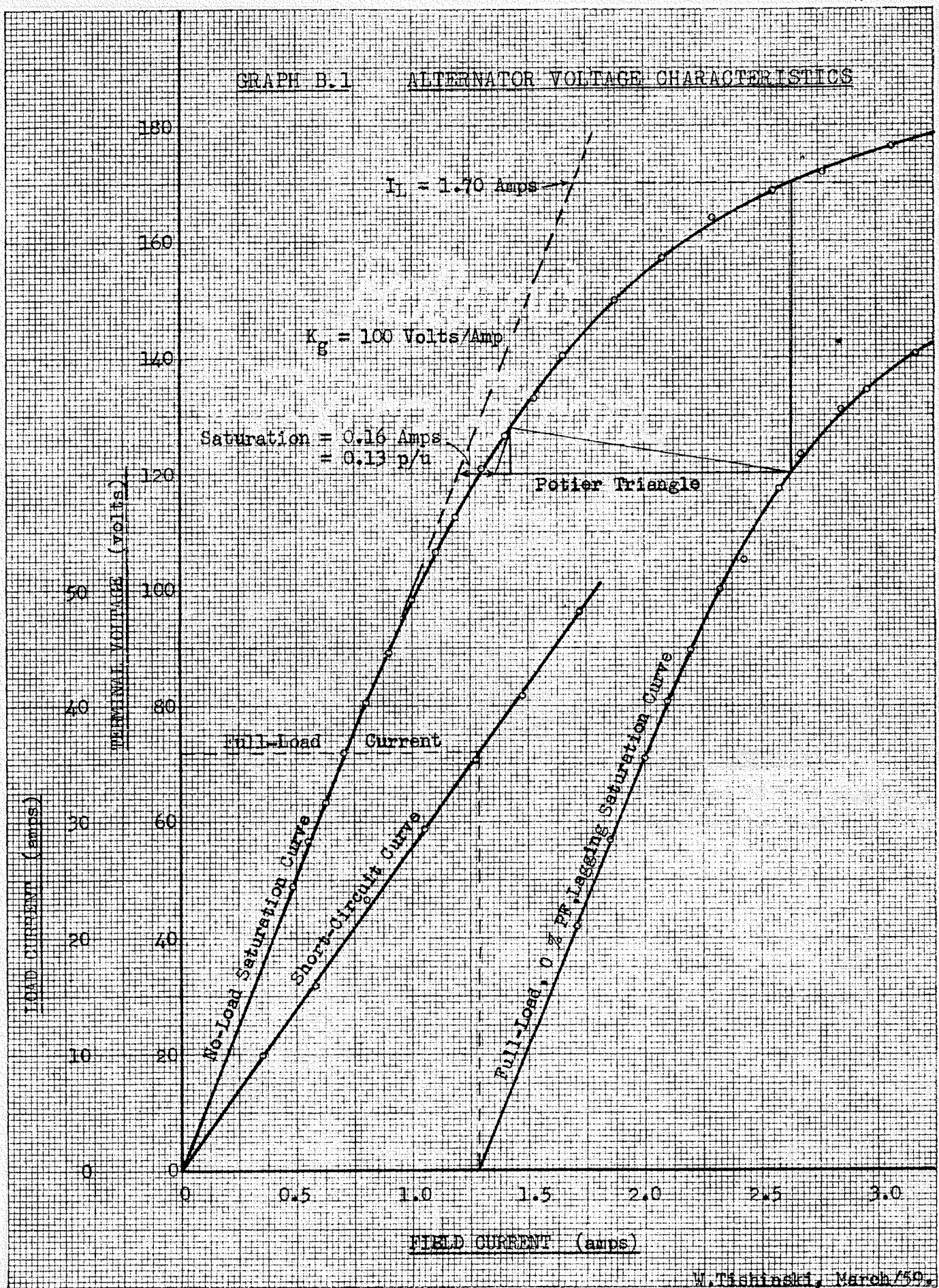

W.Tishinski, March/59.

MANUFACTURED BY RENOUF PUBLISHING CO., MONTREAL

THIS MARGIN RESERVED FOR BINDING.
IF SHEET IS READ THIS WAY (HORIZONTALLY), THIS MUST BE TOP.
IF SHEET IS READ THE OTHER WAY (VERTICALLY), THIS MUST BE LEFT-HAND SIDE.

GRAPH B.2 VOLTAGE REGULATION AND FIELD COMPOUNDING CHARACTERISTICS OF ALTERNATOR

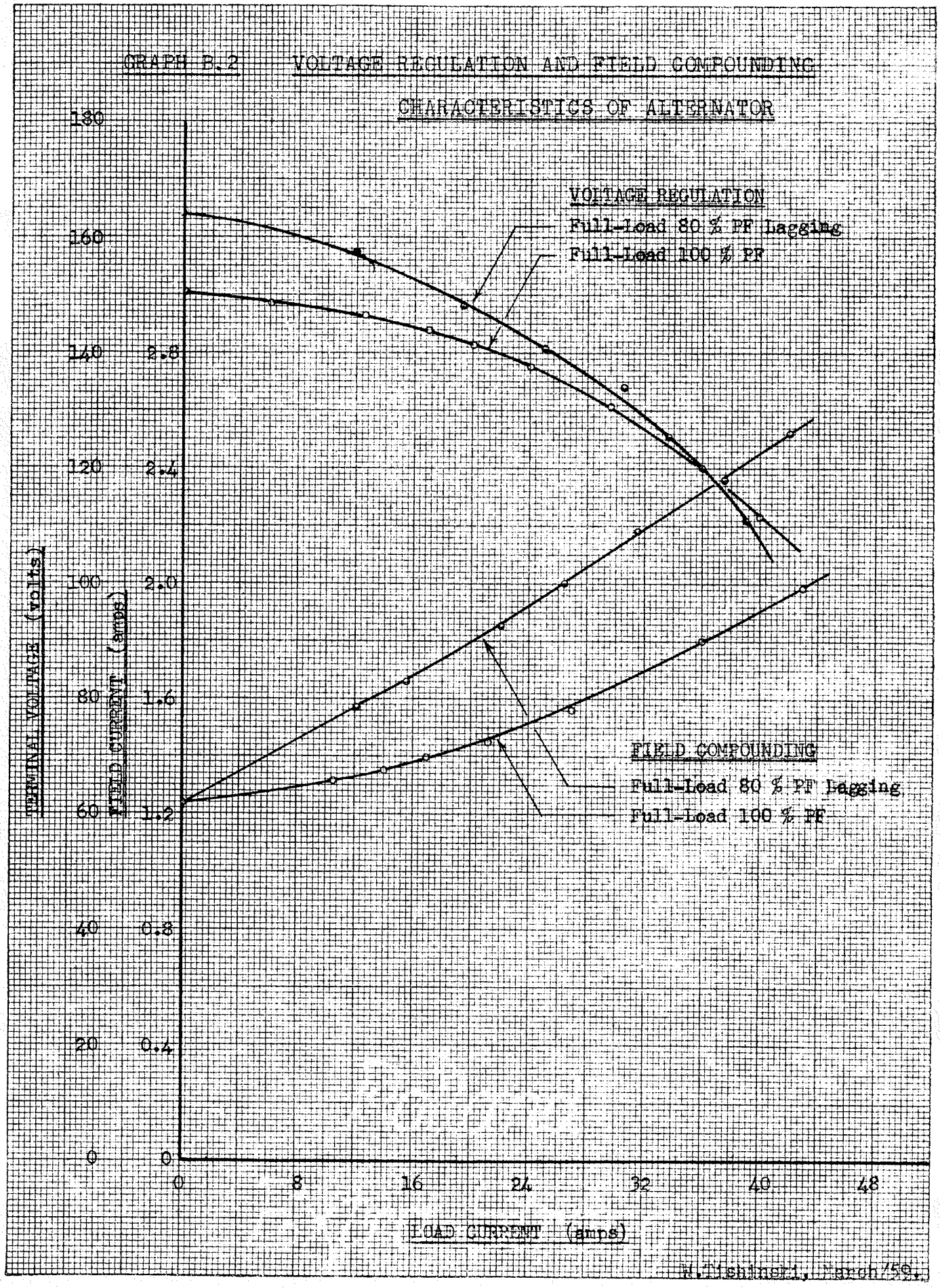

H. Tishinen, March/59.

THIS MARGIN RESERVED FOR BINDING.

IF SHEET IS READ THIS WAY (HORIZONTALLY), THIS MUST BE TOP.

IF SHEET IS READ THE OTHER WAY (VERTICALLY), THIS MUST BE LEFT-HAND SIDE.

GRAPH B.3 EXCITER SATURATION CURVES - NO-LOAD AND LOADED CONDITIONS

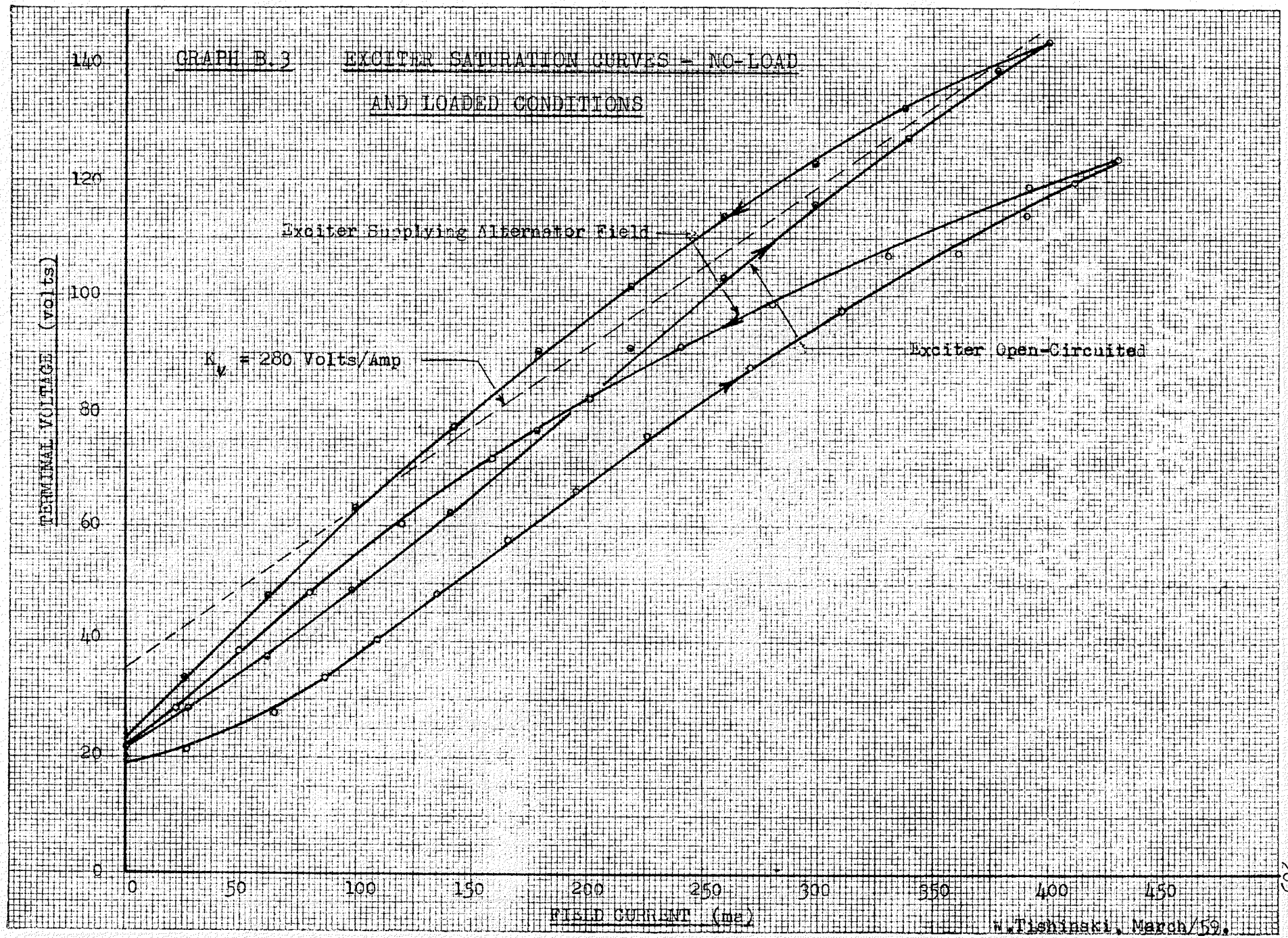

W.Tishinski, March/59.

FIELD CURRENT (ma)

W.Tishinski, March/59.

MANUFACTURED BY RENOUF PUBLISHING CO., MONTREAL

FORM 1063

THIS MARCIN RESERVED FOR BINDING.

IF SHEET IS READ THE OTHER WAY (VERTICALLY), THIS MUST BE LEFT-HAND SIDE.

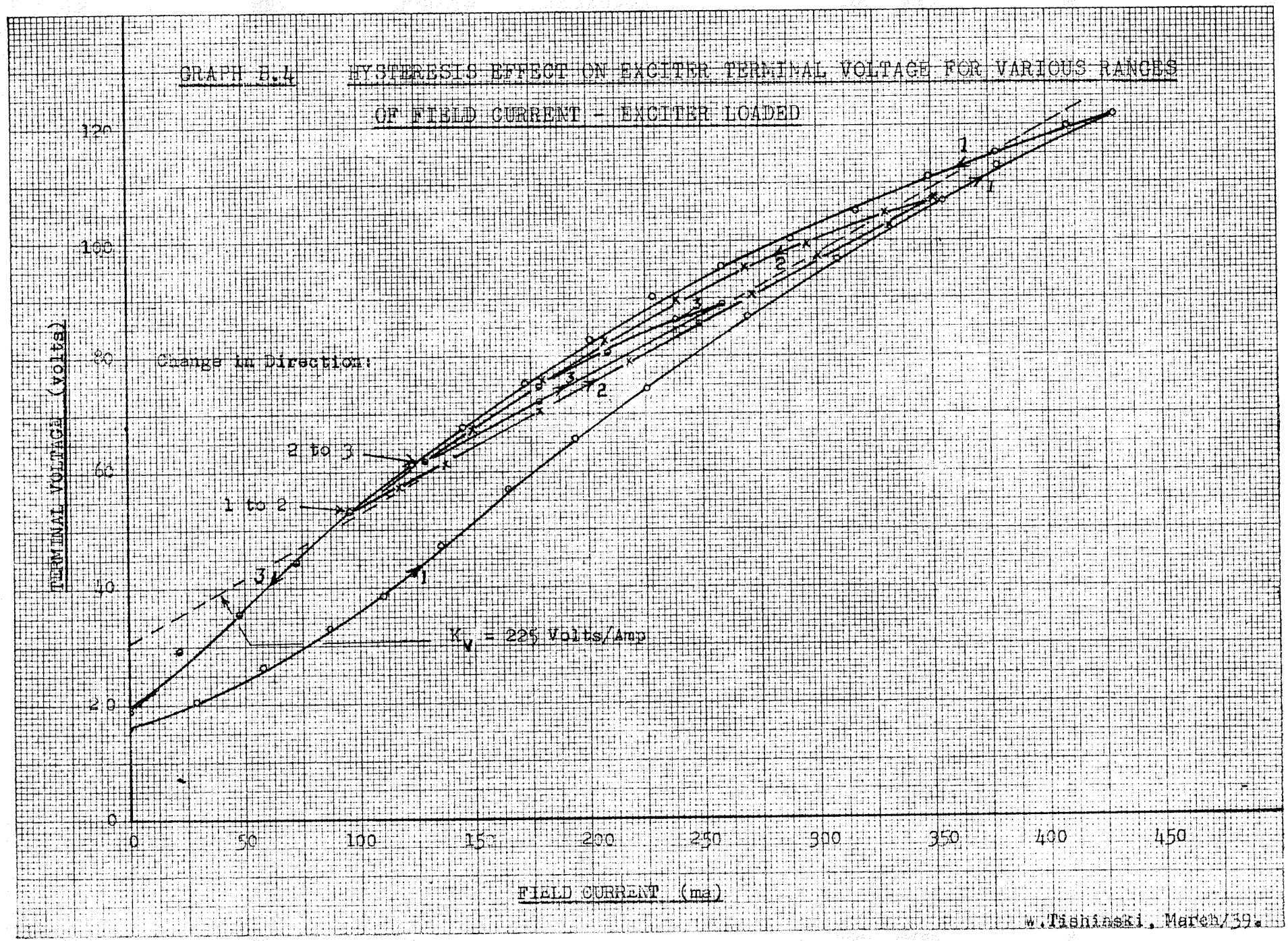

W. Tishinski, March/39.

MANUFACTURED BY RENOUF PUBLISHING CO., MONTREAL

FORM 100 MRO

THIS MARCIN RESERVED FOR BINDING.

IF SHEET IS READ THE OTHER WAY (VERTICALLY), THIS MUST BE LEFT-HAND SIDE.

GRAPH B.5 RELATION BETWEEN EXCITER AND ALTERNATOR FIELD CURRENTS

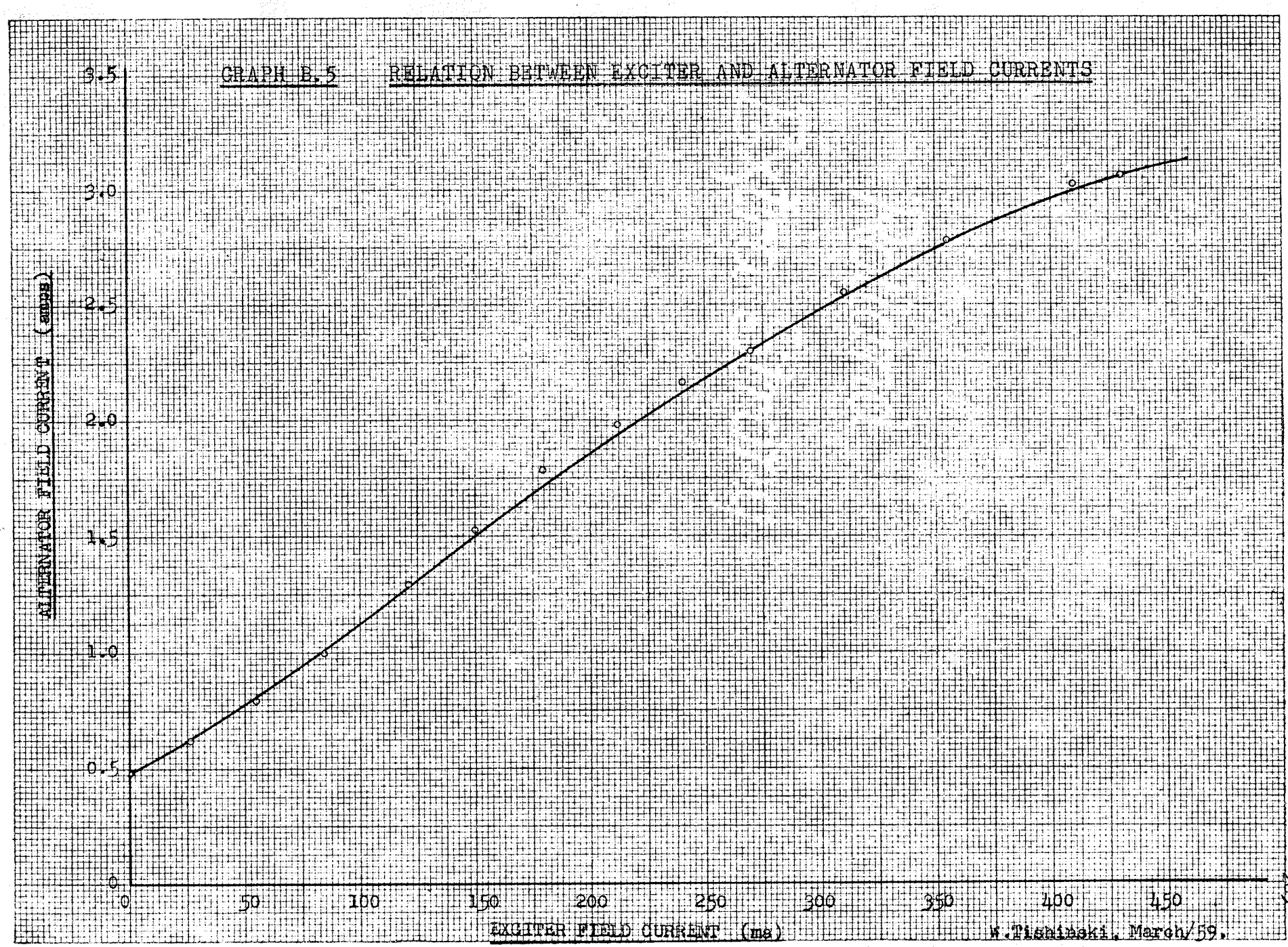

W. Tichinoski, March/59.

MANUFACTURED BY RENOUF PUBLISHING CO., MONTREAL

FORM 100

TABLE B.1

ANALYSIS OF SHORT-CIRCUIT CURRENTS

Analysis of A-Phase Current:

Time (cps)	Pos. (amps-crest)	Neg. (amps-crest)	A-C (amps-crest)	D-C (amps)
0	600	368	484	116
0.5	430	242	336	94
1.0	309	188	249	61
1.5	222	166	194	28
2.0	179	150	165	15
3.0	135	121	128	7
4.0	111	101	106	4
6.0	80	80	80	0
9.0	58	58	58	0
12.0	51	51	51	0

Analysis of B-Phase Current:

Time (cps)	Pos. (amps-crest)	Neg. (amps-crest)	A-C (amps-crest)	D-C (amps)
0	622	331	477	146
0.5	424	300	362	62
1.0	284	242	263	21
1.5	202	202	202	0
2.0	165	165	165	0
3.0	129	129	129	0
4.0	103	103	103	0
6.0	78	78	78	0
9.0	57	57	57	0
12.0	51	51	51	0

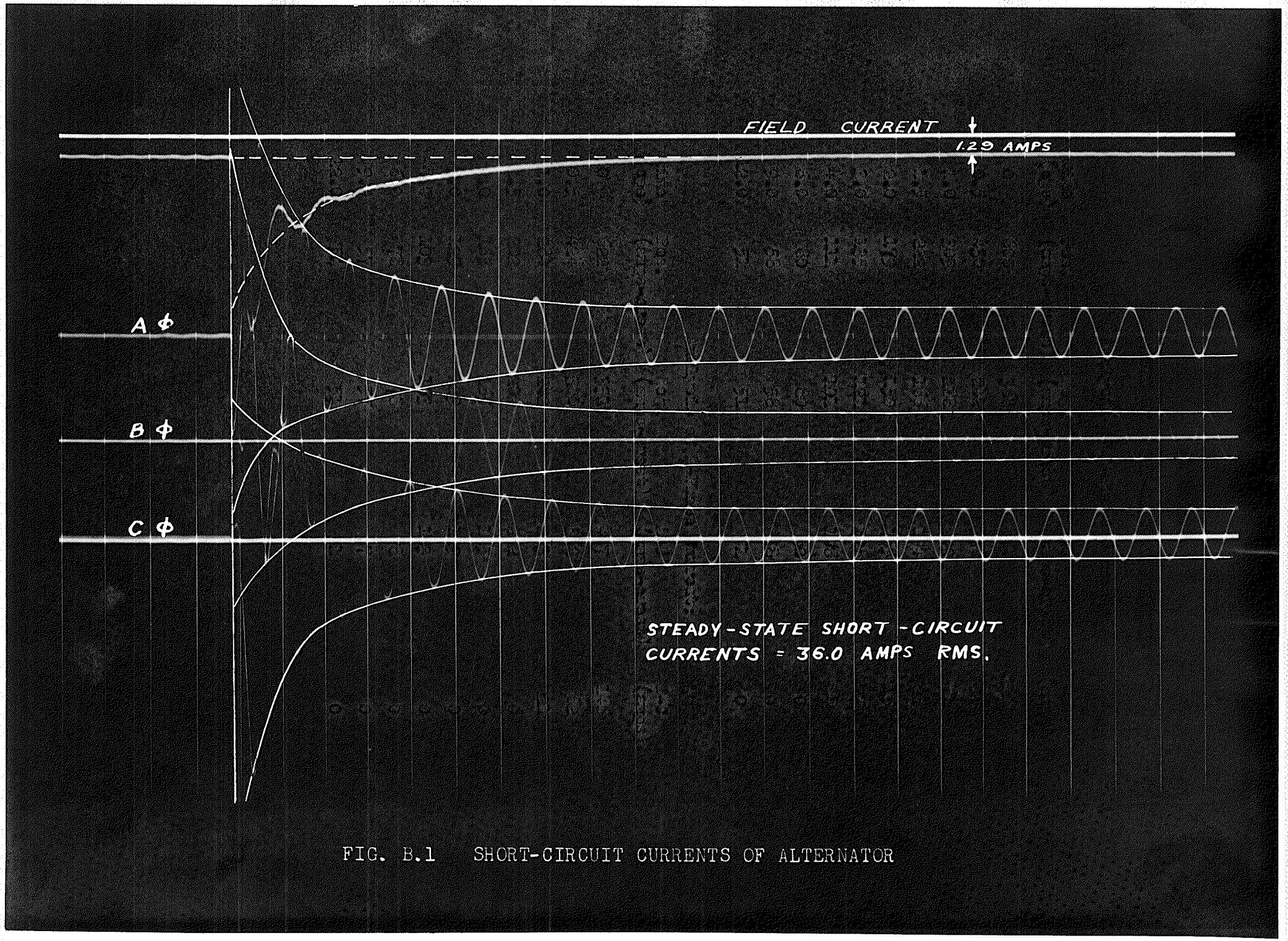

FIG. B.1 SHORT-CIRCUIT CURRENTS OF ALTERNATOR

Analysis of C-Phase Current:

Time (cps)	Pos. (amps-crest)	Neg. (amps-crest)	A-C (amps-crest)	D-C (amps)
0	285	670	478	-193
0.5	232	494	363	-131
1.0	208	324	266	- 58
1.5	176	222	199	- 23
2.0	159	174	167	- 8
3.0	131	134	133	- 2
4.0	110	112	111	- 1
6.0	78	79	79	0
9.0	61	62	62	0
12.0	51	51	51	0

Now the a-c currents can be averaged and from these the subtransient, transient and steady-state components can be separated.

Time (cps)	Total Current (amps-crest)	Subtransient and Transient Current (amps - crest)	Subtransient Current (amps-crest)
0	480	429	217
0.5	354	303	123
1.0	259	208	55
1.5	198	147	17
2.0	166	115	1
3.0	130	79	0
4.0	107	56	0
6.0	79	28	0
9.0	59	8	0
12.0	51	0	0

From Graph B.6, the transient and subtransient components of currents at t = 0 were found to be as follows:

$I_d' = 212$ amps - crest

$I_d'' = 234$ amps - crest

$$X_d = \frac{E_o}{I_d} = \frac{120/\sqrt{3}}{36.0} = 1.92 \text{ ohms per phase} = 1.00 \text{ p/u}$$

$$X_d' = \frac{E_o}{I_d + I_d'} = \frac{120/\sqrt{3}}{263/\sqrt{2}} = 0.372 \text{ ohms per phase} = 0.194 \text{ p/u}$$

$$X_d'' = \frac{E_o}{I_d + I_d' + I_d''} = \frac{120/\sqrt{3}}{480/\sqrt{2}} = 0.203 \text{ ohms per phase}$$

$$= 0.107 \text{ p/u}$$

$T_d' = 2.95$ cps $= 0.0493$ sec

$T_d'' = 0.65$ cps $= 0.0108$ sec

The short-circuit test gives a saturated value of transient reactance. An unsaturated transient reactance can be obtained by reducing the open-circuit voltage until only rated transient current is obtained on short-circuited conditions. The unsaturated[1] value may be as much as 15% greater than the saturated value. On loaded conditions the transient reactance will be an intermediate value between the saturated and unsaturated, but is nearest to the saturated transient reactance. Therefore, this value as determined by the short-circuit test is used in calculations.

The transient time constant of the a-c current can be checked by the rate of decay of the unidirectional component of the field current. This component of field current can be considered as producing the symmetrical phase currents, hence both components will decay at the same rate.

---

1. H.C. Anderson, Jr., Voltage Variation of Suddenly-Loaded Generators, G.E. Review, Vol. 48, pp. 25, August, 1945.

GRAPH B.6 SUBTRANSIENT AND TRANSIENT SHORT-CIRCUIT ARMATURE CURRENTS

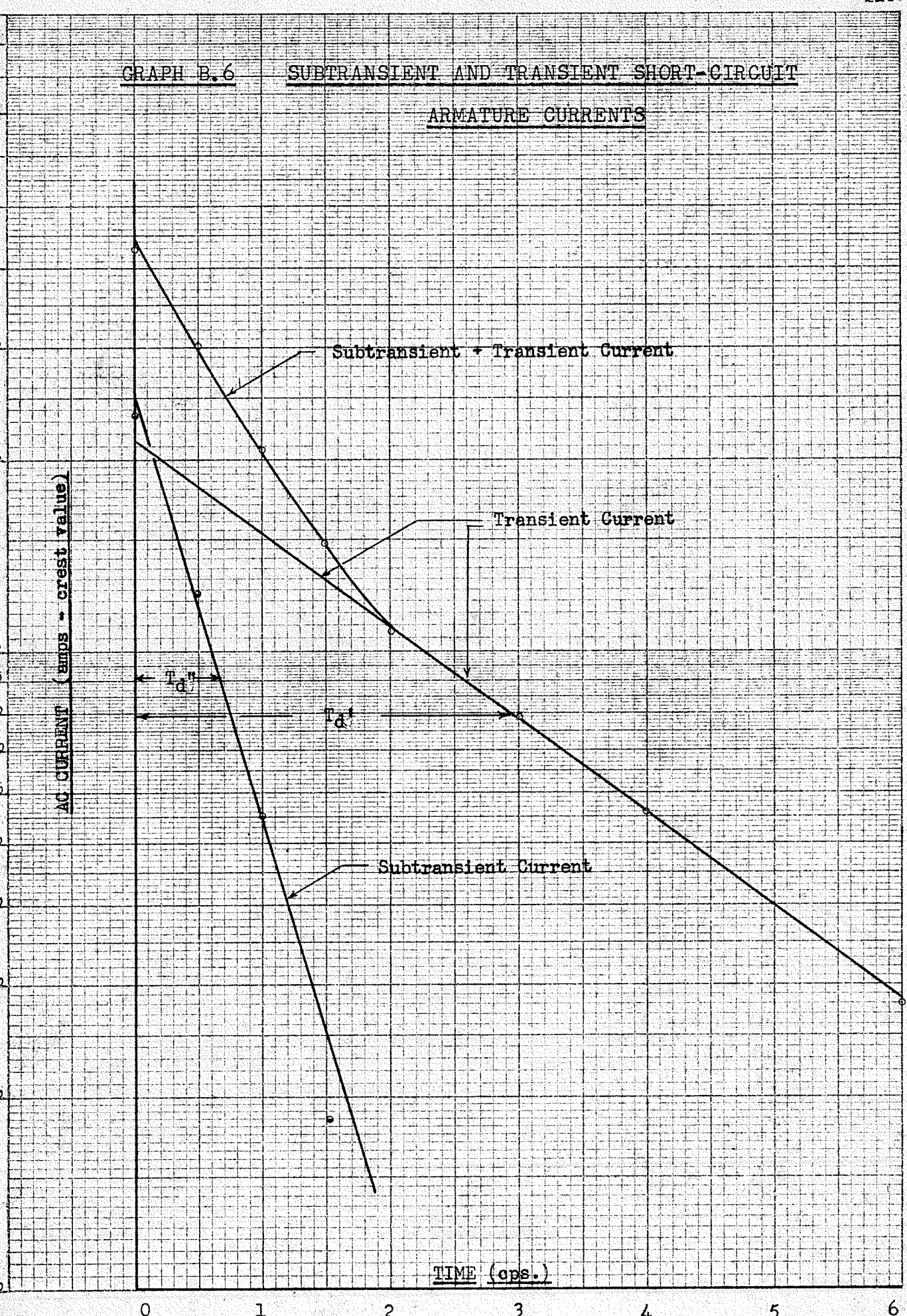

GRAPH B.7 EXCESS DC COMPONENT OF FIELD CURRENT

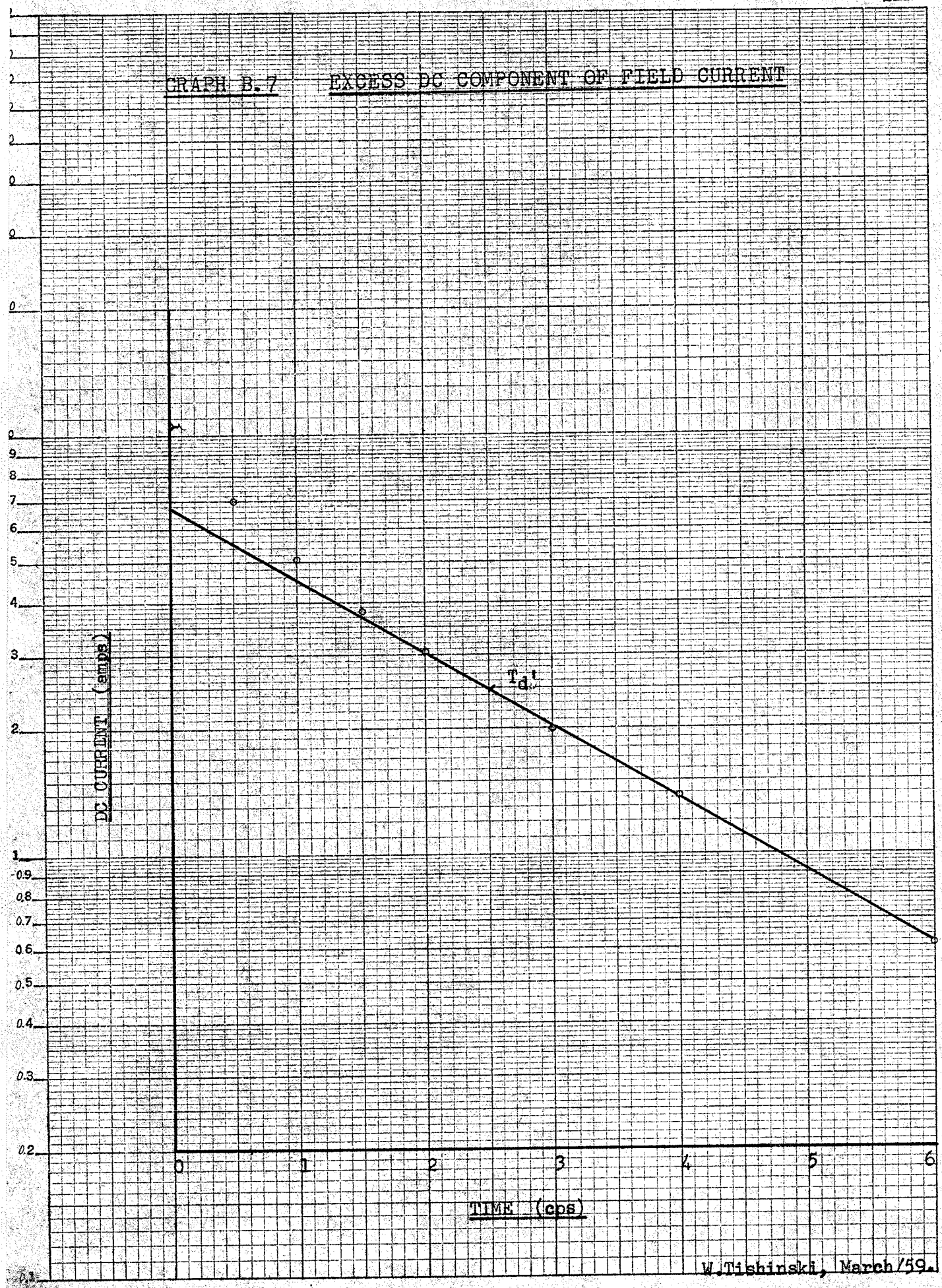

W.Tishinski, March/59.

TABLE B.2

ANALYSIS OF THE UNIDIRECTIONAL COMPONENT OF FIELD CURRENT

Time (cps)	Unidirectional Component (amps)
0	10.60
0.5	7.00
1.0	5.03
1.5	3.80
2.0	3.04
3.0	1.97
4.0	1.37
6.0	0.61
9.0	0.20
12.0	0

From Graph B.7,

$T_d' = 2.50$ cps

$= 0.0417$ sec

The average value for T_d' from both methods gives 0.0453 sec.

Having the preceding data, the open-circuit transient time constant can be found by

$$T_{do}' = \frac{X_d}{X_d'} T_d'$$

$$T_{do}' = \frac{1.00}{0.194} \times 0.0453$$

$$= 0.234 \text{ sec}$$

The armature circuit time constant is determined by plotting the d-c component of the short-circuit armature currents on Graph B.8.

$T_{a1} = 0.70$ cps

$T_{a2} = 0.52$ cps

$T_{a3} = 0.58$ cps

GRAPH B.8 D-C COMPONENTS OF THE ARMATURE SHORT-CIRCUIT CURRENTS

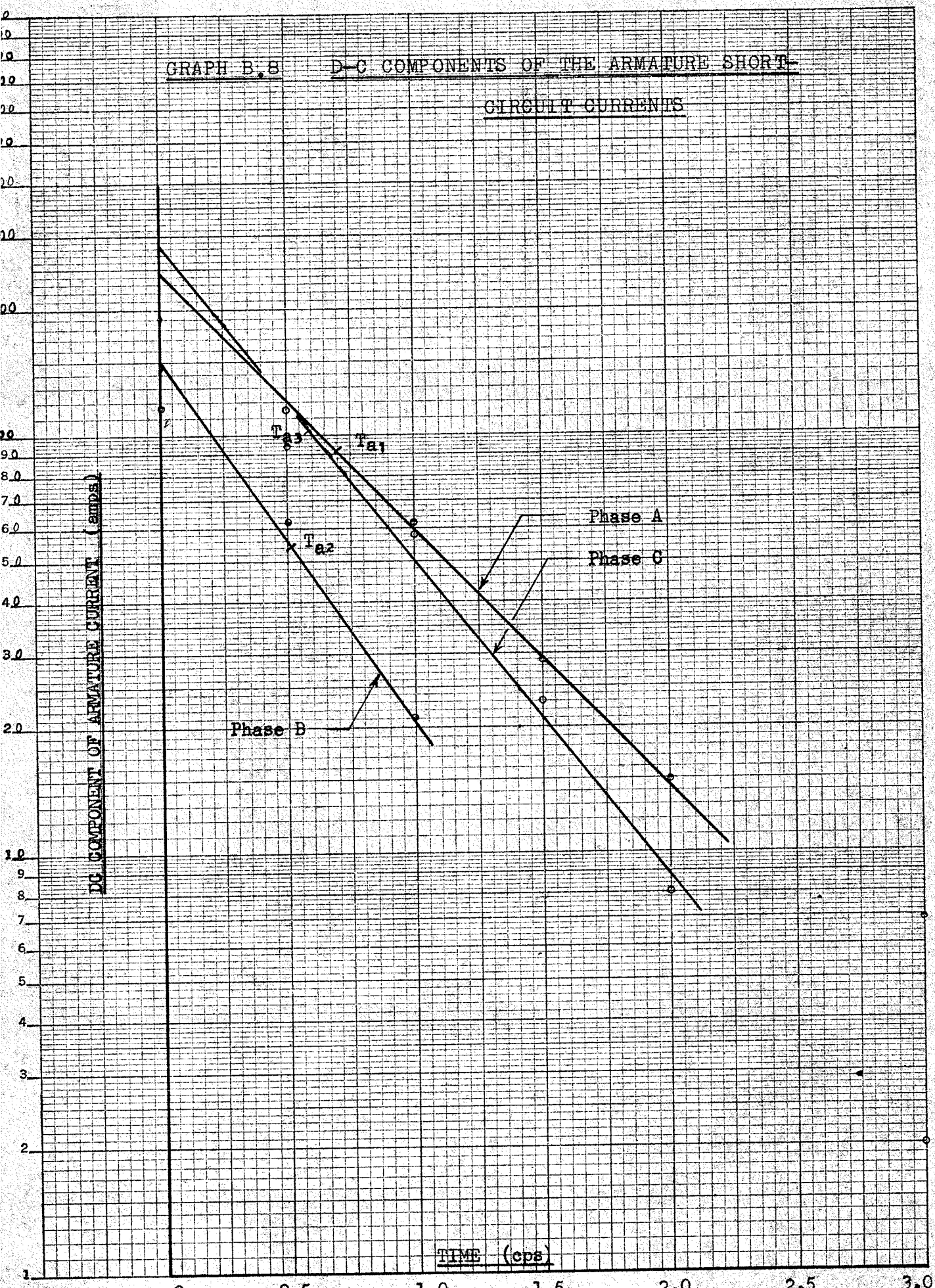

W.Tishinski, March/59.

MANUFACTURED BY RENOUF PUBLISHING CO., MONTREAL

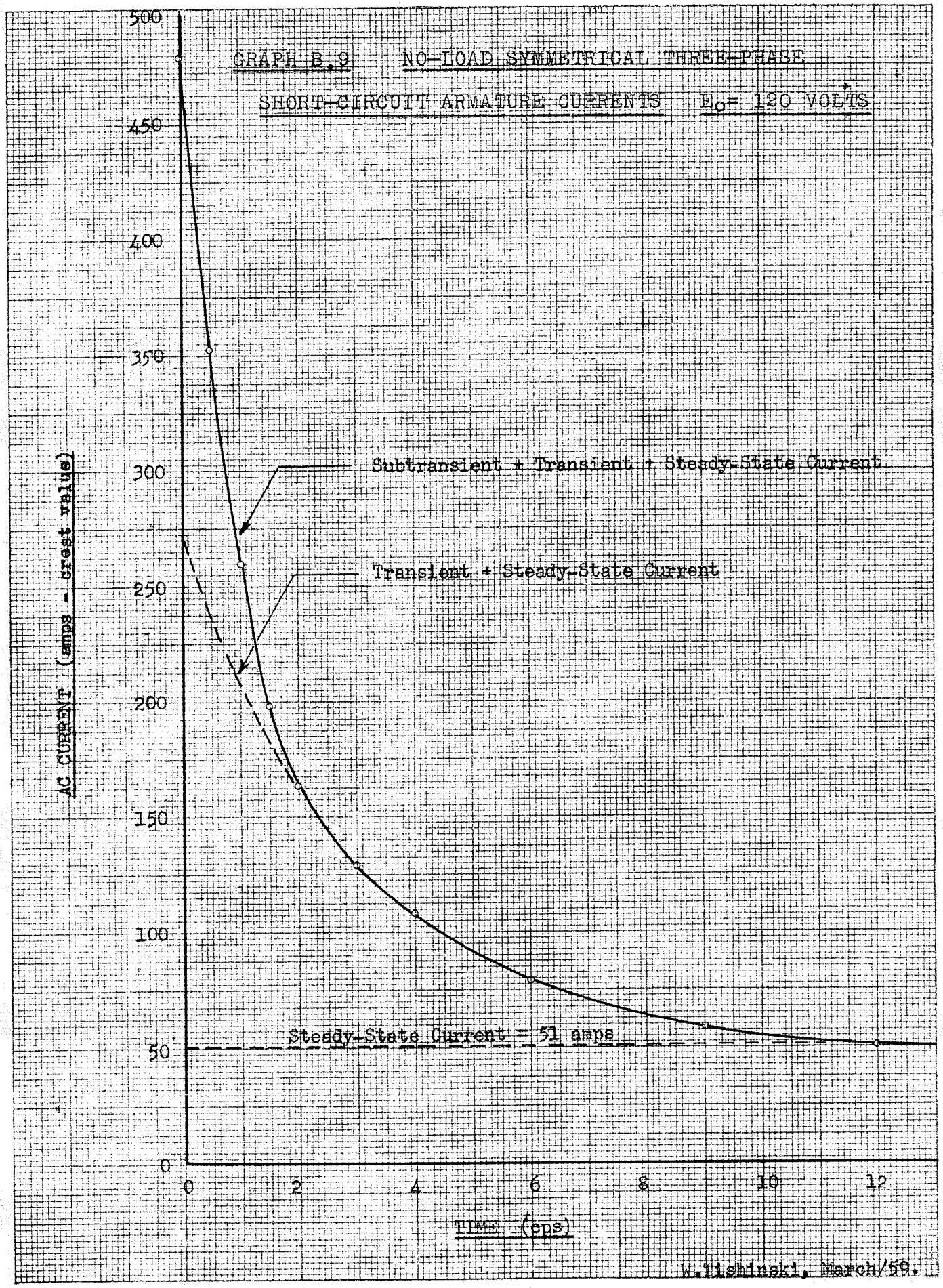

THIS MARGIN RESERVED FOR BINDING.
IF SHEET IS READ THIS WAY (HORIZONTALLY), THIS MUST BE TOP.
IF SHEET IS READ THE OTHER WAY (VERTICALLY), THIS MUST BE LEFT-HAND SIDE.

T_a (average value) = 0.60 cps

= 0.010 sec

B.2 Self-Inductance of Exciter and Alternator Fields

Bridge methods are unreliable in determining the self-inductance of a coil which has a relatively large amount of iron in its core. Because the degree of saturation affects the inductance of the field winding, the inductance should be found for the range in the saturation curve over which the machine operates. This necessitates the actual flow of field current to move the operating point on the saturation curve. If the current build-up in the field is over a linear portion of the saturation curve, the self-inductance will be constant. Thus, if a unit-step input voltage is applied to the field, the current should build-up according to

$$i = I(1 - e^{-Rt/L})$$

or $$I - i = I\, e^{-Rt/L}$$

where I = final value of current attained

i = instantaneous current at time t

R = resistance of the field circuit

L = self-inductance of the field

A brush oscillograph was used to record the build-up of current in the fields. Graph B.3 shows that the linear portion of the exciter saturation curve exists for exciter field currents from 90 ma to 250 ma. Thus, if a transient in the exciter field current varies over this portion of the saturation curve, a linear system is present and the above equation holds true. Fig. B.2 (a) and (b) show the transient response in the exciter field current to a unit-step voltage.

Values of I - i were measured at regular intervals of t and a plot was made on semi-log graph paper to determine the time constant. The inductance was then evaluated from the time constant.

TABLE B.3

EVALUATION OF THE EXCITER FIELD INDUCTANCE FROM OSCILLOGRAPH TRACINGS

Fig. B.2(a), I = 8.0 units (112 to 236 ma)
R = 212 ohms

Time (sec)	I - i (units)
0	8.0
0.04	4.9
0.08	3.0
0.12	2.0
0.20	0.8

Fig. B.2 (b) I = 9.3 units (90 to 235 ma)
R = 212 ohms

Time (sec)	I - i (units)
0	9.3
0.04	5.6
0.08	3.7
0.12	2.5
0.20	1.0

The open-circuit saturation curve of the alternator, Graph B.1, indicates that if the field current is in any range from 0 to 1.10 amps, the saturation curve is linear. This means that the self-inductance is constant for all currents within these limits. Current build-up in the alternator field may begin at 0 amps.

The self-inductance of the alternator field was determined by an identical method to that used for the exciter field.

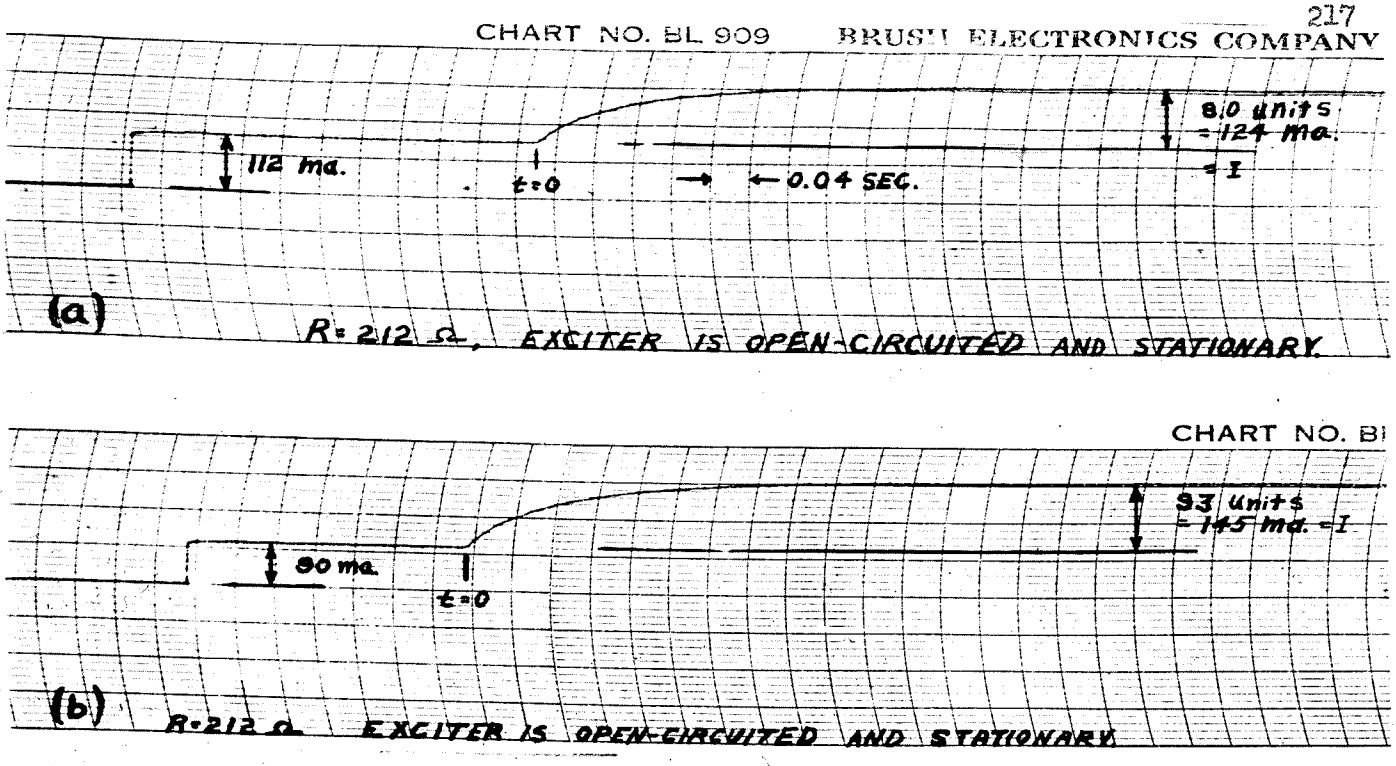

FIG. B.2 RESPONSE OF EXCITER FIELD CURRENT TO A UNIT-STEP INPUT VOLTAGE

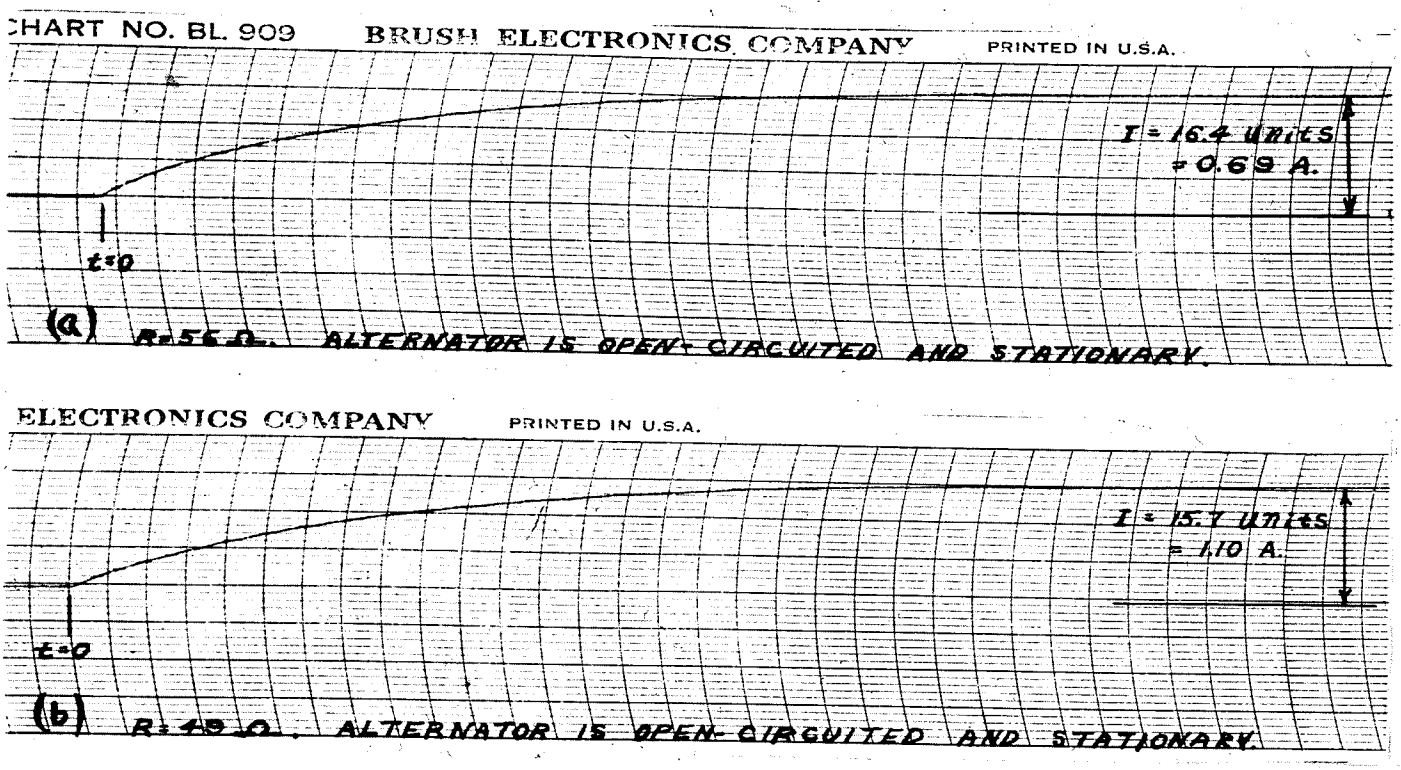

FIG. B.3 RESPONSE OF ALTERNATOR FIELD CURRENT TO A UNIT-STEP INPUT VOLTAGE

TABLE B.4

EVALUATION OF THE ALTERNATOR FIELD INDUCTANCE FROM OSCILLOGRAPH TRACINGS

Fig. B.3(a), I = 16.4 units (0 - 0.69 amps)
R = 56 ohms

Time (sec)	I - i (units)
0	16.4
0.04	13.7
0.08	11.6
0.12	10.0
0.16	8.7
0.24	6.6
0.32	4.9
0.44	3.0

Fig. B.3 (b) I = 15.7 units (0 to 1.10 amps)
R = 49 ohms

Time (sec)	I - i (units)
0	15.7
0.04	13.6
0.08	12.0
0.12	10.6
0.16	9.4
0.24	7.4
0.32	5.6
0.44	3.8

Results from Graph B.10:

Exciter Field,

$T_1 = \frac{L}{R} = 0.088$ sec

$L = 0.088 \times 212 = 18.6$ henries

$T_2 = \frac{L}{R} = 0.092$ sec

$L = 0.092 \times 212 = 19.5$ henries

Average self-inductance of the exciter field = 19.0 henries.

GRAPH B.10 - EVALUATING THE SELF-INDUCTANCE OF THE EXCITER AND ALTERNATOR FIELDS

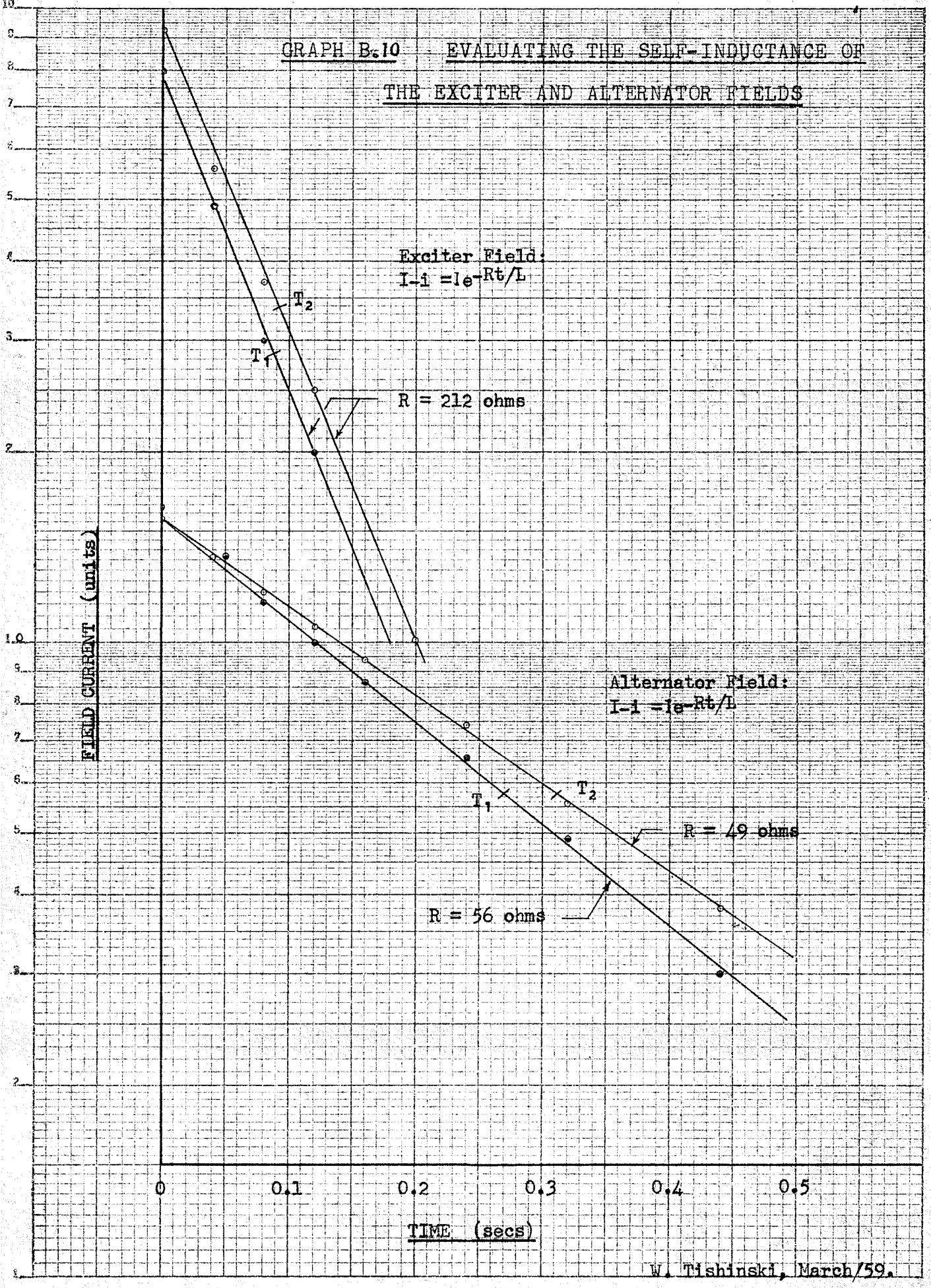

W. Tishinski, March/59.

Alternator Field,

$T_1 = \frac{L}{R} = 0.270$ sec

$L = 0.270 \times 56 = 15.1$ henries

$T_2 = \frac{L}{R} = 0.312$ sec

$L = 0.312 \times 49 = 15.3$ henries

Average self-inductance of the alternator field = 15.2 henries.

B.3 Equivalent Time Constant T_e of a Loaded Exciter

This is the build-up time constant of the exciter voltage when a unit-step voltage is impressed on the exciter field with the alternator field being supplied by the exciter at the same instant. The initial voltage on the exciter e_{x1} is the voltage that produces 120 volts at the alternator terminals at no load. This voltage is allowed to build up until the ceiling voltage, e_c is reached. The ceiling voltage is determined by the maximum exciter field current that would be supplied by the regulating system if the alternator terminal voltage failed. Two oscillograms were recorded; one with the speed of the machine at 1800 rpm and the other at 1750 rpm. The latter would simulate the condition for a suddenly-applied load. Impact loading decreases the speed of the motor-generator set.

By test the following values were determined:

(1) $e_{x1} = 48.0$ volts.

(2) $e_c = 135.0$ volts for a maximum exciter field current of 510 ma.

When the difference between the steady-state value, 135.0 volts and the instantaneous value of voltage is plotted on semi-log graph paper the result should be a straight line. The time required for the voltage to decay to 0.368 of its initial value is T_e.

The equation of the voltage build-up curve is given by

$$e = (e_c - e_{x1})(1 - e^{-t/T_e})$$

but the equation plotted on Graph B.10 is given by

$$(e_c - e_{x1}) - e = (e_c - e_{x1})\, e^{-t/T_e}$$

TABLE B.5

EVALUATION OF THE EQUIVALENT TIME CONSTANT T_e OF THE EXCITER FROM OSCILLOGRAPH TRACINGS

Figs. B.4 (a) and (b)

$e_{\chi 1}$ = 48.0 volts

e_c = 135.0 volts

Exciter field current (initial) = 107 ma

Exciter field current (final) = 510 ma

Exciter armature current (initial) = 1.29 amps

Exciter armature current (final) = 3.66 amps

Build-up curve will be expressed in terms of divisions found on the oscillogram and not in terms of voltage. This is done merely for convenience.

(a) N = 1800 rpm

Time (sec)	$(e_c - e_{\chi 1}) - e$ (units)
0	9.9
0.04	6.8
0.08	4.2
0.12	2.5
0.16	1.5
0.20	0.8
0.24	0.4

(b) N = 1750 rpm

Time (sec)	$(e_c - e_{\chi 1}) - e$ (units)
0	9.8
0.04	6.9
0.08	4.2
0.12	2.6
0.16	1.5
0.20	0.9
0.24	.6

From Graph B.11, T_e = 0.08 sec.

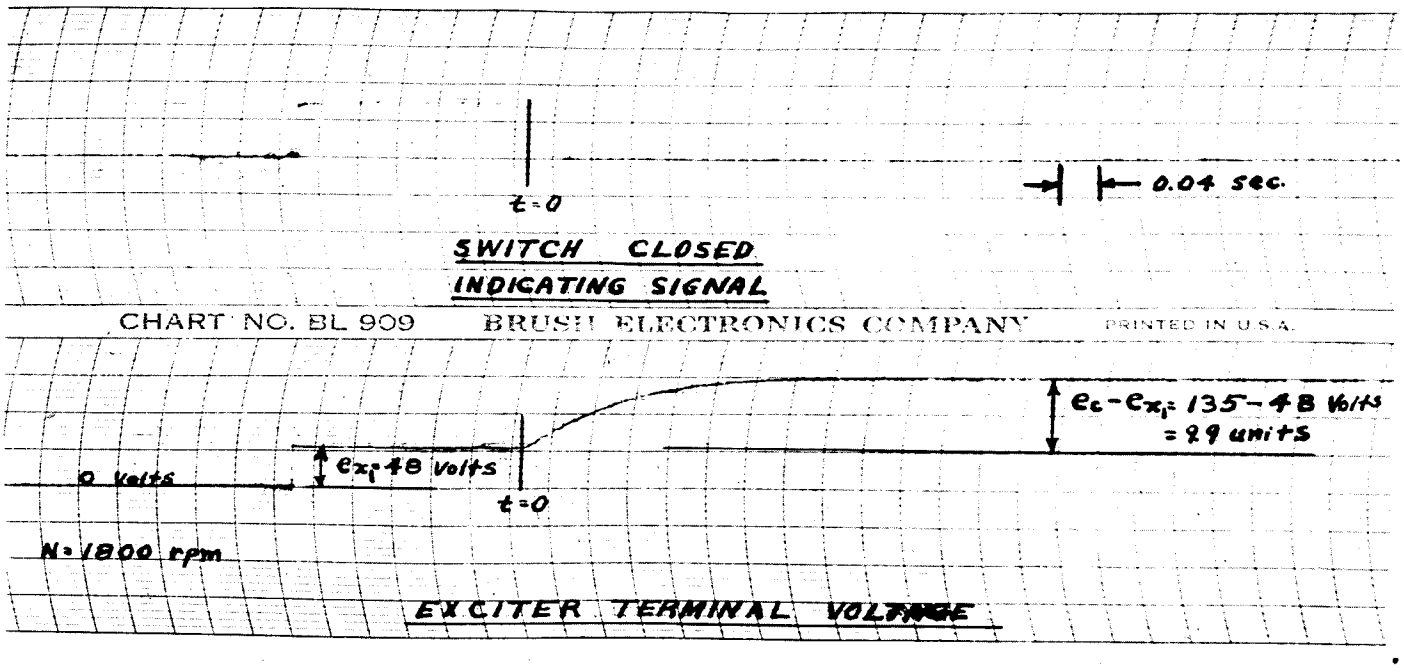

(a) N = 1800 RPM

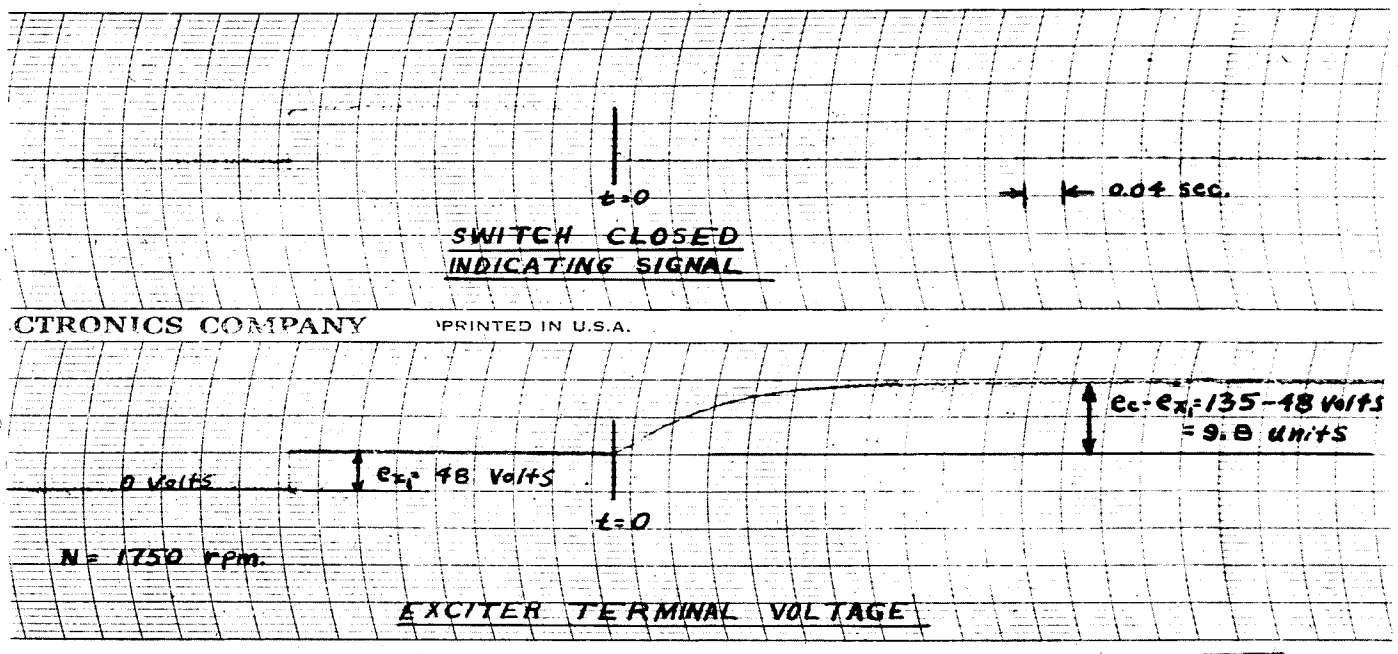

(b) N = 1750 RPM

FIG. B.4 RESPONSE OF LOADED EXCITER

GRAPH B.11 EVALUATION OF T_e, THE LOADED-EXCITER TIME CONSTANT

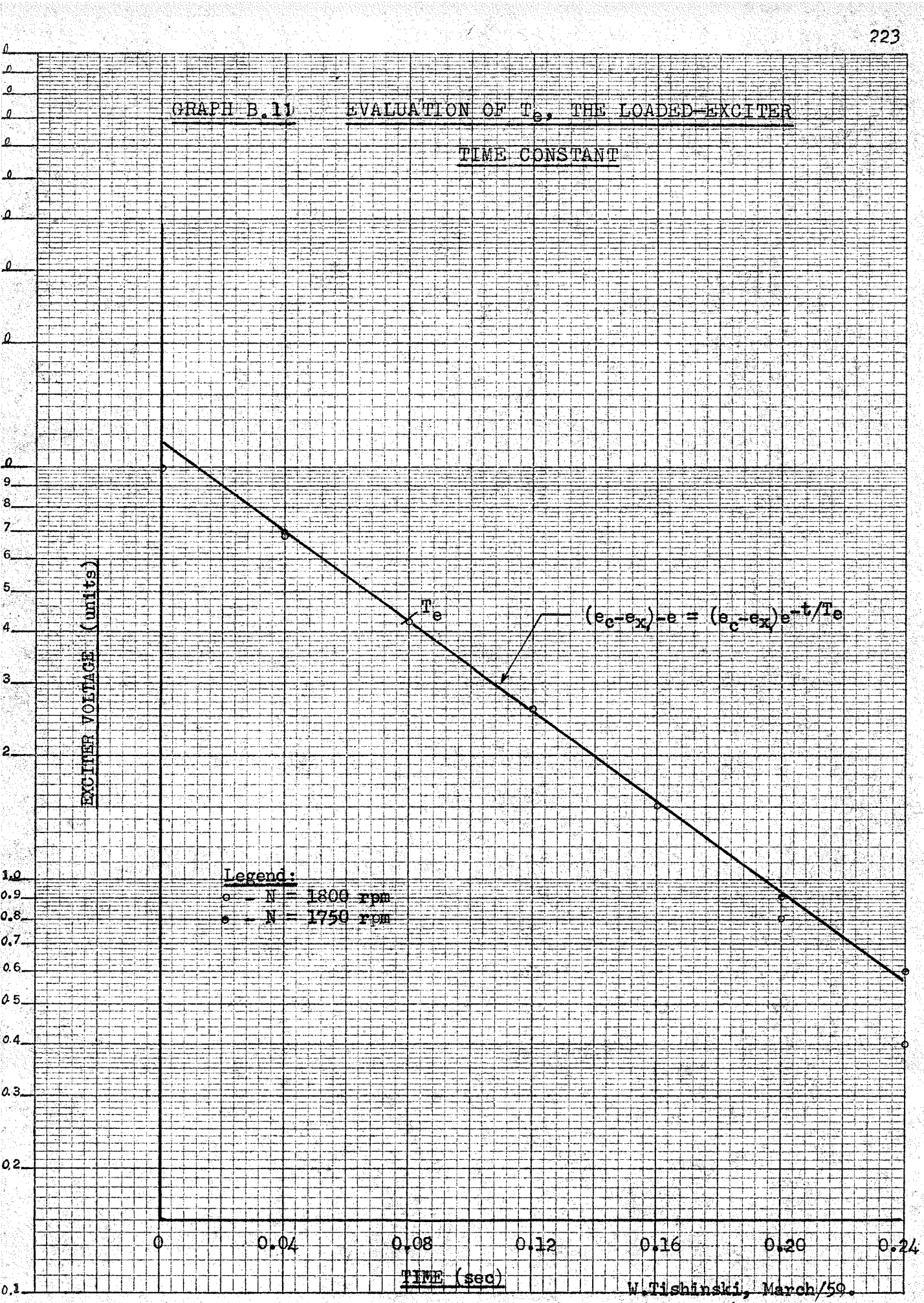

W.Tishinski, March/59.

B.4 The Slip Test

This test enables one to determine X_d, the direct-axis reactance and X_q, the quadrature-axis reactance[1]. The test machine, which is the alternator, is supplied with a reduced voltage at rated frequency by another alternator. The test alternator, however, is driven by a mechanically - coupled motor at a speed less than synchronous. This causes the line currents and voltages to pulsate. Fig. B.5 shows a record of the line current and line voltage for the above condition.

$$X_d = \frac{E_{max}/\sqrt{3}}{I_{min}} = \frac{92.0/\sqrt{3}}{28.6} = 1.87 \text{ ohms per phase} = 0.972 \text{ p/u}$$

$$X_q = \frac{E_{min}/\sqrt{3}}{I_{max}} = \frac{73.5/\sqrt{3}}{42.6} = 1.00 \text{ ohms per phase} = 0.519 \text{ p/u}$$

B.5 Exciter Armature Inductance

The exciter armature inductance can be determined by applying an a-c voltage to the armature and metering the current and power supplied.

TABLE B.6

DATA ON SUPPLYING AC POWER TO THE EXCITER ARMATURE

f = 36.5 cps

Applied Voltage (volts) #1DS1	Current (amps) #DC2	Power (watts) #391	Z (ohms)	R (ohms)
20	0.87	7.0	23.0	9.3
30	1.26	15.0	23.8	9.5
40	1.70	27.5	23.5	9.5
50	2.16	44.0	23.0	9.5
		Average -	23.2	9.5

$$X_L = \sqrt{(23.2)^2 - (9.5)^2}$$

$$= 21.2 \text{ ohms}$$

1. A.F. Puchstein, F.C. Lloyd and A.G. Conrad, Alternating Current Machines, 3rd Ed., pp. 214, J. Wiley and Sons, 1954.

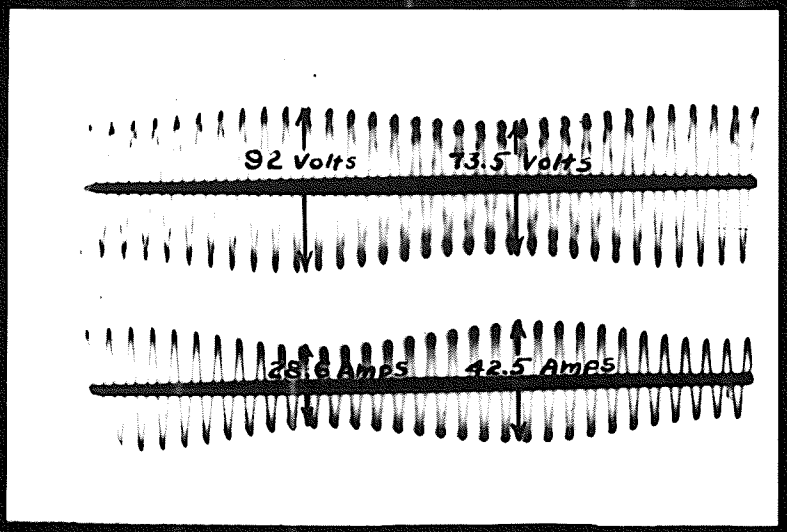

FIG. B.5 LINE CURRENT AND VOLTAGE DURING SLIP TEST

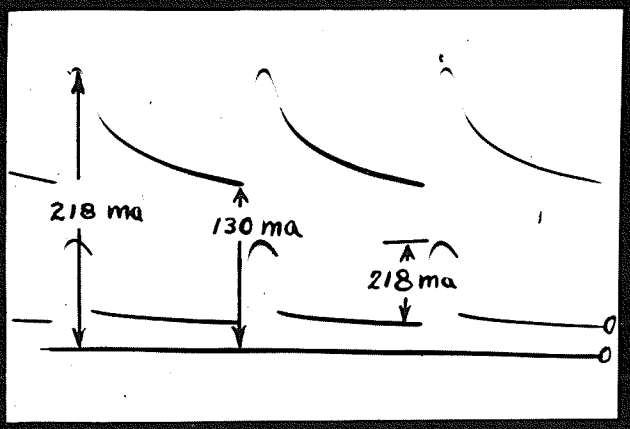

FIG. B.6 THYRATRON AND EXCITER FIELD CURRENT

Upper Trace: Field Current
Lower Trace: Thyratron Current

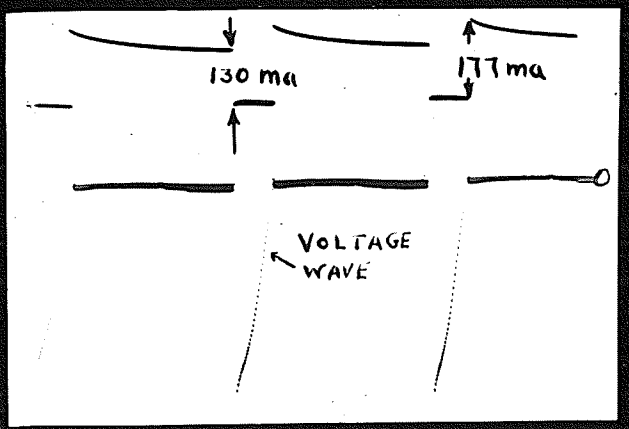

FIG. B.7 BACK-RECTIFIER CURRENT AND EXCITER FIELD VOLTAGE

$$L = \frac{21.6}{6.28 \times 36.5} = 0.0925 \text{ henries}$$

or approximately 0.1 henries

B.6 Exciter and Alternator Resistances

The various resistances were measured with a Heathkit VTVM which was calibrated with a General Radio Co., Decade Resistor, Serial No. 3726. Measurement of the alternator stator was made with a ducter.

TABLE B. 7

EXCITER AND ALTERNATOR RESISTANCES

Component	Measured Resistance at 23°C (ohms)	Corrected value to 75°C (ohms)
Exciter field	165	198
Exciter armature	9.7	11.6
Alternator field	36.5	42.5
Alternator stator	0.103 (L - L) [1]	0.125 (L - L)
	0.051 (L - N)	0.062 (L - N)

B.7 Summary of Alternator Constants

Base impedance = 69.3/36.0 = 1.925 ohms per phase

X_d (short-circuit test)	= 1.000	p/u
X_d (slip test)	= 0.972	p/u
X_d (average)	= 0.985	p/u
X_q	= 0.519	p/u
X_d'	= 0.194	p/u
X_d''	= 0.107	p/u
r_a	= 0.050	p/u
T_d'	= 0.0453	sec
T_d''	= 0.0108	sec
T_{do}'	= 0.234	sec
T_a	= 0.010	sec
T_e	= 0.080	sec

1. The stator was assumed to be wye-connected. Since the neutral was not accessible, phase resistance can be taken as half the value measured between terminals.

APPENDIX C

CURRENT WAVEFORM IN THE EXCITER FIELD

With a half-wave controlled rectifier supplying the field, Fig. 2.1(b), and the back-rectifier taking the discharge during the non-conducting portion of the thyratron, two separate equations will specify the shape of the current in the exciter field:

(1) During the conducting period of the controlled rectifier, $\beta \leq \omega t \leq \pi$, Fig. B.8.

(2) During the discharge period through the back-rectifier, $\pi \leq \omega t \leq 2\pi + \beta$.

Two points along the current wave shape are of interest:

(1) i_o, which represents the value of field current just prior to the firing of the thyratron.

(2) i_m, which represents the peak value of the current in the field. In a highly inductive load this peak occurs at the instant the a-c voltage crosses the zero axis.

With the field at room temperature (23°C) the power factor angle of the field is

$$\theta = \tan^{-1} \frac{377 \times 19.0}{165} \approx 90^{\circ}$$

For region (2)

$(\pi - \beta) \leq \omega t \leq 2\pi$ and neglecting the back-rectifier tube drop, the period is $0 \leq \omega t \leq \pi + \beta$.

$$i = i_m e^{-\frac{R}{\omega L} \omega t}$$

and $$i_o = i_m e^{-\frac{R}{\omega L}(\pi + \beta)} \qquad - - - - - - \text{(C.1)}$$

For region (1)

$$\beta \leq \omega t \leq \pi,$$

the period is $0 \leq t \leq \pi - \beta$

$$i = i_c + i_p$$

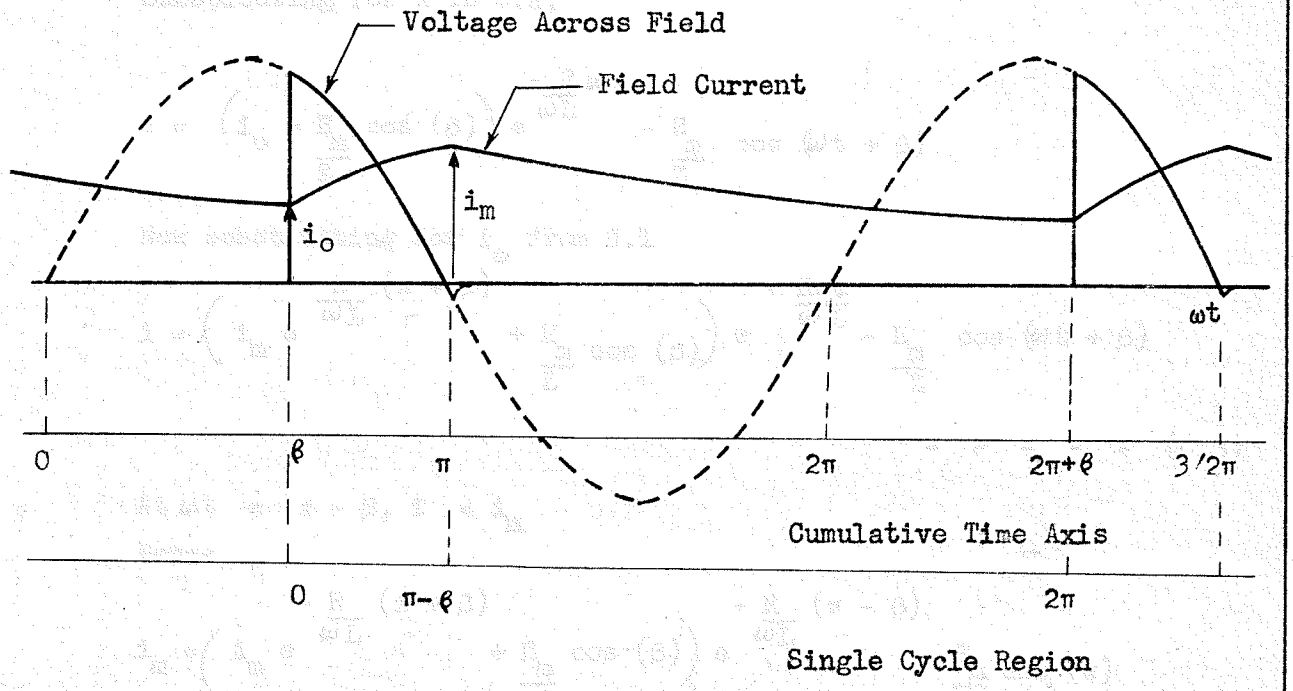

FIG. B.8 THEORETICAL VOLTAGE AND CURRENT WAVESHAPES ASSOCIATED WITH EXCITER FIELD

$$\text{or} \qquad i = K e^{-\frac{R\omega t}{\omega L}} + \frac{E_m}{Z} \sin(\omega t + \beta - \theta)$$

But, since $\theta \approx 90^\circ$,

$$i = K e^{-\frac{R\omega t}{\omega L}} - \frac{E_m}{Z} \cos(\omega t + \beta) \qquad - - - - - \quad (C.2)$$

Now at β, $\omega t = 0$ and $i = i_o$

Therefore,

$$i_o = K - \frac{E_m}{Z} \cos(\beta)$$

Substituting for K in C.2,

$$i = \left(i_o + \frac{E_m}{Z} \cos(\beta)\right) e^{-\frac{R}{\omega L}\omega t} - \frac{E_m}{Z} \cos(\omega t + \beta)$$

Now substituting for i_o from C.1

$$i = \left(i_m e^{-\frac{R}{\omega L}(\pi + \beta)} + \frac{E_m}{Z} \cos(\beta)\right) e^{-\frac{R\omega t}{\omega L}} - \frac{E_m}{Z} \cos(\omega t + \beta)$$

$$- - - - - \quad (C.3)$$

At $\omega t = \pi - \beta$, $i = i_m$

Hence,

$$i_m = \left(i_m e^{-\frac{R}{\omega L}(\pi + \beta)} + \frac{E_m}{Z} \cos(\beta)\right) e^{-\frac{R}{\omega L}(\pi - \beta)} - \frac{E_m}{Z} \cos(\pi)$$

from which

$$i_m = \frac{E_m \left(1 + e^{-\frac{R}{\omega L}(\pi - \beta)} \cos(\beta)\right)}{Z \left(1 - e^{-\frac{R}{\omega L}(2\pi)}\right)} \qquad - - - - - \quad (C.4)$$

Substituting for i_m in C.3, the final expression becomes

$$i = \left(\frac{E_m\left(1 + e^{-\frac{R}{\omega L}(\pi - \beta)} \cos\beta\right)^{e^{-\frac{R}{\omega L}(\pi + \beta)}}}{Z\left(1 - e^{-\frac{R}{\omega L}2\pi}\right)} + \frac{E_m}{Z}\cos\beta \right)^{e^{-\frac{R\omega t}{\omega L}}}$$

$$- \frac{E_m}{Z}\cos(\omega t + \beta) \qquad - - - - - - - \text{(C.5)}$$

If $(\pi - \beta)$ is substituted for ωt in C.5 the resulting expression reduces to equation C.4.

Similarly, if the substitution, $\omega t = 0$, is made in C.5, the result is equation C.1.

To check the validity of the developed equations, the theoretical and recorded current waveforms were plotted on Graph C.1. Also, on the same graph are the calculated and measured values of average current for the condition at which the current waveform was recorded.

The following constants were used in the calculations:

R = 165 ohms at 23°C. Resistance at this temperature was taken since the test was conducted on a field initially at room temperature.

L = 19.0 henries

β = 107°

E_m = 330 volts; tube drop considered

ω = 377 radians/sec

A rather large discrepancy was experienced between the two current wave shapes. This could largely be attributed to the saturating effect of the field inductance which was not considered in the calculations.

MANUFACTURED BY HENOUF PUBLISHING CO., MONTREAL

GRAPH C.1 CALCULATED AND EXPERIMENTAL CURRENT WAVE-SHAPES AND MAGNITUDES IN EXCITER FIELD

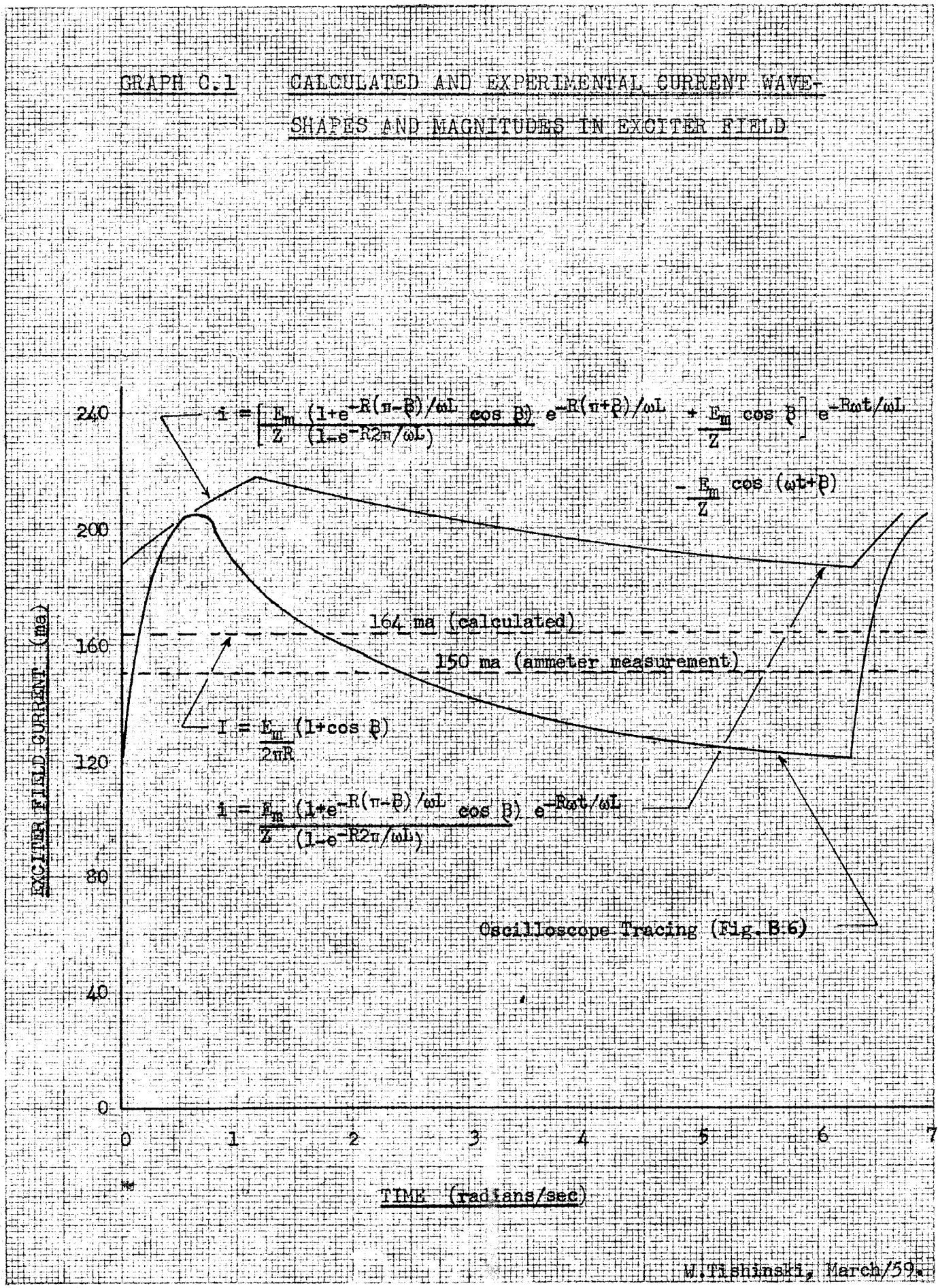

M. Tishinski, March/59.

THIS MARGIN RESERVED FOR BINDING.
IF SHEET IS READ THIS WAY (HORIZONTALLY), THIS MUST BE TOP.
IF SHEET IS READ THE OTHER WAY (VERTICALLY), THIS MUST BE LEFT-HAND SIDE.

APPENDIX D

INDUCTANCE OF THE SATURABLE REACTOR CONTROL WINDINGS

Nameplate data: General Electric Educational Amplistat
60 Cycle 115 volt
A-C Current - 1.0 amp
D-C Current - 50 ma
Resistance of the Control Winding - 415 ohms
Resistance of the load Windings (series-connected), 18 ohms
Turns in d-c winding - 4500

If the magnetization curve of an ideal saturable reactor is plotted, that is, a plot of a-c load current versus d-c control current, a sharp bend will be experienced at the "knee" of the curve. The rising portion up to the "knee" will be linear and if operation takes place along this line, the effective inductance of the control winding will be constant. With a constant effective inductance, a time constant L/R can be defined where R is the effective resistance of the control circuit and L is the inductance. Under these conditions any transient will act in an exponential manner. Thus, it is necessary to evaluate the inductance of the control winding either analytically or experimentally.

Results will be obtained by both methods. Analytical methods usually determine the transient response from the steady-state characteristics[1].

There are numerous ways of mathematically expressing the a-c saturation curve, as measured from the a-c terminals with zero d-c current. One relatively simple representation is by an equation containing a linear term and a power term[2]. The basic equation is

$$i = c_1 X + c_n X^n$$

---

1. W.C. Johnson and F.W. Latson, An Analysis of Transients and Feedback in Magnetic Amplifiers, A. I. E.E. Trans., Vol. 69, Pt. I, pp. 601, 1950.

2. W.C. Johnson, B.C. Merrell and R.E. Alley, Universal Curves for D-C Controllable Reactors, A.I.E.E. Trans., Vol. 68, Pt. I, pp. 31, 1949.

where i = the instantaneous current

χ = the instantaneous flux linkage

C_1, C_n and η = constants which depend upon the shape of the magnetization curve.

Charts have been prepared[3] to enable one to run a saturation curve for a particular reactor in question and then determine its equation by fitting the shape of the curve with one in the chart. The straight line portion must be removed first and the result is then called the reduced saturation curve. Table D.1 gives the saturation characteristics as well as some simple calculations for determining the reduced saturation curve.

TABLE D.1

REACTOR SATURATION CURVE

A-C windings series - connected in all tests

Load resistance = 0 ohms

I_{dc} = 0 ma

Applied A-C Voltage (volts) VTVM	I_{ac}(ma) Norma Wien meter	I (ma) Simpson # R238	E/E_b	I/I_b
0	0	0	Note: I is not considered in the straight line portion of the curve.	
16	2.5	0	I_b = 50 ma	
55	5.0	0	E_b = 245 volts	
94	7.5	0		
123	10.0	0	0.501	0
150	13.0	3.0	0.610	0.06
175	16.0	6.0	0.714	0.12
185	18.0	8.0	0.753	0.16
205	23.0	13.0	0.835	0.21
220	27.0	17.0	0.895	0.34
225	30.0	20.0	0.916	0.40
232	40.0	30.0	0.945	0.60
237	52.0	42.0	0.965	0.84
245	60.0	50.0	1.000	1.00

3. Ibid., pp. 33.

The preceding test data is plotted on Graph D.1. The straight line portion was taken as existing for values up to 10.0 ma load current. A base current I_b was then selected; this being the maximum value of load current obtained from the test data minus the straight line portion, that is, 60 - 10 = 50 ma. The a-c voltage, corresponding to I_b on the reduced saturation curve, is called the base voltage, E_b. It was found that when the reduced saturation curve (E/E_b vs I/I_b) was superimposed on the power curves, Graph D.2, it best fitted the 9th power curve.

Once the power of the saturation curve is established, specific universal curves are selected and these are used directly to relate the a-c voltage and current, the required direct current, and the d-c flux of the reactor when operating with d-c saturation. The curves are plotted in terms of the following dimensionless groups:

(1) E/E_b, where E is the rms voltage applied to the a-c terminals, and E_b is the rms voltage selected previously.

(2) I/I_b, where I is the rms alternating line current neglecting the straight line correction, and I_b is the rms base current selected previously.

(3) $\alpha = \psi_o/\psi_b$, where ψ_o is the d-c flux linkage of one a-c coil, and ψ_b is the maximum a-c flux linkage which would be caused by the base voltage, E_b.

($\psi_b = \sqrt{2}\, E_b/\omega$)

After the desired manipulation is carried out on the universal curves, the values corresponding to the straight line portion, which were originally subtracted from the saturation curve, must be added back. These curves are reproduced on Graph D.3.

Complete information is presented for a saturable reactor by plotting a family of curves of a-c applied voltage versus the a-c current with control current as a parameter. This data, as determined for the reactor is plotted on Graph D.1.

MANUFACTURED BY RENOUF PUBLISHING CO., MONTREAL

THIS MARGIN RESERVED FOR BINDING.
IF SHEET IS READ THIS WAY (HORIZONTALLY), THIS MUST BE TOP.
IF SHEET IS READ THE OTHER WAY (VERTICALLY), THIS MUST BE LEFT-HAND SIDE.

GRAPH D.1 — CHARACTERISTIC CURVES OF SATURABLE REACTOR

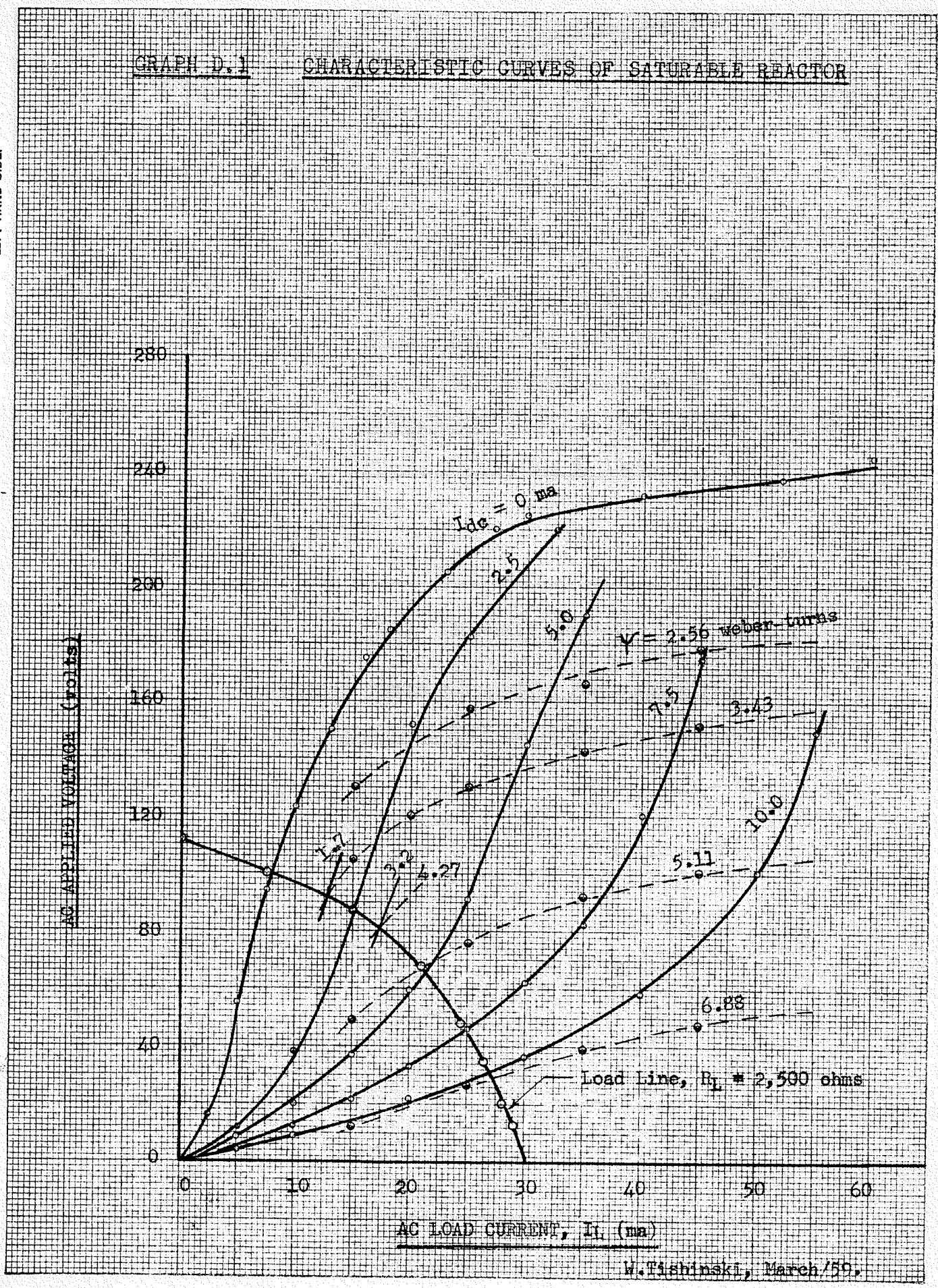

W.Tishinski, March/50.

MANUFACTURED BY, RENOUF PUBLISHING CO., MONTREAL

THIS MARGIN RESERVED FOR BINDING.

IF SHEET IS READ THIS WAY (HORIZONTALLY), THIS MUST BE TOP.

IF SHEET IS READ THE OTHER WAY (VERTICALLY), THIS MUST BE LEFT-HAND SIDE.

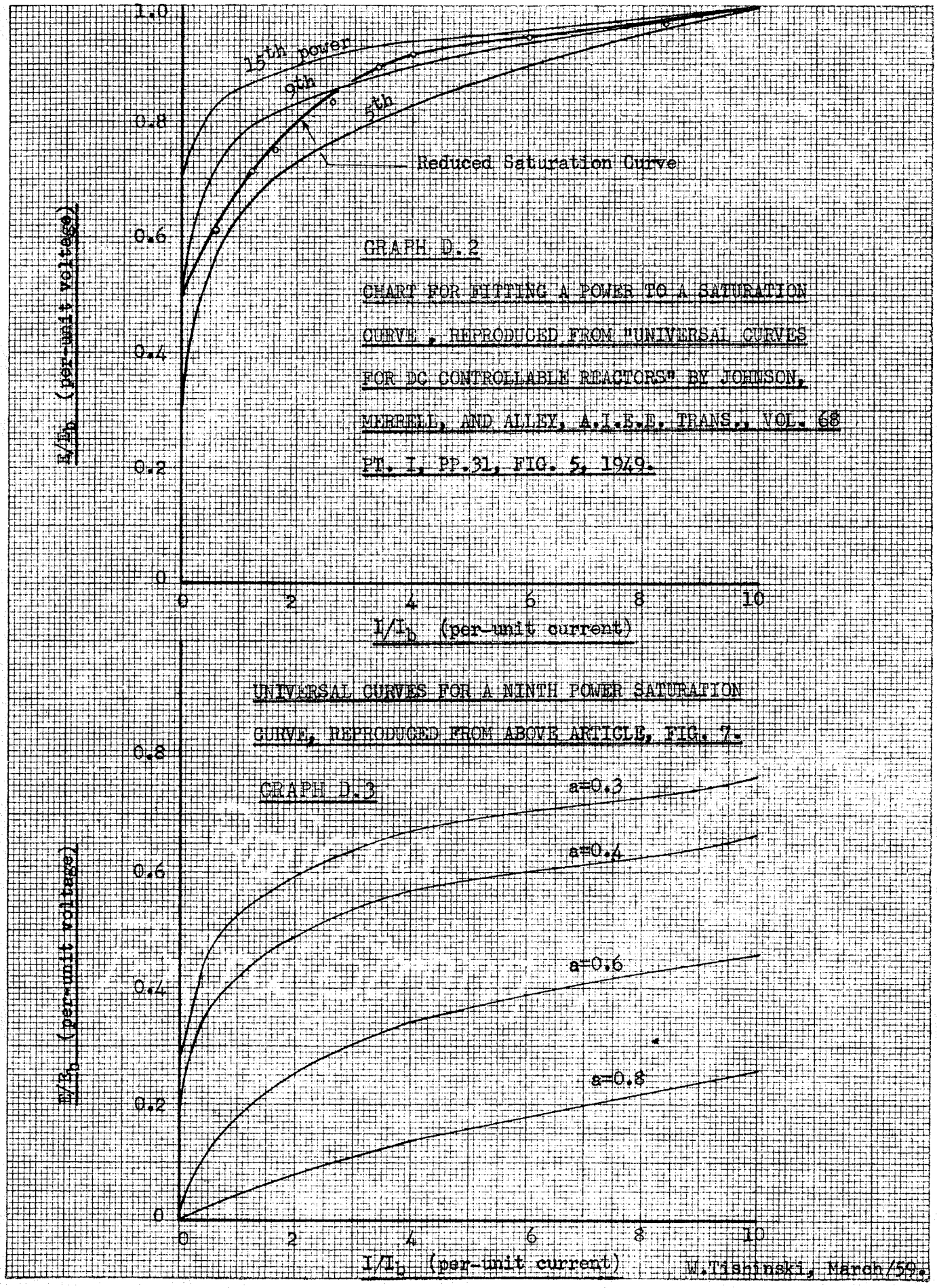

GRAPH D.2

CHART FOR FITTING A POWER TO A SATURATION CURVE, REPRODUCED FROM "UNIVERSAL CURVES FOR DC CONTROLLABLE REACTORS" BY JOHNSON, MERRELL, AND ALLEY, A.I.E.E. TRANS., VOL. 68 PT. I, PP.31, FIG. 5, 1949.

UNIVERSAL CURVES FOR A NINTH POWER SATURATION CURVE, REPRODUCED FROM ABOVE ARTICLE, FIG. 7.

GRAPH D.3

W.Tisninski, March/59.

If the load on the reactor is a resistance, the load line, when drawn on the aforementioned family of curves, will turn out to be an ellipse according to the relationship,

$$\left(\frac{E_s}{E_a}\right)^2 + \left(\frac{I_L}{E_a/R_L}\right)^2 = 1$$

where

E_s = rms voltage across the saturable reactor
E_a = rms applied voltage
I_L = rms current in the circuit
R_L = load resistance

If E_a and R_L remain constant, then the locus of the above equation can readily be plotted. However, the small 25 VA transformer used in this particular case had very poor regulation. Hence a set of data was taken to determine the exact voltages across the saturable reactor for various values of load current and the load line was plotted with this data.

TABLE D.2

DATA FOR PLOT OF LOAD LINE ON REACTOR CHARACTERISTIC CURVES

R_L = 2,500 ohms

E_a (volts) VTVM	E_s (volts) VTVM	I_L (ma) Norma Wien Meter	I_{dc} (ma) Simpson #R238
112	112	0	0
104	100	7.4	0
94	87	15.0	2.5
86	68	21.0	5.0
80	48	24.5	7.5
76	35	26.4	10.0
72	26	27.5	12.5
71	20	28.0	15.0
69	13	29.0	20.0

The above data were plotted on Graph D.1.

When the a-c coils of a saturable reactor are connected in series a change of flux which links the control circuit will induce equal and opposite voltages in the a-c coils. The transient response of a reactor due to sudden changes in the control circuit depends on the relation between the control-winding flux linkage, ψ_c and the magnetizing current, I_m, which in the case of the series-connected reactor is simply I_c. The main time lag is caused by the slowness of change of the flux that links the control winding, and so it can be assumed that the steady-state load line is followed during the transient conditions.

The flux linkages of the control winding as plotted on Graph D.1 were determined by calculation and by reference to the universal curves in the following manner:

At every point on any "a" curve (Graph D.3) a value of I/I_b will have a corresponding value of E/E_b. For example, on the "a = 0.3" curve, when $I/I_b = 0.1$, $E/E_b = 0.53$.

Hence $E = 0.53 \times E_b = 0.53 \times 245 = 130$ volts

and $I_L = I + 10.0 = (50.0 \times 0.1) + 10.0 = 15.0$ ma

From the relation listed previously, $\psi_b = \sqrt{2}\, E_b/\omega$;

$$\psi_b = \sqrt{2}\ 245/377 = 0.92$$

But $a = \psi_o/\psi_b$,

Therefore,

$\psi_o = 0.3 \times 0.92$ weber-turns (d-c flux linkage of one a-c coil).

To obtain the d-c flux linkage of the control winding, ψ_o must be multiplied by the turns ratio N_{dc}/N_{ac} and then by 2 to account for the 2 series coils,

$$\psi_c = \psi_o \times N_{dc}/N_{ac} \times 2 \text{ weber-turns}$$

The nameplate data for the reactor gave the number of d-c turns as 4,500, but no information was available concerning the a-c turns. The following test was conducted to evaluate the ratio of N_{dc}/N_{ac}.

TABLE D.3

EVALUATED TURNS RATIO OF THE SATURABLE REACTOR

Excited Terminals Section #1	Volts Applied to a-c Winding VTVM	Volts Applied to d-c Winding VTVM	$\frac{N_{dc}}{N_{ac}}$
B1 - B2 (1 coil)	10	46	4.6
A1 - A2 (1 coil)	10	46	4.6
A1 - B2 (2 coils in series)	10	46	4.6
A1 - B1 (2 coils in series)	10	2.5	0.103 This value should theoretically be zero, since with this connection the flux produced by the load windings should completely cancel out in the middle leg.
Section #2,			
F8 - F1, (control winding)	5.4 (B1-B2, 1 coil)	50	9.3
	5.2 (A1-A2, 1 coil)	50	9.6
	10.8 (A1-B2, 2 coils, in series)	50	4.6

The calculated values of N_{dc}/N_{ac} above, do not give concrete results. For instance, when one load coil was excited, a turns ratio of 4.6 was obtained, whereas when 2 coils in series were excited, the turns ratio was still 4.6 even though the a-c turns had doubled. This seemingly strange phenomenon can be explained with the aid of Fig. B.9.

The magnetomotive force relationship for a magnetic circuit is given by,

$$\text{mmf} = \frac{\Phi}{R} = NI$$

The voltage induced in the control windings is controlled by the amount of flux linking this winding. When one a-c coil is excited (coil A1-A2) a value of Φ can be considered to link the control winding. However, when the two a-c coils are connected in series, that is, terminals A2 and B1 tied together, the turns have doubled but the current I has halved since the impedance has doubled due to the increased number of turns.

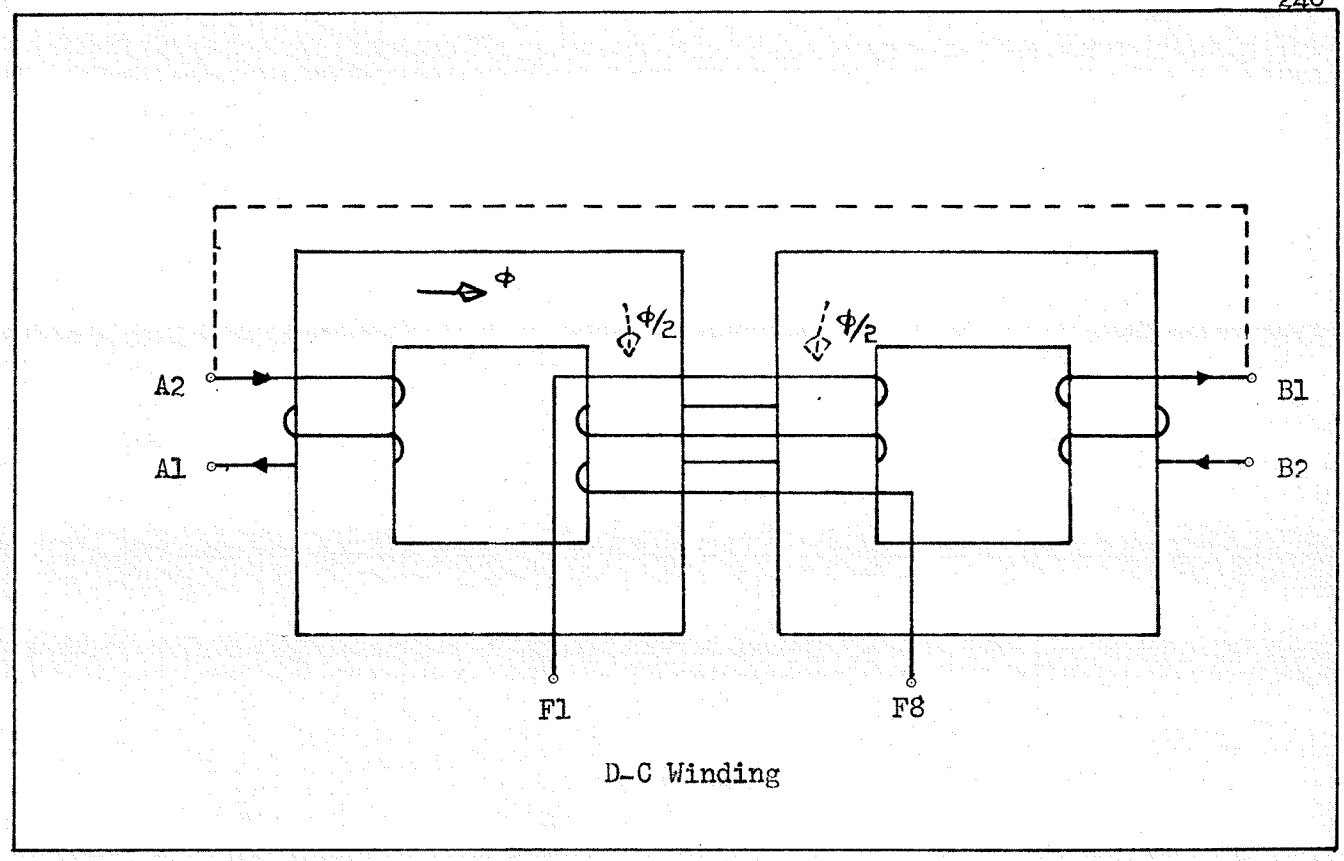

FIG. B.9 FLUX PATHS IN REACTOR WHEN A-C WINDINGS ENERGIZED

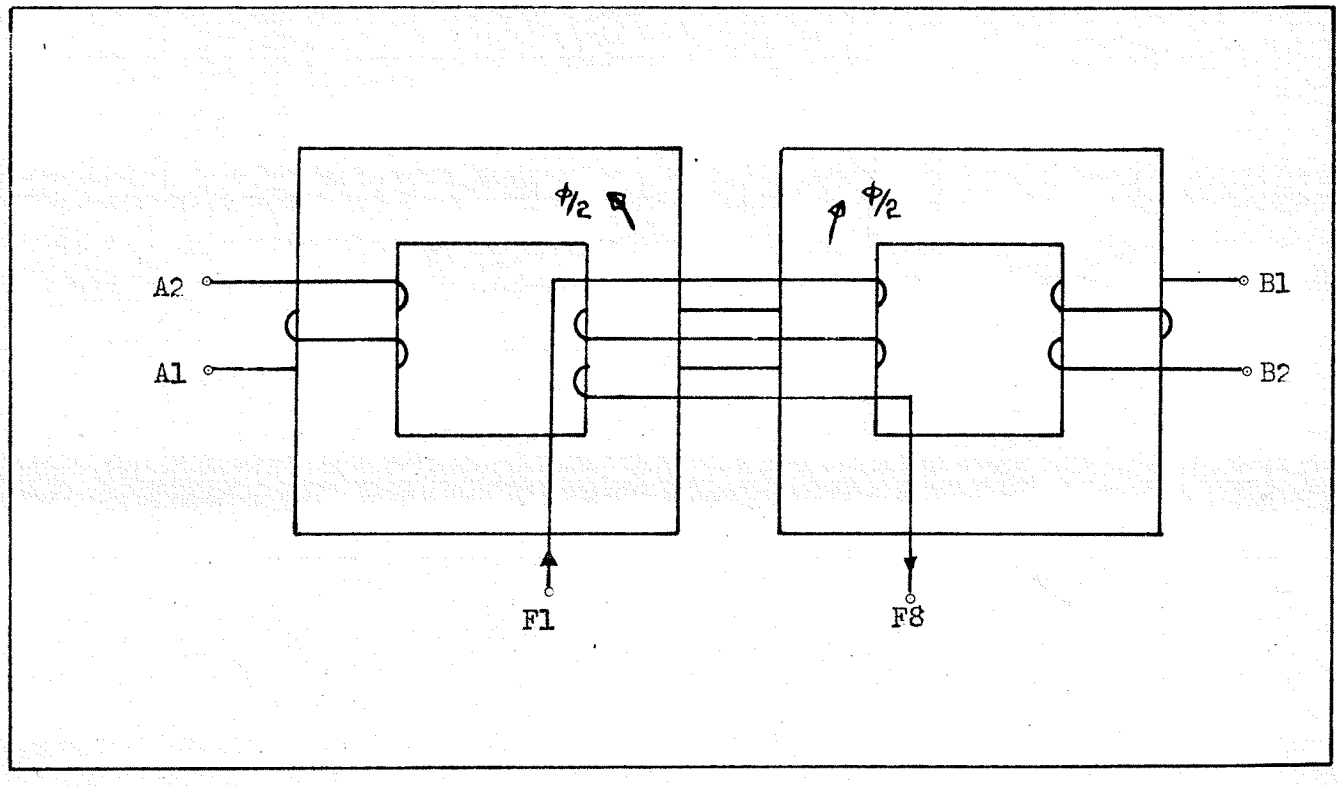

FIG. B.10 FLUX PATHS IN REACTOR WHEN CONTROL WINDINGS ENERGIZED

Effectively, the product NI remains constant and hence the flux linking the control winding remains constant. The flux path then taken is that path taken by the indicated dotted arrow. So, considering only the data in the first section of Table D.3, the turns ratio N_{dc}/N_{ac} can be taken as approximately 5.

However, the data in Section 2, Table D.3 seems to indicate that N_{dc}/N_{ac} is approximately 10, contradicting the results obtained in Section 1. This can be found to be false by reference to Fig. B.10.

A certain amount of effective current, I, will produce a value of flux, "Φ" in the middle leg of the reactor. But since there are two symmetrical paths for the flux, only $\Phi/2$ links each a-c winding. Essentially, only half the voltage is induced in the one a-c winding as would be, if all the flux from the control winding linked one a-c winding; hence, the impression that there are fewer a-c turns than actually existed. The proper turns ratio, N_{dc}/N_{ac} is, of course, approximately 5, which is very near to the averaged value of 4.63.

Having determined the turns ratio, ψ_c from the previous example may be found as,

$$\psi_c = \psi_o \times N_{dc}/N_{ac} \times 2$$

$$\psi_c = 0.276 \times 4.63 \times 2 = 2.56 \text{ weber-turns}$$

Selecting other points off the "a" curve and carrying through the same calculations as outlined, a constant ψ_c curve is evaluated and plotted on Graph D.1. The calculations and results for other ψ_c curves are arranged in tabular form.

TABLE D.4

CALCULATION OF THE CONTROL WINDING FLUX LINKAGES

E_b = 245 volts

I_b = 50.0 ma

N_{dc}/N_{ac} = 4.63

$\psi_b = \sqrt{2}\ E_b/\omega$

$\psi_o = a \cdot \psi_b$

$\psi_c = \psi_o \cdot N_{dc}/N_{ac} \cdot 2$

a	I/I_b	I (ma)	I_L (ma)	E/E_b	E(volts)	ψ_o (weber-turns)	ψ_c (weber turns)
0.3	0.1	5.00	15.00	0.53	130	0.276	2.56
	0.3	15.00	25.00	0.69	157	0.276	2.56
	0.5	25.00	35.00	0.68	167	0.276	2.56
	0.7	35.00	45.00	0.73	179	0.276	2.56
0.4	0.1	5.00	15.00	0.43	105	0.370	3.42
	0.2	10.00	20.00	0.49	120	0.370	3.42
	0.3	15.00	25.00	0.53	130	0.370	3.42
	0.5	25.00	35.00	0.58	142	0.370	3.42
	0.7	35.00	45.00	0.62	152	0.370	3.42
0.6	0.1	5.00	15.00	0.20	49	0.550	05.11
	0.3	15.00	25.00	0.31	76	0.550	05.11
	0.5	25.00	35.00	0.37	91	0.550	05.11
	0.7	35.00	45.00	0.46	100	0.550	05.11
0.8	0.1	5.00	15.00	0.05	12	0.740	6.88
	0.3	15.00	25.00	0.11	27	0.740	6.88
	0.5	25.00	35.00	0.16	39	0.740	6.88
	0.7	35.00	45.00	0.19	47	0.740	6.88

Since the operating point follows the steady-state load line during the transient conditions, points can be picked off the load line giving the relation between the control winding flux linkages and the magnetizing current (I_c).

Ψ_c (weber-turns)	I_c (ma)
3.43	1.7
3.87	2.5
4.27	3.2
5.11	4.9
6.15	7.5
6.78	10.0

The above data is plotted on Graph D.4, to give the control winding magnetization curve. The average slope between 2 points in question expressed in weber-turns per ampere, is the effective inductance of the control windings in henries.

On the same graph a relation between load current and control current is drawn to show the extent of the linear portion of the saturation curve when the reactor supplies a resistive load. The slope of the initial part of the magnetization curve is

$$\frac{5.1 - 2.6}{4.9 \times 10^{-3}} = 510 \text{ henries}$$

The inductance of the control winding can also be found by impressing a unit-step input voltage across the control winding and recording the transient response of the a-c current or d-c current. Both currents will build-up or build-down at the same rate since they are magnetically coupled. If build-up is along the linear portion of the saturation curve the load current should build up according to

$$i = I\left(1 - e^{\frac{-Rt}{L}}\right)$$

Build-up and build-down responses were recorded by the brush-oscillograph and are shown in Figs. B.11 and B.12. In Fig. B.13 is shown another build-up response as recorded by the Cossor oscilloscope.

MANUFACTURED BY RENOUF PUBLISHING CO., MONTREAL

THIS MARGIN RESERVED FOR BINDING.
IF SHEET IS READ THIS WAY (HORIZONTALLY), THIS MUST BE TOP
IF SHEET IS READ THE OTHER WAY (VERTICALLY), THIS MUST BE LEFT-HAND SIDE

GRAPH D.4 CONTROL WINDING MAGNETIZATION CURVE AND RELATION BETWEEN LOAD CURRENT AND CONTROL CURRENT FOR RESISTIVE LOAD

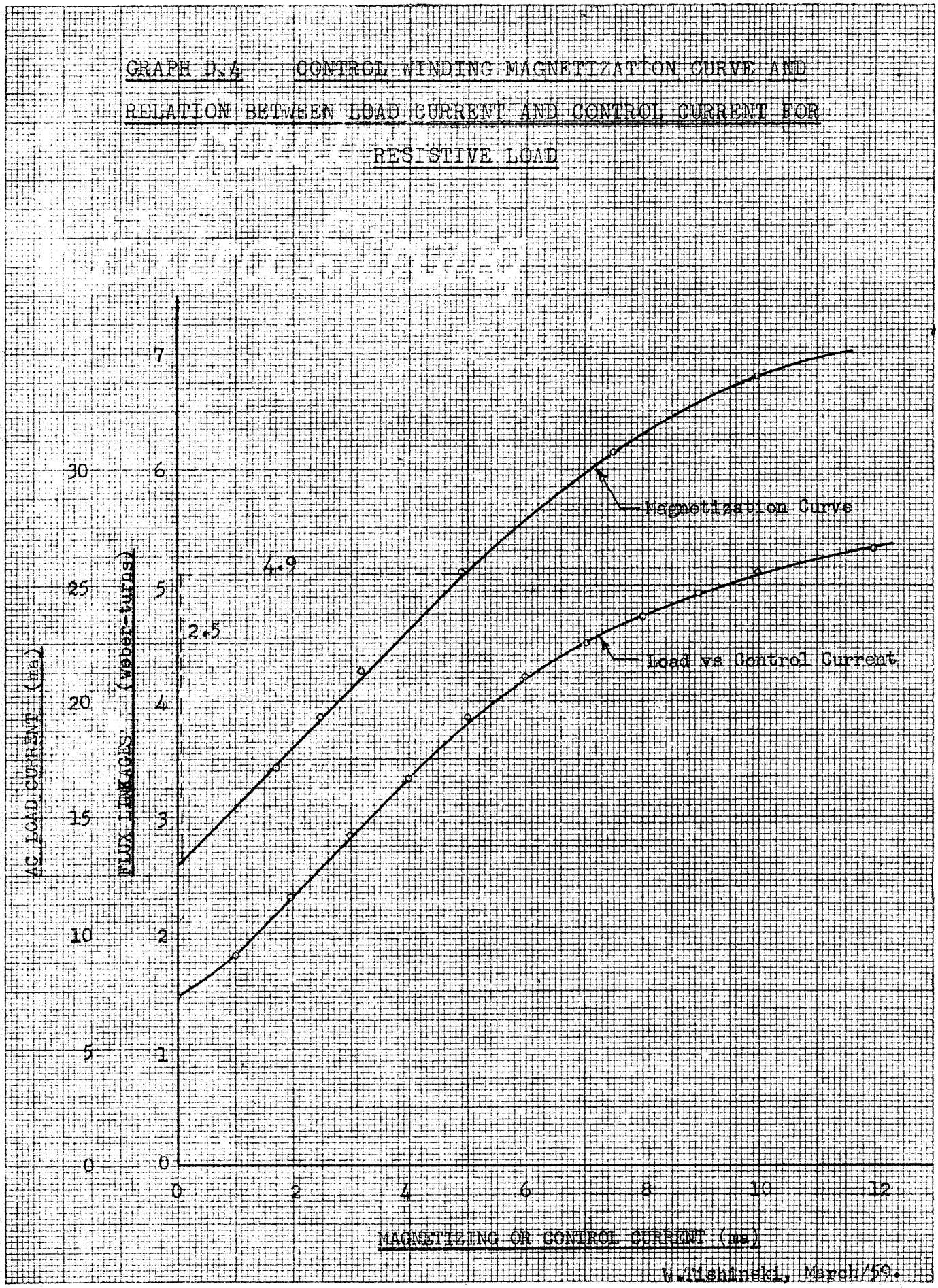

W. Tishinski, March/59.

For the build-up case, if the difference is taken between the final value and an instantaneous value the expression becomes

$$I - i = I e^{-Rt/L}$$

which when plotted on semi-log graph paper will yield the time constant.

The following table gives points from the transient response curves. Current units are of no consequences here since they do not affect the time constant.

TABLE D.5

TABULATION OF POINTS FOR EVALUATING TIME CONSTANT OF REACTOR

(a) Build-up of Saturable Reactor Load Current Recorded by Brush Oscillograph, Fig. B.11

R_L = 2500 ohms

Supply transformer : 25VA
115V/115V

R_{dc}(control windings)= 415 ohms

Time (cps)	I - i (units)
0	7.6
5	7.5
10	7.2
15	6.7
20	6.3
25	5.6
30	4.9
35	4.1
40	3.5
45	2.6
50	2.1
55	1.5
60	1.1
70	0.5

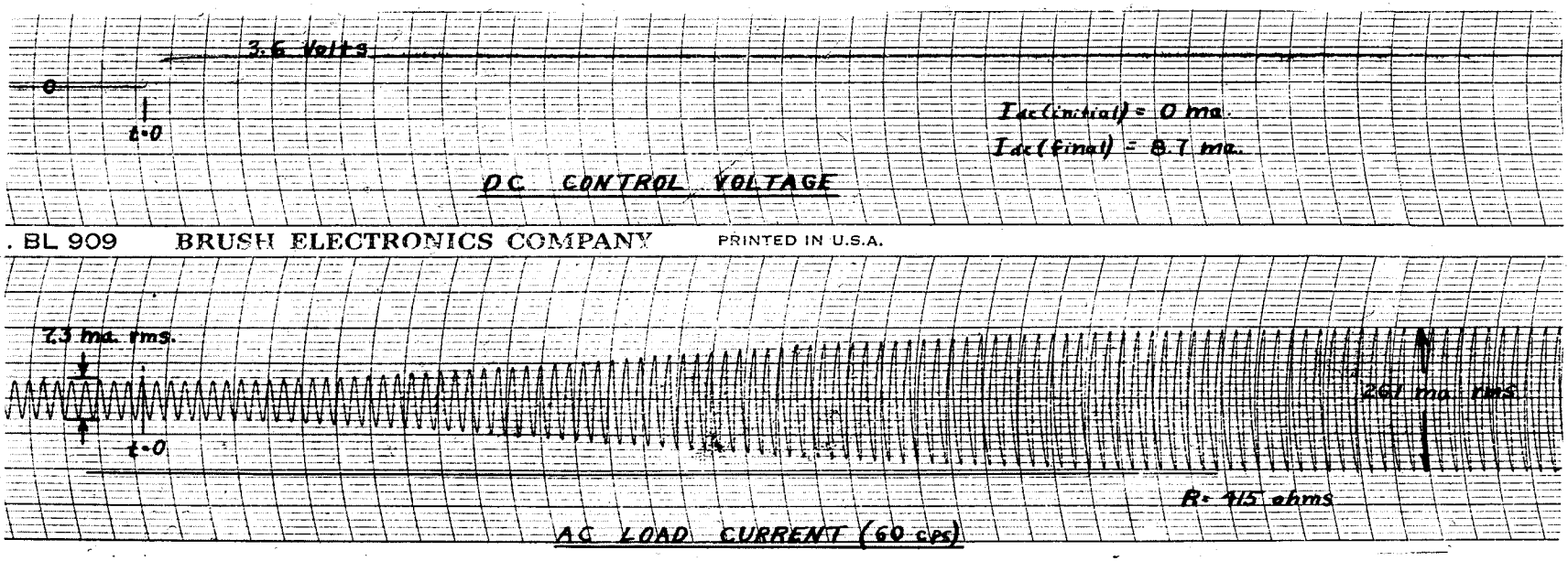

FIG. B.11 BUILD-UP OF AC CURRENT IN SATURABLE REACTOR WITH A UNIT-STEP INPUT IN CONTROL VOLTAGE

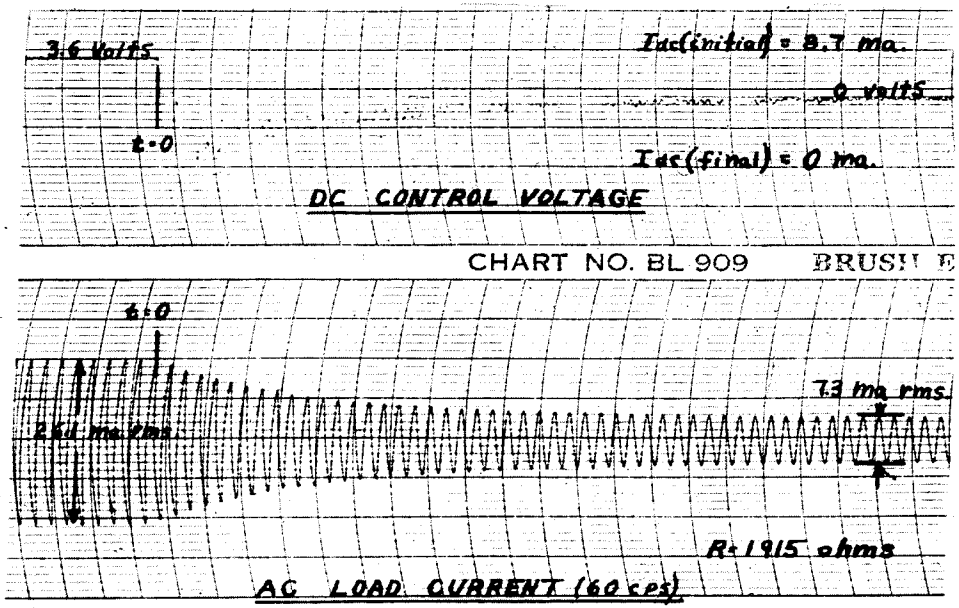

FIG. B.12 BUILD-DOWN OF SATURABLE REACTOR LOAD CURRENT WITH STEP INPUT IN CONTROL VOLTAGE

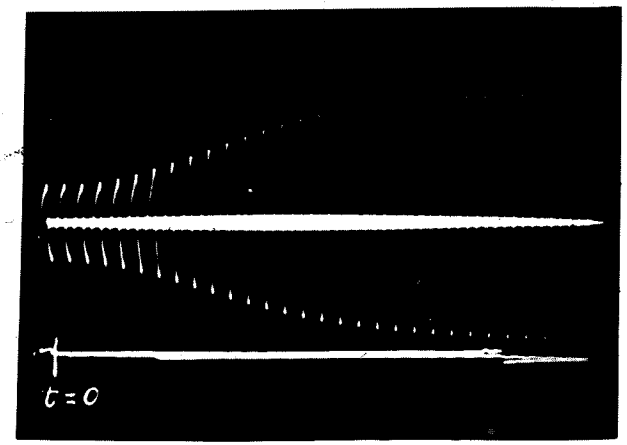

FIG. B.13 BUILD-UP OF LOAD CURRENT WITH UNIT-STEP INPUT IN CONTROL VOLTAGE

(b) Build-Down of Saturable Reactor Load Current Recorded by Brush Oscillograph, Fig. B.12.

R_{dc} (control windings and oscillograph galvanometer resistance)

= 415 + 1500 = 1915 ohms

Time (cps)	i (units)
0	7.8
2	6.2
4	5.2
6	4.2
8	3.3
10	2.8
12	2.5
16	1.9
20	1.4

(c) Build-Up of Saturable Reactor Load Current Recorded by Cossor Oscilloscope, Fig. B.13

R_{dc} (control windings + external resistance)

= 415 + 2200 = 2615 ohms

Time (cps)	I - i (units)
0	61
2	60
4	55
6	49
8	38
10	29
12	21
14	13
16	9
20	2

The time constants are selected off Graph D.5 and the results are listed below.

Test	T (cps)	R_{ac} (ohms)	L (henries)
Table (a)	37.5	415	260
Table (b)	14.5	1915	465
Table (c)	8.2	2615	358

From Graph D.5, it can be seen that during the build-up process, there is a delay of a few cycles before the a-c current begins to rise. Thus, it was rather difficult to find the proper position of the straight line. For the build-down case, the current fell rather quickly at the beginning, probably because of slight saturation, and then decayed exponentially. The build-down case would appear to present the most valid result, Therefore, the inductance can be taken as 465 henries.

There is still a third method of calculating the time constant of the reactor, and that is by the formula[1],

$$T = \frac{1}{4f} \frac{N_c^2}{N_L^2} \frac{R_L}{R_{dc}} \text{ sec} = \frac{L}{R_{dc}} \text{ sec}$$

where

f = supply frequency, 60 cps

N_c = control winding turns

N_L = load winding turns

R_L = load circuit resistance = transformer winding + reactor winding + load = 1370 + 18 + 2500 = 3898 ohms

R_{dc} = control circuit resistance

Therefore,

$$L = \frac{1}{4f} \frac{N_c^2}{N_L^2} R_L$$

$$= \frac{1}{240} \times 4.63^2 \times 3,898$$

$$= 347 \text{ henries}$$

---

1. W.A. Geyger, Magnetic Amplifier Circuits, pp. 50, McGraw - Hill, 1954.

GRAPH D.5 BUILD-UP AND BUILD-DOWN CURRENTS IN A SATURABLE REACTOR WITH A UNIT-STEP INPUT CONTROL VOLTAGE

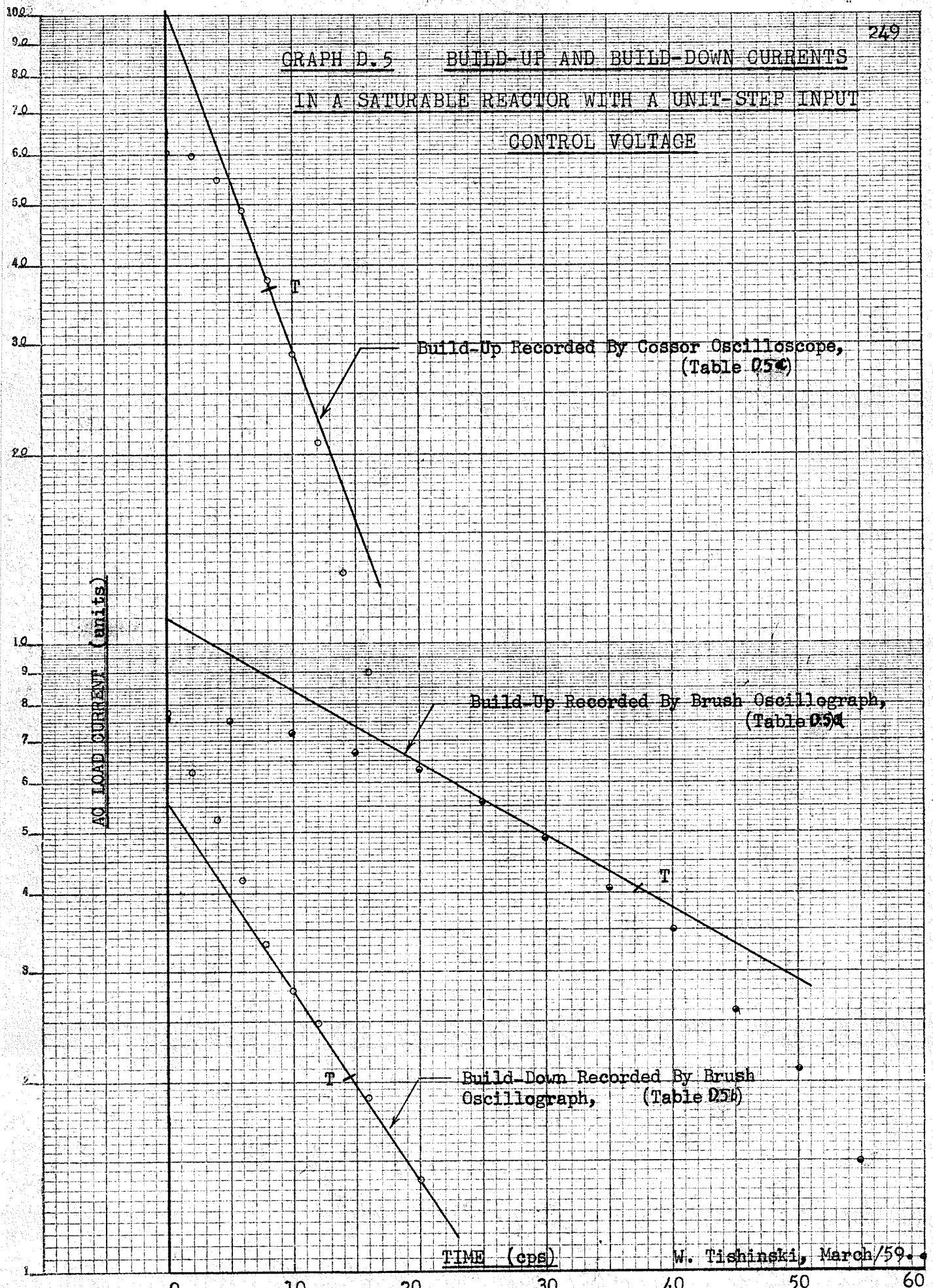

W. Tishinski, March/59.

Summary

(1) By graphical analysis L = 510 henries

(2) By test L = 467 henries

(3) By calculations L = 347 henries

Average value of the control winding inductance = 440 henries.

APPENDIX E

CONSTANTS OF 25VA TRANSFORMER, # 50711, USED IN FEEDBACK CIRCUIT

Short-Circuit Test

Voltage was applied to the primary, transformer ratio, 115:230. The primary is a 230-volt winding with a centre-tap, but only one-half of the winding was utilized.

Applied Voltage (volts) VTVM	I_{sc} (ma) Norma Wien Meter	Z_{o1} (ohms)
5.45	11.8	462
12.65	27.8	455
26.20	57.5	456

D-C resistance of primary = 320 ohms (VTVM)

D-C resistance of secondary = 720 ohms (VTVM)

Therefore, $R_{o1} = R_1 + a^2 R_2$

$= 320 + \frac{720}{4} = 500$ ohms

It is seen that R_{o1} is greater than Z_{o1} which is impossible. Error could be due to the inaccuracy of the VTVM. Nevertheless, the fact that can be established is that the inductance of the above transformer is negligible. For calculating purposes the impedance can be considered as pure resistance. Hence, the resistance referred to the secondary side of the transformer is

$R_{o2} = 730 + (4 \times 320) = 2{,}010$ ohms

An identical transformer was used to supply power to the saturable reactor load windings. For this application the total primary winding was utilized making the transformation ratio 230/230. Hence $R_{o2} = 730 + (2 \times 320) = 1{,}370$ ohms.

APPENDIX F

OPERATING PROCEDURE

The following procedure is recommended in placing the voltage-regulating system into operation:

(1) Start the M-G set and bring up to rated speed.

(2) Close the reference supply switch.

(3) Close the detector supply switch.

(4) Turn the anti-hunt control to position 10 in order to provide maximum available damping in the system.

(5) Check the position of the 6AC7 pentode screen voltage control. This should be at position 6 for a screen voltage of 124 volts.

(6) Turn on the B+ power supply.

(7) Close the thyratron heater supply switch. Wait for at least 20 seconds in order to provide ample time for the heaters to warm up.

(8) Close the switch controlling the thyratron plate supply voltage.

When step 8 is completed the alternator terminal voltage should rise to a value determined by the voltage control. This control is merely the potentiometer in the reference supply. Clockwise rotation of the dial "taps-off" a larger portion of the reference supply and increases the terminal voltage. The available range of voltage control at rated speed is from 65 volts to 133 volts.

The anti-hunt control may be decreased from position 10 to any limiting setting, beyond which oscillations occur, and yet operate satisfactorily. The limiting settings for various terminal voltages were determined by test and the results were plotted on Graph 7.6. If the system is stable on open-circuit conditions, it will certainly be stable under loaded conditions since some of the components in the system will operate at greater saturation.

It has been found by test that an optimum setting for the anti-hunt control is at 7. This setting reduces the ripple from the exciter provided with maximum feedback and yet provides stability throughout the entire controllable voltage range.

BIBLIOGRAPHY

A. BOOKS

1. Adkins, B., The General Theory of Electrical Machines, Wiley, 1957.
2. Bendz, W.I., Electronics for Industry, Wiley, 1947.
3. Brown, G.S., and Campbell, D.P., Principles of Servomechanisms, Wiley, 1948.
4. Bower, J.L., and Schultheiss, P.M., Introduction to the Design of Servomechanisms, Wiley, 1958.
5. Chance, B., and others, Electronic Time Measurements, MIT Radiation Laboratory Series, Vol. 20, McGraw-Hill, 1949.
6. Chestnut, H., and Mayer, R.W., Servomechanisms and Regulating System Design, Vol. I, Wiley, 1951.
7. Chestnut, H., and Mayer, R.W., Servomechanisms and Regulating System Design, Vol. II, Wiley, 1955.
8. Concordia, C., Synchronous Machines, Wiley, 1951.
9. Clarke, E., Circuit Analysis of A-C Power Systems, Vol. II, Wiley, 1950.
10. Cockrell, W.D., Industrial Electronic Control, Second edition, McGraw-Hill, 1950.
11. Davis, W.L., and Weed, H.R., Industrial Electronic Engineering, Prentice-Hall, 1954.
12. Dahl, O.G.C., Electric Power Circuits: Theory and Applications, Vol. II, McGraw-Hill, 1938.
13. Fitzgerald, S.E., and Kingsley, C., Electric Machinery, McGraw-Hill, 1952.
14. Fich, S., Transient Analysis in Electrical Engineering, Prentice-Hall, 1957.
15. Geyger, W.A., Magnetic Amplifier Circuits, McGraw-Hill, 1954
16. Gardner, M.F., and Barnes, J.L., Transients in Linear Systems, Wiley, 1942.
17. Gray, T.S., Applied Electronics, second edition, Wiley, 1954.
18. Kimbark, E.W., Power System Stability, Vol. III, Wiley, 1956.
19. Kerchner, R.M., and Corcoran, G.F., Alternating-Current Circuits, Third Edition, Wiley, 1953.
20. LePage, W.R., and Seely, S., General Network Analysis, McGraw-Hill, 1952.

21. LePage, W.R., Analysis of Alternating - Current Circuits, McGraw-Hill, 1952.

22. Langsdorf, A.S., Theory of Alternating - Current Machinery, Second edition, McGraw-Hill, 1955.

23. Lawrence, R.R., and Richards, H.E., Principles of Alternating-Current Machinery, Fourth edition, McGraw-Hill, 1953.

24. Lyon, W.O., Transient Analysis of Alternating-Current Machinery, Wiley, 1954.

25. Millman, J. and Taub, H., Pulse and Digital Circuits, McGraw-Hill, 1953.

26. Puchstein, A.F., Lloyd, T.C., and Conrad, A.G., Alternating-Current Machines, Third edition, Wiley, 1954.

27. Pipes, L.A., Applied Mathematics for Engineers and Physicists, McGraw-Hill, 1946.

28. RCA Receiving Tube Manual, Radio Corporation of America, 1954.

29. Reddick, H.W., Differential Equations, Second edition, Wiley, 1953.

30. Tustin, A., Direct-Current Machines for Control Systems, Spon, London, 1952.

31. Thaler, G.J., and Brown, R.G., Servomechanism Analysis, McGraw-Hill, 1953.

32. Wylie, C.R., Jr., Advanced Engineering Mathematics, McGraw-Hill, 1951.

33. Electrical Transmission and Distribution Reference Book, By Central Station Engineers of the Westinghouse Electric Corporation, Fourth edition, Westinghouse Electric Corporation, 1950.

34. Industrial Electronics Reference Book, by Electronics Engineers of the Westinghouse Electric Corporation, Wiley, 1948.

35. Standard Mathematical Tables, Tenth edition, Chemical Rubber Company, 1954.

B. TECHNICAL PAPERS

1. Anderson, H.C., Voltage Variation of Suddenly-Loaded Generators, General Electric Review, Vol. 48, p. 25, August, 1945.

2. Burnett, J.H., Fast Response, High Current Thyratron Supplies for Inductive Loads, Electrical Engineering, Vol. 72, p. 627, April, 1953.

3. Brady, T.W., Cathode-Coupled Valves, Wireless Engineer, Vol. 31, p. 111, May 1954.

4. Boice, W.K. and others, The Direct-Acting Generator Voltage Regulator, AIEE Trans., Vol. 59, p. 149, 1940.

5. Bothwell, F.E., Stability of Voltage Regulators, AIEE Trans., Vol. 69, part II, p. 1430, 1950.

6. Chin, P.T., and Walter, G.E., Transient Response of Controlled Rectifier Circuits, AIEE Trans., Vol. 64, p. 208, 1945.

7. Cornelius, H.A., and others, Experience with Automatic Voltage Regulation on a 115-Megawatt Turbogenerator, AIEE Trans., Vol. 71, part III, p. 184, 1952.

8. Close, R.N., and Lebenbaum, M.T., Design of Phantastron Time Delay Circuits, Electronics, Vol. 21, p. 100, April, 1948.

9. Colaico, A.P., Johnson, A.A., and Reilly, J.E., Design and Test on Electronic Exciter Supplied from Common Shaft-Driven Generator, AIEE Trans., Vol. 69, part I, p. 328, 1950.

10. Doherty, R.E., and Nickle, C.A., Synchronous Machines, - I and II, AIEE Trans., Vol. 45, p. 912, 1926.

11. Doherty, R.E., and Nickle, C.A., Synchronous Machines - V, Three-Phase Short Circuit, AIEE Trans., Vol. 49, p. 700, April, 1930.

12. Goldmuntz., L.A., A Cathode-Coupled Clipper, Proc. IRE, Vol. 36, p. 1172, September, 1948.

13. Harty, E.A., Characteristics and Applications of Selenium-Rectifier Cells, AIEE Trans., Vol. 62, p. 624, 1943.

14. Holloway, V.C., Transient Characteristics of Aircraft A-C Generators, AIEE Trans., Vol. 73, part II, p. 187, 1954.

15. Harder, E.L., and Cheek, R.C., Regulation of A-C Generators with Suddenly Applied Loads, AIEE Trans., Vol. 63, p. 310, June 1944.

16. Hanna, C.R., Oplinger, K.A., and Valentine, C.E., Recent Developments in Generator Voltage Regulation, AIEE Trans., Vol. 58, p. 838, 1939.

17. Harder, E.L., Solution of the General Voltage Regulator Problem by Electrical Analogy, AIEE Trans., Vol. 66, p. 815, 1947.

18. Harder, E.L., Cheek, R.C., and Clayton, J.M., Regulation of A-C Generators with Suddenly Applied Loads, Part II, AIEE Trans., p. 395, 1950.

19. Harder, E.L., and Horton, W.F., Response Time of Magnetic Amplifiers, AIEE Trans., Vol. 69, part II, p. 1130, 1950.

20. Johnson, W., Merrell, B., and Alley, R., Universal Curves for D-C Controllable Reactors, AIEE Trans., Vol. 68, p. 31, 1949.

21. Johnson, W., and Latson, F.W., An Analysis of Transients and Feedback in Magnetic Amplifiers, AIEE Trans., Vol. 69, part I, p. 601, 1950.

22., James, H.B., The Use of an Analog Computer to Optimize the Transient Response of an Aircraft-Type Generator-Regulator System, AIEE Trans., Vol. 72, part II, p. 363, 1953.

23. Johnson, E.E., Jr., Sinusoidal Analysis of Feedback Control System Containing Non-linear Elements, AIEE Trans., Vol. 71, part II, p. 169, 1952.

24. Kochenburger, R.J., A Frequency Response Method for Analyzing and Synthesizing Contactor Servomechanisms, AIEE Preprint, 50, Jan. 1950.

25. Kilgore, L.A., Calculation of Synchronous Machine Constants - Reactance and Time Constants Affecting Transient Characteristics, AIEE Trans., Vol. 50, p. 1201, 1931.

26. Kingsley, C. Jr., Saturated Synchronous Reactance, AIEE Trans., Vol. 54, p. 300, 1935.

27. Kilgore, L.A., Effects of Saturation on Machine Reactances, AIEE Trans., Vol. 54, p. 545, 1935.

28. Kuyper, W.W., Analysis of Short-Circuit Oscillograms, AIEE Trans., Vol. 60, p. 151, 1941.

29. Kirschbaum, H.S., Per-Unit Inductances of Synchronous Machines, AIEE Trans., Vol. 69, part I, p. 231, 1950.

30. Koenig, H.E., Transient Response of Direct-Current Dynamos, AIEE Trans., Vol. 69, part I, p. 139, 1950.

31. Klokow, R.E., Maximum Overvoltage on Aircraft A-C Generators After Sudden Removal of Load, AIEE Trans., Vol. 74, part II, p. 417, 1955.

32. Lewis, W.A., Quick-Response Excitation, Elec. Jour., Vol. 31, p. 308, August, 1934.

33. Langstaff, H.A.P., Vaughan, H.R., and Lawrence, R.F., Application and Performance of Electronic Exciters for Large A-C Generators, AIEE Trans., (Elec. Eng.), Vol. 65, p. 246, 1946.

34. May, J.C., and others, Thyratron Phase-Control Circuits, Electronics, Vol. 21, p. 107, July, 1948.

35. McClure, J.B., Whittlesey, S.I., and Hartman, M.E., Modern Excitation Systems for Large Synchronous Machines, AIEE Trans., Vol. 65, p. 939, 1946.

36. Mellor, A.G., and Tomoshok, M., Excitation System Performance with Motor-Driven Exciters, AIEE Trans., Vol. 69, part i, p. 321, 1950.

37. Park, R.H., Definition of an Ideal Synchronous Machine and Formula for the Armature Flux Linkages, Gen. Elec. Rev., Vol. 31, p. 332, June, 1928.

38. Park, R.H., Two-Reaction Theory of Synchronous Machines - I, Generalized Method of Analysis, AIEE Trans., Vol. 48, p. 716, 1929.

39. Park, R.H., Two-Reaction Theory of Synchronous Machines - II, AIEE Trans., Vol. 52, p. 352, 1933.

40. Powel, C.A., Quick-Response Excitation for Alternating-Current Synchronous Machinery, Elec. Jour., Vol. 24, p. 157, April, 1927.

41. Porter, F.M., and Kinghorn, J.H., The Development of Modern Excitation Systems for Synchronous Condensers and Generators, AIEE Trans., Vol. 65, p. 1020, 1946.

42. Phillips, A.H., Lambert, W.H., and Pattison, D.R., Excitation Improvement - Electronic Excitation and Regulation of Electric Generators as Compared to Conventional Methods, AIEE Trans., Vol. 69, part I, p. 338, 1950.

43. Rankin, A.W., The Equations of the Idealized Synchronous Machine, Gen. Elec. Rev., Vol. 47, p. 31, June, 1944.

44. Rankin, A.W., Per-Unit Impedances of Synchronous Machines, AIEE Trans., Vol. 64, p. 569, 1945.

45. Rankin, A.W., Per-Unit Impedances of Synchronous Machines, II, AIEE Trans., Vol. 64, p. 839, 1945.

46. Rankin, A.W., The Direct- and Quadrature-Axis Equivalent Circuits of the Synchronous Machine, AIEE Trans., Vol. 64, p. 861, 1945.

47. Rosenberg, L.T., A semiempirical Approach to Voltage-Dip, with Suddenly Applied Loads on A-C Generators, AIEE Trans., Vol. 68, part I, p. 160, 1949.

48. Storm, H.F., Some Fundamentals of D-C Controlled Reactors with resistive Load, AIEE Trans., Vol. 68, part I., p. 188, 1949.

49. Storm, H.F., Transient Response of Saturable Reactors with Resistive Load, AIEE Trans., Vol. 70, part I, p. 95, 1951.

50. Scott, H.J., Rectifier Filter Design, Electronics, Vol. II, p. 28, June, 1938.

51. Snively, H.D., and Robinson, P.B., Measurement and Calculation of D-C.Machine Armature Circuit Inductance, AIEE Trans., Vol. 69, part II, p. 1228, 1950.

52. Stewart, C., Automatic Voltage Control of Generators, Jour. IEE, Vol. 94, part IIA, p. 39, May 1947.

53. Tschudi, E.W., Transfer Functions for R-C and R-L Equalizer Networks, Electronics, Vol. 22, p. 116, May 1949.

54. Ver Planck, D.W., Finzi, L.A., and Beaumariage, D.C., An Analysis of Transients in Magnetic Amplifiers, AIEE Trans., Vol. 69, part I, p. 498, 1950.

55. Wright, S.H., Determination of Synchronous Machine Constants by Test-Reactances, Resistances, and Time Constants, AIEE Trans., Vol. 50, p. 1331, December, 1931.

56. Whiteley, A.L., Fundamental Principles of Automatic Regulators and Servomechanisms, Jour. IEE, part IIA, No. 1, Vol. 94, p. 5, 1947.